Chemische Modifizierung von Polyoxovanadaten mit Übergangsmetallkomplexen und deren Charakterisierung

Löslichkeitsstudien, Transformationsreaktionen, Versuche zur rationalen Syntheseplanung sowie Synthese eines neuen Isomers des $\{V_{14}Sb_8O_{42}\}$-Clusters

Kumulative Dissertation

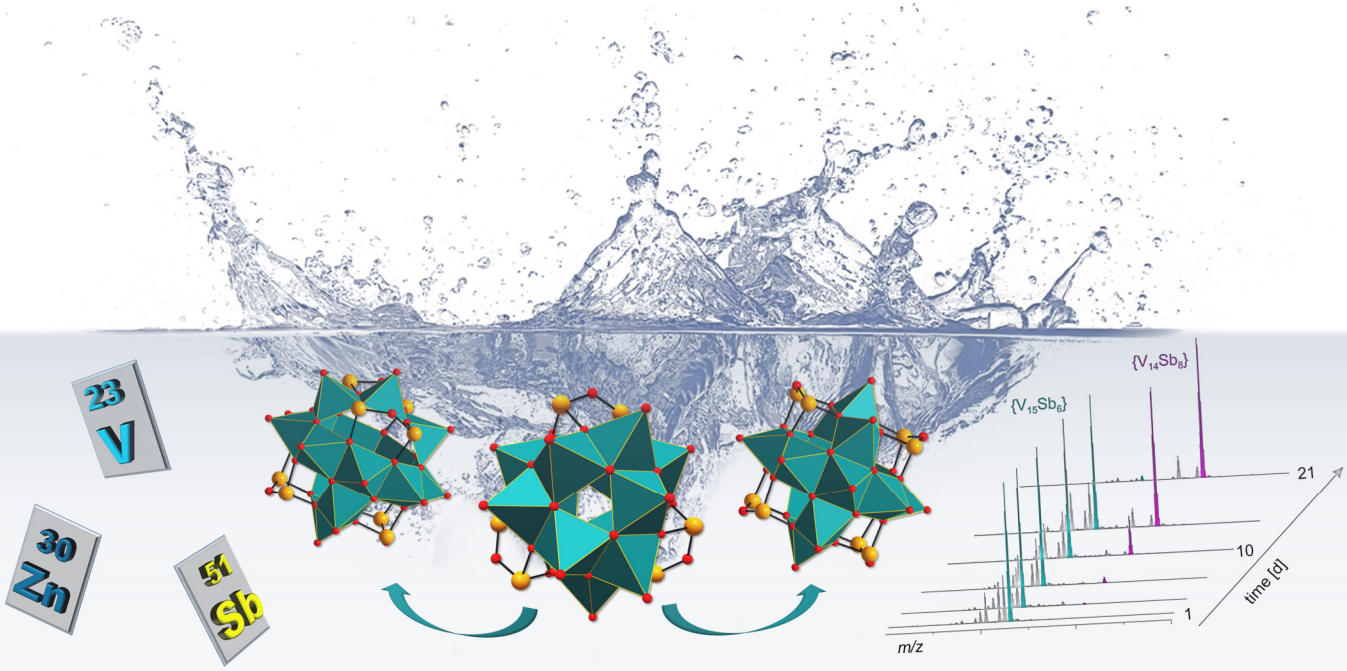

Zur Erlangung des Doktorgrades an der Mathematisch Naturwissenschaftlichen Fakultät der Christian-Albrechts-Universität zu Kiel

Bearbeitet und vorgelegt von

Lisa Katharina Mahnke

Kiel 2019

Chemische Modifizierung von Polyoxovanadaten mit Übergangsmetall-komplexen und deren Charakterisierung

Löslichkeitsstudien, Transformationsreaktionen, Versuche zur rationalen Syntheseplanung sowie Synthese eines neuen Isomers des $\{V_{14}Sb_8O_{42}\}$-Clusters

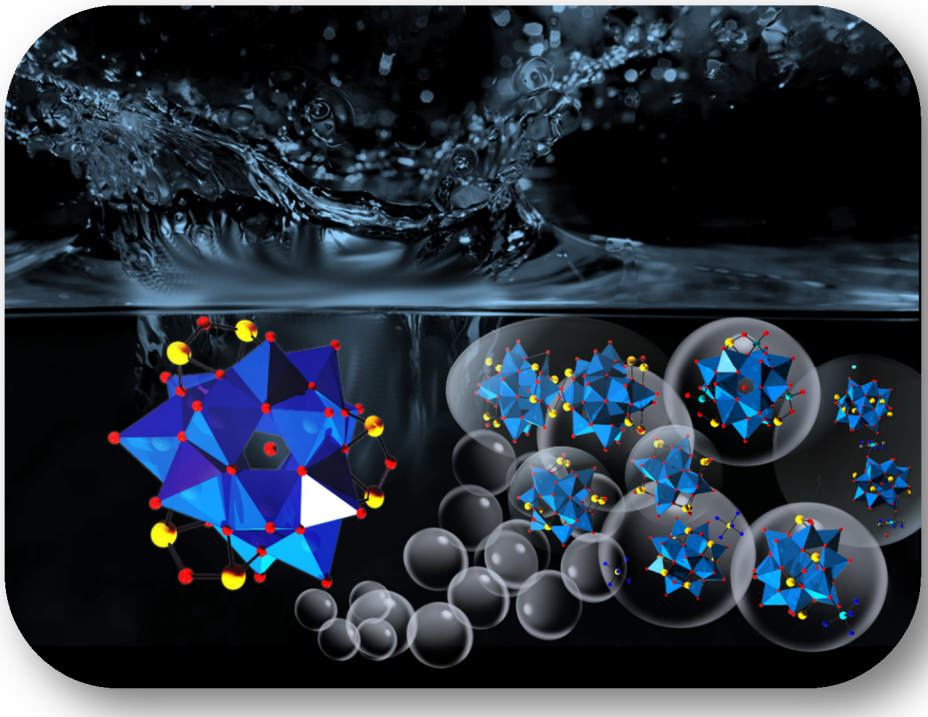

Kumulative Dissertation

Zur Erlangung des Doktorgrades an der Mathematisch Naturwissenschaftlichen Fakultät der Christian-Albrechts-Universität zu Kiel

Bearbeitet und vorgelegt von

Lisa Katharina Mahnke

Kiel, 2019

Für meine Familie

Die vorliegende Dissertation wurde unter Anleitung von

Prof. Dr. Wolfgang Bensch

in der Zeit von

Juni 2016 bis Mai 2019

am Institut für Anorganische Chemie

der Christian-Albrechts-Universität zu Kiel

angefertigt

Referent:	Prof. Dr. Wolfgang Bensch
Koreferent:	Prof. Dr. Norbert Stock
Tag der Prüfung:	24.06.19
Zum Druck genehmigt:	Kiel, 24.06.19

Prof. Dr. Frank Kempken, Dekan der Mathematisch-Naturwissenschaftlichen Fakultät

„Look up at the stars and not down at your feet. Try to make sense of what you see, and wonder about what makes the universe exist. Be curious. And however difficult life may seem, there is always something you can do and succeed at. It matters that you don't just give up."

Steven Hawking

Eidesstattliche Erklärung

Ich erkläre, dass ich meine vorliegende Dissertation mit dem Thema: „Chemische Modifizierung von Polyoxovanadaten mit Übergangsmetallkomplexen und deren Charakterisierung - Löslichkeitsstudien, Transformationsreaktionen, Versuche zur rationalen Syntheseplanung sowie Synthese eines neuen Isomers des $\{V_{14}Sb_8O_{42}\}$-Clusters“ selbstständig und ohne Benutzung anderer als der angegebenen Hilfsmittel angefertigt habe und dass ich alle Stellen, die ich wörtlich oder sinngemäß aus Veröffentlichungen entnommen habe, als solche kenntlich gemacht habe. Die Arbeit hat bisher in gleicher oder ähnlicher Form oder auszugsweise noch keiner Prüfungsbehörde vorgelegen und wurde unter Einhaltung der Regeln guter wissenschaftlicher Praxis der Deutschen Forschungsgemeinschaft angefertigt. Ich bestätige, dass mir kein akademischer Grad entzogen wurde.

Ich versichere, dass die eingereichte schriftliche Fassung der auf dem beigefügten Medium gespeicherten Fassung entspricht.

Kiel, Lisa K. Mahnke

Kurzzusammenfassung

Polyoxovanadate (POVs) stellen eine Untergruppe der Polyoxometallate dar und sind durch eine große Struktur- und Zusammensetzungsvielfalt gekennzeichnet. Durch das erste wasserlösliche antimonsubstituierte Polyoxovanadat, $\{Ni(en)_3\}_3[V_{15}Sb_6O_{42}(H_2O)_x]\cdot\approx 15\ H_2O$ (en = Ethylendiamin) ergab sich eine völlig neue synthetische Chemie für Postfunktionalisierungsreaktionen, welche vorher nicht möglich war.

Die vorliegende Doktorarbeit fokussiert sich auf die Synthese und Charakterisierung neuer Heterometall-Polyoxovanadate (Sb-POVs und Ge/Sb-POVs), welche durch Verwendung der Precursoren $\{Ni(en)_3\}_3[V_{15}Sb_6O_{42}(H_2O)_x]\cdot\approx 15\ H_2O$ (Ni-$\{V_{15}Sb_6\}$) und $\{Zn(en)_3\}_3[V_{15}Sb_6O_{42}(H_2O)]\cdot 3\ en\cdot 10\ H_2O$ (Zn-$\{V_{15}Sb_6\}$) hergestellt werden konnten. Die Vorläuferverbindung Zn-$\{V_{15}Sb_6\}$ wurde im Laufe der Arbeit synthetisiert und charakterisiert und ist im Vergleich zu Ni-$\{V_{15}Sb_6\}$ besser löslich sowie deutlich stabiler in wässriger Lösung. Die umfassende Charakterisierung der gelösten Spezies gelang mit Elektrosprayionisations-Massenspektrometrie (ESI-MS) Untersuchungen in Zusammenarbeit mit ULRIKE WARZOK und CHRISTOPH A. SCHALLEY (FU Berlin). Die Ergebnisse belegen, dass sich beide Precursoren langsam in den $\{V_{14}Sb_8O_{42}\}$-Cluster umwandeln, wobei diese Umwandlung bei Zn-$\{V_{15}Sb_6\}$ sehr viel langsamer verläuft. Die Umwandlung kann beschleunigt werden, wenn der pH-Wert erniedrigt wird. Diese Befunde eröffneten völlig neue Perspektiven für die gezielte Synthese neuer Verbindungen.

Besonders spektakulär sind zwei Verbindungen, die mit Ni-$\{V_{15}Sb_6\}$ hergestellt werden konnten. Die erste Verbindung, $\{Ni(cyclen)(en)\}_2[V_{14}Sb_8O_{42}(H_2O)]\cdot ca\ 10\ H_2O$, enthält ein neues Konfigurationsisomer des $\{V_{14}Sb_8O_{42}\}$-Clusters als herausragendes Strukturmotiv. Während normalerweise die Spitzen der $\{VO_5\}$-Pyramiden der Cluster nach außen weisen, zeigt eine $\{VO_5\}$-Pyramide des neuen Isomers nach innen. Diese Ausrichtung des $\{VO_5\}$-Polyeders wird durch die kurzen Sb-O-Abstände zwischen zwei benachbarten Clustern verursacht, so dass ein Dimer ausgebildet wird und die Koordinationssphäre um das V^{IV}-Zentrum auf 5+1 (verzerrter Oktaeder) erweitert wird. ESI-MS-Untersuchungen beweisen, dass das Dimer auch in Lösung vorhanden ist. Die zweite Verbindung, $\{Ni(en)_3\}_3[V_{15}Sb_3Ge_3O_{42}(OH)_3(H_2O)]\cdot\sim 9\ H_2O$, ist ein seltenes

Beispiel für gemischte Sb/Ge-POVs und konnte bei der Reaktion von Ni-{$V_{15}Sb_6$} mit GeO_2 erhalten werden. In der Struktur sind die Sb- und Ge-Positionen geordnet besetzt, was nur mit einer *in situ* Substitution von SbO_3-Hanteln durch GeO_4-Tetraeder erklärt werden kann.

Durch postsynthetische Funktionalisierung von Zn-{$V_{15}Sb_6$} konnten {$Zn(phen)_3$}$_2$[$Zn(en)_2V_{15}Sb_6O_{42}(H_2O)$]·23 H_2O und {$(Zn(en)_2(H_2O)_2)(Zn(en)_2)$}-[$Zn(en)_2V_{15}Sb_6O_{42}(H_2O)$]·8.5 H_2O synthetisiert und charakterisiert werden. Durch gezieltes Einstellen des pH-Wertes konnten des Weiteren {$Zn(phen)_3$}$_2$[$V_{14}Sb_8O_{42}(H_2O)$]· 0.5 phen·17 H_2O, [{$Zn(en)_2$}$_2V_{14}Sb_8O_{42}$]·7 H_2O und {$Fe(phen)_3$}$_2$[$V_{14}Sb_8O_{42}(H_2O)$]·11 H_2O synthetisiert werden. Bei diesen Synthesen gelang nicht nur die *in situ* Umwandlung des {$V_{15}Sb_6O_{42}$}-Clusters, sondern parallel der Austausch der Übergangsmetallkomplexe.

Abstract

Polyoxovanadates (POVs) are a subgroup of polyoxometallates characterized by a fascinating structural variety and flexible compositions. The discovery of the first water-soluble antimony-substituted polyoxovanadate (Sb-POV), $\{Ni(en)_3\}_3[V_{15}Sb_6O_{42}(H_2O)_x]\cdot \approx 15\ H_2O$ (en = ethylenediamine) resulted in a completely new synthetic chemistry of post-functionalization reactions, which was previously not possible.

The present dissertation focuses on the synthesis and characterization of new hetero-polyoxovanadates (Sb-POVs and Ge/Sb-POVs) by using the precursors $\{Ni(en)_3\}_3[V_{15}Sb_6O_{42}(H_2O)_x]\cdot \approx 15\ H_2O$ (Ni-$\{V_{15}Sb_6\}$) and $\{Zn(en)_3\}_3[V_{15}Sb_6O_{42}(H_2O)]\cdot 3\ en\cdot 10\ H_2O$ (Zn-$\{V_{15}Sb_6\}$). The precursor Zn-$\{V_{15}Sb_6\}$ was synthesized and characterized during this work and the main characteristics are the better solubility compared to Ni-$\{V_{15}Sb_6\}$ and a significantly enhanced stability in aqueous solution. The extensive characterization of the dissolved species was achieved by electrospray ionization mass spectrometry (ESI-MS) in collaboration with ULRIKE WARZOK and CHRISTOPH A. SCHALLEY (FU Berlin). The results demonstrated that both precursors slowly transform into the $\{V_{14}Sb_8O_{42}\}$-cluster, and this process is much slower for Zn-$\{V_{15}Sb_6\}$. The conversion can be accelerated by lowering the pH value. These investigations opened up completely unexpected perspectives for the targeted synthesis of new compounds.

Particularly noteworthy are two compounds that have been synthesized from the Ni-$\{V_{15}Sb_6\}$ compound. The first example, $\{Ni(cyclen)(en)\}_2[V_{14}Sb_8O_{42}(H_2O)]\cdot ca\ 10\ H_2O$, contains a new configurational isomer of the $\{V_{14}Sb_8O_{42}\}$-cluster as prominent structural motif. While normally the vanadyl group of the $\{VO_5\}$ pyramids point outward, one $\{VO_5\}$ pyramid of the new isomer faces inward. This arrangement of the $\{VO_5\}$ polyhedron is caused by the short Sb-O distances between two neighboring clusters, forming a dimer and expanding the coordination sphere around the V^{IV} center to 5 + 1 (distorted octahedron). ESI-MS investigations proved that the dimer is also present in solution. The second compound, $\{Ni(en)_3\}_3[V_{15}Sb_3Ge_3O_{42}(OH)_3(H_2O)]\cdot \sim 9\ H_2O$, is a rare examples of mixed Sb/Ge-POVs and was obtained by a reaction of Ni-$\{V_{15}Sb_6\}$ with GeO_2. Sb and Ge are ordered on distinct crystallographic positions in the structure. This

observation strongly indicates that a partial substitution of SbO_3 with GeO_4 tetrahedral occurred *in situ* during the reaction.

Via postsynthetic functionalization of Zn-$\{V_{15}Sb_6\}$, the new compounds $\{Zn(phen)_3\}_2[Zn(en)_2V_{15}Sb_6O_{42}(H_2O)]\cdot 23\ H_2O$ and $\{(Zn(en)_2(H_2O)_2)(Zn(en)_2)\}$-$[Zn(en)_2V_{15}Sb_6O_{42}(H_2O)]\cdot 8.5\ H_2O$ have been synthesized and characterized. Through the adjustment of the pH value the synthesis of $\{Zn(phen)_3\}_2[V_{14}Sb_8O_{42}(H_2O)]\cdot 0.5$ phen$\cdot 17\ H_2O$, $[\{Zn(en)_2\}_2V_{14}Sb_8O_{42}]\cdot 7\ H_2O$ and $\{Fe(phen)_3\}_2[V_{14}Sb_8O_{42}(H_2O)]\cdot 11\ H_2O$ was possible. Not only the *in situ* transformation of the $\{V_{15}Sb_6O_{42}\}$-clusters was achieved, but also the exchange of entire transition-metal complexes.

Inhaltsverzeichnis

Abkürzungsverzeichnis

Tabelle 1: Übersicht über die verwendeten Abkürzungen und deren Bedeutung.

Abkürzung	Bedeutung
aep	2-Piperazin-N-Ethylamin
bipy	2,2-Bipyridin
BVS	Bond Valence Sum Analyse
CHNS	Elementaranalyse
cyclen	1,4,7,10-Tetraazacyclododecan
d	Tage
dach	1,2-Diaminocyclohexan
dest.	destilliert
DESY	Deutsches Elektronen Synchrotron
dien	Diethylentriamin
DTA	Differenzthermoanalyse
EDX	Energy dispersive X-ray analyses (deutsch: Energie-dispersive-Röntgenspektroskopie)
en	Ethylendiamin
enMe	1,2-Propandiamin
ESI	Elektrosprayionisation
g	Gramm
h	Stunden
IL	Ionic Liquid (Ionische Flüssigkeit)
i.Vak.	Im Vakuum
IR	Infrarot
JMAK	Johnson-Mehl-Avrami-Kolmogorow
ma	Methylamin
mg	Milligramm
mL	Milliliter
mmol	Millimol
MS	Massenspektrometrie
phen	1,10-Phenanthrolin
POM	Polyoxometallate
POMo	Polyoxomolybdate
PONb	Polyoxoniobate
POV	Polyoxovanadate
POW	Polyoxowolframate
ppz	Piperazin
rpm	rounds per minute (deutsch: Umdrehungen pro Minute)
SEM	Scanning Electron Microscopy
SILP	Supported Ionic Liquid Phase
synRAC	**syn**chrotron-based **r**eaction cell for the **a**nalysis of **c**hemical reactions
teta	Triethylentetraamine
TG	Thermogravimetrie
tren	Tris(2-aminoethyl)amin
XRD	Röntgenpulverdiffraktometrie

1. Motivation und theoretischer Hintergrund

Die Synthese neuartiger Polyoxometallate ist eine Herausforderung in der synthetischen Chemie. Für Polyoxometallat-Chemiker eröffnen sich vielversprechende Anwendungsgebiete wie die (Photo[1]-) Katalyse[2] oder neuartige Batteriematerialen[3] [4] [5] mit überraschend hohen spezifischen Kapazitäten sowie die photokatalytische Reinigung von Trinkwasser[6] [7].

Im Folgenden werden die herausfordernden synthetischen Aspekte und Versuche zur Vereinfachung der Synthesen vorgestellt.

1.1. Polyoxometallate

Seit der Entdeckung des ersten Polyoxometallates (POM) durch BERZELIUS 1826[8] und der kristallografischen Aufklärung der Struktur durch KEGGIN über hundert Jahre später im Jahre 1933[9] ist das Interesse an Polyoxometallaten stetig gewachsen. Durch immer leistungsfähigere Charakterisierungsmethoden und die erheblichen Weiterentwicklungen synthetischer Methoden sind POMs heute mit einer außerordentlichen Zusammensetzungs- und Strukturvielfalt bekannt.

Polyoxometallate sind Metall-Sauerstoff-Verbindungen der Elemente Vanadium, Niob, Tantal, Molybdän und Wolfram, die häufig hohlraumartige Strukturen ausbilden. Die Metall-Sauerstoff-Polyeder ($\{MO_x\}$-Polyeder, x = 4-7, Abb. 1) weisen in wässrigen Lösungen eine ausgeprägte Tendenz zur Selbstorganisation auf. Neben den POMs der frühen Übergangsmetalle gibt es auch Beispiele für Edelmetall-POMs[10] [11] [12] [13], welche jedoch nicht Gegenstand der vorliegenden Arbeit sind.

Die frühen Übergangsmetalle liegen in den POMs oft in ihren höchsten Oxidationsstufen vor und die freien *d*-Orbitale (d^0–/ d^1– Elektronenkonfiguration) stehen für starke pπ-dπ-Bindungen mit Sauerstoff zur Verfügung. Daraus resultiert eine kurze terminale Metall-Sauerstoff-Bindung und durch den sogenannten *trans*-Effekt werden die Metallzentren in Richtung der terminalen Metall-Sauerstoff-Bindung verschoben, so dass eine Schwächung der *trans*-ständigen Bindung bedingt wird. Diese Metall-Sauerstoff-

Bindung kann daher leichter in den ablaufenden Kondensationsreaktionen durch Bindungsbruch agieren.[14]

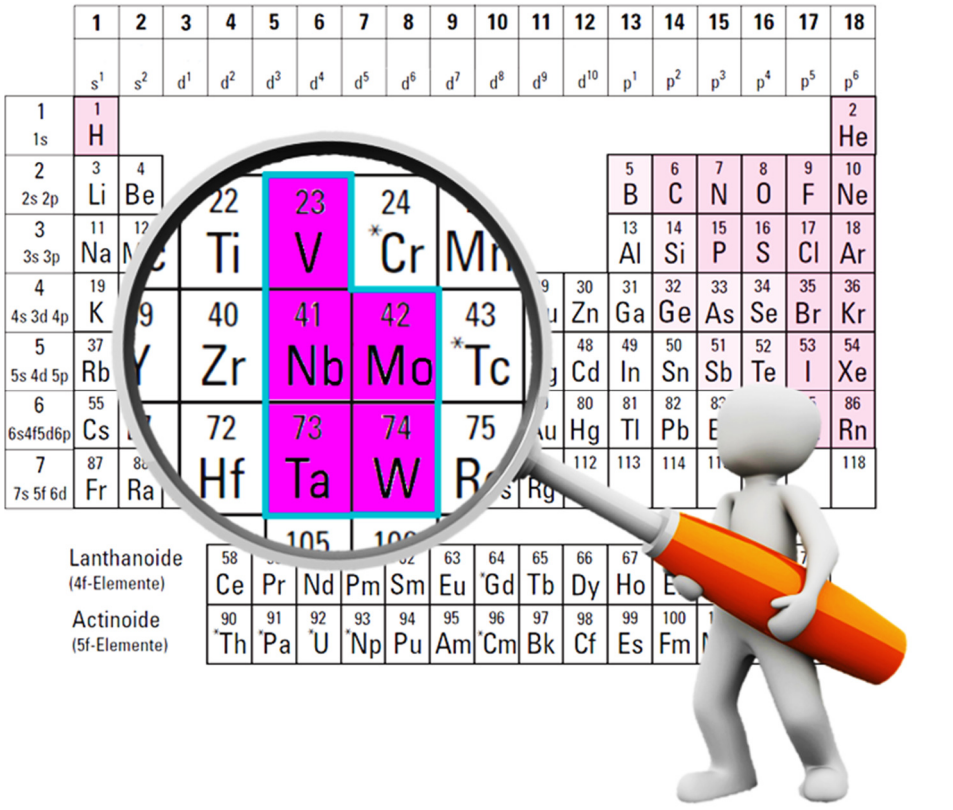

Abbildung 1: Elemente, die zur Bildung von Polyoxometallaten neigen sind in pink hervorgehoben. Vanadium, Niob, Tantal, Molybdän und Wolfram sind dabei die Übergangsmetalle, die neben Edelmetallen wie z. B. Palladium und Gold besonders viele POMs bilden.[15]

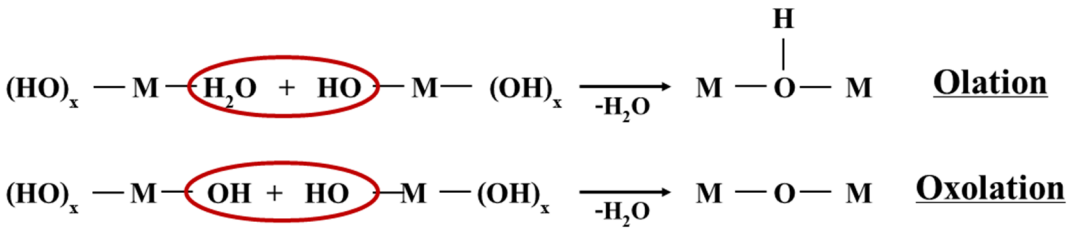

Abbildung 2: Schematischer Ablauf der zwei Kondensationsreaktionen, der Olation (oben), bei welcher eine koordinierte Wassergruppe und eine Hydroxidgruppe der Übergangsmetalle zu einer verbrückenden Hydroxidgruppe unter Wasserabspaltung reagieren, sowie die Oxolation (unten), bei welcher zwei Hydroxidgruppen unter Wasserabspaltung zu einer verbrückenden Oxogruppe reagieren.

Die Kondensationsreaktionen können in Oxolation und Olation unterschieden werden (Abb. 2). Die Oxolation läuft meist unter Wasserabspaltung zwischen zwei Metallzentren mit koordinierten Hydroxid-Gruppen ab. Dabei wird eine Metall-Sauerstoff-Metall-Bindung, ein μ-O-verbrückendes Sauerstoffatom, gebildet. Aufgrund der stärker gebundenen Hydroxid-Gruppen ist diese Reaktion kinetisch gehemmter als die Olation.[16] Bei der Olation liegt an einem Metallzentrum mindestens ein koordinierter Wasserligand vor, welcher mit einer Hydroxid-Gruppe eines weiteren Metallzentrums ebenfalls unter Wasserabspaltung reagieren kann. Die Olation ist aufgrund der labilen Wasserliganden normalerweise sehr viel schneller als die Oxolation.[16] Die Metall-Hydroxid-Metall Verknüpfung kann im nächsten Schritt an einer weiteren Kondensationsreaktion beteiligt sein und so ein μ_3-verbrückendes Sauerstoffatom ausbilden (Abb. 3). Die Kondensationsreaktionen laufen selbstorganisiert in wässrigen Lösungen ab.[17]

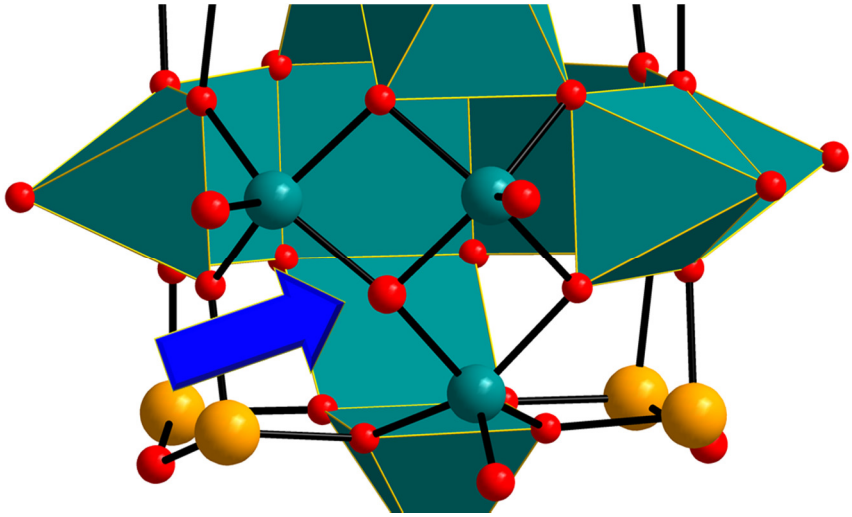

Abbildung 3: Der blaue Pfeil hebt das μ_3-verbrückende Sauerstoffatom hervor, welches bei der Oxolation nach bereits erfolgter Olation gebildet werden kann.

Eine weitere wichtige Eigenschaft für die Ausbildung von POMs der Kationen der Elemente der fünften und sechsten Gruppe ist das passende Ladungs-zu-Radius Verhältnis, wobei Chrom differenziert betrachtet werden muss. Chrom bevorzugt in der höchsten Oxidationsstufe die tetraedrische Koordination, welche eine höhere, sphärische Kondensation nicht begünstigt. In den Oxidationsstufen +5 und +6 liegt zudem ein ungünstiges Ladungs-zu-Radius Verhältnis für die selbstorganisierte Bildung von POMs vor.

Die Kondensation zu größeren sphärischen Anionen wird bei Polyoxowolframaten (POW) und Polyoxomolybdaten (POMo) häufig im sauren pH-Wert Bereich erreicht, während die POMs der fünften Gruppe meist unter basischen Bedingungen gebildet werden.

Die Gruppe der Polyoxometallate kann weiterhin in verschiedene Untergruppen unterteilt werden.

a) Isopolyoxometallate sind Metall-Oxid-Cluster, welche aus einem Übergangsmetall bestehen ohne weitere Heteroatom-Elemente. Iso-POMs sind aufgrund der hohen negativen Ladung meist weniger stabil als ihre Heteroatom-Geschwister. Eines der bekanntesten und am besten erforschten Vanadium-basierten Isopolyoxometallate ist das Decavanadation $[V_{10}O_{28}]^{6-}$, welches 1956 erstmals von ROSSOTTI und ROSSOTTI[18] entdeckt wurde und aus $\{VO_6\}$-Oktaedern gebildet wird (Abb. 4a). Die Decavanadate sind in einem weiten pH-Wert Bereich stabil.
b) Heteropolyoxometallate sind stabilere Polyoxoanionen, welche mindestens ein Übergangsmetall sowie Heteroatome wie Phosphor, Schwefel, Silizium, Germanium, Arsen oder Antimon enthalten. Die Heteropolyoxometallate sind aufgrund ihrer interessanten katalytischen, elektronischen und magnetischen Eigenschaften die am besten untersuchte Klasse der Polyoxoanionen. Das erste vollständig charakterisierte Heteropolyoxometallat ist das KEGGIN Anion $[XM_{12}O_{40}]^{n-}$ mit M = Mo, W und X = z. B. PO_4^{3-},SiO_4^{2-} und SO_4^{2-}, welches 1826 von BERZELIUS[8] entdeckt aber erst über hundert Jahre später 1933 von KEGGIN[9] [19] [20] vollständig charakterisiert wurde (Abb. 4b).
c) Die letzte Kategorie bilden die sogenannten „Riesen-Cluster“. Vor allem die Molybdänblau und –braun-Cluster, welche 1995 bzw. 1998 von MÜLLER *et al.* synthetisiert und charakterisiert wurden, gehören zu dieser Kategorie. Die Ring-Topologie von Molybdänblau besteht aus insgesamt 154 Molybdänatomen, der sphärische Molybdänbraun-Cluster setzt sich aus 132 Molybdänzentren zusammen. Die Abmessungen der Cluster liegen im Nanometerbereich (Abb. 4c).[21] [22] [23]

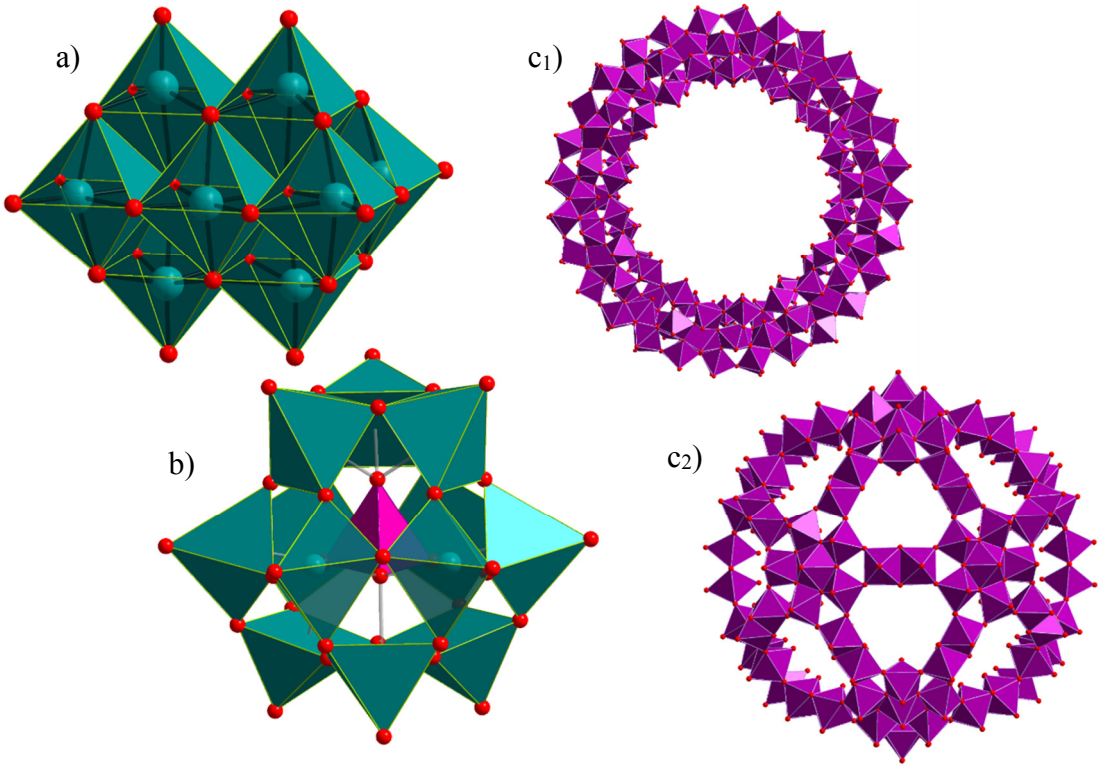

Abbildung 4: Polyederdarstellungen der Strukturen der Untergruppen der Polyoxometallate, a) Das Isopolyoxometallat $[V_{10}O_{28}]^{6-}$ (Decavanadatanion); b) Das Keggin-Anion $[XM_{12}O_{40}]^{n-}$ mit M= Mo, W und X= z. B. PO_4^{3-},SiO_4^{2-} und SO_4^{2-}, ein Heteropolyoxometallat; c_1) Molybdänblau-Cluster; c_2) Molybdänbraun-Cluster.

1.2. Synthetische Herausforderungen

Polyoxometallate werden meistens solvothermal bzw. hydrothermal hergestellt. Die Solvothermalsynthese wird oft als „weiche Chemie“ (auch: „soft chemistry“ oder „chimie douce“) bezeichnet, da unter diesen Bedingungen molekulare Baueinheiten und schwache Wechselwirkungen wie Wasserstoffbrücken, van-der-Waals-, hydrophile-hydrophobe Wechselwirkungen, etc. erhalten bleiben.[17] Allerdings wird die Solvothermalsynthese auch als „Black Box“ betitelt, da bei den meisten Reaktionen eventuell auftretende Intermediate und die ablaufenden Reaktionsmechanismen nicht bekannt sind. Zusätzlich hängen die verschiedenen Reaktionsparameter wie Temperatur, autogener Druck, Viskosität, pH-Wert, Redoxpotential etc. in komplizierter und wenig verstandener Weise voneinander ab. Um Licht in das Dunkel zu bringen, wurden solvothermale Reaktionen unter *in situ* Bedingungen mit z. B. Synchrotron Strahlung untersucht, um den Einfluss

verschiedener Reaktionsparameter auf die Produktbildung zu verstehen (mehr dazu im Abschnitt 1.5 Zeitaufgelöste *in situ* Röntgenpulverdiffraktometrie und 2.1 Methoden). Aber auch andere *in situ* Verfolgungsmethoden zeigen großes Potential wie der Review-Artikel von WOLFGANG BENSCH und NICOLE PIENACK eindrucksvoll belegt.[24]

Für die Herstellung von Polyoxometallaten stehen verschiedene „Precursoren“ oder sog. Vorläuferverbindungen zur Verfügung, welche die Synthese und Modifizierung von POMs vereinfachen. Über solche Vorläuferverbindungen sind z. B. lakunare Strukturen zugänglich, die eine aktive Metallbindungsstelle aufweisen, welche eine Vielzahl neuer Anwendungsmöglichkeiten eröffnet. Die Arbeiten von SVEN HERRMANN und der Arbeitsgruppe um CARSTEN STREB befassen sich mit lakunaren Polyoxometallaten, welche mit ionischen Flüssigkeiten sowohl als selbstreparierender Korrosionsschutz[6] als auch in Bezug auf die Wasseraufbereitung untersucht wurden. Das Polyoxowolframat $[\alpha\text{-}SiW_{11}O_{39}]^{8-}$ weist für die Anwendung in der Wasseraufbereitung eine freie Metallbindungsstelle auf und kann daher Kationen der Elemente Blei, Nickel, Kupfer, Chrom, Kobalt und Uran aus dem Wasser entfernen, aber auch für *E.coli* Bakterien konnten selektive Adsorptionseigenschaften beobachtet werden (Abb. 5). Wird $[\alpha\text{-}SiW_{11}O_{39}]^{8-}$ auf Silicat als Trägermaterial aufgebracht, wird ein leicht schüttbares, einfach zu handhabendes Material erhalten. Bei der Herstellung der lakunaren Keggin-Ionen fungiert ein lösliches Keggin-Ion als Precursor, welches durch Erhöhung des pH-Wertes eine oder zwei vakante Positionen freigibt, die z. B. durch Übergangsmetalle besetzt werden können und so die Eigenschaften des Polyoxowolframates verändert werden aber die vakanten Positionen können auch durch ionische Flüssigkeiten stabilisiert und als unbesetzte Kontaktstellen genutzt werden.[7]

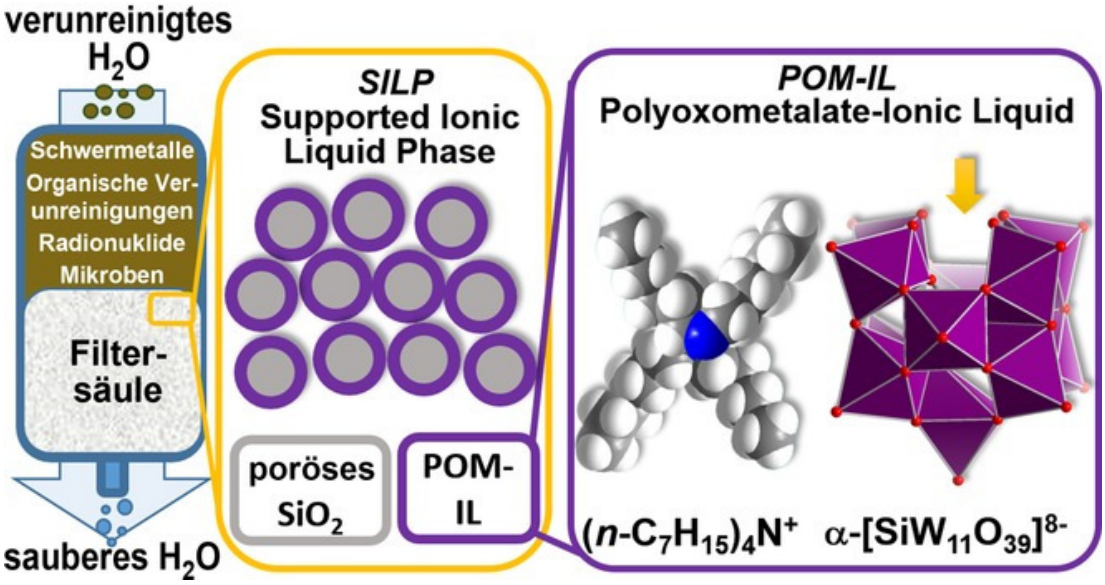

Abbildung 5: Schematische Darstellung der Wasseraufbereitung mit lipophilen POM-basierten ionischen Flüssigkeiten immobilisiert auf porösem SiO_2 (POM-SILPs). POM-SILP-Filter entfernen Schwermetallkationen (wie: Ni^{2+}, Pb^{2+}, UO_2^{2+}), aromatische Verunreinigungen (Trityl-Farbstoffe) oder *E. coli* Bakterien durch die Verwendung antimikrobieller Tetraalkylammonium-Kationen und lakunarer POW-Anionen mit spezifischen Metallbindungsstellen (oranger Pfeil). Reprinted with permission from STREB *et al.*, *Angew. Chem.* (© 2017 Wiley-VCH Verlag GmbH & Co. KGaA, Weinheim).[7]

Innerhalb der Klasse der Polyoxovanadate ist die Anzahl geeigneter Precursoren stark limitiert. Das Decavanadatanion scheint ein prädestinierter Kandidat zu sein, jedoch ist dieses ein relativ stabiles Anion und in einem weiten pH-Wert Bereich das thermodynamisch begünstigte Produkt und daher eher ungeeignet als Vorläuferverbindung.[18]

Typischerweise werden Polyoxovanadate unter Verwendung niedernuklearer Edukte solvothermal hergestellt, wobei die Reaktionszeiten zwischen fünf Tagen und zwei Wochen betragen. Neue Produkte können meistens nur durch Variation der stöchiometrischen Verhältnisse der Edukte erhalten werden denn bei pH-Werten von ca. 12 ist die Zahl geeigneter Ausgangsverbindungen limitiert. Um diese Nachteile zu reduzieren sind geeignete Precursoren notwendig, welche neue Strukturmotive generieren können und kürzere und weniger harsche Synthesebedingungen erlauben.

1.3. Polyoxovanadate

Die Polyoxovanadate (POVs) heben sich in der Gruppe der Polyoxometallate besonders durch die Koordinationsvielfalt ab, was zu unterschiedlichen Strukturmotiven führt. Die Bildung von POVs ist zudem stark vom pH-Wert abhängig: bei pH > 6 beträgt die bevorzugte Koordinationszahl von Vanadium sechs und es wird das Decavanadat gebildet, welches als starke Säure agiert und für weitere Kondensationsreaktionen nicht zur Verfügung steht (Abb. 6).[17] Für die Synthese von clusterartigen POVs muss daher im basischen Bereich gearbeitet werden, während POMos und POWs eher im sauren Medium gebildet werden.

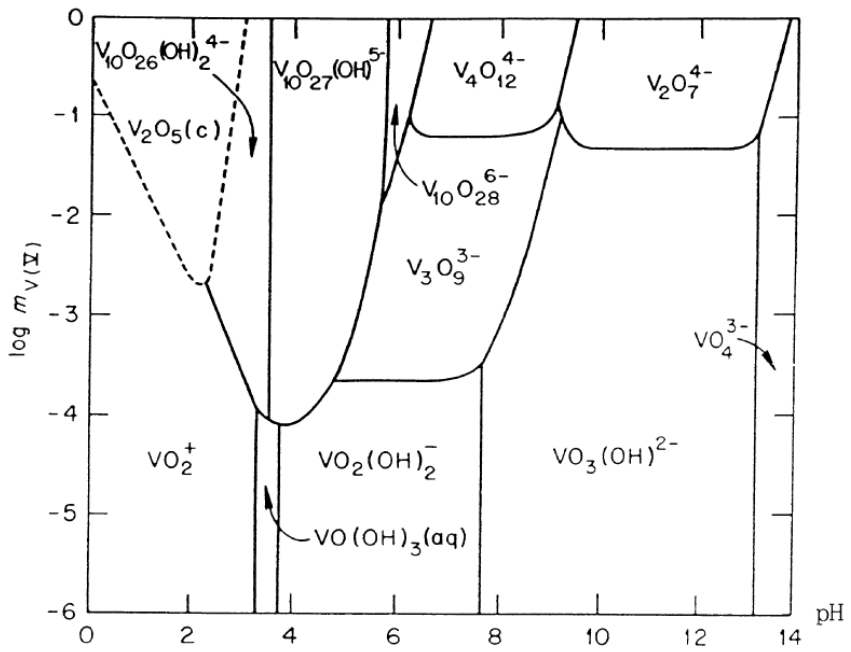

Abbildung 6: Vorliegende Vanadat-Spezies in wässriger Lösung in Abhängigkeit von Konzentration und dem pH-Wert. Reprinted from *Synthesis of Polyoxovanadates from Aqueous Solutions* by LIVAGE (2001) with permission from Elsevier. (© 2001 Elsevier)[17]

Eine weitere Besonderheit der Polyoxovanadate ist, dass die V-Zentren in unterschiedlichen Oxidationsstufen vorliegen können (gemischt-valente Cluster). Daher werden die POVs in vier Gruppen eingeteilt: vollständig oxidierte POVs welche ausschließlich V^V enthalten; gemischt-valente POVs mit V^V/V^{IV} in nahezu jedem Verhältnis; vollständig reduzierte POVs, welche ausschließlich V^{IV} enthalten und höchst reduzierte POVs mit ausschließlich V^{III}.[25]

Die Integration von Heteroatomen in POV-Cluster ist ein aktuelles Forschungsthema, da dadurch die oft große negative Ladung reduziert wird und die Stabilität gleichzeitig verbessert wird. Die Strukturen der Hetero-POVs können von dem sogenannten vollständig reduzierten „Archetypen“ $[V^{IV}_{18}O_{42}]^{12-}$, welcher 1978 von JOHNSON und SCHLEMPER[26] entdeckt wurde, abgeleitet werden. Die Struktur besteht aus 18 ecken- und kantenverknüpften $\{VO_5\}$-Pyramiden und der Cluster weist eine ideale T_d-oder D_{4d}-Symmetrie auf. Durch die formale Substitution von zwei, drei oder vier $\{VO_5\}$-Pyramiden durch zwei, drei oder vier $\{E_2O_x\}$ Gruppen (weniger häufig $\{E_2O_xS_2\}$; mit E = Si, Ge, As, Sb und x = 5 oder 7) ergeben sich unterschiedliche Polyoxovanadat-Cluster: $\{V_{14}E_8O_{42+a}\}$, $\{V_{15}E_6O_{42+b}\}$ und $\{V_{16}E_4O_{42+c}\}$. Für die Antimonato-Polyoxovanadate ergeben sich folgende Anionen: $[V_{16}Sb_4O_{42}]^{8-}$, $[V_{15}Sb_6O_{42}]^{6-}$ und $[V_{14}Sb_8O_{42}]^{4-}$. Eine Übersicht der bereits publizierten Antimonato-Polyoxovanadate findet sich in Tabelle 2.

Tabelle 2 Übersicht der Antimonato-Polyoxovanadate.

Sb-POV – Typ	**Verbindung**	**Lit**
***α* - $V_{14}Sb_8$**	$(enH_2)_2\{V_{14}Sb_8O_{42}(H_2O)\}](en) \cdot 4\ H_2O$ en = Ethylendiamin	[27]
***α* - $V_{14}Sb_8$**	$\{Ni(phen)_3\}_2[V_{14}Sb_8O_{42}] \cdot phen \cdot 12\ H_2O$ phen = 1,10-Phenanthrolin	[28]
***α* - $V_{14}Sb_8$**	$\{Co(enMe)_3\}_2[V_{14}Sb_8O_{42}(H_2O)]$ enMe = 1,2-Propandiamin	[29]
***α* - $V_{14}Sb_8$**	$[\{Zn(en)_2\}_2V_{14}Sb_8O_{42}] \cdot 7\ H_2O$	[30]
***β* - $V_{14}Sb_8$**	$[H_4V_{14}Sb_8O_{42}(H_2O)] \cdot 5\ H_2O$	[29]
***β* - $V_{14}Sb_8$**	$(NH_4)_4[V_{14}Sb_8O_{42}] \cdot 2\ H_2O$	[31]
***β* - $V_{14}Sb_8$**	$(enH_2)_2[V_{14}Sb_8O_{42}(H_2O)] \cdot 3\ H_2O$	[32]
***β* - $V_{14}Sb_8$**	$(ppzH_2)_2[V_{14}Sb_8O_{42}(H_2O)]$ ppz = Piperazin	[32]
***β* - $V_{14}Sb_8$**	$\{Zn_2(dien)_2\}_2[\{Zn(dien)\}_2V_{14}Sb_8O_{42}(H_2O] \cdot 4\ H_2O$ dien = Diethylentriamin	[33]

β - $V_{14}Sb_8$	$[V_{14}Sb_8(aepH)_4O_{42}(H_2O)] \cdot 4\ H_2O$ aep = 2-Piperazin-N-Ethylamin	[34]
β - $V_{14}Sb_8$	$[\{Ni(en)_2\}_2V_{14}Sb_8O_{42}] \cdot 5.5\ H_2O$	[35]
β - $V_{14}Sb_8$	$[\{Co(en)_2\}_2V_{14}Sb_8O_{42}(H_2O)] \cdot 6\ H_2O$	[36]
β - $V_{14}Sb_8$	$\{Zn(phen)_3\}_2[V_{14}Sb_8O_{42}(H_2O)] \cdot 0.5\ phen \cdot 17\ H_2O$	[30]
β - $V_{14}Sb_8$	$\{Fe(phen)_3\}_2[V_{14}Sb_8O_{42}(H_2O)] \cdot 11\ H_2O$	[30]
α* - $V_{14}Sb_8$	$\{Ni(cyclen)(en)\}_2[V_{14}Sb_8O_{42}(H_2O)] \cdot ca.10\ H_2O$ cyclen = 1,4,7,10-Tetraazacyclododecan	[37] [38]
α/ β - $V_{14}Sb_8$	$\{Co(phen)_{2.4}(2,2'\text{-bipy})_{0.6}\}_4[\alpha\text{-}V_{14}Sb_8O_{42}(H_2O)][\beta\text{-}V_{14}Sb_8O_{42}(H_2O)] \cdot 10.5\ H_2O$ bipy = Bipyridin	[39]
α - $V_{14}Sb_5Ge_3$	$\{Ni(phen)_3\}_2[V_{14}Sb_5Ge_3O_{42}(OH)_3(H_2O)] \cdot \approx 16\ H_2O$	[40]
$V_{15}Sb_6$	$\{Cd(en)_3\}_3[V_{15}Sb_6O_{42}(H_2O)] \cdot 8\ H_2O$	[29]
$V_{15}Sb_6$	$\{Ni(en)_3\}_2[H_2V_{15}Sb_6O_{42}(H_2O)] \cdot 5\ H_2O$	[29]
$V_{15}Sb_6$	$\{Co(en)_3\}_2[H_2V_{15}Sb_6O_{42}(H_2O)] \cdot 5\ H_2O$	[29]
$V_{15}Sb_6$	$(aepH_2)_2[V_{15}Sb_6(aepH)_2O_{42}(H_2O)] \cdot 2.5\ H_2O$	[34]
$V_{15}Sb_6$	$(trenH_3)_2[V_{15}Sb_6O_{42}] \cdot 0.33\ tren \cdot n\ H_2O$ tren = Tris(2-aminoethyl)amin	[41]
$V_{15}Sb_6$	$\{Ni(dien)_2\}_3[V_{15}Sb_6O_{42}(H_2O)] \cdot 12\ H_2O$	[42]
$V_{15}Sb_6$	$\{Ni(dien)_2\}_3[V_{15}Sb_6O_{42}(H_2O)] \cdot 8\ H_2O$	[42]
$V_{15}Sb_6$	$\{Co(tren)(H_2O)\}_3[V_{15}Sb_6O_{42}(H_2O)] \cdot H_2O$	[43]
$V_{15}Sb_6$	$\{Co_2(tren)_3\}_2\{Co(tren)(en)\}[\{V_{15}Sb_6O_{42}(H_2O)(Co(tren)_2)\}\text{-}V_{15}Sb_6O_{42}(H_2O)] \cdot n\ H_2O$	[43]
$V_{15}Sb_6$	$\{[Fe(dach)_2]_3[V_{15}Sb_6O_{42}(H_2O)]\} \cdot 8\ H_2O$ dach = 1,2-Diaminocyclohexan	[44]
$V_{15}Sb_6$	$\{Co(N_3C_5H_{15})_2\}_2[\{Co(N_3C_5H_{15})_2\}V_{15}Sb_6O_{42}(H_2O)] \cdot 5\ H_2O$ $N_3C_5H_{15}$ = N-(2-aminoethyl)-1,3-propandiamin	[45]
$V_{15}Sb_6$	$\{Ni(N_3C_5H_{15})_2\}_2[\{Ni(N_3C_5H_{15})_2\}V_{15}Sb_6O_{42}(H_2O)] \cdot 8\ H_2O$ $N_3C_5H_{15}$ = N-(2-aminoethyl)-1,3-propandiamin	[45]

$V_{15}Sb_6$	$\{Ni(en)_3\}_3[V_{15}Sb_6O_{42}(H_2O)_x] \cdot n\ H_2O$ (n » 15)	[46]
$V_{15}Sb_6$	$\{Co(en)_3\}_3[V_{15}Sb_6O_{42}(H_2O)_x] \cdot n\ H_2O$ (n » 15)	[46]
$V_{15}Sb_6$	$\{Fe(en)_3\}_3[V_{15}Sb_6O_{42}(H_2O)_x] \cdot n\ H_2O$ (n » 15)	[46]
$V_{15}Sb_6$	$\{Ni(en)_3\}_3[V_{15}Sb_6O_{42}(H_2O)_x] \cdot n\ H_2O$ (n » 28)	[46]
$V_{15}Sb_6$	$\{Ni(trenH)_2\}[Ni_2(tren)_3(V_{15}Sb_6O_{42}(H_2O)_{0.5}] \cdot 2\ H_2O$	[47]
$V_{15}Sb_6$	$\{Ni(phen)_3\}_2[\{Ni(en)_2\}V_{15}Sb_6O_{42}(H_2O)] \cdot 19\ H_2O$	[48]
$V_{15}Sb_6$	$[\{Co(teta)_2\}\{Co_2(tren)(teta)_2\}V_{15}Sb_6O_{42}(H_2O)] \cdot$ *ca.* $9\ H_2O$ teta = Triethylentetraamin	[49]
$V_{15}Sb_6$	$\{Zn(en)_3\}_3\ [V_{15}Sb_6O_{42}(H_2O)] \cdot 3$ en $\cdot 10\ H_2O$	[50]
$V_{15}Sb_6$	$\{(Zn(en)_2(H_2O)_2)(Zn(en)_2)\}[\{Zn(en)_2\}V_{15}Sb_6O_{42}(H_2O)] \cdot$ $8.5\ H_2O$	[50]
$V_{15}Sb_6$	$\{Zn(phen)_3\}_2[Zn(en)_2V_{15}Sb_6O_{42}(H_2O)] \cdot 23\ H_2O$	[50]
$V_{15}Sb_6$	$\{Ni(dien)_2\}_2[(aepH)_2V_{15}Sb_6O_{42}(H_2O)] \cdot 7.5\ H_2O$	[51]
$V_{15}Sb_2Ge_4$	$\{Ni(en)_3\}_3[V_{15}Sb_2Ge_4O_{42}(OH)_4(H_2O)] \cdot en \cdot \approx 10\ H_2O$	[52]
$V_{15}Sb_3Ge_3$	$\{Ni(en)_3\}_3[V_{15}Sb_3Ge_3O_{42}(OH)_3(H_2O)] \cdot \approx 9\ H_2O$	[52]
$V_{15}Sb_3Ge_3$	$\{Ni(en)_3\}_3[V_{15}Sb_3Ge_3O_{42}(OH)_3(H_2O)] \cdot \approx 15\ H_2O$	[52]
α - $V_{16}Sb_4$	$\{aepH_2\}_4[V_{16}Sb_4O_{42}] \cdot 2\ H_2O$	[31]
α - $V_{16}Sb_4$	$[V_{16}Sb_4O_{42}(H_2O)\{VO(dach)_2\}_4]$	[53]
α - $V_{16}Sb_4$	$\{Ni(dien)_2\}_4[V_{16}Sb_4O_{42}(H_2O)]$	[54]
α - $V_{16}Sb_4$	$\{Zn_2(dien)_3\}[\{Zn(dien)\}_2V_{16}Sb_4O_{42}(H_2O] \cdot 4\ H_2O$	[33]
α - $V_{16}Sb_4$	$\{[Mn(teta)]_4V_{16}Sb_4O_{42}\}_n \cdot [(H_2O)_{12}]_n$	[55]
β - $V_{16}Sb_4$	$\{Co(tren)(trenH_2)\}_2[V_{16}Sb_4O_{42}(H_2O)] \cdot 6\ H_2O$	[43]
β - $V_{16}Sb_4$	$\{(trenH_2)Zn(tren)\}_2[V_{16}Sb_4O_{42}(H_2O)] \cdot n\ H_2O$	[43]

Die Integration von As(III) und Sb(III), führt im Vergleich zu Si(IV) oder Ge(IV) zu unterschiedlichen Reaktivitäten und lokalen strukturellen Umgebungen, da die beiden ersteren Beispiele ein freies Elektronenpaar aufweisen.[25] [34] [43] [49]

Mit DFT-Berechnungen und der Elektronlokalisationsfunktion (ELF) konnte z. B. der kurze Sb-N-Abstand (Sb (4) – N (51) = 2.559 Å) in der Verbindung [{$Co^{II}(teta)_2$}-{$Co^{II}_2(tren)(teta)_2$}$V^{IV}_{15}Sb^{III}_6O_{42}(H_2O)$]·*ca.*9 H_2O (teta = triethylentetraamin) als kovalente Bindung identifiziert werden, welche einer Sb-O Bindung sehr ähnlich ist (Abb. 7).[49]

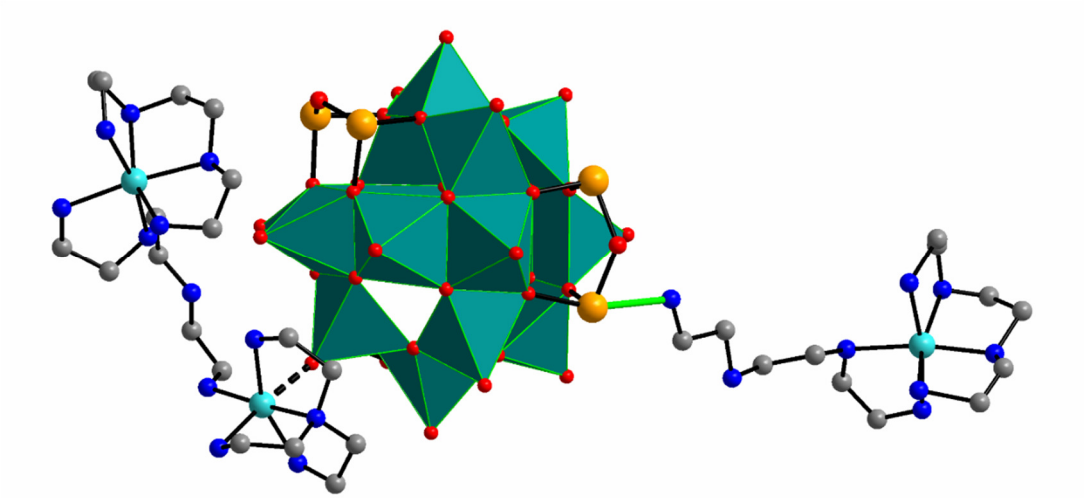

Abbildung 7: Der kurze Sb-N-Abstand (grüne Linie) in der Struktur der Verbindung [{$Co^{II}(teta)_2$}{$Co^{II}_2(tren)(teta)_2$}$V^{IV}_{15}Sb^{III}_6O_{42}(H_2O)$]·*ca.*9 H_2O.[49]

Der Einbau von Heteroatomen beeinflusst die Eigenschaften und das Verhalten von POVs enorm. Dies wird besonders beim magnetischen Verhalten von {$V_{15}E_6$}-Clustern deutlich. Das spezielle magnetische Verhalten wurde von MÜLLER *et al.* erstmalig für $K_6[V^{IV}_{15}As_6O_{42}(H_2O)]$·8 H_2O beobachtet und ist immer noch ein Thema von aktuellem Interesse. Der {$V_{15}E_6$}-Cluster zeigt neben starken antiferromagnetischen Austauschwechselwirkungen zwischen den V^{IV}-Zentren auch Spinfrustration, welche bei tiefen Temperaturen auftritt. Die Struktur des {$V_{15}E_6$}-Clusters kann formal in zwei Sechsringe aus V^{4+}-Ionen unterteilt werden, in welchen die Spins antiferromagnetisch koppeln. Diese Sechsringe sind durch drei weitere V^{4+}-Ionen verbunden, die formal ein Dreieck aufspannen (Abb. 9, rechts). Die ungerade Anzahl an V^{IV} führt dazu, dass ein Spin-frustriertes System vorliegt.

1.3.1. Isomere antimonsubstituierter POVs

Bei Clusteranionen der Zusammensetzungen $[V_{16}Sb_4O_{42}]^{8-}$, $[V_{15}Sb_6O_{42}]^{6-}$ und $[V_{14}Sb_8O_{42}]^{4-}$ können Isomere unterschieden werden: einige konnten experimentell verifiziert werden, andere sind bislang lediglich mittels DFT-Kalkulationen vorhergesagt.

Die Struktur des $\{V_{16}Sb_4O_{42}\}$-Clusters wird aus 16 $\{VO_5\}$-Pyramiden gebildet, welche über Kanten miteinander verknüpft sind. In dem α-Isomer bilden acht $\{VO_5\}$-Pyramiden über Kantenverknüpfung je einen Achterring, die sich an zwei Positionen schneiden (Abb. 8, links unten), was zur D_{2h}-Symmetrie führt. Die Struktur des β-Isomers besteht ebenfalls aus einem achtgliedrigen Ring aus $\{VO_5\}$-Pyramiden, wobei um 40-45° zueinander verdrehte $\{VO_5\}$-Triaden ober- und unterhalb des Achterrings lokalisiert sind (Abb. 8, rechts unten). Daher weist das β- Isomer die niedrigere C_2-Symmetrie auf.

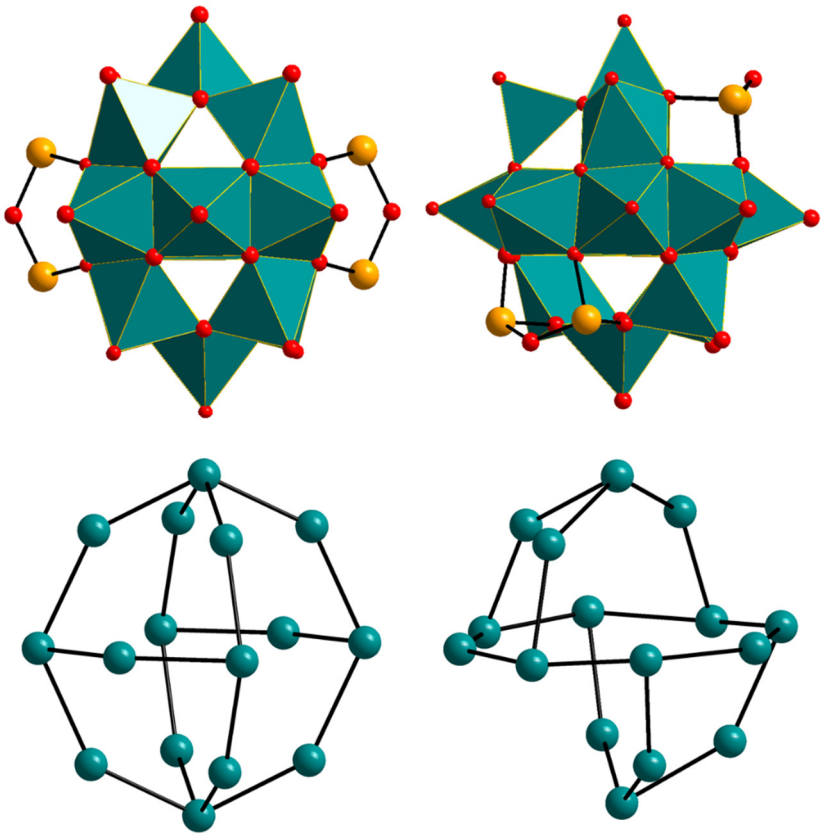

Abbildung 8: Die Strukturen der zwei Isomere des $\{V_{16}Sb_4O_{42}\}$-Clusters: oben in Polyederdarstellung, unten das Vanadium-Gerüst. Das α-Isomer mit D_{2h}-Symmetrie ist links dargestellt, das β-Isomer mit der niedrigeren C_2-Symmetrie ist rechts gezeigt.

Von dem $\{V_{15}Sb_6O_{42}\}$-Cluster ist bislang nur ein Isomer bekannt (Abb. 9, rechts). Je sechs $\{VO_5\}$-Pyramiden sind zu zwei V_6-Ringen verknüpft (Abb. 9, rechts, rot und türkis). Diese sind über drei weitere $\{VO_5\}$-Polyeder miteinander verknüpft (lila).

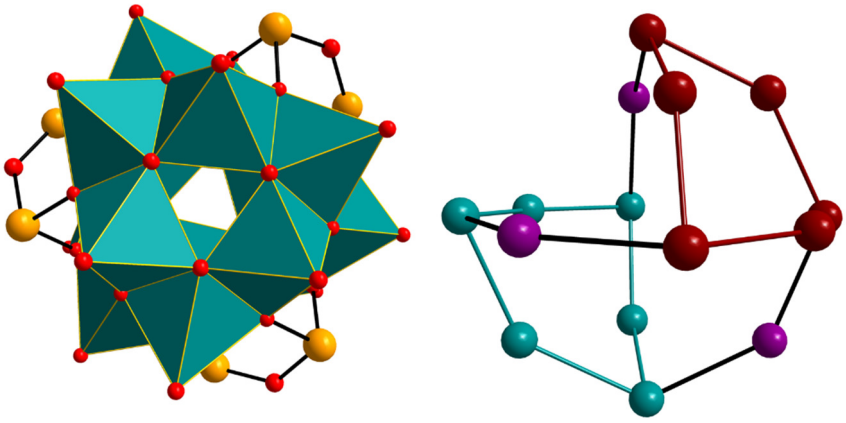

Abbildung 9: Der $\{V_{15}Sb_6O_{42}\}$-Cluster in Polyederdarstellung (links) und als eingefärbtes Vanadiumatomgerüst mit den zwei, um 60° zueinander verdrehten, Dreiecken aus je sechs V^{4+}-Ionen (rot und türkis) sowie den verbrückenden drei V^{4+}-Ionen (lila).

Der $\{V_{14}Sb_8O_{42}\}$-Cluster ist in Form des α-Isomers mit D_{2d}-Symmetrie bzw. des β-Isomers mit D_{2h}-Symmetrie bekannt. DFT-Kalkulationen belegen, dass das γ-Isomer (Abb. 10) isolierbar sein sollte und durchaus auch der Einbau von Heteroatomen wie Sn möglich sind.[56]

Vor einiger Zeit wurde über das γ-Isomer berichtet.[57] Ein genauer Blick auf die Struktur zeigt jedoch, dass es sich um ein Gemisch aus dem α- und dem β-Isomer handelt, welche co-kristallisiert vorliegen.[25]

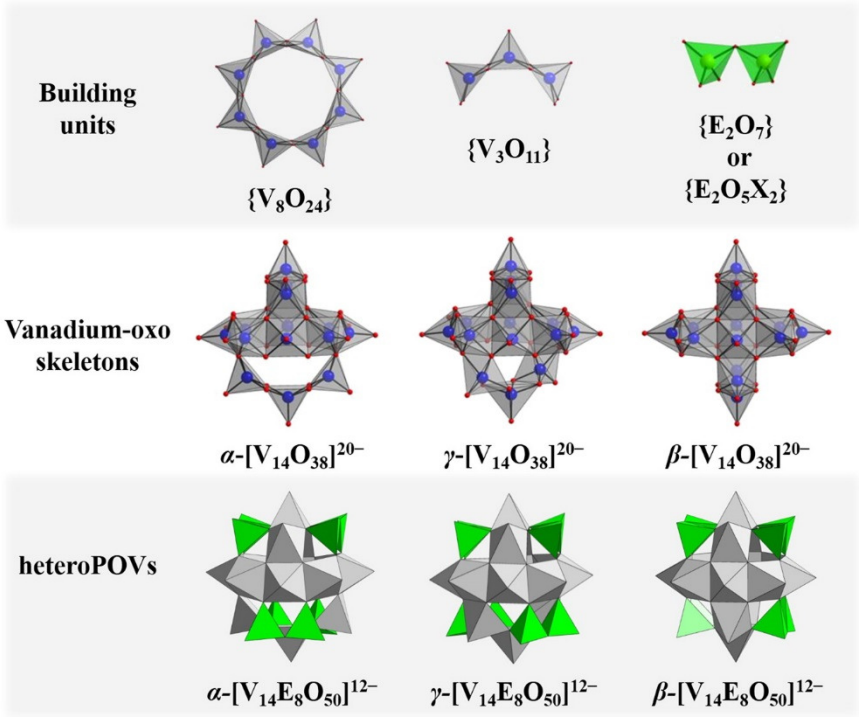

Abbildung 10: DFT-Kalkulationsergebnisse der bekannten Isomere des $\{V_{14}Sb_8O_{42}\}$-Clusters und des γ-Isomers. Reprinted with permission from MONAKHOV *et al.* (© 2016 American Chemical Society).[56]

Das α-Isomer ist aus einem Achterring aus kantenverknüpften $\{VO_5\}$-Pyramiden aufgebaut, sowie aus zwei Triaden aus $\{VO_5\}$-Pyramiden, die um 90° zueinander verdreht an den Achterring binden (Abb. 11, links). Die Struktur des α-Isomer des $\{V_{14}Sb_8O_{42}\}$-Clusters weist eine D_{2d}-Symmetrie auf. Das β-Isomer, mit D_{4h}-Symmetrie, besteht aus zwei senkrecht zueinanderstehenden Achterringen kantenverknüpfter $\{VO_5\}$-Polyeder (Abb. 11, rechts).

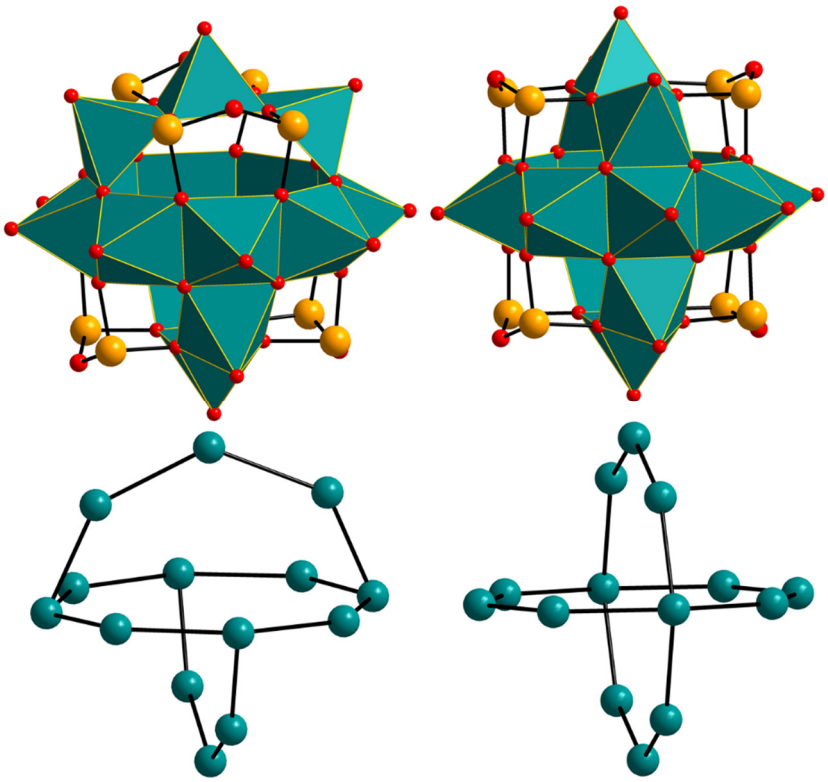

Abbildung 11: Links ist das α-Isomer des $\{V_{14}Sb_8O_{42}\}$-Clusters gezeigt, mit D_{2d}-Symmetrie, oben in der Polyederdarstellung, unten das Vanadium-Gerüst. Rechts ist das β-Isomer, mit D_{4h} Symmetrie dargestellt.

Während der Doktorarbeit konnte ein weiteres Isomer des $\{V_{14}Sb_8O_{42}\}$-Clusters synthetisiert und charakterisiert werden. Mit DFT-Kalkulationen wurde die relative Stabilität des neuen Isomers mit nach innen gerichteter Vanadyleinheit, sowie potentiell möglicher Isomere des $\{V_{14}Sb_8O_{42}\}$-Clusters, bestimmt (Abb. 12).

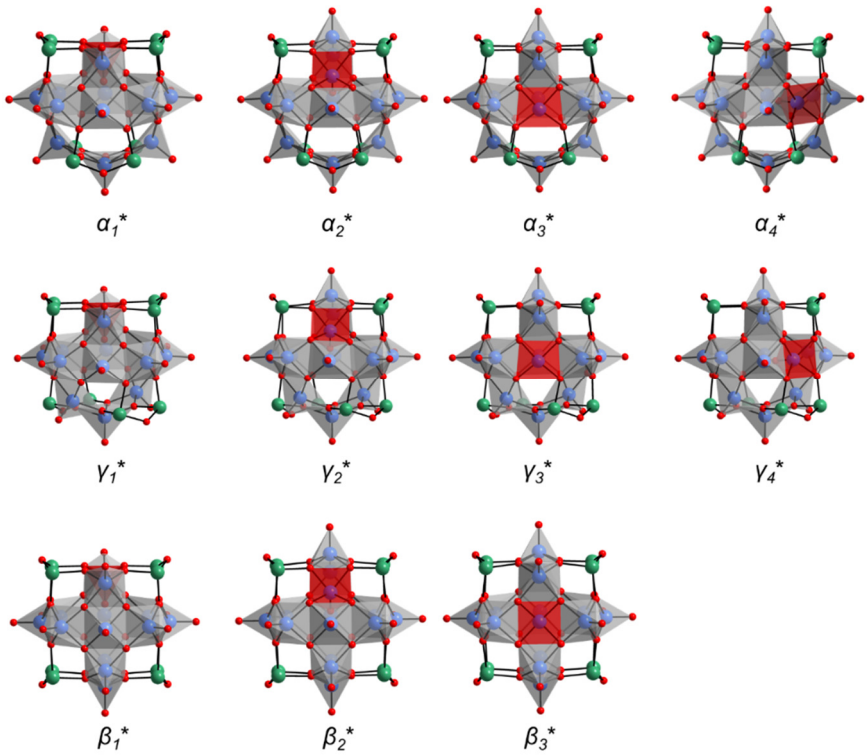

Abbildung 12: Die mittels DFT-Kalkulationen berechneten möglichen Isomere des $\{V_{14}Sb_8O_{42}\}$-Clusters mit nach innen gerichteter $\{VO_5\}$-Pyramide (roter Polyeder).[37] [38]

1.3.2. Chemische Modifizierung von POVs

Neben den Sb-POVs (Tabelle 2) sind auch gemischte Heteroatom-POVs bekannt, wobei als Heteroatome Sb und Ge in die POV-Cluster integriert sind. Die Synthese dieser Ge/Sb-POVs erfolgt mit den herkömmlichen Edukten NH_4VO_3, Sb_2O_3, GeO_2 und einem Übergangsmetallsalz bei hohen pH-Werten. Oft dauern die Synthesen mehrere Tage bis geeignete Kristalle erhalten werden. In diesen Verbindungen sind die Heteroatompositionen meist statistisch von Ge und Sb besetzt. Eine Ausnahme bildet die Verbindung $\{Ni(en)_3\}_3[V_{15}Sb_3Ge_3O_{42}(OH)_3(H_2O)] \cdot \approx 9\,H_2O$ welche durch Postfunktionalisierung einer wasserlöslichen Vorläuferverbindung (ugs. Precursor) hergestellt wurde.[52] Mit einem solchen Precursor kann die Reaktionszeit auf Stunden verkürzt werden und deutlich moderatere pH-Werte sind notwendig. Der Einsatz von Precursoren war vor allem bei den Mo- und W-basierten POMs wohl bekannt. Jedoch

waren für heteroatomsubstituierte POVs lange keine adäquaten Vorläuferverbindungen verfügbar. Dies änderte sich 2016 als der erste wasserlösliche Sb-POV publiziert wurde.[46] In der Folgezeit wurde die postsynthetische Modifizierung zu einem wichtigen Werkzeug für die Synthese neuer POVs.

1.4. Anwendungen von POVs

Polyoxometallate finden in vielen interessanten Bereichen Anwendungen, die zum einen auf die redoxaktiven Eigenschaften der POMs zurück zu führen sind, aber auch auf die große sauerstoffbasierte Oberfläche. Die möglichen Anwendungsgebiete sind sehr vielfältig und daher sollen nur einige ausgewählte Beispiele vorgestellt werden.

POMs werden antivirale, antitumorale und anti-HIV Wirkungen zugeschrieben, was durch mehrere Patentschriften und Publikationen bestätigt wurde.[58] [59] LI und WANG *et al.* synthetisierten die Verbindungen $\{Ni(en)_3\}_5H\{V^VNb_8V^{IV}{}_8O_{44}\}\cdot 9\ H_2O$, $(H_2en)Na_2[\{Zn(en)_2(Hen)\}\{Zn(en)_2(H_2O)\}_2\{PNb_8V^{IV}{}_8O_{44}\}]\cdot 11\ H_2O$ sowie $Na\{Cu(en)_2\}_3\{[Cu(en)_2]_2[\{PNb_8V^{IV}{}_8O_{44}]\}\cdot 11\ H_2O$, von denen die ersten beiden Verbindungen eine hohe Aktivität gegenüber Magenkrebszellen (SGC-7901 cells), Lungenkarzinomen (SC-1680 cells) und osteogenem Sarkom „Knochenkrebs“ (MG-63 cells) zeigten. Diese Verbindungen stellen die ersten Beispiele für höhernukleare V-substituierte Heteropolyoxoniobate dar. Die Strukturen bestehen aus einem $\{VO_5\}$-Achterring mit je vier ecken- und kantenverknüpften $\{NbO_6\}$-Oktaedern ober- und unterhalb des Achterrings (Abb. 13).

Da die Einzelbestandteile nur geringe antitumorale Aktivitäten aufweisen, konnte auf einen synergistischen Effekt geschlossen werden. Außerdem zeigten die Verbindungen eine hohe Selektivität, da gesunde Zellen in niedrigerem Konzentrationsbereich kaum bis gar nicht beeinträchtigt wurden, während die Krebszellen zu mindestens 60-80 % zerstört wurden, bei höheren Konzentrationen sogar bis zu 99 %.[60]

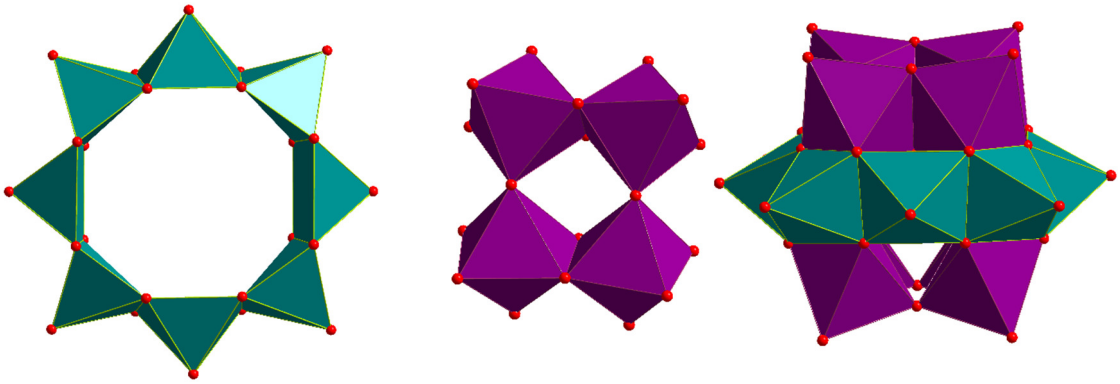

Abbildung 13: links: $\{V_8\}$-Ring aus kantenverknüpften $\{VO_5\}$-Pyramiden (türkis), mitte: $\{NbO_6\}$-Oktaeder (lila) über ecken- und kantenverknüpft, rechts: $\{Nb_8V_8O_{40}\}$-Einheit.

Die photoinduzierte Farbstoffdegradation[61], der Einsatz als Ionentauscher oder Sorptionsmaterial[62] [63] zeigen weitere Eigenschaften der POMs auf. Für die Entfernung organischer und anorganischer Verunreinigungen aus Trinkwasser[7] [6] oder zur Synthese organischer Moleküle sind POMs ebenfalls geeignet[64] [65].

Der Einsatz von POMs als Katalysatoren und besonders von POVs ist besonders viel versprechend.[2] HILL und HU *et al.* haben diese Eigenschaft für die gleichzeitige oxidative und hydrolytische Dekontamination von Simulanzien für chemische Kampfstoffe untersucht, wobei ein V-substituiertes Polyoxoniobat verwendet wurde. Als Nervengift Simulant wurde Diethyl-Cyanophosphonat (DECP) eingesetzt und als Senfgas Simulant 2-Chloroethyl-ethyl-sulfid (CEES), welche beide in ungiftige Endprodukte zersetzt werden konnten. Mit hohen 'Turnover'-Zahlen und Effizienzen über 90 % konnte für diese Material eine hervorragende katalytische Aktivität nachgewiesen werden.[66]

GÜTTEL und STREB *et al.* untersuchten die aerobe oxidative Katalyse des Modellsystems 9,10-Dihydrogenanthracen zu Anthrachinon mit $[Ba_4(dmso)_{14}V_{14}O_{38}(NO_3)]$ als Katalysator. Bei der homogenen Katalyse unter Sauerstoffüberdruck (8 bar) wurde in 7 h eine fast 60 %ige Konversion erreicht, während das literaturbekannte katalytische System nur 46 % erreichte.[67]

Die Entwicklung neuer Energiespeichermaterialien steht im Fokus der Materialforschung sowohl in Bezug auf die Elektromobilität als auch bei erneuerbaren Energien. Auch auf diesem Gebiet entwickeln sich POVs zu interessanten Vertretern. SONOYAMA *et al.*[68]

zeigten mit $K_7MnV_{13}O_{38}$ als Kathodenmaterial erste Erfolge. Kürzlich zeigten CRONIN *et al.*, dass POVs sowohl für Lithium-Ion-Batterien als auch für Na-Ionen-Batterien geeignet sind, anhand des POVs $Li_7V_{15}O_{36}(CO_3)$.[3] [5]

Die Spinfrustation der $\{V^{IV}_{15}E_6\}$-Cluster (E = As, Sb, Ge oder Si) bei tiefen Temperaturen und der resultierende magnetische Grundzustand S = ½ sind besonders im Bereich der Datenverarbeitung ein viel diskutiertes Anwendungsgebiet.[69] [70] So genannte Quantenbits sollen durch gezielte Informationsspeicherung in Form von 'Spin up' und 'Spin down' auf molekularer Ebene erzeugt werden. Dies ist besonders unter dem Gesichtspunkt der immer kleiner werdenden Speicher mit immer größeren Speicherkapazitäten ein interessantes Gebiet der aktuellen Forschung.[71]

1.5. Zeitaufgelöste *in situ* Röntgenpulver-diffraktometrie

Eine hervorragende Methode, um Erkenntnisse über die Bildung von Polyoxovanadaten zu erhalten, stellt die zeitaufgelöste *in situ* Röntgenpulverdiffraktometrie dar. Mit Hilfe von Synchrotron Strahlen (z. B. Deutsches-Elektronen-Synchrotron, DESY, Hamburg) kann deren Bildung unter solvothermalen Bedingungen mit hoher Zeitauflösung verfolgt werden, ohne in die Reaktionsabläufe einzugreifen.

Die Aufklärung von Reaktionsmechanismen stellt in der anorganischen Chemie nach wie vor eine große Herausforderung dar, da besonders heterogen ablaufende Reaktionen komplex sind und nur wenig über die Einzelschritte bis hin zum fertigen Kristall bekannt ist. Die Evaluation der Reaktionskinetik stellt einen ersten Schritt dar, die Bildung von POVs besser zu verstehen.

Für die Evaluation der Kinetik können unterschiedliche Nukleations-Kristallisations-Theorien herangezogen werden, welche unterschiedliche Randbedingungen voraussetzen. Mit dem Ansatz nach JMAK (JOHNSON-MEHL-AVRAMI-KOLMOGOROW), im Allgemeinen oft nur als AVRAMI-EROFÉEV (Gl. 1) bezeichnet, wird der Reaktionsfortschritt z. B. anhand der normierten Intensität eines Reflexes über die Zeit

beschrieben.[72] [73] [74] Ursprünglich wurde der JMAK-Formalismus für Phasenumwandlungen von Festkörpern entwickelt.

$$\boldsymbol{\alpha(t) = 1 - e^{[-(kt_{red})^m]}} \qquad \textbf{(1)}$$

Mit α dem Reaktionsfortschritt, k der Ratenkonstante, t_{red} der sogenannten Induktionszeit; meistens definiert als der Zeitpunkt, bei dem das Wachstum der Produktreflexe beginnt, und m dem Reaktionsexponent.

Die AVRAMI-EROFÉEV Gleichung kann linearisiert werden, was als SHARP-HANCOCK-Formalismus (Gl. 2) bezeichnet wird. Ändert sich der Reaktionsmechanismus während der Reaktion nicht so resultiert eine Gerade.

$$\boldsymbol{ln[-ln(1-\alpha)] = m \cdot ln(t_{red}) + m \cdot ln(k)} \qquad \textbf{(2)}$$

Aus dem Schnittpunkt der extrapolierten Gerade mit der y-Achse wird $m \cdot \ln(k)$ erhalten. Der Reaktionsexponent m kann aus der Steigung der Geraden bestimmt werden. Allerdings stecken in der Entwicklung der Formalismen einige Annahmen, die selten unter solvothermalen Bedingungen erfüllbar sind wie die homogene Nukleation ohne Berührung der sphärischen Partikel und dass die Nukleation statistisch erfolgt.[75] [76] [77] [78]

Für die quantitative Beschreibung der Bildung kristalliner Feststoffe aus fluiden Medien wird seit einiger Zeit die Theorie nach GUALTIERI (Gl. 3) herangezogen. Diese Methode wurde zur Ermittlung der Reaktionskinetik von Zeolithen entwickelt, die in Bezug auf Nukleations- und Kristallisationsverhalten eher dem Verhalten der POVs ähneln. Die Nukleations- und Kristallisationsphase werden mit unterschiedlichen Aktivierungsenergien und daher als individuelle Prozesse beschrieben.[79]

$$\alpha = \frac{1}{1 + e^{-\frac{t-a}{b}}} \cdot \left[1 - e^{-(k_g t)^n}\right] \quad (3)$$

k_g ist die Ratenkonstante des Wachstum-Prozesses, *a* und *b* sind Konstanten, welche mit der Nukleation verbunden sind. Die Ratenkonstante des Nukleations-Prozesses (k_n) kann aus dem Wert für *a* ermittelt werden (Gl. 4).[80]

$$k_n = \frac{1}{a} \quad (4)$$

Der Exponent *n* beschreibt die Dimensionalität des Kristallwachstums (n = 3 - Wachstum in allen drei Raumrichtungen) und kann aus SEM-Bildern ermittelt werden. Der Parameter *b* lässt Schlüsse über die Nukleation zu (Tab. 3).

Tabelle 3: Nukleationsmodelle abgeleitet vom Wert *b* nach GUALTIERI.[80]

***b* [min^{-1}]**	**Mechanismus der Nukleation**
< 15	Heterogen
~ 20	Homogen
> 20	Autokatalytisch

Mit Hilfe von Gleichung 5 kann zusätzlich die zeitabhängige Wahrscheinlichkeit der Nukleation P_N berechnet werden, wofür die Parameter *a* und *b* aus Gleichung 3 bekannt sein müssen.

$$P_N = e^{-\left[\frac{(t-a)^2}{2b^2}\right]} \quad (5)$$

Wird eine bestimmte Reaktion bei unterschiedlichen Temperaturen durchgeführt, kann aus den unterschiedlichen Ratenkonstanten mithilfe der ARRHENIUS Gleichung die Aktivierungsenergie für den Nukleations- und den Kristallisationsprozess bestimmt werden (Gl. 6 und 7). Für diese Analyse wird ln(*k*) gegen 1/*T* aufgetragen und

anschließend die jeweilige Aktivierungsenergie aus der Steigung der resultierenden Geraden bestimmt.

$$\boldsymbol{k = A \cdot e^{\left(-\frac{E_a}{RT}\right)}} \quad \textbf{(6)}$$

$$\boldsymbol{ln(k) = \ln(A) - \frac{E_a}{RT}} \quad \textbf{(7)}$$

Mit k = Ratenkonstante, A = präexponentieller Faktor, E_a =Aktivierungsenergie, R = universelle Gaskonstante und T = Temperatur.

2. Charakterisierungsmethoden

Die weiteren Charakterisierungsmethoden sind in Tabelle 4 zusammengefasst.

2.1. Methoden

Tabelle 4: Verwendete Charakterisierungsmethoden.

Methode	Bezeichnung	Bemerkung
Einkristallstruktur-analyse	IPSD-2 (Stoe)	Mo-Kα; Graphit Monochromator
Pulver-diffraktometrie	STADI-P (Stoe)	Transmissionsgeometrie Cu-Kα mit einem 1K Mythen Detektor
IR-Spektroskopie	ATR-IR-Spektrometer (Bruker)	375-4000 cm^{-1}; Diamant aus ATR-Kristall; Auflösung: 4 cm^{-1}
UV/Vis Spektroskopie	Agilent 8453 Spektrometer, Agilent Technologies, Waldbronn	190 – 1100 nm, im flüssigen Medium
UV/Vis Spektroskopie	UV/Vis Cary5Varian TechtronPty. Darmstadt	250 – 2000 nm, Probe in $BaSO_4$-Referenzmatrix
Elementaranalyse	EuroEA3000 Elementar Analyzer (Eurovector)	Verbrennung in O_2 bei 1000 °C; Helium-Trägergas, Detektion über Wärmeleitzelle
DTA-TG	STA 409 CD (Netzsch)	Pt-Pt/Rh-Thermoelement Gasstrom: 75 cm^3/min; Heizrate: 4 K/min
Magnetmessungen	Quantum Design MP MS-4XL SQUID	T = 2 – 300 K, H = 0.1 – 5 T

Rasterelektronen-mikroskopie (ESEM) – Energiedispersive Röntgen-spektroskopie (EDX)	ESEM XL (Philips)	200000-fache Vergrößerung, Rasterelektro-nenmikroskop gekoppelt mit EDX Detektor U = 20 kV, I = 33 A
Weitwinkel-Synchrotron-Diffraktometrie	DESY, P07 DESY, P08 SynRAC	Perkin Elmer XRD1621 Flat Panel Detektor; pixel: 200x200 µm; Laue Kristalle Si(111) und Si(220) sowie einen single bounce Monochromator (SBM)
Massenspektrometrie ESI-Q-TOF-HRMS	Synapt G2-S HDMS Waters Co., Milford, MA, USA	Flussrate: 10 μL/min, USpray = 1.6 kV, UKegel = 10 V, Verneblergas 6 bar
Tandem MS/CID	Synapt G2-S HDMS Waters Co., Milford, MA, USA	Kollisionsenergie 15 – 25 V

Der *in situ* Reaktor „SynRAC“ (**syn**chrotron-based **r**eaction cell for the **a**nalysis of **c**hemical reactions, Abb. 14) wird für Solvothermalsynthesen im Kulturröhrchen (bis 180 °C) verwendet, wenn die Reaktionen *in situ* verfolgt werden sollen. Unter dem Reaktorblock befindet sich ein Magnetrührer (max. 1200 rpm). Über den Heizmantel aus Kupferdrähten wird das Kulturröhrchen auf eine definierte Temperatur erhitzt. Der Reaktor hält die Temperatur über einen in die Reaktionslösung eintauchenden Temperaturfühler konstant, ggf. wird mit Druckluft gekühlt. Die Temperatur kann dabei auf ± 0.6 °C genau gehalten werden (häufig sehr viel genauer, abhängig vom System).[81] Zum Schutz der Umgebung ist eine Verschlusskappe aus Aluminium vorhanden, die mittels Dichtringen und Schellen mit dem Reaktorblock verbunden werden kann. Der Röntgenstrahl tritt durch zwei Aluminiumfenster und wird hinter dem Reaktorblock detektiert (Abb. 14).[81]

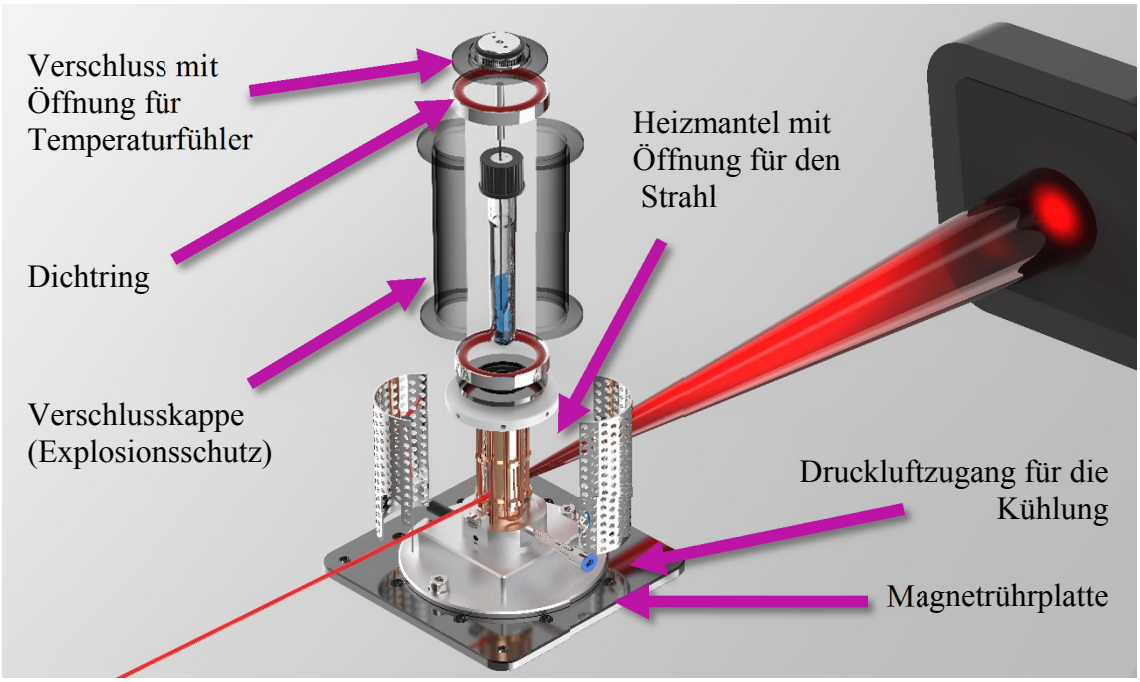

Abbildung 14: *In situ*-Reaktor „SynRAC“, der im Rahmen des MATsynCELL Projekts des Röntgen-Ångstrøm Clusters entwickelt wurde.[82]

3. Experimenteller Teil

Die Synthese von POVs erfolgte meist in Duran©-Kulturröhrchen mit einem Innenvolumen von 11 mL. Der maximale Befüllungsgrad lag bei 40-50 %. Die Röhrchen wurden mit einer Verschlusskappe aus Polybutylenterephthalat (PBT) und einer Dichtung aus Polytetrafluorethylen verschlossen, welche für Temperaturen bis 180 °C geeignet sind. In einem Aluminiumblock (Abb. 15) können bis zu sechs Kulturröhrchen parallel getempert werden. Da bei diesem Vorgehen das Reaktionsgemisch nicht gerührt oder geschüttelt wird, wird diese als statische Solvothermalsynthese bezeichnet.[83] [84] [85]

Die Synthese unter dynamischen Bedingungen, also Rühren des Reaktionsgemisches (Abb. 16) bietet den Vorteil, dass die Bildung kristalliner Produkte während der Reaktion verfolgt werden können und auf diese Weise die Kristallisationskinetik bestimmt werden kann. Nicht jede Verbindung, die unter statischen Bedingungen gebildet wird, kann auch unter dynamischen Bedingungen synthetisiert werden. D. h., die optimalen Bedingungen müssen iterativ gefunden werden.

Zur Analyse der Reaktionsprodukte wurden die Infrarot (IR)-Spektroskopie, die Elementar (CHNS-)Analyse, UV/Vis-Spektroskopie, Differenzthermoanalyse - Thermogravimetrie (DTA-TG), Röntgenpulverbeugung (XRD) und Einkristallstrukturanalyse eingesetzt. Am Deutschen Elektronen Synchrotron in Hamburg (DESY) wurden *in situ* Röntgenbeugungsuntersuchungen mit dem SynRAC Reaktor[81] durchgeführt. Massenspektrometrische Untersuchungen wurden von Kooperationspartnern (Prof. SCHALLEY, Dr. WARZOK, FU Berlin) durchgeführt. Magnetmessungen und dichtefunktionaltheroretische Rechnungen (DFT) wurden von Kooperationspartnern an der RWTH Aachen (Prof. KÖGERLER, Prof. MONAKHOV, Dr. KONDINSKI, Dr. VAN LEUSEN) durchgeführt.

Abbildung 15: Duran©-Kulturröhrchen (links) und im Aluminiumblock (rechts).

Abbildung 16: Magnetheizrührer mit Aluminiumblock und Kontaktthermometer.

3.1. Verwendete Chemikalien

Tabelle 5: Verwendete Chemikalien mit Reinheitsgrad und Herstellerangabe.

Name		Reinheitsgrad	Hersteller
1,10-Phenanthrolin	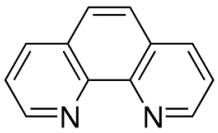	99 %	abcr
Ammoniummeta-vanadat	NH_4VO_3	99 %	Merck
Antimonoxid	Sb_2O_3	Reinst	Merck
Cyclen (1,4,7,10-Tetraazacyclododecan)	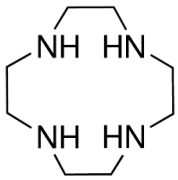	min. 98 %	strem chemicals, INC.
Eisenchlorid-Tetra-hydrat	$FeCl_2 \cdot 4H_2O$	Reinst >99 %	Honeywell/ Fluka
Eisenperchlorat-Hydrat	$Fe(ClO_4)_2 \cdot xH_2O$	98 %	Aldrich
Nickelchlorid-Hexahydrat	$NiCl_2 \cdot 6H_2O$	Reinst, >97 %	Merck
Nickelperchlorat-Hexahydrat	$Ni(ClO_4)_2 \cdot 6H_2O$	99 %	abcr
Zinkacetat-Dihydrat	$Zn(CH_3COO)_2 \cdot 2H_2O$	Reinst	Merck
Zinkchlorid	$ZnCl_2$	Reinst	Merck
Zinknitrat-Hexahydrat	$Zn(NO_3)_2 \cdot 6H_2O \cdot$	Reinst, >99 %	Merck
Zinkperchlorat-Hexahydrat	$Zn(ClO_4)_2 \cdot 6H_2O$	99 %	abcr

Tabelle 6: Verwendete flüssige Amine.

Name		Reinheitsgrad	Hersteller
Ethylendiamin (en)	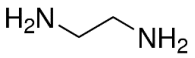	99 %	Grüssing
Methylamin (MA)	CH_3NH_2	40 % aq. solution	abcr
Tris(2-aminoethyl)amin (tren)	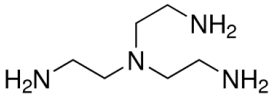	96 %	Aldrich

3.2. Verwendete Programme

Tabelle 7: Verwendete Programme mit Beschreibung.

Programm	Beschreibung	Quelle
STOE WinXPow	Visualisierung von Pulverdiffraktogrammen, Berechnung von Pulverdiffraktogrammen aus Einkristallstrukturdaten und Programmpaket zur Datensammlung von Pulver-diffraktogrammen.	[86]
SHELXS 97 – 2015:	Strukturlösung aus Messdaten der Einkristallstruktur-analyse.	[87]
SHELXL 97 – 2015	Strukturverfeinerung der Einkristallstrukturdaten.	[88]
STOE X-RED, X-SHAPE, X-AREA:	Durchführung von Absorptionskorrekturen der Einkristalldaten.	[89] [90] [91]
Diamond 3.2k	Visualisierung von Strukturbildern.	[92]
Netzsch TA4:	Auswertung thermischer Untersuchungen (DTA-TG).	[93]
EDXPowd 3.155	Ermittlung der Reflexintensitäten aus *in situ* EDXRD-Daten.	[94]
calf3	Ermittlung der Reflexintegrale aus *in situ* XRD Daten.	[95]
olex^2	Visulisierung der nicht ausgefüllten Freiräume in einer Verbindung zur Ermittlung des hypothetischen Wassergehaltes.	[96] [97]
Powerpoint	Erstellung unterschiedlicher Grafiken.	
Fit2D	Integration der 2D Pulverdiffraktogramme aus *in situ* Beugungsdaten	[98]
Gimp2	Erstellung unterschiedlicher Grafiken.	[99]

4. Ergebnisse: Kumulativer Hauptteil

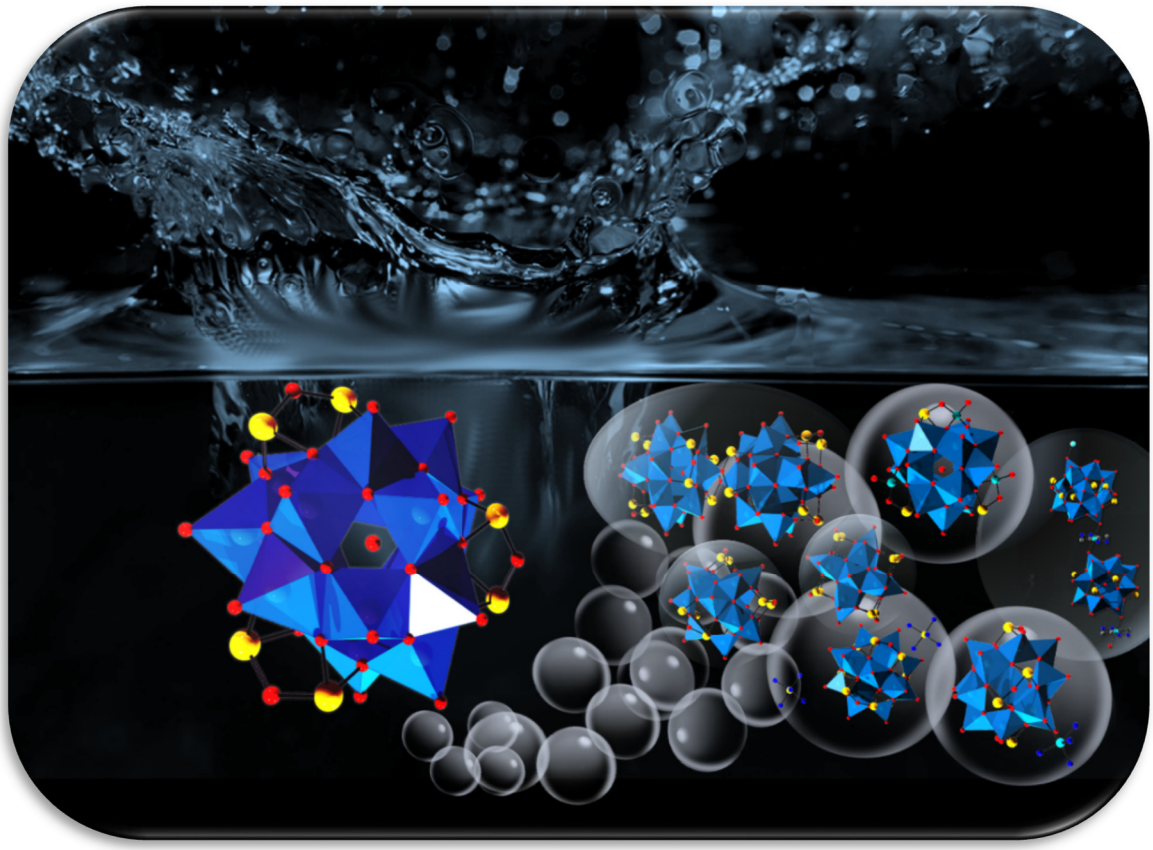

4.1. Die Publikation *„Nucleation and Crystal Growth of a {$V_{14}Sb_8O_{42}$}-Cluster from a {$V_{15}Sb_6O_{42}$} Polyoxovanadate: In Situ XRD Studies"*

Die Transformation der Precursorverbindung $\{Ni(en)_3\}_3[V_{15}Sb_6O_{42}(H_2O)_x]\cdot\approx 15\ H_2O$ in Wasser zu dem V-ärmeren aber Sb-reicheren Produkt $[\{Ni(en)_2\}_2V_{14}Sb_8O_{42}]\cdot 5.5\ H_2O$ wurde mittels *in situ* Röntgenbeugung bei unterschiedlichen Temperaturen untersucht. Die *in situ*-Untersuchungen zeigten, dass nach kurzer Aufheizphase die Reflexe des Precursors (T > 130°C) verschwinden und die Verbindung wahrscheinlich gelöst oder amorphisiert wird. Die Intensitätszunahme im Kleinwinkelbereich deutet auf die Bildung von Nanoteilchen hin. Nach einer Induktionszeit, welche mit der Temperatur korreliert, sind die Reflexe des Produkts zu beobachten sowie die Abnahme der Intensität im Kleinwinkelbereich der Diffraktogramme. Die Transformationsreaktion, welche unter statischen Bedingungen drei Tage in Anspruch nimmt, konnte durch den Einsatz von NH_4VO_3 als Additiv signifikant beschleunigt werden und war unter dynamischen Bedingungen innerhalb von drei Stunden vollständig abgeschlossen. Die Auswertung der Kinetik bei unterschiedlichen Temperaturen ergeben nach dem Modell von AVRAMI einen 3D Nukleationsprozess. Dieser ist ebenfalls der geschwindigkeitsbestimmende Schritt. Zusätzlich liegt ein heterogener Nukleationsprozess vor, was durch die Präsenz von röntgenamorphen Nanopartikel erklärt werden kann. Die Aktivierungsenergien sowohl des Nukleations- (34.4 kJ/mol) als auch des Kristallisationsschrittes (43.8 kJ/mol) sind vergleichbar gering, und weisen Werte auf, welche für Zeolithe (40-100 kJ/mol), Thiometallate (40-70 kJ/mol) oder MOFs

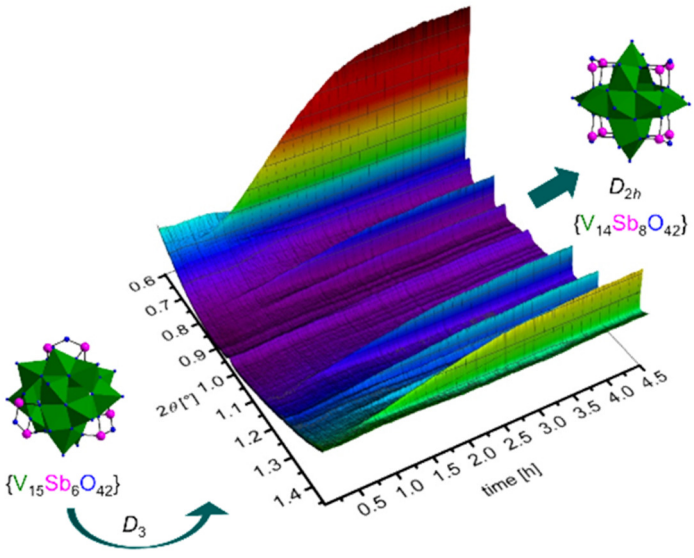

Abbildung 17: TOC Grafik der Publikation *„Nucleation and Crystal Growth of a {$V_{14}Sb_8O_{42}$}-Cluster from a {$V_{15}Sb_6O_{42}$} Polyoxovanadate: In Situ XRD Studies"*.

(50-140 kJ/mol) berichtet wurden. Diese niedrigen Energiebarrieren belegen das vielversprechende Potential dieser synthonartigen Verbindung in Bezug auf Postfunktionalisierungsreaktionen.

Veröffentlicht in *Eur. J. Inorg. Chem.* **2016**, *34*, 5393.
DOI: 10.1002/ejic.201601025

ChemPubSoc Europe

DOI: 10.1002/ejic.201601025

EurJIC European Journal of Inorganic Chemistry

Full Paper

Vanadium Chalcogenide Clusters

Nucleation and Crystal Growth of a {$V_{14}Sb_8O_{42}$} Cluster from a {$V_{15}Sb_6O_{42}$} Polyoxovanadate: In Situ XRD Studies

Michael Wendt,[a] Lisa K. Mahnke,[a] Niclas Heidenreich,[a] and Wolfgang Bensch*[a]

Abstract: The hydrothermal transformation of the heteroatom polyoxovanadate compound {$Ni(en)_3]_3[V_{15}Sb_6O_{42}(H_2O)$]·≈$15H_2O$ (en = ethylenediamine) in water into [{$Ni(en)_2]_2V_{14}Sb_8O_{42}$]·$5.5H_2O$ was investigated by in situ XRD experiments at different temperatures. First, the precursor undergoes very fast amorphization or dissolution, and an induction period is observed that depends on the reaction temperature. Crystal growth of the product is completed within 3 h, while higher temperatures lead to accelerated reaction progress. Evaluation of the kinetics showed that heterogeneous nucleation is the rate-limiting step of the reaction. The activation energies for nucleation and crystal growth are very low compared to data reported in the literature for several other chemical systems.

Introduction

The formation mechanisms of crystalline solids from solution are still scarcely understood due to the complexity of chemical reactions during nucleation and crystallization steps.[1] In recent years the analytical tools for in situ investigations of chemical reactions under real reaction conditions were significantly developed.[2–13] We and others demonstrated that a wealth of information is gained by applying in situ XRD, in-situ total scattering, or in-situ X-ray absorption spectroscopy during chemical reactions.[10, 14–29] Despite the increasing efforts to gain insight into mechanisms of chemical reactions, in situ X-ray scattering studies under real reaction conditions are still rarely performed. Several reasons may be responsible for preventing broader application of such experiments: (i) special reaction cells must be developed to meet the requirements of the reaction conditions; (ii) a high temporal resolution requires high-intensity X-rays, and therefore the experiments are mainly performed at synchrotron radiation facilities. In any case, for direct syntheses of new materials the reaction mechanisms including formation of metastable intermediate phases must be known.

Syntheses under solvo- or hydrothermal conditions are widely used for the preparation of new materials. Heteroatom-modified high-nuclearity polyoxovanadates (POVs) are a class of compounds that can only be prepared under solvothermal conditions. Because the reaction mechanisms are not well understood, almost all hetero-POVs were obtained by systematic variation of the reaction conditions. Hetero-POVs with Sb as heteroatom having the general formula {$V_{18-2n}Sb_{2n}O_{42}$} (n = 2–4) were synthesized and characterized.[30–36] The clusters can be expanded by, for example, transition metal complexes or organic ammonium cations,[30,32,37–43] and this leads to an increase in complexity of the chemical reactions. In contrast to polyoxomolybdates or polyoxotungstates, no suitable preformed high-nuclearity clusters are available for the generation of Sb-POVs, which can be regarded as an obstacle to the development of Sb-POV chemistry. In a recent in situ energy-dispersive X-ray diffraction (EDXRD) study[44] we investigated the formation of Sb-POVs in the presence of 1-(2-aminoethyl)piperazine at the same ratio of Sb_2O_3/NH_4VO_3. The main result of this study was that all $[V^{IV}_{18-n}Sb_{2n}O_{42}]^{2n-}$ clusters with n = 2–4 can be obtained by varying the amine concentration, that is, the amine concentration and consequently the pH value controls the nuclearity of the cluster anion.

During our systematic research into Sb-POV chemistry we were able to prepare {$Ni(en)_3]_3[V_{15}Sb_6O_{42}(H_2O)_x$]·≈$15H_2O$ (**I**; en = ethylenediamine, x = 0 or 1),[45] which is the first water-soluble hetero-POV. The cluster core is successively transformed within several days in water at room temperature into the Sb-richer {$V_{14}Sb_8O_{42}$} moiety. Using **I** as synthon in the reaction slurry causes conversion of the {$V_{15}Sb_6O_{42}$} cluster into [{$Ni(en)_2]_2V_{14}Sb_8O_{42}$]·$5.5H_2O$ (**II**)[46] containing the β-isomer of {$V_{14}Sb_8O_{42}$} (Figure 1) over 3 d.

The addition of $[Ni(phen)_3](ClO_4)_2$·$0.5H_2O$ (phen = 1,10-phenanthroline) to an aqueous solution of **I** resulted in the crystallization of {$Ni(phen)_3]_2[V_{14}Sb_8O_{42}$]·phen·$12H_2O$ (**III**) containing α-{$V_{14}Sb_8O_{42}$}.[47] Performing the reaction in the presence of Sb_2O_3 reduced the reaction time to 1 d. On the basis of the observation that the {$V_{14}Sb_8O_{42}$} cluster can be obtained with Sb_2O_3 in short reaction times, we performed syntheses with NH_4VO_3 with the aim of preparing the V-richest cluster {$V_{16}Sb_4O_{42}$}. Surprisingly, compound **II** could be identified in the reaction product after heating for 1 d. All these intriguing observations encouraged us to investigate the reaction of **I** by in situ powder XRD under real reaction conditions.

[a] *Institute of Inorganic Chemistry, Christian-Albrechts-University of Kiel, 24118 Kiel, Germany*
E-mail: wbensch@ac.uni-kiel.de
http://www.ac.uni-kiel.de/de/bensch

Supporting information and ORCID(s) from the author(s) for this article are available on the WWW under http://dx.doi.org/10.1002/ejic.201601025.

ChemPubSoc Europe

EurJIC European Journal of Inorganic Chemistry

Full Paper

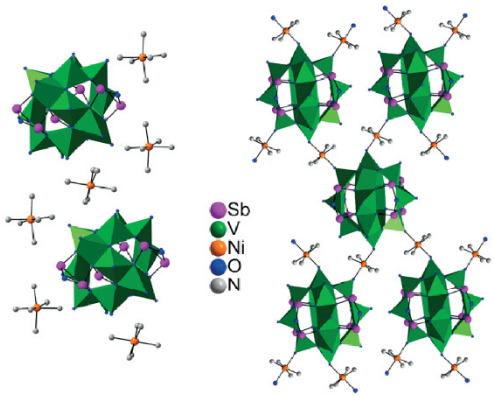

Figure 1. Structure of precursor **I** with the isolated complexes and cluster anions (left) and the structure of product **II** featuring a 2D layer by interconnection of the anions through V–O–Ni–O–V bridges (right). C and H atoms are omitted for clarity.

Results and Discussion

The transformation of a {$V_{15}Sb_6O_{42}$} cluster into a {$V_{14}Sb_8O_{42}$} cluster proceeds by several structural and chemical changes.[47] The {$V_{15}Sb_6O_{42}$} cluster with D_3 symmetry contains 15 edge-sharing square-pyramidal VO_5 moieties. Two V_6 hexagons (V_6) composed of six edge-sharing VO_5 polyhedra enwrap three VO_5 (V_3) units in a V_6–V_3–V_6 sequence. The three Sb_2O_5 units bridge the hexagons by Sb–O bonds to the hexagons. The total charge of the anion is 6–. During formation of the {$V_{14}Sb_8O_{42}$} cluster the chemical composition changes, and formally one VO_5 unit is replaced by an Sb_2O_5 moiety. This cluster exhibits a lower charge of 4–, and the structure contains two perpendicular V_8 rings formed by edge sharing of VO_5 pyramids. The symmetrical arrangement of the four Sb_2O_5 units and of the V_8 rings leads to the symmetry D_{2h}.

Evaluation of the Kinetics

The reflection intensities were normalized against the Al (100) reflection due to the window of the in situ cell to account for beam flux fluctuations [$I_n(t) = I_{exp}/I_{Al}$]. The reaction time at which the first reflections appeared was set as t_0 (induction period). The real time t_{red} was estimated as $t_{red} = t - t_0$. Crystal growth was evaluated by plotting the extent of reaction $\alpha(t)$ [$\alpha(t) = I_n(t)/I_n(t_\infty)$, t_∞ = end of reaction] versus time. The extent of reaction was analyzed with the JMAK (Johnson–Mehl–Avrami–Kolmogorov) approach[48–50] according to Equation (1).

$$\alpha(t) = 1 - \exp[-(kt_{red})^m] \quad (1)$$

where k is the rate constant and m the reaction exponent. By using a Sharp–Hancock (SH) plot[51] [Equation (2)] the parameters m can be derived from the slope and k from the intersection with the y, axis and different growth models can be derived.

$$\ln[-\ln(1 - \alpha)] = m\ln(k) + m\ln(t_{red}) \quad (2)$$

Note that the JMAK approach was developed for solid-state reactions with severe constraints, and one should be careful in the interpretation of the kinetic data. Nevertheless, first indications of the dominant reaction mechanism can be obtained by JMAK analysis. Another approach was established by Gualtieri[52] for the nucleation and crystallization of zeolites [Equation (3)] which seems to be more appropriate for the analysis of kinetic data for crystallization of crystalline solids from solution.

$$\alpha = \{1/(1 + \exp[-(t - a)/b])\}\cdot\{1 - \exp[-(k_g t)^n]\} \quad (3)$$

where α is the extent of crystallization and t the time, as in Equations (1) and (2), a the maximum rate of nucleation, b the distribution of the probability of nucleation with time, k_g the rate constant of the crystal growth, and n the dimension of crystal growth. The crystal shape is described by n and was set to $n = 3$ on the basis of the rhombohedral particle morphology seen in SEM images (Figure S3). The b value indicates different nucleation models: $b < 15$ heterogeneous; $b \approx 20$ homogeneous; and $b > 20$ autocatalytic. If the values a and b are known, the nucleation and the crystal-growth processes can be separated according to Equation (4) describing the time-dependent probability of nuclei development P_N.

$$P_N = \exp\{-[(t - a)^2/2b^2]\} \quad (4)$$

Results of the Kinetics

The in situ XRD patterns displayed in Figure 2 were collected while heating the sample to the desired temperature. Powder patterns were recorded in a fast step rate every 5 s with a heating rate of 1 °C/s to obtain a time-resolved set of patterns to follow the evolution of the Bragg reflections of the starting material. At the beginning of heating the Bragg reflections of **I** are clearly visible until they disappear after ca. 2.5 min (T = 137 °C). Similar observations were made at all three reaction temperatures and indicate that **I** is either dissolved or transforms into an amorphous state.

Exemplarily, the evolution of the XRD patterns collected at T = 144 °C is shown in Figure 3. After dissolution/amorphization of **I**, no reflections could be observed for a period of time t_{red} between ca. 46.5 min (T = 144 °C) and 30.5 min (T = 164 °C) until reflections of the product **II** appeared in the powder patterns. Interestingly, while the reflections of the starting material decrease, the background at small angles increases and indicates the presence of an amorphous phase. With further reaction progress the modulation of the background is successively reduced and disappears when the product starts to crystallize. After 150 min, the reaction seems to be finished, because no further increase in the intensities of the Bragg reflections could be detected (Figure 3, top). Comparison of the powder pattern of the final product with that calculated for **II** shows good agreement (Figure 3, bottom and Figure S1).

For kinetic analyses the most intense ($\bar{1}01$) reflection was used for T = 144, 154, and 164 °C. The extent of reaction $\alpha(t)$ shown in Figure 4 demonstrates the temperature dependence

ChemPubSoc Europe

EurJIC European Journal of Inorganic Chemistry

Full Paper

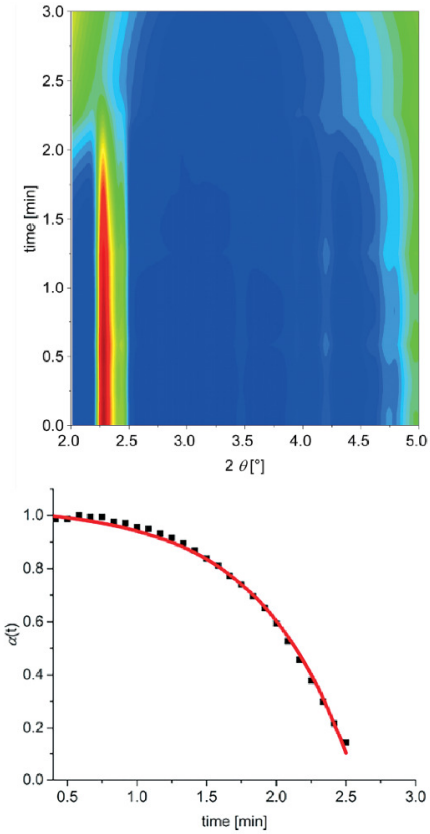

Figure 2. Powder XRD patterns (top; λ = 0.4959 Å) collected every 5 s during heating of the precursor {Ni(en)$_3$}$_3$[$V_{15}Sb_6O_{42}(H_2O)$]·≈15H_2O (**I**) to $T \geq 137$ °C. Intensity scale: intensity decreases from red to blue; (bottom) change of the intensity of the most intense reflection with time plotted as extent of reaction $\alpha(t)$. The red line is a guide for the eye.

of the induction period and the growth of the product. A higher reaction temperature leads to a shorter induction period and accelerates the formation of the product. Once reflections could be detected, fast growth was observed, and the reactions are finished in a time depending on the temperature: 144 °C: 150.5 min; 154 °C: 128.5 min; 164 °C: 76.5 min. The signal at 2θ = 3.00° is caused by a damaged pixel of the detector.

In Table S1 the mathematical expressions of different growth models are summarized together with values for *m* reported in refs.[51,53] A plot of these theoretical different growth models together with the experimental data (Figure 5) suggests that a nucleation-controlled process dominates the crystal growth (A3, Avrami–Erofeev; see Supporting Information, Figure S4 for the corresponding plots at T = 144 and 154 °C).

Using Equation (3) and fitting $\alpha(t)$ versus t assuming n = 3 (the value of 3 indicates 3D growth, see SEM image in the Supporting Information) gave values for b indicating heterogeneous nucleation processes for all three temperatures (Table 1). Most likely X-ray-amorphous particles formed from the precursor (see discussion above) act as nucleation centers. Evaluation

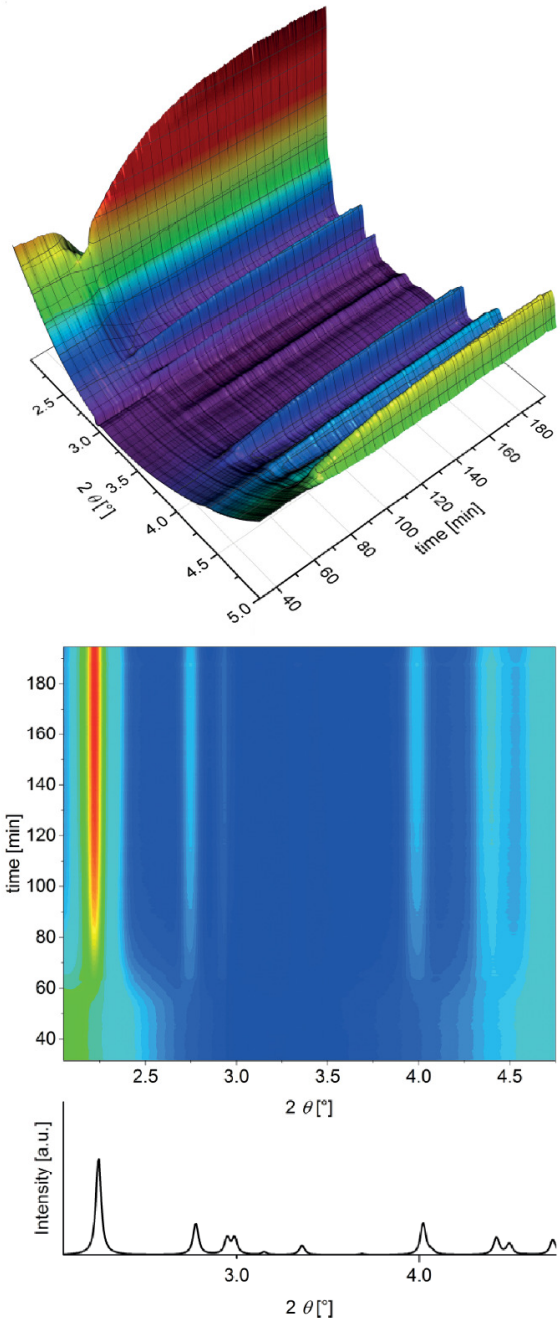

Figure 3. In-situ XRD patterns (λ = 0.4959 Å) collected during the reaction progress of the formation of [{Ni(en)$_2$}$_2$$V_{14}Sb_8O_{42}$]·5.5$H_2O$ (**II**). Patterns were recorded every 30 s at 144 °C: top: 3D plot; bottom: corresponding waterfall plot; color code: intensity increases in the order blue–green–yellow–red.

of the data with Equation (4) revealed that the nucleation phase and crystal growth scarcely overlap and gave further proof of the observed nucleation processes (Figure 6). Furthermore, the

ChemPubSoc Europe

EurJIC European Journal of Inorganic Chemistry

Full Paper

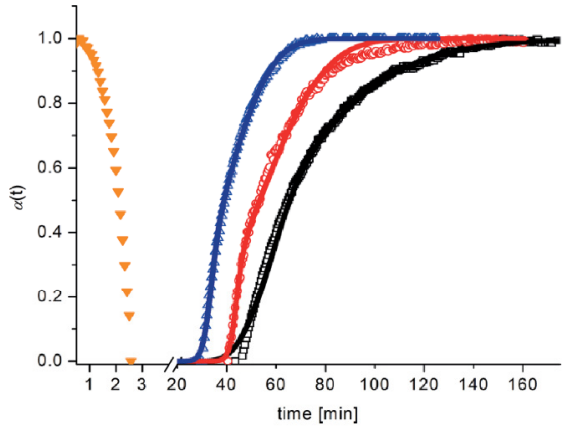

Figure 4. Extent of reaction $\alpha(t)$ for three different temperatures: 144 (black points), 154 (red points) and 164 °C (blue points) and the fits according to Equation (3) (corresponding colored lines) based on evaluation of the ($\bar{1}$01) reflection. The orange curve shows the fast decrease of the intensity of reflections corresponding to the precursor.

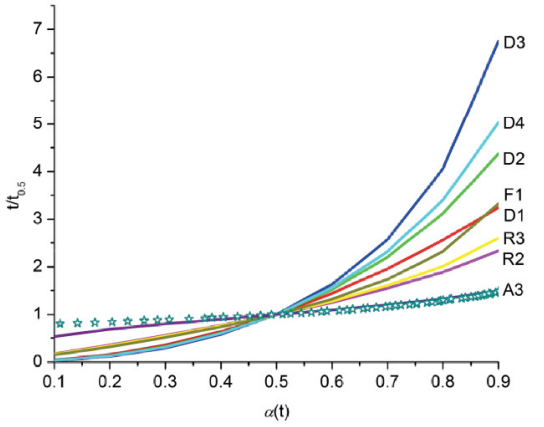

Figure 5. Comparison of the experimental data $t/t_{0.5}$ at 164 °C (points) as a function of $\alpha(t)$ with different kinetic growth models (listed in Table S1).

Table 1. Kinetic parameters for the three different reaction temperatures (t_{red} = induction time, k_n = rate constant of the nucleation process, k_g = rate constant of crystal growth, adj. R^2 = regression coefficient, and a, b = Gualtieri parameters; see text).

T [°C]	144 °C	154 °C	164 °C
t_{red} [min]	46.5	41.0	30.5
Growth model	A_3 nucleation	A_3 nucleation	A_3 nucleation
k_n [min^{-1}]	0.01607	0.01967	0.02531
Adj. R^2	0.995		
k_g [min^{-1}]	0.019(1)	0.024(3)	0.033(1)
Adj. R^2	0.999		
a [min^{-1}]	62(3)	50(4)	39(5)
b [min^{-1}]	19(1)	14(1)	7(2)
Adj. R^2	0.995	0.994	0.995

values of k_n and k_g indicate that nucleation is the rate-limiting step at all temperatures, because k_n is slightly smaller than k_g ($k_n = 1/a$) (Table 1). Analysis of the full widths at half-maximum of the most intense reflection shows only a moderate narrowing with reaction time, which suggests that not enough "monomers" are in solution for further crystal growth. Once the nuclei formed exceed the critical size, these newly formed nanocrystallites consume the "monomers".

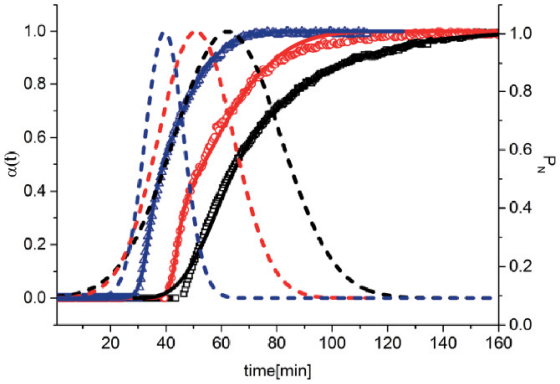

Figure 6. Temperature-dependent probability of nuclei development P_N (dotted lines), crystal growth of the ($\bar{1}$01) peak (points), and the Gualtieri fit (lines) for reaction temperatures of 164 (blue), 154 (red), and 144 °C (black).

The apparent activation energies for nucleation E_n and crystal growth E_g were calculated from an Arrhenius plot (Figure 7). The values of 34.4 kJ/mol for E_n and 43.8 kJ/mol for E_g are in the lower region of values reported for the formation of metal–organic frameworks (50–140 kJ/mol),[18,54–58] thiostannates (ca. 42 kJ/mol),[16] thioantimonates (ca. 70 kJ/mol,[21,59] and zeolites (ca. 40–100 kJ/mol).[60]

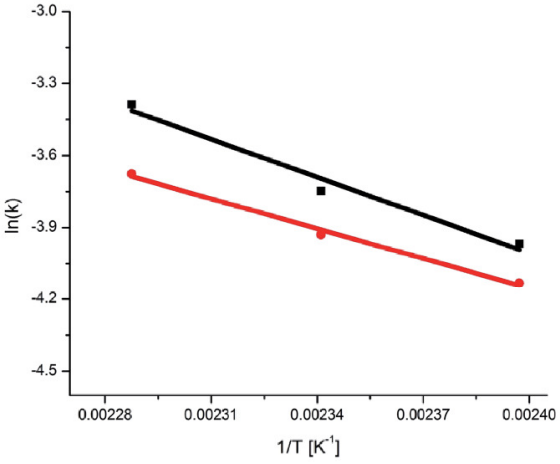

Figure 7. Arrhenius plots to determine the activation energies of the nucleation process (red) and crystal growth (black).

Conclusion

In situ XRD investigations were performed during the transformation of the $[V_{15}Sb_6O_{42}]^{6-}$ cluster into the layered compound

ChemPubSoc Europe

EurJIC European Journal of Inorganic Chemistry

Full Paper

[{Ni(en)$_2$}$_2$$V_{14}Sb_8O_{42}$]·5.5$H_2O$. The precursor is either dissolved or amorphized during heating to the desired reaction temperature. The dissolution or amorphization is reflected by an initial increase in intensity of the small-angle region in the X-ray powder patterns followed by a decrease of this signal once crystallization is observable. After disappearance of reflections of the precursor, an induction period follows, which becomes shorter with increasing reaction temperature. Kinetic evaluation of the data showed that nucleation is the rate-limiting step at all temperatures. The nucleation process is heterogeneous, which may be rationalized by the presence of X-ray-amorphous nanoparticles. The reaction progress depends on the temperature and crystallization is faster at higher temperatures. The activation energies for nucleation and crystal growth are low compared to those of other groups of compounds. Especially the low nucleation barrier is promising for further investigations concerning the synthesis of new Sb-POVs in short reaction times.

Experimental Section

Materials and Methods: The in situ XRD measurements were performed at DESY in Hamburg, Germany, at the beamlines P07b[61] and P08.[62] The data discussed herein were obtained at P08, and measurements were performed at P07b to ensure reproducibility. A Perkin–Elmer XRD1621 Flat Panel detector with a pixel size of 200 × 200 µm and an array size of 2048 × 2048 pixel was used. Laue crystals Si(111) and Si(220) and a single bounce monochromator (SBM) for P07b enabled a maximum beam size of 0.5 × 0.5 mm with an energy of 87 keV (λ = 0.14235 Å), and a Laue crystal Si(511) with a large-offset monochromator for P08 enabled a maximum beam size of 1 × 1 mm with an energy of 25 keV (λ = 0.4959 Å). The reactions were performed in Duran® glass vessels with a maximum volume of ca. 11 mL. These reaction vessels were heated in a custom-built reactor that was developed at CAU Kiel in collaboration with the beamline staff of beamline P08, PETRA III, DESY, and further details will be published in the near future. A PTFE-coated thermocouple is located inside the reaction vessel to monitor the temperature. The mixtures were stirred by using an electromagnetic stirring device. In situ XRD patterns could be collected every 30 s. The data were evaluated with the program "f3tools" which was developed by A. Rothkirch (Hasylab, DESY) and is already well established.[58,59,63] The compounds formed were further characterized by IR spectroscopy [Genesis FTIRTM spectrometer (ATI Mattson)], CHN elemental analysis (EUROEA Elemental Analyzer), and EDX (Philips ESEM XL30 equipped with an EDAX detector). Powder XRD patterns were recorded with a STOE STADI-P diffractometer equipped with a 1K Mythen detector in transmission geometry by using Cu-$K_{\alpha1}$ radiation (λ = 1.540598 Å).

Synthetic Details of the In Situ Experiments: The compound [Ni(en)$_3$]$_3${$V_{15}Sb_6O_{42}(H_2O)_x$}·≈15H_2O (**I**) was synthesized according to the literature.[45] NH_4VO_3, Sb_2O_3, and $NiCl_2$·6H_2O (Merck) as well as ethylenediamine (Grüssing) were purchased and used without further purification. Reaction times of days are not suitable for in situ XRD studies at synchrotron radiation facilities. Hence, the reaction time must be significantly reduced. In the past, we demonstrated for several solvothermal systems that the reaction time can be drastically reduced by stirring the mixture.[28,47] During experiments in the laboratory the shortest reaction times were identified for the reaction of compound **I** (0.045 mmol) with NH_4VO_3 (0.125 mmol) in a glass tube (inner volume 11 mL) and distilled water (4 mL). The syntheses were performed between 144 and 164 °C for 3 h while stirring the slurry (dynamic conditions). Powder XRD demonstrated that phase-pure **II** is formed in this temperature range. Elemental analysis: C 3.72, H 1.88, N 3.92 %; calcd. ($C_8H_{44}N_8Ni_2V_{14}Sb_8O_{47.5}$): C 3.40, H 1.57, N 3.97 %. EDX analysis: V 40.01, Sb 53.01, Ni 6.99 %; calcd. ($V_{14}Sb_8Ni_2$): V 39.5, Sb 54.0, Ni 6.5 %. For further characterization of the product (powder XRD, IR, SEM image), see Figures S1–S3.

Acknowledgments

We thank M. Köppen for programming the evaluation tools, the MATsynCELL project, and especially Prof. Dr. N. Stock for letting us use the in situ cell and DESY for allocation of beamtime. Furthermore, we would like to thank the HZG, Uta Rütt, Norbert Schell, and Karthick Perumal for their support at the beamlines.

Keywords: X-ray diffraction · Polyoxometalates · Structural transformation · Vanadium · Crystal growth

[1] N. Pienack, W. Bensch, *Angew. Chem. Int. Ed.* **2011**, *50*, 2014; *Angew. Chem.* **2011**, *123*, 2062.
[2] J. Keating, G. Sankar, T. I. Hyde, S. Kohara, K. Ohara, *Phys. Chem. Chem. Phys.* **2013**, *15*, 8555.
[3] U. Bentrup, J. Radnik, U. Armbruster, A. Martin, J. Leiterer, F. Emmerling, A. Brückner, *Top. Catal.* **2009**, *52*, 1350.
[4] O. Paris, C. Li, S. Siegel, G. Weseloh, F. Emmerling, H. Riesemeier, A. Erko, P. Fratzl, *J. Appl. Crystallogr.* **2007**, *40*, 466.
[5] M. Wuithschick, B. Paul, R. Bienert, A. Sarfraz, U. Vainio, M. Sztucki, R. Kraehnert, P. Strasser, K. Rademann, F. Emmerling, J. Polte, *Chem. Mater.* **2013**, *25*, 4679.
[6] J. Polte, R. Erler, A. F. Thünemann, S. Sokolov, T. T. Ahner, K. Rademann, F. Emmerling, R. Kraehnert, *ACS Nano* **2010**, *4*, 1076.
[7] J. Becker, M. Bremholm, C. Tyrsted, B. Pauw, K. M. O. Jensen, J. Eltzholt, M. Christensen, B. B. Iversen, *J. Appl. Crystallogr.* **2010**, *43*, 729.
[8] K. M. O. Jensen, C. Tyrsted, M. Bremholm, B. B. Iversen, *ChemSusChem* **2014**, *7*, 1594.
[9] M. Zobel, R. B. Neder, S. A. J. Kimber, *Science* **2015**, *347*, 292.
[10] J. Cravillon, C. A. Schroeder, R. Nayuk, J. Gummel, K. Huber, M. Wiebcke, *Angew. Chem. Int. Ed.* **2011**, *50*, 8067; *Angew. Chem.* **2011**, *123*, 8217.
[11] S. Saha, S. Springer, M. E. Schweinefuss, D. Pontoni, M. Wiebcke, K. Huber, *Cryst. Growth Des.* **2016**, *16*, 2002.
[12] J. Cravillon, C. A. Schroeder, H. Bux, A. Rothkirch, J. Caro, M. Wiebcke, *CrystEngComm* **2012**, *14*, 492.
[13] G. Muncaster, A. T. Davies, G. Sankar, C. R. A. Catlow, J. M. Thomas, S. L. Colston, P. Barnes, R. I. Walton, D. O'Hare, *Phys. Chem. Chem. Phys.* **2000**, *2*, 3523.
[14] K. M. Ø. Jensen, M. Christensen, P. Juhas, C. Tyrsted, E. D. Bøjesen, N. Lock, S. J. L. Billinge, B. B. Iversen, *J. Am. Chem. Soc.* **2012**, *134*, 6785.
[15] H. Jensen, M. Bremholm, R. P. Nielsen, K. D. Joensen, J. S. Pedersen, H. Birkedal, Y.-S. Chen, J. Almer, E. G. Sogaard, S. B. Iversen, B. B. Iversen, *Angew. Chem. Int. Ed.* **2007**, *46*, 1113; *Angew. Chem.* **2007**, *119*, 1131.
[16] L. Engelke, M. Schaefer, M. Schur, W. Bensch, *Chem. Mater.* **2001**, *13*, 1383.
[17] C. Tyrsted, J. Becker, P. Hald, M. Bremholm, J. S. Pedersen, J. Y. Chevallier, S. B. Iversen, B. B. Iversen, *Chem. Mater.* **2010**, *22*, 1814.
[18] F. Millange, R. El Osta, M. E. Medina, R. I. Walton, *CrystEngComm* **2011**, *13*, 103.
[19] R. Kiebach, M. Schaefer, F. Porsch, W. Bensch, *Z. Anorg. Allg. Chem.* **2005**, *631*, 369.
[20] A. Michailovski, J.-D. Grunwaldt, A. Baiker, R. Kiebach, W. Bensch, G. R. Patzke, *Angew. Chem. Int. Ed.* **2005**, *44*, 5643; *Angew. Chem.* **2005**, *117*, 5787.
[21] R. Kiebach, N. Pienack, M.-E. Ordolff, F. Studt, W. Bensch, *Chem. Mater.* **2006**, *18*, 1196.
[22] R. Kiebach, N. Pienack, W. Bensch, J.-D. Grunwaldt, A. Michailovski, A. Baiker, T. Fox, Y. Zhou, G. R. Patzke, *Chem. Mater.* **2008**, *20*, 3022.

ChemPubSoc Europe

EurJIC European Journal of Inorganic Chemistry

Full Paper

[23] Y. Zhou, E. Antonova, W. Bensch, G. R. Patzke, *Nanoscale* **2010**, *2*, 2412.
[24] Y. Zhou, E. Antonova, Y. Lin, J.-D. Grunwaldt, W. Bensch, G. R. Patzke, *Eur. J. Inorg. Chem.* **2012**, 783.
[25] Y. Zhou, Q. Zhang, Y. Lin, E. Antonova, W. Bensch, G. R. Patzke, *Sci. China Chem.* **2013**, *56*, 435.
[26] F. Millange, M. I. Medina, N. Guillou, G. Férey, K. M. Golden, R. I. Walton, *Angew. Chem. Int. Ed.* **2010**, *49*, 763; *Angew. Chem.* **2010**, *122*, 775.
[27] H. H.-M. Yeung, Y. Wu, S. Henke, A. K. Cheetham, D. O'Hare, R. I. Walton, *Angew. Chem. Int. Ed.* **2016**, *55*, 2012; *Angew. Chem.* **2016**, *128*, 2052.
[28] B. Seidlhofer, E. Antonova, J. Wang, D. Schinkel, W. Bensch, *Z. Anorg. Allg. Chem.* **2012**, *638*, 2555.
[29] I. Engelke, M. Schaefer, F. Porsch, W. Bensch, *Eur. J. Inorg. Chem.* **2003**, 506.
[30] L. Zhang, X. Zhao, J. Xu, T. Wang, *J. Chem. Soc., Dalton Trans.* **2002**, 3275.
[31] R. Kiebach, C. Näther, W. Bensch, *Solid State Sci.* **2006**, *8*, 964.
[32] E. Antonova, C. Näther, W. Bensch, *CrystEngComm* **2012**, *14*, 6853.
[33] E. Antonova, C. Näther, P. Kögerler, W. Bensch, *Dalton Trans.* **2012**, *41*, 6957.
[34] E. Antonova, C. Näther, W. Bensch, *Dalton Trans.* **2012**, *41*, 1338.
[35] E. Antonova, A. Wutkowski, C. Näther, W. Bensch, *Solid State Sci.* **2011**, *13*, 2154.
[36] K. Yu. Monakhov, W. Bensch, P. Kögerler, *Chem. Soc. Rev.* **2015**, *44*, 8443.
[37] E. Antonova, P. Kögerler, C. Näther, W. Bensch, *Angew. Chem. Int. Ed.* **2011**, *50*, 764; *Angew. Chem.* **2011**, *123*, 790.
[38] E. Antonova, C. Näther, P. Kögerler, W. Bensch, *Inorg. Chem.* **2012**, *51*, 2311.
[39] A. Wutkowski, C. Näther, P. Kögerler, W. Bensch, *Inorg. Chem.* **2013**, *52*, 3280.
[40] H. Lühmann, C. Näther, P. Kögerler, W. Bensch, *Inorg. Chim. Acta* **2014**, *421*, 549.
[41] X.-X. Hu, J.-Q. Xu, X.-B. Cui, J.-F. Song, T.-G. Wang, *Inorg. Chem. Commun.* **2004**, *7*, 264.
[42] Y. Gao, Z. Han, Y. Xu, C. Hu, *J. Cluster Sci.* **2010**, *21*, 163.
[43] A. Wutkowski, C. Näther, P. Kögerler, W. Bensch, *Inorg. Chem.* **2008**, *47*, 1916.
[44] E. Antonova, B. Seidlhofer, J. Wang, M. Hinz, W. Bensch, *Chem. Eur. J.* **2012**, *18*, 15316.
[45] M. Wendt, U. Warzok, C. Näther, J. van Leusen, P. Kögerler, C. A. Schalley, W. Bensch, *Chem. Sci.* **2016**, *7*, 2684.
[46] L. Yu, J.-P. Liu, J.-P. Wang, J.-Y. Niu, *Chem. Res. Chin. Univ.* **2009**, *25*, 426.
[47] M. Wendt, C. Näther, W. Bensch, *Chem. Eur. J.* **2016**, *22*, 7747.
[48] M. Avrami, *J. Chem. Phys.* **1941**, *9*, 177.
[49] M. Avrami, *J. Chem. Phys.* **1940**, *8*, 212.
[50] M. Avrami, *J. Chem. Phys.* **1939**, *7*, 1103.
[51] J. D. Hancock, J. H. Sharp, *J. Am. Ceram. Soc.* **1972**, *55*, 74.
[52] A. F. Gualtieri, *Phys. Chem. Miner.* **2001**, *28*, 719.
[53] J. H. Sharp, G. W. Brindley, B. N. N. Achar, *J. Am. Ceram. Soc.* **1966**, *49*, 379.
[54] T. Ahnfeldt, J. Moellmer, V. Guillerm, R. Staudt, C. Serre, N. Stock, *Chem. Eur. J.* **2011**, *17*, 6462.
[55] T. Ahnfeldt, N. Stock, *CrystEngComm* **2012**, *14*, 505.
[56] F. Niekiel, M. Ackermann, P. Guerrier, A. Rothkirch, N. Stock, *Inorg. Chem.* **2013**, *52*, 8699.
[57] H. Reinsch, N. Stock, *CrystEngComm* **2013**, *15*, 544.
[58] C. Schmidt, N. Stock, *Cryst. Growth Des.* **2011**, *11*, 5682.
[59] B. Seidlhofer, N. Pienack, W. Bensch, *Z. Naturforsch. B* **2010**, *65*, 937.
[60] R. W. Thompson in *Molecular Sieves, Science and Technology*, vol. 1 (Eds.: H. G. Karge, J. Weitkamp), Springer, Berlin, **1998**, p. 21.
[61] N. Schell, A. King, F. Beckmann, T. Fischer, M. Müller, A. Schreyer, *Mater. Sci. Forum* **2014**, *772*, 57.
[62] O. H. Seeck, C. Deiter, K. Pflaum, F. Bertam, A. Beerlink, H. Franz, J. Horbach, H. Schulte-Schrepping, B. M. Murphy, M. Greve, O. Magnussen, *J. Synchrotron Radiat.* **2012**, *19*, 30.
[63] C. Schmidt, M. Feyand, A. Rothkirch, N. Stock, *J. Solid State Chem.* **2012**, *188*, 44.

Received: August 18, 2016
Published Online: October 27, 2016

4.2. Die Publikation *„Conformational Isomerism in Polyoxovanadates"*

Der Einsatz des Precursors Ni-$\{V_{15}Sb_6\}$ ermöglichte die Synthese eines neuen Isomers des $\{V_{14}Sb_8O_{42}\}$-Clusters. Die chemische Reaktion wird durch einen Ligandenaustausch im $[Ni(en)_3]^{2+}$-Komplex durch cyclen eingeleitet.

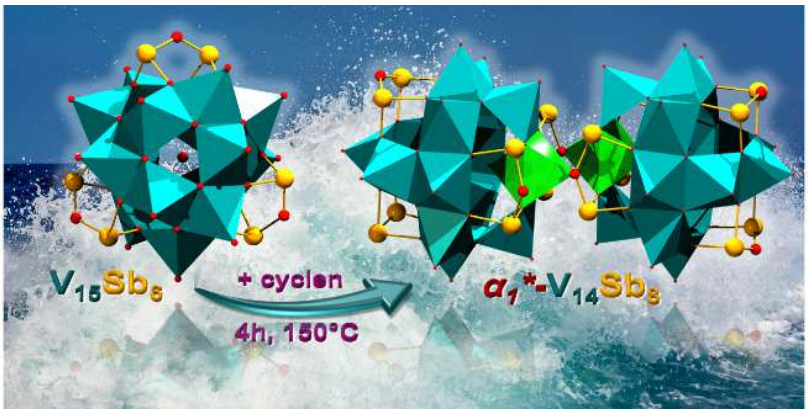

Abbildung 19: TOC Grafik der Publikation *„Conformational Isomerism in Polyoxovanadates"*.

Das α*-Konfigurationsisomer hat im Gegensatz zu allen bisher bekannten Polyoxovanadatschalen eine nach innen gerichtete Vanadyleinheit. Zwischen benachbarten Cluster werden kurze Sb-O···V- sowie Sb-O···Sb-Abstände gefunden, welche kovalenten Bindungen entsprechen. Diese supramolekulare Wechselwirkungen führen zur Bildung eines $\{V_{14}Sb_8O_{42}\}_2$-Dimers, welches im Festkörper ausgebildet wird. Dieses Dimer wurde in Lösung mit ESI-MS-Experimenten nachgewiesen und intensiv in der Gasphase untersucht. Ergebnisse von DFT-Rechnungen zeigten, dass das Isomer ca. 50 bzw. 12 kJ/mol energiereicher ist als die bereits bekannten α- und β-Isomere. Außerdem wurden mit diesen Rechnungen weitere mögliche Isomere mit nach innen gerichteter Vanadyleinheit der $\{V_{14}Sb_8O_{42}\}$-Cluster vorhergesagt.

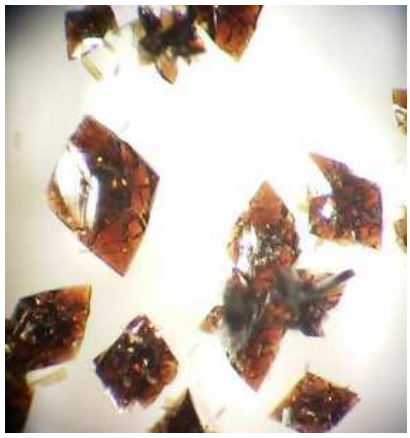

Abbildung 18: Foto der Kristalle des α*-Isomers.

Veröffentlicht in *Angew. Chem.* **2018**, *130*, 3024.
DOI: 10.1002/ange.201712417
Angew. Chem. Int. Ed. **2018**, *57*, 2972.
DOI: 10.1002/anie.201712417

GDCh Zuschriften Angewandte Chemie

Polyoxometallate

Deutsche Ausgabe: DOI: 10.1002/ange.201712417
Internationale Ausgabe: DOI: 10.1002/anie.201712417

Konfigurationsisomerie in Polyoxovanadaten

Lisa K. Mahnke, Aleksandar Kondinski, Ulrike Warzok, Christian Näther, Jan van Leusen, Christoph A. Schalley, Kirill Yu. Monakhov,* Paul Kögerler* und Wolfgang Bensch**

Abstract: *Ein wasserlöslicher Abkömmling des Polyoxovanadat-Archetyps $\{V_{15}E_6O_{42}\}$ (E = Halbmetall) ermöglicht die Untersuchung supramolekular induzierter Clusterschalen-Umwandlungen. Eine für E = Sb spezifische Reaktion, die durch einen Ligandenaustausch in $[Ni(ethylendiamin)_3]^{2+}$-Gegenionen eingeleitet wird, resultiert in der Bildung des metastabilen α_1*-Konfigurationsisomers des $\{V_{14}Sb_8O_{42}\}$-Clustertyps. Im Unterschied zu allen bisher bekannten Polyoxovanadat-Schalenarchitekturen weist dieses Isomer eine nach innen ausgerichtete Vanadylgruppe auf und ist ca. 50 bzw. 12 kJ mol^{-1} energiereicher als die zuvor isolierten α- und β-Isomere. Diese unerwartete Reaktion wird im Hinblick auf supramolekulare Sb-O···V- und Sb-O···Sb-Bindungen diskutiert, die sich in $\{V_{14}Sb_8O_{42}\}_2$-Dimeren im Festkörper manifestieren. ESI-MS-Experimente untermauern die Stabilität dieser Dimere auch in Lösung und in der Gasphase. DFT-Rechnungen zufolge sollten so auch weitere, bislang noch nicht gefundene $\{V_{14}Sb_8\}$-Isomere zugänglich sein.*

Halbmetall-funktionalisierte Polyoxovanadate[1] (POVs) werden vorwiegend unter solvothermalen Bedingungen gebildet. Dies beschränkt die Verwendung der für Polyoxomolybdate und -wolframate entwickelten vielseitigen Synthesetechniken zur gezielten Beeinflussung der Selbstorganisationsmechanismen, die aber tiefere Temperaturen voraussetzen.[2] Dementsprechend sind die Synthesen von Halbmetall-funktionalisierten POVs oftmals aus Zufallsentdeckungen hervorgegangen. In der am besten untersuchten Klasse der Antimonato-POVs (Sb-POVs)[3] sind darüber hinaus die isolierbaren Clusterverbindungen üblicherweise nahezu unlöslich, was die Untersuchung von Folgereaktionen limitiert. Mit der wasserlöslichen Sb-POV-Verbindung $\{Ni(en)_3\}_3[V^{IV}{}_{15}Sb^{III}{}_6O_{42}(H_2O)_x]\cdot$ca. $15\,H_2O$ (**1**; $x = 0, 1$; en = Ethylendiamin) entdeckten wir jüngst eine geeignete Vorstufe für die In-situ-Erzeugung neuartiger Sb-POV-Verbindungen.[4,5] Die Zugabe von Cyclen (1,4,7,10-Tetraazacyclododecan) zu einer wässrigen Lösung dieses Reaktanten führte zur schnellen Bildung von $\{Ni(cyclen)(en)\}_2[V_{14}Sb_8O_{42}(H_2O)]\cdot$ca. $10\,H_2O$ (**2**), das einen $\{V_{14}Sb_8O_{42}\}$-Cluster in Form seines α_1*-Isomers aufweist. Darin ist eine der eckenverknüpften VO_5-Pyramiden invertiert (also ins Clusterinnere hin orientiert), was die Molekülsymmetrie auf C_{2v} reduziert. Verbindung **2** enthält das erste Hetero-POV, das Konfigurationsisomerie aufweist. Da die Isomerisierung der Vanadylgruppen an verschiedenen Positionen stattfinden kann, können für dieses Sb-POV zudem weitere Regioisomere unterschieden werden,[6] was die Synthese und Isolierung eines bestimmten Isomers erschweren kann.

Die Strukturen aller bislang bekannten Sb-POV-Clusterschalen lassen sich vom $\{V^{IV}{}_{18}O_{42}\}$-Archetyp ableiten, in dem zwei, drei oder vier quadratische $\{VO_5\}$-Pyramiden durch hantelförmige $\{Sb^{III}{}_2O_5\}$-Einheiten ersetzt werden. Von allen möglichen $[V_{14}Sb_8O_{42}(H_2O)]^{4-}$-Isomeren (siehe Abbildung S1 in den Hintergrundinformationen) wurden bisher das D_{2d}-symmetrische α-[7] und das D_{2h}-symmetrische β-Isomer[8–13] beobachtet. Alle Isomere enthalten einen Ring aus acht kantenverknüpften VO_5-Pyramiden, der von oben und unten mit Bögen aus drei kantenverknüpften VO_5-Pyramiden überbrückt wird. Deren Orientierung relativ zueinander differenziert das $\alpha(90°)$-, das $\beta(0°)$- und das (hypothetische) $\gamma(45°)$-Isomer. Sb_2O-Hanteln überbrücken die vier Nischen zwischen den beiden V_3-Bögen und dem V_8-Ring, wobei jedes Sb-Atom an ein O-Atom des V_8-Rings und ein O-Atom eines V_3-Bogens gebunden ist. Während in den α-, β- und γ-Isomeren alle V=O-Gruppen nach außen gerichtet sind, ist der zentrale Hohlraum in der $\{V_{14}Sb_8O_{42}\}$-Struktur ausreichend groß für eine nach innen orientierte Vanadylgruppe, womit elf zusätzliche, hypothetische Isomere möglich werden (α_{1-4}*, β_{1-3}*, γ_{1-4}*; Schema 1 sowie Abbildungen S1 und S2).

Verbindung **2** kristallisiert in der monoklinen Raumgruppe $P2_1/n$ mit allen Atomen auf allgemeinen Positionen. Die verzerrt oktaedrischen N_6-Koordinationsumgebungen der Ni^{2+}-Zentren werden von einem Cyclen- und einem en-Liganden gebildet (Ni-N: 2.096(11)–2.155(10) Å). Innerhalb der Clusterschale des α_1*-$\{V_{14}Sb_8O_{42}\}$-Isomers in **2** ist die mittlere Vanadylgruppe eines der V_3-Bögen nach innen ausgerichtet (V7-O42; Abbildung 1). Diese einzigartige „out-in-out"-Konfiguration der VO_5-Pyramiden bewirkt einen V-V-V-Winkel von etwa 162° (gegenüber 132° für die übliche „out-

[*] M. Sc. L. K. Mahnke, Prof. Dr. C. Näther, Prof. Dr. W. Bensch
Institut für Anorganische Chemie
Christian-Albrechts-Universität zu Kiel
24118 Kiel (Deutschland)
E-Mail: wbensch@ac.uni-kiel.de
Dr. A. Kondinski, Dr. J. van Leusen, Dr. K. Yu. Monakhov, Prof. Dr. P. Kögerler
Institut für Anorganische Chemie
RWTH Aachen University
52074 Aachen (Deutschland)
E-Mail: kirill.monakhov@ac.rwth-aachen.de
paul.koegerler@ac.rwth-aachen.de
M. Sc. U. Warzok, Prof. Dr. C. A. Schalley
Institut für Chemie und Biochemie
Freie Universität Berlin
Takustraße 3, 14195 Berlin (Deutschland)
E-Mail: c.schalley@fu-berlin.de
Dr. A. Kondinski
Derzeitige Adresse: Department of Chemistry
KU Leuven, Celestijnenlaan 200F, 3001 Leuven (Belgien)
Hintergrundinformationen und die Identifikationsnummern (ORCIDs) einiger Autoren sind unter: https://doi.org/10.1002/ange.201712417 zu finden.

GDCh Zuschriften Angewandte Chemie

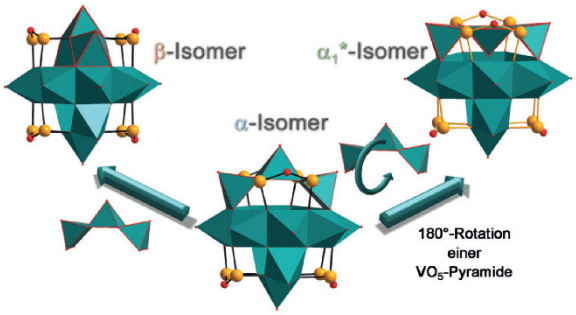

Schema 1. Ausgewählte Isomere des $\{V_{14}Sb_8O_{42}\}$-Clusters (V türkis, Sb gelb, O rot); es variiert der in Rot umrandet hervorgehobene V_3-Bogen.

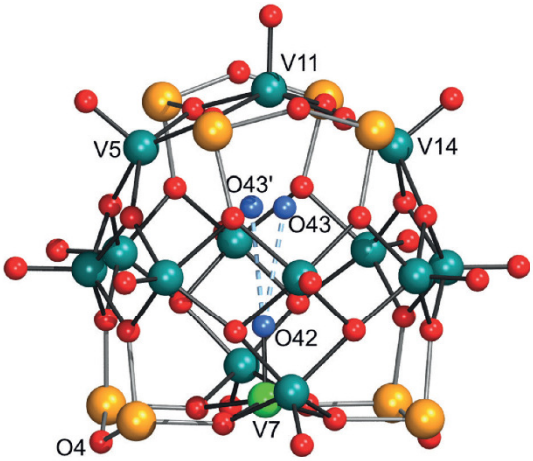

Abbildung 1. Kugel-Stab-Darstellung der Molekülstruktur des α_1*-Isomers von $\{V_{14}Sb_8O_{42}\}$ in **2**. O rot, Sb orange, V türkis, Sb-O-Bindungen hellgrau, V-O dunkelgrau. Hervorgehoben sind V7 (grün) und O42 (blau) der invertierten VO_5-Pyramide sowie die 50:50-fehlgeordneten O43/O43′-Positionen des H_2O-Gastes.

out-out"-Konfiguration). Alle anderen geometrischen Parameter entsprechen denen bekannter POV-Strukturen.[4,5,7–14] Die Bindungsvalenzsummen (BVS) für Sb reichen von 3.14 bis 3.57 (im Mittel 3.35) und von 3.71 bis 4.05 (im Mittel 3.98) für V und bestätigen die formalen Oxidationszahlen V^{IV} und Sb^{III}.[15]

Das endständige O42-Atom der V(7)O_5-Pyramide ist in Reichweite für eine Wasserstoffbrücke (2.6 Å) zum zentralen H_2O-Gastmolekül, das über zwei Positionen fehlgeordnet ist (50:50). Der H_2O-Gast ist zu V11 (gegenüber V7) hin verschoben, was kleine V11-O43/O43′(H_2)-Abstände von 2.58/2.65 Å bewirkt. Darüber hinaus betragen die kleinsten V5/V14-O43(H_2)-Abstände etwa 2.75 Å, in deutlichem Gegensatz zum α-$[V_{14}Sb_8O_{42}(H_2O)]^{4-}$-Polyanion mit kleinsten V-O-(H_2)-Abständen von ca. 3.7 Å.[6–12]

Eine V7-O4-Intercluster-Bindung (2.348(2) Å) erweitert die Koordinationsumgebung von V7 in eine oktaedrische und erhöht seine BVS von 3.71 auf 3.92 (Abbildung 2), womit ein $[V_{28}Sb_{16}O_{84}(H_2O)_2]^{8-}$-Anion mit zwei VO_6-Oktaedern gebildet wird, was bislang einmalig in der Chemie der Polyoxovanadate ist. Die meisten $\{V_{14}Sb_8O_{42}\}$-Verbindungen weisen zwischen benachbarten Clustern supramolekulare Sb-O···Sb-Abstände von 2.73 bis 2.96 Å auf,[7–13] die auch in der Kristallstruktur von **2** vorhanden sind, in der die α_1*-$[V_{14}Sb_8O_{42}(H_2O)]^{4-}$-Clusterschalen kurze Sb-O···Sb-intra-Dimer-Kontakte (2.71 und 2.76 Å) aufweisen.[16] Zusätzliche schwache Sb-O···Sb-inter-Dimer-Kontakte (2.91 Å) ordnen die Cluster in Ketten entlang [100] (Abbildungen S12 und S13).

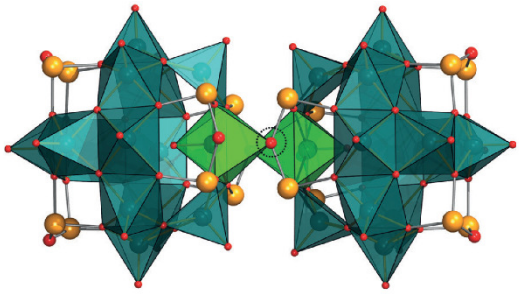

Abbildung 2. V(7)O_6-Oktaeder (grün) verbinden benachbarte Polyanionen zu $\{V_{14}Sb_8\}_2$-Dimeren in **2** (umkreist: O4).

Elektrosprayionisations-Massenspektrometrie (ESI-MS) ermöglicht die Überführung von intakten, nicht-kovalent gebundenen Komplexen wie dem Clusterdimer in **2** aus der Lösung in die Gasphase und erlaubt somit einen Einblick in dessen Struktur und Reaktivität. Das im negativen Ionisationsmodus aufgenommene ESI-Massenspektrum einer wässrigen Lösung von **2** (60 μM) zeigt Signale der intakten Clusterionen $[\mathbf{N}{\cdot}H_2O]^{3-}$/$[\mathbf{N}{\cdot}H{\cdot}H_2O]^{3-}$ und $[\mathbf{N}{\cdot}H_2O]^{2-}$/$[\mathbf{N}{\cdot}H{\cdot}H_2O]^{2-}$ bei *m/z* 792 bzw. 1188 sowie $[\mathbf{N}{\cdot}H_2O{\cdot}Ni(cyclen)]^{2-}$/$[\mathbf{N}{\cdot}H{\cdot}H_2O{\cdot}Ni(cyclen)]^{2-}$ bei *m/z* 1304 als die häufigsten Spezies ($\mathbf{N} = \{V_{14}Sb_8O_{42}\}$; Abbildung 3). **N** durchläuft im Ionisationsprozess eine oder zwei Ein-Elektronen-Oxidationsreaktionen von V^{IV} nach V^{V}, was in zwei- und dreifach geladenen Anionen resultiert, wenn die Clusterionen nicht mit Kationen gepaart sind. Das Massenspektrum von **2** ist ähnlich dem seiner eingehend untersuchten Vorstufe **1**[4] (siehe Abbildung S18 für eine detaillierte Analyse des Isotopenmusters). Von besonderer Bedeutung sind die ausgeprägten Peaks, die den dimeren Komplexen $[\mathbf{N}{\cdot}H_2O{\cdot}Ni(cyclen)]_2^{4-}$/$[\mathbf{N}{\cdot}H{\cdot}H_2O{\cdot}Ni(cyclen)]_2^{4-}$ und $[\mathbf{N}{\cdot}H_2O{\cdot}Ni(cyclen)]_2^{3-}$/$[\mathbf{N}{\cdot}H{\cdot}H_2O{\cdot}Ni(cyclen)]_2^{3-}$ bei *m/z* 1304 und 1738 zugeordnet

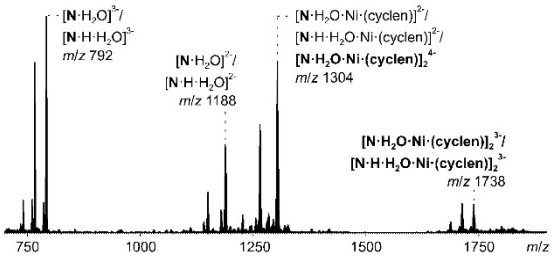

Abbildung 3. ESI-Q-TOF-HR-Massenspektrum von **2** (60 μM in H_2O, $\mathbf{N} = \{V_{14}Sb_8O_{42}\}$). Eine detaillierte Analyse und Diskussion finden sich in den Hintergrundinformationen.

werden können. Diese Komplexe bestehen formal entweder aus zwei dreifach geladenen oder einem dreifach und einem zweifach geladenen Clusterkern sowie einem ladungskompensierenden Ni^{2+}-Komplex. Die Peaks des vierfach negativ geladenen Dimerkomplexes und des zweifach geladenen monomeren Clusters überlappen einander bei gleichem *m/z*-Wert, können aber mittels Traveling-Wave-Ionenmobilitäts-Massenspektrometrie aufgetrennt werden (Abbildung S19). Die dimeren Ionen werden in einem weiten Konzentrationsbereich beobachtet, was darauf schließen lässt, dass die Dimerbildung nicht auf bloße unspezifische Aggregation während des ESI-Prozesses zurückgeht. Darüber hinaus zeigt ein Kontrollexperiment mit dem α-$\{V_{14}Sb_8O_{42}\}$-Isomer[17] keine Dimerbildung (Abbildung S20). Demnach ist die nicht-kovalente Inter-Cluster/Intra-Dimer-Sb-O···V-Bindung spezifisch für das α_1*-$\{V_{14}Sb_8O_{42}\}$-Isomer in **2** und sowohl in Lösung als auch in der Gasphase vorhanden.

Schon unmittelbar nach der solvothermalen Synthese von **2** und der Filtration der Reaktionslösung wurde die Bildung von **N** und dem entsprechenden Dimer im ESI-MS beobachtet (Abbildungen S21 und S22), ebenso wie Ionen des Reaktanten **1**. Demnach ist die Bildung des α_1*-Clusterkerns schon beim Erhitzen der Reaktionslösung abgeschlossen. Das Produkt fiel innerhalb von drei Tagen (teilweise) aus der Reaktionslösung aus, und die Intensität der von **2** abgeleiteten Peaks verringerte sich.

Darauf untersuchten wir die Gasphasenreaktivität des α_1*-Dimers, indem zunächst die $[\mathbf{N}{\cdot}H_2O{\cdot}Ni(cyclen)]_2^{3-}$/$[\mathbf{N}{\cdot}H{\cdot}H_2O{\cdot}Ni(cyclen)]_2^{3-}$-Ionen bei *m/z* 1738 massenselektiert und danach kollisionsinduzierter Dissoziierung ausgesetzt wurden (CID; Abbildung 4). Die auffälligste Fragmentierung besteht in der Spaltung der dimeren in monomere Ionen, gefolgt von der Abspaltung von Wasser und Hydroxyl-Radikalen, vergleichbar dem zuvor beschriebenen, in situ gebildeten $\{V_{14}Sb_8\}$-Cluster (Abbildung S23).[4] Interessanterweise kann ein zweiter Fragmentierungsprozess hiermit konkurrieren: Die direkte Abspaltung von zwei neutralen H_2O- und OH-Gruppen aus den intakten $[\mathbf{N}{\cdot}H_2O{\cdot}Ni(cyclen)]_2^{3-}$/$[\mathbf{N}{\cdot}H{\cdot}H_2O{\cdot}Ni(cyclen)]_2^{3-}$-Ionen, was im dimeren $[(\mathbf{N}{\cdot}H\text{-}OH){\cdot}Ni(cyclen)]_2^{3-}$-Komplex resultiert (Abbildung 4). Da der erste Fragmentierungsverlauf infolge verringerter Coulomb-Abstoßung klar favorisiert ist, weist der weniger

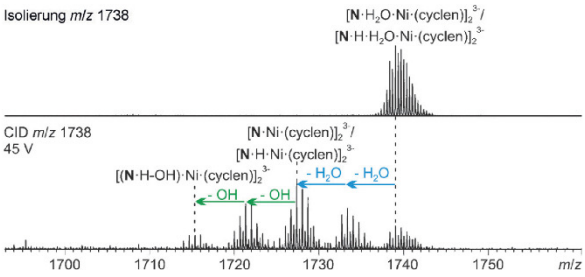

Abbildung 4. Tandem-MS-Experiment mit den massenselektierten Ionen $[\mathbf{N}{\cdot}H_2O{\cdot}Ni(cyclen)]_2^{3-}$/$[\mathbf{N}{\cdot}H{\cdot}H_2O{\cdot}Ni(cyclen)]_2^{3-}$ ($\mathbf{N} = \{V_{14}Sb_8O_{42}\}$).

ausgeprägte, aber dennoch charakteristische Verlust von Neutralspezies aus dem dimeren Komplex auf eine bemerkenswerte Bindungsenergie zwischen den beiden α_1*-Monomeren in der Gasphase hin.

Die Bildung von α_1*-$[V_{14}Sb_8O_{42}]^{4-}$ und seine Stabilität relativ zu jener der anderen $[V_{14}Sb_8O_{42}]^{4-}$-Isomere wurde mittels relativistischer Dichtefunktionaltheorie (DFT) untersucht. Eine DFT-basierte Geometrieoptimierung der Polyoxoanionen zeigte eine gute Übereinstimmung mit den experimentell abgeleiteten Strukturparametern (Tabelle S1), und die Simulationen ergaben die Spin-Elektronendichten für das voll reduzierte Polyanion α_1*-$[V_{14}Sb_8O_{42}]^{4-}$, mit je einem Elektron in den d_{xy}/d_{yz}-Orbitalen eines jeden V-Zentrums (Abbildung S4), in Übereinstimmung mit den BVS. Dem publizierten Standardprotokoll[18] folgende Rechnungen zeigten, dass die Gesamtbindungsenergie E_b von α_1*-$[V_{14}Sb_8O_{42}]^{4-}$ um ca. 50, 33 bzw. 12 kJ mol^{-1} höher liegt als die der „konventionellen" α-/γ-/β-$[V_{14}Sb_8O_{42}]^{4-}$-Isomere und dieses daher thermodynamisch weniger stabil ist (Tabelle S3). Im Vergleich zu den anderen zehn Regioisomeren ist der E_b-Wert von α_1*-$[V_{14}Sb_8O_{42}]^{4-}$ etwa vergleichbar dem des γ_2*- und des γ_4*-Isomers ($\Delta E_b < 1$ kJ mol^{-1}), während α_2* und α_4* energetisch um 21 bzw. 15 kJ mol^{-1} günstiger sind. Alle anderen Regioisomere liegen energetisch deutlich über α_1* (Abbildung S5). α_1*-$\{V_{14}Sb_8O_{42}\}$ und seine $\{V_{15}Sb_6O_{42}\}$-Vorstufe sind strukturell über ein gemeinsames $\{V_7Sb_4O_{21}\}$-Fragment verbunden (Abbildung 5), das aus fünf quadratischen $\{VO_5\}$-Pyramiden, zwei $\{Sb_2O_5\}$-Einheiten und zwei daran endständig gebundenen Vanadylgruppen besteht. Die gewölbten $\{V_7Sb_4O_{21}\}$-Fragmente können in Bezug auf die Orientierung der V=O-Gruppen Konfigurationsisomere bilden. Diese Isomerisierung innerhalb der $\{V_7Sb_4O_{21}\}$-Fragmente ist als Auslöser für die Bildung von α_1*-$\{V_{14}Sb_8O_{42}\}$ wahrscheinlicher als der alternative Reaktionspfad – die direkte Isomerisierung von α-$\{V_{14}Sb_8O_{42}\}$ zu α_1*-$\{V_{14}Sb_8O_{42}\}$ (Schema 1) –, der infolge sterischer Beschränkungen mit hohen Energiebarrieren für eine Rotation der V=O-Einheit verbunden wäre. Da α_1*-$\{V_{14}Sb_8O_{42}\}$ ausschließlich aus der $\{V_{15}Sb_6O_{42}\}$-Vorstufe herstellbar ist, ist vermutlich das entscheidende Synthon das $\{V_7Sb_4O_{21}\}$-Fragment, das zudem nur in den α-$\{V_{14}Sb_8O_{42}\}$- und α*-$\{V_{14}Sb_8O_{42}\}$-Strukturen auftritt. Untermauert wird dies dadurch, dass die formale Dimerisierung der verschiedenen $\{V_7Sb_4O_{21}\}$-Konfigurationsisomere ausschließlich zu den α-$\{V_{14}Sb_8O_{42}\}$-, α_1*-$\{V_{14}Sb_8O_{42}\}$- und

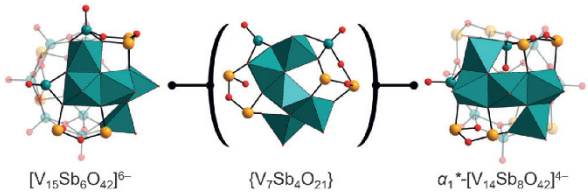

Abbildung 5. Das gemeinsame $\{V_7Sb_4O_{21}\}$-Fragment (Mitte), das in den Polyanionen $[V_{15}Sb_6O_{42}]^{6-}$ (links) und α_1*-$[V_{14}Sb_8O_{42}]^{4-}$ (rechts) enthalten ist (Farbschema wie in Abbildung 2).

α_4*-$\{V_{14}Sb_8O_{42}\}$-Strukturen führen kann. Die zugehörigen relativen Energien und das Konzept des $\{V_7Sb_4O_{21}\}$-Synthons grenzen die Umwandlungen des $\{V_{15}Sb_6O_{42}\}$-Gerüsts effektiv auf die α-/α*-$\{V_{14}Sb_8O_{42}\}$-Cluster ein.

Die unerwartete solvothermale Bildung des energetisch hoch liegenden α_1*-$\{V_{14}Sb_8O_{42}\}$-Konfigurationsisomers ist das Ergebnis verschiedener schwächerer kooperativer Effekte, die von Änderungen in der Koordinationssphäre der Gegenionen bis hin zu intramolekularen nichtkovalenten Wechselwirkungen sowie Sb-O···V- und Sb-O···Sb-Kontakten zwischen den Clustern reicht. Die Einkristallstrukturanalyse und ESI-MS-Experimente bestätigen das Auftreten ungewöhnlich stabiler α_1*-$\{V_{14}Sb_8O_{42}\}$-Dimere im Festkörper, in Lösung und in der Gasphase. Die Notwendigkeit einer Vorstufenstruktur, die schon eine kritische Untermenge an Strukturmerkmalen vorgebildet enthält, geht aus der Tatsache hervor, dass andere V/Sb-Vorstufen unter ansonsten identischen Synthesebedingungen nicht zu **2** führen. DFT-Rechnungen lassen auf interessante elektronische Eigenschaften der α_1*-$[V_{14}Sb_8O_{42}]^{4-}$-Spezies schließen, die bestimmte Folgereaktionen möglich machen könnten (siehe Hintergrundinformationen), während die mittlere relative Stabilität des α_1*-Isomers in Relation zu den anderen Isomeren nahelegt, dass supramolekulare Aspekte offenbar eine Schlüsselrolle für die Bildung und Isolierung dieser dimeren Cluster einnehmen. Weitere Regio- und Konfigurationsisomere des $\{V_{14}Sb_8\}$-Typs sollten daher realisierbar sein.

Experimentelles

Alle Ausgangsmaterialien wurden ohne vorherige Aufreinigung verwendet. Die Vorstufe $\{Ni(en)_3\}_3[V_{15}Sb_6O_{42}(H_2O)_x]\cdot$ca. $15\,H_2O$ (**1**) wurde gemäß Literaturvorschrift synthetisiert.[3] Verbindung **2**[19] wurde unter Solvothermalbedingungen in DURAN-Glasröhren mit einem Reaktionsvolumen von 11 mL synthetisiert. 0.1373 g (0.045 mmol) der Vorstufe **1** ($\{Ni(en)_3\}_3[V_{15}Sb_6O_{42}(H_2O)_x]\cdot$ca. $15\,H_2O$) wurden mit 0.0240 g (0.135 mmol) Cyclen und 4 mL entionisiertem Wasser in der Glasröhre gemischt und 4 h unter Rühren auf 150 °C erhitzt. Die heiße Reaktionsmischung wurde abfiltriert und das Filtrat in einem Schnappdeckelgläschen aufbewahrt. Nach neun Tagen wurden rhomboedrische Kristalle von **2** durch Filtration abgetrennt und mit entionisiertem Wasser und Ethanol gewaschen. Ausbeute: ca. 10 mg; weitere Details siehe Hintergrundinformationen. Elementaranalyse [%] für $C_{40}H_{112}N_{24}Ni_4O_{86}Sb_{16}V_{28}$ (5914.7 g mol^{-1}): gef.: C 8.09, H 2.06, N 5.45 %; ber.: C 8.12, H 1.91, N 5.68. EDX-Analyse [%] für $V_{14}Sb_8Ni_2$: gef.: V 39.55, Sb 53.71, Ni 6.74; ber.: V 39.52, Sb 53.97, Ni 6.50.

Danksagung

Diese Arbeit wurde vom Land Schleswig-Holstein und der Deutschen Forschungsgemeinschaft (DFG, CRC 1109) unterstützt. K.Y.M. dankt der DFG für ein Emmy-Noether-Stipendium. Wir danken Michael Wendt für Vorarbeiten.

Interessenkonflikt

Die Autoren erklären, dass keine Interessenkonflikte vorliegen.

Stichwörter: Antimonatopolyoxovanadate · Dichtefunktionalrechnungen · ESI-MS · Konfigurationsisomerie

Zitierweise: *Angew. Chem. Int. Ed.* **2018**, *57*, 2972–2975
Angew. Chem. **2018**, *130*, 3024–3028

[1] K. Y. Monakhov, W. Bensch, P. Kögerler, *Chem. Soc. Rev.* **2015**, *44*, 8443.
[2] Siehe z. B. a) L. Vilà-Nadal, A. Rodríguez-Fortea, L.-K. Yan, E. F. Wilson, L. Cronin, J. M. Poblet, *Angew. Chem. Int. Ed.* **2009**, *48*, 5452; *Angew. Chem.* **2009**, *121*, 5560; b) Z.-L. Lang, W. Guan, L.-K. Yan, S.-Z. Wen, Z.-M. Su, L.-Z. Hao, *Dalton Trans.* **2012**, *41*, 11361.
[3] H.-Y. Guo, X. Zhang, X.-B. Cui, Q.-S. Huo, J.-Q. Xu, *CrystEngComm* **2016**, *18*, 5130.
[4] M. Wendt, U. Warzok, C. Näther, J. van Leusen, P. Kögerler, C. A. Schalley, W. Bensch, *Chem. Sci.* **2016**, *7*, 2684.
[5] M. Wendt, C. Näther, W. Bensch, *Chem. Eur. J.* **2016**, *22*, 7747.
[6] Siehe z. B. a) M. T. Pope, T. F. Scully, *Inorg. Chem.* **1975**, *14*, 953; b) L. Pettersson, I. Andersson, J. H. Grate, A. Selling, *Inorg. Chem.* **1994**, *33*, 982; c) „Complexity in Chemistry and Beyond": L. Vilà-Nadal, S. Romo, X. López, J. M. Poblet in *NATO Science for Peace and Security Series B* (Hrsg.: C. Hill, D. G. Musaev), Springer, Dordrecht, **2012**; d) S. Spillane, R. Sharma, A. Zavras, R. Mulder, C. A. Ohlin, L. Goerigk, R. J. O'Hair, C. Ritchie, *Angew. Chem. Int. Ed.* **2017**, *56*, 8568; *Angew. Chem.* **2017**, *129*, 8691.
[7] X.-X. Hu, J.-Q. Xu, X.-B. Cui, J.-F. Song, T.-G. Wang, *Inorg. Chem. Commun.* **2004**, *7*, 264.
[8] R. Kiebach, C. Näther, W. Bensch, *Solid State Sci.* **2006**, *8*, 964.
[9] E. Antonova, A. Wutkowski, C. Näther, W. Bensch, *Solid State Sci.* **2011**, *13*, 2154.
[10] Y. Gao, Z. Han, Y. Xu, C. Hu, *J. Cluster Sci.* **2010**, *21*, 163.
[11] E. Antonova, C. Näther, P. Kögerler, W. Bensch, *Angew. Chem. Int. Ed.* **2011**, *50*, 764; *Angew. Chem.* **2011**, *123*, 790.
[12] L. Zhang, X. Zhao, J. Xu, T. Wang, *Dalton Trans.* **2002**, 3275.
[13] H.-Y. Guo, Y. Zhang, L.-N. Xiao, X.-B. Cui, *Dalton Trans.* **2017**, *46*, 8022.
[14] a) E. Antonova, C. Näther, W. Bensch, *Dalton Trans.* **2012**, *41*, 1338; b) E. Antonova, C. Näther, W. Bensch, *CrystEngComm* **2012**, *14*, 6853; c) E. Antonova, C. Näther, P. Kögerler, W. Bensch, *Dalton Trans.* **2012**, *41*, 6957; d) E. Antonova, C. Näther, P. Kögerler, W. Bensch, *Inorg. Chem.* **2012**, *51*, 2311; e) E. Antonova, B. Seidlhofer, J. Wang, M. Hinz, W. Bensch, *Chem. Eur. J.* **2012**, *18*, 15316; f) R. Kiebach, C. Näther, P. Kögerler, W. Bensch, *Dalton Trans.* **2007**, 3221; g) A. Wutkowski, C. Näther, P. Kögerler, W. Bensch, *Inorg. Chem.* **2013**, *52*, 3280; h) A. Wutkowski, C. Näther, P. Kögerler, W. Bensch, *Inorg. Chem.* **2008**, *47*, 1916.
[15] a) I. D. Brown, D. Altermatt, *Acta Crystallogr. Sect. B* **1985**, *41*, 244; b) M. O'Keefe, N. E. Brese, *J. Am. Chem. Soc.* **1991**, *113*, 3226.
[16] a) A. Bondi, *J. Phys. Chem.* **1964**, *68*, 441; b) A. Bondi, *J. Phys. Chem.* **1966**, *70*, 3006; c) M. Mantina, A. C. Chamberlin, R. Valero, C. J. Cramer, D. G. Truhlar, *J. Phys. Chem. A* **2009**, *113*, 5806.
[17] Analog zu: a) M. Wendt, L. K. Mahnke, N. Heidenreich, W. Bensch, *Eur. J. Inorg. Chem.* **2016**, 5393–5398; b) L. Yu, J.-p. Liu, J.-p. Wang, J.-y. Niu, *Chem. Res. Chinese U.* **2009**, *25*, 426–429.
[18] A. Kondinski, T. Heine, K. Y. Monakhov, *Inorg. Chem.* **2016**, *55*, 3777.
[19] Kristallographische Daten für **2**: $C_{40}H_{112}N_{24}Ni_4O_{86}Sb_{16}V_{28}$, 5914.69 g mol^{-1}, $T = 170(2)$ K, monoklin, $P2_1/n$; $a = 19.4201(4)$, $b = 24.4157(4)$, $c = 20.6579(4)$ Å; $\alpha, \gamma = 90$, $\beta = 117.1620(10)°$; $V = 8714.8(3)$ Å^3, $Z = 2$, $\rho = 2.254$ Mg m^{-3}, $\mu = 4.351$ mm^{-1}, $0.06 \times 0.10 \times 0.16$ mm^3, STOE IPDS-2 mit einer Mo-Kα-Quelle

(0.71073 Å), $2\theta_{max} = 26.005°$; 92336 gemessene Reflexe (R_{int}: 0.0652), wR_2 für 17119 unabhängige Reflexe = 0.1696, R_1 für 14585 Reflexe mit $F_0 > 4\sigma(F_0) = 0.0624$, Restelektronendichte: 2.219/−1.328 e Å^{-3}. CCDC 1552878 enthält die ausführlichen kristallographischen Daten zu dieser Veröffentlichung. Die Daten sind kostenlos beim The Cambridge Crystallographic Data Centre erhältlich.

Manuskript erhalten: 4. Dezember 2017
Akzeptierte Fassung online: 12. Januar 2018
Endgültige Fassung online: 12. Februar 2018

GDCh **Communications** Angewandte International Edition Chemie

Polyoxometalates

International Edition: DOI: 10.1002/anie.201712417
German Edition: DOI: 10.1002/ange.201712417

Configurational Isomerism in Polyoxovanadates

Lisa K. Mahnke, Aleksandar Kondinski, Ulrike Warzok, Christian Näther, Jan van Leusen, Christoph A. Schalley, Kirill Yu. Monakhov,* Paul Kögerler,* and Wolfgang Bensch**

Abstract: *A water-soluble derivative of the polyoxovanadate $\{V_{15}E_6O_{42}\}$ (E = semimetal) archetype enables the study of cluster shell rearrangements driven by supramolecular interactions. A reaction unique to E = Sb, induced exclusively by ligand metathesis in peripheral $[Ni(ethylenediamine)_3]^{2+}$ counterions, results in the formation of the metastable α_1* configurational isomer of the $\{V_{14}Sb_8O_{42}\}$ cluster type. Contrary to all other polyoxovanadate shell architectures, this isomer comprises an inward-oriented vanadyl group and is ca. 50 and 12 kJ mol^{-1} higher in energy than the previously isolated α and β isomers, respectively. We discuss this unexpected reaction in light of supramolecular Sb–O···V and Sb–O···Sb contacts manifested in $\{V_{14}Sb_8O_{42}\}_2$ dimers detected in the solid state. ESI MS experiments confirm the stability of these dimers also in solution and in the gas phase. DFT calculations indicate that other, as of yet elusive isomers of $\{V_{14}Sb_8\}$, might be accessible as well.*

Semimetal-functionalized polyoxovanadates[1] (POVs) are predominantly formed under solvothermal conditions. This inherently limits us in adopting concepts for interfering with the clusters' self-assembly reaction mechanisms, as have been established, for example, in polyoxomolybdate and polyoxotungstate chemistry.[2] As such, the syntheses of semimetal-functionalized POVs often are entirely serendipitous. Moreover, within the most widely explored class of antimonato polyoxovanadates,[3] the obtained cluster compounds usually are nearly insoluble, limiting the study of consecutive reactions. Very recently, we discovered a water-soluble antimonato polyoxovanadate (Sb-POV), $\{Ni(en)_3\}_3[V^{IV}{}_{15}Sb^{III}{}_6O_{42}(H_2O)_x]\cdot ca.15\,H_2O$ (**1**; $x = 0$, 1; en = ethylenediamine), representing a suitable starting material for the in situ generation of novel Sb-POV compounds.[4,5] The addition of cyclen (1,4,7,10-tetraazacyclododecane) to an aqueous solution of this precursor results in the rapid formation of $\{Ni(cyclen)(en)\}_2[V_{14}Sb_8O_{42}(H_2O)]\cdot ca.10\,H_2O$ (**2**), as the α_1*-$\{V_{14}Sb_8O_{42}\}$ isomer. This isomer is characterized by the inverted orientation (that is, pointing inwards) of one of its edge-sharing VO_5 pyramids, reducing the molecular symmetry to C_{2v}. Compound **2** features the first hetero-POV displaying configurational isomerism, and as the isomerization of the vanadyl moieties can occur at different positions, this Sb-POV is furthermore subject to positional isomerism,[6] an aspect that may complicate synthesis and isolation of a targeted isomer.

The structures of all hitherto known Sb-POV cluster shells can be derived from the $\{V^{IV}{}_{18}O_{42}\}$ archetype by substitution of 2, 3, or 4 $\{VO_5\}$ square pyramids with dumbbell-like $\{Sb^{III}{}_2O_5\}$ units. Of all possible $[V_{14}Sb_8O_{42}(H_2O)]^{4-}$ isomers (see Supporting Information, Figure S1), the D_{2d}-symmetric α[7] and the D_{2h}-symmetric β[8–13] isomers have so far been observed. All isomers comprise one eight-membered ring of edge-sharing VO_5 pyramids that is capped from above and from below by arcs consisting of three edge-sharing VO_5 pyramids. The relative orientation of these arcs differentiates the α (90°), the β (0°), and the (hypothetical) γ (45°) isomer. The four niches formed between the two V_3 arcs and the V_8 ring are then occupied by Sb_2O subunits, whereby each Sb atom binds to one O of the V_8 ring and one O of a V_3 arc. Whereas the α, β, and γ isomers are characterized by all-outward oriented V=O vanadyl groups, the central cavity of the $\{V_{14}Sb_8O_{42}\}$ structure is sufficiently large to accommodate one inward-orientated vanadyl group, leading to eleven additional, hypothetical isomers ($\alpha_{1\text{-}4}$*, $\beta_{1\text{-}3}$*, $\gamma_{1\text{-}4}$*, Scheme 1 and Figures S1,S2).

Compound **2** crystallizes in the monoclinic space group $P2_1/n$ with all atoms on general positions. The Ni^{2+} centers

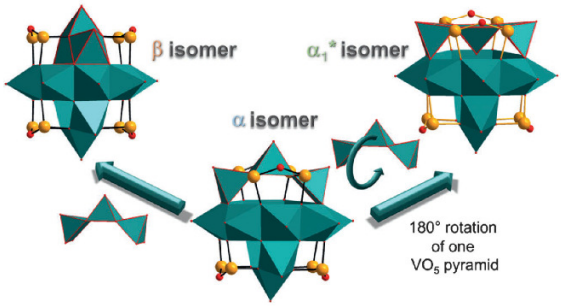

Scheme 1. Selected isomers of the $\{V_{14}Sb_8O_{42}\}$ cluster (V turquoise, Sb yellow, O red), with the modified V_3 arc outlined in red.

[*] M. Sc. L. K. Mahnke, Prof. Dr. C. Näther, Prof. Dr. W. Bensch
Institut für Anorganische Chemie
Christian-Albrechts-Universität zu Kiel
24118 Kiel (Germany)
E-mail: wbensch@ac.uni-kiel.de
Dr. A. Kondinski, Dr. J. van Leusen, Dr. K. Yu. Monakhov, Prof. Dr. P. Kögerler
Institut für Anorganische Chemie
RWTH Aachen University
52074 Aachen (Germany)
E-mail: kirill.monakhov@ac.rwth-aachen.de
paul.koegerler@ac.rwth-aachen.de
M. Sc. U. Warzok, Prof. Dr. C. A. Schalley
Institut für Chemie und Biochemie
Freie Universität Berlin
Takustrasse 3, 14195 Berlin (Germany)
E-mail: c.schalley@fu-berlin.de
Supporting information and the ORCID identification number(s) for the author(s) of this article can be found under: https://doi.org/10.1002/anie.201712417.

reside in distorted octahedral N_6 environments from one cyclen and one en ligand (Ni–N: 2.096(11)–2.155(10) Å). Within the cluster shell of the α_1*-$\{V_{14}Sb_8O_{42}\}$ isomer present in **2**, the central vanadyl group of one V_3 arc points to the center of the cluster sphere (V7–O42; Figure 1). This unique

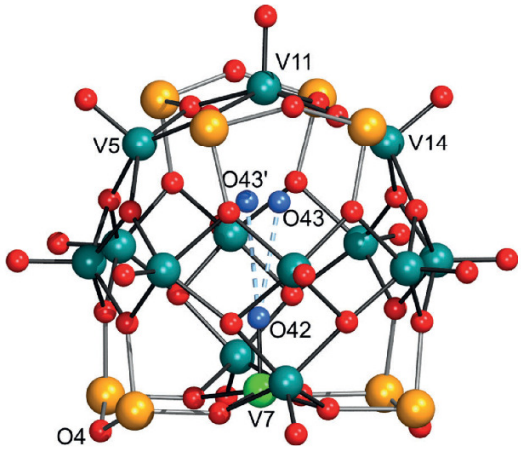

Figure 1. The molecular structure of the α_1* isomer of $\{V_{14}Sb_8O_{42}\}$ in **2**. O red, Sb orange, V turquoise, Sb–O bonds: light gray, V–O: dark gray. Highlighted are V7 (green) and O42 (blue) of the inverted VO_5 pyramid and the 50:50 disordered O43/O43′ of the H_2O guest.

out-in-out arrangement of the VO_5 pyramids generates a V–V–V angle of about 162° (vs. 132° for the usual out-out-out configuration). All geometric parameters are in line with known POV structures.[4,5,7–14] Bond valence sums (BVS) for Sb range from 3.14 to 3.57 (avg. 3.35), and from 3.71 to 4.05 (avg. 3.98) for V, confirming the formal oxidation states V^{IV} and Sb^{III}.[15]

The terminal O42 atom of the V(7)O_5 pyramid is in hydrogen-bonding range (2.6 Å) to an internal H_2O guest molecule that is disordered (50:50) over two positions. The H_2O guest is shifted towards V11 (opposite to V7), leading to short V11–O43/O43′(H_2) contacts of 2.58/2.65 Å. In comparison, the shortest V5/V14–O43(H_2) separations are about 2.75 Å, in stark contrast to α-$[V_{14}Sb_8O_{42}(H_2O)]^{4-}$ with shortest V-O(H_2) distances of approximately 3.7 Å.[6–12]

An inter-cluster V7–O4 bond (2.348(2) Å) generates an octahedral environment for V7 and increases its BVS from 3.71 to 3.92 (Figure 2). This results in a $[V_{28}Sb_{16}O_{84}(H_2O)_2]^{8-}$ anion containing two VO_6 octahedra, unique in polyoxovanadate chemistry. Most $\{V_{14}Sb_8O_{42}\}$ polyoxovanadate compounds display supramolecular inter-cluster Sb–O···Sb separations of 2.73–2.96 Å[7–13] that are also present in the structure of **2**, where the α_1*-$[V_{14}Sb_8O_{42}(H_2O)]^{4-}$ cluster shells form short intra-dimer Sb–O···Sb contacts of 2.71 and 2.76 Å;[16] additional weak inter-dimer Sb–O···Sb contacts of 2.91 Å arrange the clusters into chains along [100] (Figures S12,S13).

Electrospray ionization mass spectrometry (ESI-MS) enables the transfer of intact non-covalently bound complexes, such as the cluster dimers in **2**, from solution into the

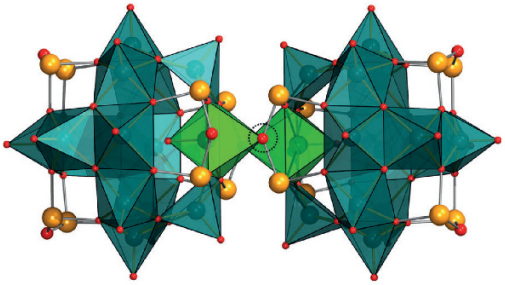

Figure 2. V(7)O_6 octahedra (in green) joining neighboring cluster anions into $\{V_{14}Sb_8\}_2$ dimers in **2** (encircled: O4).

gas phase and thereby allows us to study its structure and reactivity. The negative-mode ESI mass spectrum of an aqueous solution of **2** (60 μM) exhibits signals of the intact cluster ions $[\mathbf{N}\cdot H_2O]^{3-}$/$[\mathbf{N}\cdot H\cdot H_2O]^{3-}$ and $[\mathbf{N}\cdot H_2O]^{2-}$/$[\mathbf{N}\cdot H\cdot H_2O]^{2-}$ at *m/z* 792 and 1188, respectively, as well as $[\mathbf{N}\cdot H_2O\cdot Ni(cyclen)]^{2-}$/$[\mathbf{N}\cdot H\cdot H_2O\cdot Ni(cyclen)]^{2-}$ at *m/z* 1304 as the most abundant species ($\mathbf{N} = \{V_{14}Sb_8O_{42}\}$, Figure 3). **N** undergoes one or two one-electron oxidations of

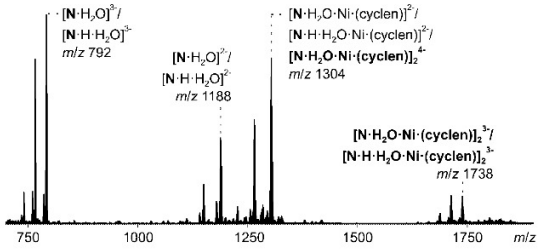

Figure 3. ESI-Q-TOF-HRMS spectrum of compound **2** (60 μM in H_2O, $\mathbf{N} = \{V_{14}Sb_8O_{42}\}$). See Supporting Information for a detailed analysis and discussion.

V^{IV} to V^{V} during the ionization process, yielding doubly and triply charged ions in case of the cluster ions without charge-compensating cations. We note that the mass spectrum of **2** is quite similar to that of its well-studied precursor **1**[4] (see Figure S18 for a detailed isotope pattern analysis). Most importantly, the spectrum contains prominent peaks that correspond to the dimeric complexes $[\mathbf{N}\cdot H_2O\cdot Ni(cyclen)]_2^{4-}$/$[\mathbf{N}\cdot H\cdot H_2O\cdot Ni(cyclen)]_2^{4-}$ and $[\mathbf{N}\cdot H_2O\cdot Ni(cyclen)]_2^{3-}$/$[\mathbf{N}\cdot H\cdot H_2O\cdot Ni(cyclen)]_2^{3-}$ at *m/z* 1304 and 1738, respectively. Formally, these complexes consist of either two triply charged or one triply and one doubly charged cluster core and a charge-compensating Ni^{2+} complex. The peak of the tetra-anionic dimer complex overlaps with the peak of the doubly charged monomeric complex at the same *m/z*, but can be separated via traveling-wave ion-mobility mass spectrometry (Figure S19). The dimer ions are seen over a wide range of sample concentrations indicating that dimer formation is not merely unspecific aggregation during the ESI process. Furthermore, a control experiment with the α-$\{V_{14}Sb_8O_{42}\}$[17] isomer did not show any dimer formation (Figure S20). Thus, the non-covalent inter-cluster/intra-dimer Sb–O···V

interaction is specific to the α_1*-{$V_{14}Sb_8O_{42}$} isomer **2** and is also retained in solution and the gas phase.

Already directly after solvothermal synthesis of **2** and filtration of the crude mixture, the formation of **N** and the corresponding dimer was observed by ESI-MS (Figures S21,S22). In addition, ions of the precursor **1** have also been observed. This implies that the formation of the α_1* cluster core is already completed during the heating of the reaction mixture. Over three days, the product (partially) precipitated from the reaction mixture and the intensity of signals corresponding to **2** decreased.

We then investigated the gas-phase reactivity of the α_1* dimer by first mass-selecting the $[\mathbf{N}{\cdot}H_2O{\cdot}Ni(cyclen)]_2^{3-}$/$[\mathbf{N}{\cdot}H{\cdot}H_2O{\cdot}Ni(cyclen)]_2^{3-}$ ions at *m/z* 1738 and subsequently subjecting them to collision-induced dissociation (CID, Figure 4). The most prominent fragmentation is the cleavage

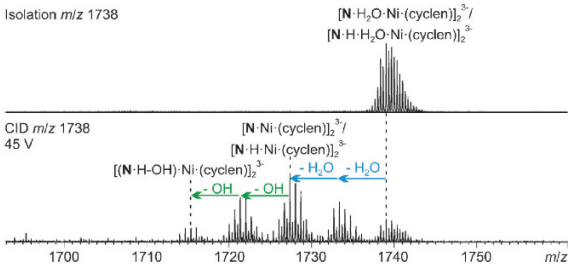

Figure 4. Tandem MS experiment performed with mass-selected ions $[\mathbf{N}{\cdot}H_2O{\cdot}Ni(cyclen)]_2^{3-}$/$[\mathbf{N}{\cdot}H{\cdot}H_2O{\cdot}Ni(cyclen)]_2^{3-}$ ($\mathbf{N} = \{V_{14}Sb_8O_{42}\}$).

of the dimeric into monomeric ions, followed by the loss of water and hydroxyl radicals as previously described for the in situ-formed $\{V_{14}Sb_8\}$ cluster (Figure S23).[4] Most interestingly, a second fragmentation pathway is able to compete: The loss of two neutral H_2O and OH units originating directly from the intact $[\mathbf{N}{\cdot}H_2O{\cdot}Ni(cyclen)]_2^{3-}$/$[\mathbf{N}{\cdot}H{\cdot}H_2O{\cdot}Ni(cyclen)]_2^{3-}$ ions, yielding the dimeric $[(\mathbf{N}\text{-}H\text{-}OH){\cdot}Ni(cyclen)]_2^{3-}$ complex (Figure 4). As the first fragmentation pathway is clearly favored by the reduction of charge repulsion, the less intense yet characteristic loss of neutral species from the dimeric complex clearly points to a remarkable binding energy connecting the two α_1* monomers in the gas phase.

To rationalize the formation of α_1*-$[V_{14}Sb_8O_{42}]^{4-}$ and its stability relative to the other $[V_{14}Sb_8O_{42}]^{4-}$ isomers, we applied relativistic density functional theory (DFT). DFT geometry optimization of the polyoxoanions resulted in a good match with the experimentally determined structural parameters (Table S1). The calculations predict the spin electron densities for the "fully reduced" α_1*-$[V_{14}Sb_8O_{42}]^{4-}$ polyoxoanion, featuring a single electron in d_{xy}/d_{yz} orbitals at each V center (Figure S4), in line with BVS results. Following a published method,[18] the total bonding energy E_b of α_1*-$[V_{14}Sb_8O_{42}]^{4-}$ exceeds the E_b of the "conventional" α-/γ-/β-$[V_{14}Sb_8O_{42}]^{4-}$ isomers by approximately 50, 33, and 12 kJ mol^{-1}, meaning a lower thermodynamic stability of α_1* (Table S3). However, with respect to the remaining ten positional isomers, α_1*-$[V_{14}Sb_8O_{42}]^{4-}$ has a total E_b comparable to the γ_2* and γ_4* isomers ($\Delta E_b < 1$ kJ mol^{-1}), whereas α_2* and α_4* are more favorable by 21 and 15 kJ mol^{-1}, respectively. All other positional isomers are significantly higher in energy than α_1* (Figure S5). α_1*-$\{V_{14}Sb_8O_{42}\}$ and its $\{V_{15}Sb_6O_{42}\}$ precursor are structurally related through a common $\{V_7Sb_4O_{21}\}$ fragment (Figure 5), consisting of five

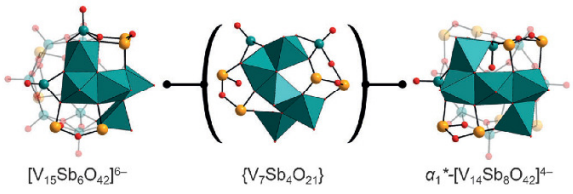

Figure 5. The common $\{V_7Sb_4O_{21}\}$ fragment (middle) present in $[V_{15}Sb_6O_{42}]^{6-}$ (left) and α_1*-$[V_{14}Sb_8O_{42}]^{4-}$ (right; colors as in Figure 2).

$\{VO_5\}$ square pyramids, two $\{Sb_2O_5\}$ units and two dangling and chemically inequivalent vanadyl moieties. The $\{V_7Sb_4O_{21}\}$ fragments are subject to configurational isomerism, where the V=O groups can rotate toward or outward the inner cavity. The isomerization of the $\{V_7Sb_4O_{21}\}$ fragments is more likely the origin of the isomerization vector leading to α_1*-$\{V_{14}Sb_8O_{42}\}$ when compared to the alternative direct isomerization of α-$\{V_{14}Sb_8O_{42}\}$ into α_1*-$\{V_{14}Sb_8O_{42}\}$ (Scheme 1) that is associated with high energy barriers for rotation of the V=O moiety as a result of the steric hindrance by the neighboring O atoms. As α_1*-$\{V_{14}Sb_8O_{42}\}$ is produced only from the $\{V_{15}Sb_6O_{42}\}$ precursor, we tentatively regard the $\{V_7Sb_4O_{21}\}$ fragment as a key synthon, which is only encountered in α-$\{V_{14}Sb_8O_{42}\}$ and α*-$\{V_{14}Sb_8O_{42}\}$ structures, while formal combinatorial dimerization of the different $\{V_7Sb_4O_{21}\}$ configurational isomers can lead exclusively to the formation of α-$\{V_{14}Sb_8O_{42}\}$, α_1*-$\{V_{14}Sb_8O_{42}\}$, and α_4*-$\{V_{14}Sb_8O_{42}\}$ structures. The relative energies and the concept of $\{V_7Sb_4O_{21}\}$ synthons thus narrow down the conversion of $\{V_{15}Sb_6O_{42}\}$ to α-/α*-$\{V_{14}Sb_8O_{42}\}$ clusters.

In summary, the unexpected solvothermal formation of the high-energy configurational α_1*-$\{V_{14}Sb_8O_{42}\}$ isomer is driven by a host of seemingly minor yet cooperative effects, ranging from changes to the countercation ligand environment to intramolecular non-covalent interactions and intercluster Sb–O···V and Sb–O···Sb contacts. X-ray crystal structure analysis and ESI-MS experiments confirm the emergence of surprisingly stable α_1*-$\{V_{14}Sb_8O_{42}\}$ dimers in the solid state, in solution and in the gas phase. The need for a precursor structure that already comprises a critical subset of structural features of the intended product is furthermore underlined by the fact that other V/Sb precursors do not result in **2** under otherwise identical synthetic conditions. DFT calculations point to interesting electronic properties of the α_1*-$[V_{14}Sb_8O_{42}]^{4-}$ species that make them potential candidates for subsequent reactions (see Supporting Information), while the medium rank of their relative stability among other isomers again suggests that supramolecular aspects are apparently key to the formation and isolation of

these dimeric clusters. As such, further positional and configurational $\{V_{14}Sb_8\}$ isomers of comparable stability represent viable synthetic targets.

Experimental Section

All chemicals were used as purchased without further purifications. The precursor $\{Ni(en)_3\}_3[V_{15}Sb_6O_{42}(H_2O)_x]\cdot ca.15\,H_2O$ (**1**) was synthesized using the published method.[3] Compound **2**[19] was prepared under solvothermal conditions in DURAN glass tubes with an inner volume of 11 mL. 0.1373 g (0.045 mmol) of the precursor **1** ($\{Ni(en)_3\}_3[V_{15}Sb_6O_{42}(H_2O)_x]\cdot ca.15\,H_2O$) were mixed with 0.0240 g (0.135 mmol) cyclen and 4 mL deionized water in a glass tube and heated for 4 h under stirring at 150 °C. The hot mixture was filtered and the filtrate was transferred to a beaded rim bottle. After 9 d brown rhombohedral crystals of **2** were obtained that were collected by filtration and washed with deionized water and ethanol. Yield: ca. 10 mg; see Supporting Information for further details. Elemental analysis (%) for $C_{40}H_{112}N_{24}Ni_4O_{86}Sb_{16}V_{28}$ (5914.7 g mol^{-1}) C 8.09, H 2.06, N 5.45; calcd: C 8.12, H 1.91, N 5.68. EDX analysis (%) for $V_{14}Sb_8Ni_2$: V 39.55, Sb 53.71, Ni 6.74; calcd: V 39.52, Sb 53.97, Ni 6.50.

Acknowledgements

This work was supported by the State of Schleswig-Holstein and by the Deutsche Forschungsgemeinschaft (DFG, CRC 1109). K.Y.M. is grateful to the DFG for an Emmy Noether fellowship. We thank Michael Wendt for previous work and support.

Conflict of interest

The authors declare no conflict of interest.

Keywords: antimonato polyoxovanadates · configurational isomerism · DFT calculations · ESI MS · polyoxometalates

[1] K. Y. Monakhov, W. Bensch, P. Kögerler, *Chem. Soc. Rev.* **2015**, *44*, 8443.
[2] See, for example, a) L. Vilà-Nadal, A. Rodríguez-Fortea, L.-K. Yan, E. F. Wilson, L. Cronin, J. M. Poblet, *Angew. Chem. Int. Ed.* **2009**, *48*, 5452; b) Z.-L. Lang, W. Guan, L.-K. Yan, S.-Z. Wen, Z.-M. Su, L.-Z. Hao, *Dalton Trans.* **2012**, *41*, 11361.
[3] H.-Y. Guo, X. Zhang, X.-B. Cui, Q.-S. Huo, J.-Q. Xu, *CrystEngComm* **2016**, *18*, 5130.
[4] M. Wendt, U. Warzok, C. Näther, J. van Leusen, P. Kögerler, C. A. Schalley, W. Bensch, *Chem. Sci.* **2016**, *7*, 2684.
[5] M. Wendt, C. Näther, W. Bensch, *Chem. Eur. J.* **2016**, *22*, 7747.
[6] See, for example, a) M. T. Pope, T. F. Scully, *Inorg. Chem.* **1975**, *14*, 953; b) L. Pettersson, I. Andersson, J. H. Grate, A. Selling, *Inorg. Chem.* **1994**, *33*, 982; c) "Complexity in Chemistry and Beyond": L. Vilà-Nadal, S. Romo, X. López, J. M. Poblet in *NATO Science for Peace and Security Series B* (Eds.: C. Hill, D. G. Musaev), Springer, Dordrecht **2012**; d) S. Spillane, R. Sharma, A. Zavras, R. Mulder, C. A. Ohlin, L. Goerigk, R. J. O'Hair, C. Ritchie, *Angew. Chem. Int. Ed.* **2017**, *56*, 8568; *Angew. Chem.* **2017**, *129*, 8691.
[7] X.-X. Hu, J.-Q. Xu, X.-B. Cui, J.-F. Song, T.-G. Wang, *Inorg. Chem. Commun.* **2004**, *7*, 264.
[8] R. Kiebach, C. Näther, W. Bensch, *Solid State Sci.* **2006**, *8*, 964.
[9] E. Antonova, A. Wutkowski, C. Näther, W. Bensch, *Solid State Sci.* **2011**, *13*, 2154.
[10] Y. Gao, Z. Han, Y. Xu, C. Hu, *J. Clust. Sci.* **2010**, *21*, 163.
[11] E. Antonova, C. Näther, P. Kögerler, W. Bensch, *Angew. Chem. Int. Ed.* **2011**, *50*, 764.
[12] L. Zhang, X. Zhao, J. Xu, T. Wang, *Dalton Trans.* **2002**, 3275.
[13] H.-Y. Guo, Y. Zhang, L.-N. Xiao, X.-B. Cui, *Dalton Trans.* **2017**, *46*, 8022.
[14] a) E. Antonova, C. Näther, W. Bensch, *Dalton Trans.* **2012**, *41*, 1338; b) E. Antonova, C. Näther, W. Bensch, *CrystEngComm* **2012**, *14*, 6853; c) E. Antonova, C. Näther, P. Kögerler, W. Bensch, *Dalton Trans.* **2012**, *41*, 6957; d) E. Antonova, C. Näther, P. Kögerler, W. Bensch, *Inorg. Chem.* **2012**, *51*, 2311; e) E. Antonova, B. Seidlhofer, J. Wang, M. Hinz, W. Bensch, *Chem. Eur. J.* **2012**, *18*, 15316; f) R. Kiebach, C. Näther, P. Kögerler, W. Bensch, *Dalton Trans.* **2007**, 3221; g) A. Wutkowski, C. Näther, P. Kögerler, W. Bensch, *Inorg. Chem.* **2013**, *52*, 3280; h) A. Wutkowski, C. Näther, P. Kögerler, W. Bensch, *Inorg. Chem.* **2008**, *47*, 1916.
[15] a) I. D. Brown, D. Altermatt, *Acta Crystallogr. Sect. B* **1985**, *41*, 244; b) M. O'Keefe, N. E. Brese, *J. Am. Chem. Soc.* **1991**, *113*, 3226.
[16] a) A. Bondi, *J. Phys. Chem.* **1964**, *68*, 441; b) A. Bondi, *J. Phys. Chem.* **1966**, *70*, 3006; c) M. Mantina, A. C. Chamberlin, R. Valero, C. J. Cramer, D. G. Truhlar, *J. Phys. Chem. A* **2009**, *113*, 5806.
[17] Analogous to: a) M. Wendt, L. K. Mahnke, N. Heidenreich, W. Bensch, *Eur. J. Inorg. Chem.* **2016**, 5393–5398; b) L. Yu, J.-p. Liu, J.-p. Wang, J.-y. Niu, *Chem. Res. Chinese U.* **2009**, *25*, 426–429.
[18] A. Kondinski, T. Heine, K. Y. Monakhov, *Inorg. Chem.* **2016**, *55*, 3777.
[19] Crystallographic data for **2**: $C_{40}H_{112}N_{24}Ni_4O_{86}Sb_{16}V_{28}$, 5914.69 g mol^{-1}, $T=170(2)$ K, monoclinic, $P2_1/n$, $a=19.4201(4)$, $b=24.4157(4)$, $c=20.6579(4)$ Å, α, $\gamma=90°$, $\beta=117.1620(10)°$, $V=8714.8(3)$ Å^3, $Z=2$, $\rho=2.254$ Mg m^{-3}, $\mu=4.351$ mm^{-1}, $0.06\times0.10\times0.16$ mm^3, STOE IPDS-2 with Mo-Kα radiation (0.71073 Å), $2\theta_{max}=26.005°$; 92336 measured reflections (R_{int}: 0.0652), wR_2 for 17119 independent reflections = 0.1696, R_1 for 14585 reflections with $F_0>4\sigma(F_0)=0.0624$, residual electron density: 2.219/−1.328 e Å^{-3}. CCDC 1552878 contains the supplementary crystallographic data for this paper. These data can be obtained free of charge from The Cambridge Crystallographic Data Centre.

Manuscript received: December 4, 2017
Accepted manuscript online: January 12, 2018
Version of record online: ■■ ■■, ■■■■

Communications

Polyoxometalates

L. K. Mahnke, A. Kondinski, U. Warzok, C. Näther, J. van Leusen, C. A. Schalley,* K. Yu. Monakhov,* P. Kögerler,* W. Bensch* ——— ■■■■–■■■■

Configurational Isomerism in Polyoxovanadates

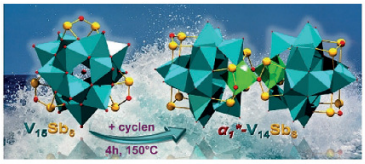

Supramolecular intra- and inter-cluster interactions support the energetically uphill formation of a configurational isomer (α_1*) of the $\{V_{14}Sb_8\}$ family of antimonato polyoxovanadates.

4.3. Die Publikation *„Ordnung muss sein: heteroelement order and disorder in polyoxovanadates"*

Die ersten gemischten Antimonato-Germanato POVs wurden über zwei synthetische Strategien hergestellt mit besonderem Augenmerk auf die Synthese mit dem Precursors Ni-{$V_{15}Sb_6$}. Die traditionelle Syntheseroute mit niedernuklearen Edukten wie NH_4VO_3, Sb_2O_3, GeO_2 und $NiCl_2{\cdot}6\,H_2O$ führte zur Kristallisation von $\{Ni(en)_3\}_3[V_{15}Sb_2Ge_4O_{42}(OH)_4(H_2O)]{\cdot}en{\cdot}{\approx}10\,H_2O$ sowie $\{Ni(en)_3\}_3[V_{15}Sb_3Ge_3O_{42}(OH)_3(H_2O)]{\cdot}{\approx}15\,H_2O$. In den Strukturen sind die Heteroatompositionen sowohl von Ge als Sb besetzt. Dies deutet darauf hin, dass Cluster mit unterschiedlicher Zusammensetzung, welche aber im Gleichgewicht vorliegen, in Lösung gebildet werden. Interessanterweise ist die Struktur des Anions in der Verbindung, $\{Ni(en)_3\}_3[V_{15}Sb_3Ge_3O_{42}(OH)_3(H_2O)]{\cdot}{\approx}9\,H_2O$, welche mit dem Precursor erhalten wurde, nicht von Mischbesetzungen der Heteroatompositionen betroffen, sondern Ge und Sb sind voll ausgeordnet. Daher kann angenommen werden, dass die Reaktion über partielle Substitution der SbO_3-Pyramiden durch GeO_4-Tetraeder abläuft. Die Verbindungen wurden mittels ESEM-EDX, IR, XRD, CHNS, DTA-TG charakterisiert. Mit den Daten der Einkristallstrukturanalysen und der Bond Valence Sum Analyse konnten in allen drei Verbindungen Hydroxylgruppen eindeutig identifiziert werden.

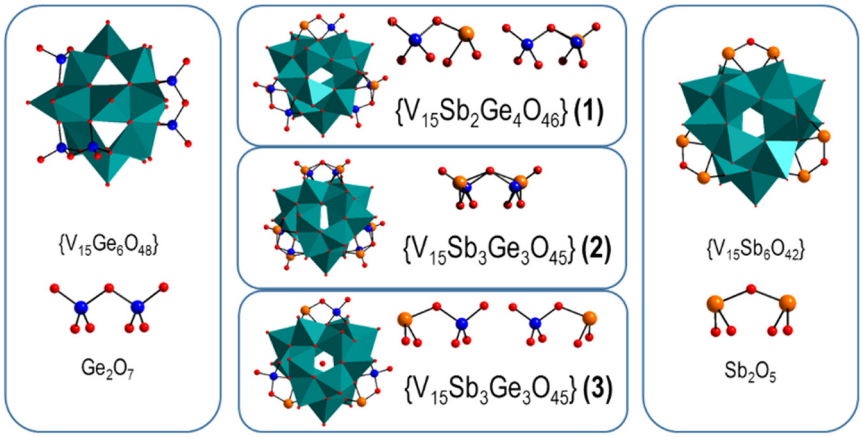

Abbildung 20: TOC Grafik der Publikation *„Ordnung muss sein: heteroelement order and disorder in polyoxovanadates"*.

Veröffentlicht in *Dalton Trans.* **2018**, *47*, 6672.
DOI: 10.1039/c8dt00715b

Dalton Transactions

COMMUNICATION

Cite this: *Dalton Trans.*, 2018, **47**, 6672

Received 22nd February 2018,
Accepted 9th April 2018

DOI: 10.1039/c8dt00715b

rsc.li/dalton

Ordnung muss sein: heteroelement order and disorder in polyoxovanadates†

M. Wendt,[a] L. K. Mahnke,[a] C. Näther,[a] J. van Leusen,[b] P. Kögerler[b] and W. Bensch*[a]

The first mixed antimonato–germanato polyoxovanadates were synthesized using two different strategies, highlighting the critical role of the precursors. Following the traditional route using multiple single sources as precursors the polyanions $[V_{15}Sb_2Ge_4O_{42}(OH)_4(H_2O)]^{6-}$ (1) and $[V_{15}Sb_3Ge_3O_{42}(OH)_3(H_2O)]^{6-}$ (2) are obtained, which display disorder of their Sb/Ge positions, indicating that clusters of different compositions are in equilibrium in solution. In contrast, if the water-soluble single-source precursor $\{Ni(en)_3\}_3[V_{15}Sb_6O_{42}(H_2O)]$·*ca.* $15H_2O$ is reacted with GeO_2, $\{Ni(en)_3\}_3[V_{15}Sb_3Ge_3O_{42}(OH)_3(H_2O)]\cdot\approx 9H_2O$ (3) forms, in which Sb and Ge occupy distinct positions that might have been formed *via* partial substitution reactions in the $\{V_{15}Sb_6\}$ precursor.

While arsenato-polyoxovanadates, with the most prominent example $[V^{IV}_{15}As^{III}_6O_{42}(H_2O)]^{6-}$ (abbreviated as $\{V_{15}As_6\}$)[1] exhibiting unusual magnetic properties,[2] can be prepared at moderate temperatures, the analogous antimonato-polyoxovanadate $\{V_{15}Sb_6\}$ requires solvothermal conditions.[3,4] The structure of the cluster anion is formally derived from the $\{V_{18}O_{42}\}$ archetype by replacement of three VO_5 square pyramids with three E_2O_5 (E = As, Sb) moieties, formed by two corner-sharing of EO_3 units.[5] Replacing E(III) by Ge(IV) yields Ge-POVs which differ significantly in their composition, charge, geometry and structural dimensionality.[5] It is noteworthy that Ge-POVs are also prepared only under solvothermal conditions. Structurally, instead of E_2O_5 units, two, three or four Ge_2O_7 moieties (two corner-sharing GeO_4 tetrahedra) enter the $\{V_{18}O_{42}\}$ archetype, thereby forming $[V_{16}Ge_4O_{46}]^{12-}$, $[V_{15}Ge_6O_{48}]^{12-}$ and $[V_{14}Ge_8O_{50}]^{12-}$.[6–8] In contrast to the E_2O_5 handles, the Ge_2O_7 groups contain terminal O atoms (O_t), which affect the chemical reactivity, and consequentially Ge-POVs can display terminal expansion of their cluster shells.[2,7] But not only the geometric parameters of E_2O_5 and Ge_2O_7 moieties significantly differ, the E(III) cations are additionally characterized by a stereochemically active electron lone pair (LEP). Traditionally, such semi-metal containing polyoxovanadates (POVs) are synthesized mainly using single source educts like *e.g.* E_2O_3, GeO_2, AVO_3 (A = NH_4, Na, K) or V_2O_5. Until now no mixed Ge-E-POVs were known, but it would be of interest to combine the physico-chemical properties of Ge-POVs with those of E-POVs. By applying the traditional synthesis procedure NH_4VO_3 could be reacted with mixtures of Sb_2O_3 and GeO_2 under solvothermal conditions. However, in this case, physical mixtures of pure Sb-POVs or Ge-POVs might form, which would not be surprising given their differing geometries and chemical behavior. Moreover, even if mixed compounds will form, different cluster cores might be in equilibrium which can crystallize simultaneously due to their similar shape, leading to strong disorder, which can be proven because different Sb and Ge positions might be expected due to the different bond lengths. However, a second, maybe more elegant strategy would be reacting a water-soluble precursor like $\{Ni(en)_3\}_3[V_{15}Sb_6O_{42}(H_2O)]$·*ca.*$15H_2O$[9] with GeO_2. Under *in situ* conditions one may expect that Sb may be fully replaced by Ge, leading to compounds with ordered structures. This assumption is not unrealistic because we have demonstrated a similar strategy to transform this precursor into a $\{V_{14}Sb_8\}$ cluster core.[9]

In the present work we compared both routes. The reaction of NH_4VO_3, Sb_2O_3, GeO_2 and $NiCl_2\cdot 6H_2O$ in identical molar ratios (ESI†) in an aqueous en solution, but with different absolute amounts of solid precursors (ESI†), yielded two new mixed-semimetal derivatives $\{Ni(en)_3\}_3[V_{15}Sb_2Ge_4O_{42}(OH)_4(H_2O)]\cdot en\cdot\approx 10H_2O$ (1) and $\{Ni(en)_3\}_3[V_{15}Sb_3Ge_3O_{42}(OH)_3(H_2O)]\cdot\approx 15H_2O$ (2), in which Ge and Sb are disordered. Interestingly, a compound of the same cluster composition as in 2, $\{Ni(en)_3\}_3[V_{15}Sb_3Ge_3O_{42}(OH)_3(H_2O)]\cdot\approx 9H_2O$ (3), was obtained by the second route, in which the water-soluble pre-

[a]*Institut für Anorganische Chemie, Christian-Albrechts-Universität zu Kiel, 24118 Kiel, Germany. E-mail: wbensch@ac.uni-kiel.de*

[b]*Institut für Anorganische Chemie, RWTH Aachen University, 52074 Aachen, Germany*

†Electronic supplementary information (ESI) available: Crystal structure refinement results, geometric parameters, EDX data, IR spectra, figures of the structures, XRD patterns, and TG curves. CCDC 1503959, 1503958 and 1820425. For ESI and crystallographic data in CIF or other electronic format see DOI: 10.1039/c8dt00715b

cursor $\{Ni(en)_3\}_3[V_{15}Sb_6O_{42}(H_2O)]\cdot ca.\ 15H_2O$[9] was reacted with GeO_2 in a water/en mixture at 150 °C.

In **1**, three out of the six semimetal positions are occupied by Ge/Sb and in **2** all positions show mixed occupancy by Ge/Sb, while in **3** Sb and Ge are fully ordered. EDX data (Table S1†) and CHN analyses support the compositions determined by single-crystal X-ray diffraction structure refinements. Bond valence sum (BVS) data for the V atoms are nearly +4 in all compounds, in line with all-vanadyl configurations (Table S2†) and the characteristic intense V–O stretching mode in the IR spectra at 959 cm^{-1} (**1** and **2**) and 962 cm^{-1} (**3**) (Fig. S1–S3†). BVS data also clearly indicate that the terminal O atom of each GeO_4 tetrahedron is monoprotonated, *i.e.* in all compounds $GeO_3(OH)$ tetrahedra are present (Table S3†). This observation is in line with theoretical calculations that identify the terminal O atoms of GeO_4 units as potential protonation sites.[10]

All three compounds crystallize in non-centrosymmetric chiral space groups (**1**: $P2_1$; **2**: $C2$; **3**: $P2_1$, Table S4,† powder patterns: Fig. S4–S6†). The anions in **1–3** comprise the classical $\{V_{15}E_6\}$ structure of 15 edge- and corner-sharing VO_5 square pyramids and three E_2O_{5+x} handle-like units composed of two corner-shared EO_3 trigonal pyramids (E = Sb) or EO_4 tetrahedra (E = Ge). The spherical cluster shell encloses a water guest molecule. The VO_5 polyhedra are organized into two C_3-symmetric hexagons of edge-sharing VO_5 pyramids, which are interlinked by three additional VO_5 groups, themselves oriented in a C_3-symmetric fashion. In **1** three unique $[Ni(en)_3]^{2+}$ complexes adopt Λ configuration, while both Δ and Λ isomers are observed in **2** and **3** (Fig. S7–S9†). The V–O, Sb–O and Ge–O bond lengths and angles (Tables S5–S13†) are in the range reported for other polyoxovanadates. In the $\{V_{15}Sb_2Ge_4\}$ cluster (**1**) one of the three semimetal bridges is formed by a SbO_3 pyramid condensed to a GeO_4 tetrahedron with fully occupied Sb/Ge positions thus forming an $O_2Ge(OH)$–O–SbO_2 group (Fig. 1, bottom row a). In the two other bridging units the Ge/Sb positions exhibit mixed occupancies (Fig. 1, bottom row b), see also Table S14.†

One N atom of the co-crystallized en molecule is at a distance of 2.53 Å to a Sb atom, indicating covalent Sb–N bonding.[4,11] A short Sb···O intercluster distance of 2.86 Å suggests weak interaction (sum of van der Waals radii:[12] 3.58 Å that results in a packing featuring cluster chains along [100] (ESI, Fig. S10†). In the $\{V_{15}Sb_3Ge_3\}$ structure in **2** a mixed occupancy (Ge1 : Sb1 = 30 : 70, Ge2 : Sb2 = 65 : 35, and Ge3 : Sb3 = 55 : 45) leads to bridges with three different chemical compositions (Fig. 1, bottom row c). Significant intercluster interactions are absent in the crystal structure of **2**, where cations and cluster anions alternate along all three crystallographic directions (Fig. S11, ESI†). The Ge/Sb atom distribution over the crystallographic positions however drastically differs in the $\{V_{15}Sb_3Ge_3\}$ core of **3** because all semimetal positions are exclusively occupied either by Ge or Sb, resulting in three $O_2Ge(OH)$–O–SbO_2 handles (Fig. 1, bottom row d and e). This is surprising as it requires the removal of SbO_3 units from the Sb_2O_5 handles present in the $\{V_{15}Sb_6\}$ precursor and bond formation to GeO_4 tetrahedra that are *in situ* delivered by reaction between GeO_2 and the basic solution.

The key line of evidence for our hypothesis that three SbO_3 groups are effectively removed from the $\{V_{15}Sb_6\}$ precursor cluster is derived from syntheses performed with different GeO_2 : $\{V_{15}Sb_6\}$ ratios: if the concentration of GeO_2 is lower than required for the replacement of all three SbO_3 units, compound **3** is obtained but in a correspondingly lower yield. In contrast, a higher GeO_2 : cluster ratio results in the crystallization of **3**, yet limited to the same yield obtained in the original synthesis.

Remarkably, in **3** the Sb atoms of neighboring cluster anions are in close contact with the μ_2-O bridge of the $O_2Ge(OH)$–O–SbO_2 (Fig. 1e) unit (inter-cluster Sb···O: 2.74 Å) and to an adjacent vanadyl apex (Sb···O=V: 2.94 Å). Considering these Sb···O separations, zig-zag chains are formed along [010] (Fig. S12†). Along [001], cations and anions alternate, while rods consisting of cations and of cations and anions are arranged along [010].

The magnetic data of **1–3** are shown in Fig. 2 as $\chi_m T$ *vs.* T plots at 0.1 Tesla, and M_m *vs.* B plots at 2.0 K. At 290 K, the $\chi_m T$ values of **1** (5.29 cm^3 K mol^{-1}), **2** (5.46 cm^3 K mol^{-1}) and **3** (5.29 cm^3 K mol^{-1}) are well below the expected range

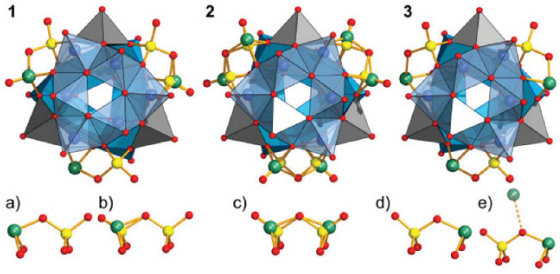

Fig. 1 Polyhedral representation of the cluster anions in **1**, **2**, and **3** (top row) and the heterometal bridges with different occupations (bottom row). Blue and grey polyhedra: V; yellow: Ge; green: Sb; red: O.

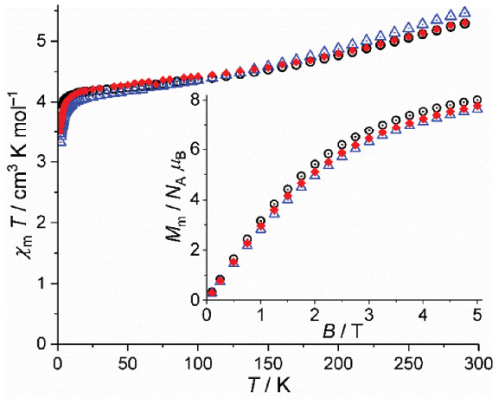

Fig. 2 Temperature dependence of $\chi_m T$ at 0.1 T of **1** (black open circles), **2** (blue open triangles) and **3** (red full diamonds); inset: molar magnetization M_m *vs.* applied magnetic field B at 2.0 K for **1–3**.

(8.05–10.61 cm^3 K mol^{-1}) for three high-spin (S = 1) Ni^{II} and 15 vanadyl groups (S = 1/2) in the absence of any coupling interactions. This is in line with the strong antiferromagnetic exchange interactions between the centers of fully reduced $\{V_{15}E_6\}$ polyoxovanadates. Upon cooling the compounds, $\chi_m T$ almost linearly decreases down to approximately 20 K with a distinct change of the slope at about 160–170 K for all compounds. Below 20 K, $\chi_m T$ decreases to 3.77 cm^3 K mol^{-1} (**1**), 3.32 cm^3 K mol^{-1} (**2**), and 3.51 cm^3 K mol^{-1} (**3**), respectively, at 2.0 K. The curves of all compounds are therefore similar with slightly different slopes and a more pronounced drop off in the case of **2**. For all fields, the molar magnetization curves at 2.0 K are similar. At this temperature, the observed order of $\chi_m T$ values translates to the molar magnetization: the magnetization of **1** slightly exceeds that of **2** and **3**, reaching $8.0 N_A \mu_B$ (**1**), $7.6 N_A \mu_B$ (**2**), and $7.7 N_A \mu_B$ (**3**), respectively, at 5.0 T without saturation.

Based on the coordination environments of the Ni^{II} ions, they can be approximated as isotropic S = 1 centers with $g_{iso} \geq 2.0$. They thus contribute to $\chi_m T$, except at very low temperatures, as a constant value within the above-mentioned range for three isolated Ni^{II} centers. Additionally, the saturation value of $3 g_{iso} N_A \mu_B$ serves as a good approximation to estimate their contribution to the molar magnetization at 5.0 T and 2.0 K. The correspondingly reduced $\chi_m T$ *vs.* T and M_m *vs.* B plots are similar to those of the $\{V_{15}E_6\}$ compounds[1–6] confirming the observation that the strong antiferromagnetic exchange interactions between the 15 V^{IV} centers are only slightly affected by the Sb_2O_5 and Ge_2O_7 moieties, respectively. Comparing the data of **1–3** with the data of $\{Ni(en)_3\}_3[V_{15}Sb_6O_{42}(H_2O)]$[9c] reveals minor differences. They can be attributed to different distortions and coordination modes of the $[Ni(en)_3]^{2+}$ complexes and uncertainties in the water contents besides the varying occupation of Sb positions by Ge in the $\{V_{15}\}$ cores: the $\chi_m T$ *vs.* T curve for T < 100 K is even flatter, while the slope for T > 150 K is similar to that of **1** and **3**. Additionally, the slope of the molar magnetization M_m *vs.* B is slightly larger than for **1–3**.

Conclusions

Summarizing, we have synthesized the first mixed Ge–Sb-POVs which were prepared by two different routes. In particular, using the water-soluble precursor cluster seems to be very promising, because it offers more control leading to structurally ordered compounds as observed in the case of **3**. Consequently this route has much potential for the directed synthesis of defined clusters with desired compositions and this will be the subject of further investigations. The formation of **2** is of high interest, because it indicates that several different species must be in equilibria in solution. Unfortunately, based on our structural work one cannot prove if different mixed Sb–Ge clusters formed exclusively or if such clusters are superimposed with pure Sb and/or Ge clusters. For detection and possible isolation of further isomers *in situ* investigations like *e.g.* circular dichroism spectroscopy are projected.

Conflicts of interest

There are no conflicts to declare.

Acknowledgements

Financial support by the State of Schleswig-Holstein is acknowledged.

References

1 A. Müller and J. Döring, *Angew. Chem., Int. Ed. Engl.*, 1988, **27**, 1721.
2 P. Kögerler, B. Tsukerblat and A. Müller, *Dalton Trans.*, 2010, 21–36.
3 R. Kiebach, C. Näther, P. Kögerler and W. Bensch, *Dalton Trans.*, 2007, 3221–3223.
4 E. Antonova, C. Näther, P. Kögerler and W. Bensch, *Angew. Chem., Int. Ed.*, 2011, **50**, 764–767.
5 K. Y. Monakhov, W. Bensch and P. Kögerler, *Chem. Soc. Rev.*, 2015, **44**, 8443–8483.
6 J. Zhou, J. Zhang, W.-H. Fang and G.-Y. Yang, *Chem. – Eur. J.*, 2010, **16**, 13253–13261.
7 J. Wang, C. Näther, M. Speldrich, P. Kögerler and W. Bensch, *CrystEngComm*, 2013, **15**, 10238–10245.
8 (*a*) M. Wendt, M. Rasmussen, C. Näther and W. Bensch, *Z. Anorg. Allg. Chem.*, 2017, **643**, 155–159; (*b*) Y. Gao, Y. Xu, K. Huang, Z. Han and C. Hu, *Dalton Trans.*, 2012, **41**, 6122–6129.
9 (*a*) M. Wendt, C. Näther and W. Bensch, *Chem. – Eur. J.*, 2016, **22**, 7747–7751; (*b*) M. Wendt, L. K. Mahnke, N. Heidenreich and W. Bensch, *Eur. J. Inorg. Chem.*, 2016, **2016**, 5393–5398; (*c*) M. Wendt, U. Warzok, C. Näther, J. van Leusen, P. Kögerler, C. A. Schalley and W. Bensch, *Chem. Sci.*, 2016, **7**, 2684–2694; (*d*) M. Wendt, P. Polzin, J. van Leusen, C. Näther, P. Kögerler and W. Bensch, *Dalton Trans.*, 2017, **46**, 1618–1623.
10 A. Kondinski, T. Heine and K. Y. Monakhov, *Inorg. Chem.*, 2016, **55**, 3777–3788.
11 (*a*) X. Ma, Y. Ding, H. W. Roesky, S. Sun and Z. Yang, *Z. Anorg. Allg. Chem.*, 2013, **639**, 49–52; (*b*) A. J. Edwards, N. E. Leadbeater, M. A. Paver, P. R. Raithby, C. A. Russell and D. S. Wright, *J. Chem. Soc., Dalton Trans.*, 1994, **105**, 1479–1482; (*c*) J. A. Lessa, D. C. Reis, I. C. Mendes, N. L. Speziali, L. F. Rocha, V. R. Pereira, C. M. Melo and H. Beraldo, *Polyhedron*, 2011, **30**, 372–380; (*d*) H. D. Yin and J. Zhai, *Inorg. Chim. Acta*, 2009, **362**, 339–345; (*e*) S. K. Hadjikakou, C. D. Antoniadis, N. Hadjiliadis, M. Kubicki, J. Binolis, S. Karkabounas and K. Charalabopoulos, *Inorg. Chim. Acta*, 2005, **358**, 2861–2866; (*f*) M. Rasmussen, C. Näther, J. van Leusen, P. Kögerler, L. Zhechkov, T. Heine and W. Bensch, *Inorg. Chem.*, 2017, **56**, 7120–7126.
12 (*a*) A. Bondi, *J. Phys. Chem.*, 1966, **70**, 3006–3007; (*b*) A. Bondi, *J. Phys. Chem.*, 1964, **68**, 441–451.

4.4. Die Publikation *„The New Water-Soluble Cluster Compound $\{Zn(en)_3\}_3[V_{15}Sb_6O_{42}(H_2O)]\cdot(ethylene-diamine)_3\cdot 10\ H_2O$ as a Synthon for the Generation of two New Antimonato Polyoxovanadates"*

Die Verbindung $\{Zn(en)_3\}_3[V_{15}Sb_6O_{42}(H_2O)]\cdot 3en\cdot 10\ H_2O$, welche unter solvothermalen Bedingungen synthetisiert wurde, weist eine bemerkenswert hohe Löslichkeit in Wasser auf. In der Struktur werden sehr kurze Sb-N-Abstände zu den Ethylendiamin-molekülen beobachtet. ESI-MS-Untersuchungen bestätigten, dass der Cluster über 72 Stunden vollständig intakt in der wässrigen Lösung vorliegt und erst nach 14 Tagen ca. 50 % des Anions in das $[V_{14}Sb_8O_{42}]^{4-}$-Anion umgewandelt sind. Weiterführende ESI-MS-Untersuchungen ergaben, dass die Transformation $\{V_{15}Sb_6\} \rightarrow \{V_{14}Sb_8\}$ durch Zugabe von NH_4OAc beschleunigt werden kann und die Umwandlung nach 23 Stunden bei Raumtemperatur abgeschlossen ist. Die ausgeprägte Stabilität des $\{V_{15}Sb_6O_{42}\}$-Clusters erlaubte die Synthese der zwei neuen Verbindungen $\{Zn(phen)_3\}_2[Zn(en)_2V_{15}Sb_6O_{42}(H_2O)]\cdot 23\ H_2O$ und $\{(Zn(en)_2(H_2O)_2)(Zn(en)_2)\}$-$[Zn(en)_2V_{15}Sb_6O_{42}(H_2O)]\cdot 8.5\ H_2O$. In den Strukturen sind Zn^{2+}-Komplexe über Zn-O-V-Bindungen an das Anion gebunden. Diese Postfunktionalisierung des intakten Anions konnte wahrscheinlich nur aufgrund der ausgeprägten Stabilität des Clusters erreicht werden.

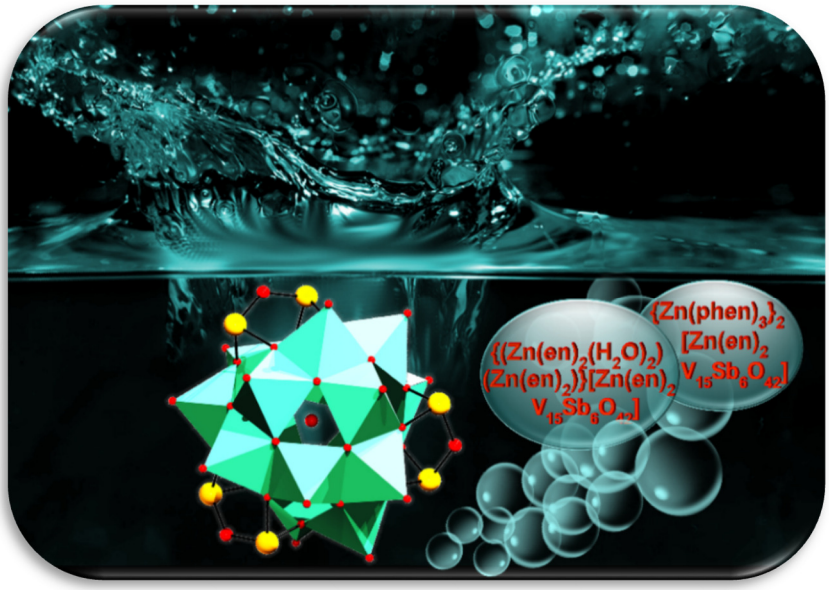

Abbildung 21: TOC Grafik der Publikation *„The New Water-Soluble Cluster Compound $\{Zn(en)_3\}_3[V_{15}Sb_6O_{42}(H_2O)]\cdot(ethylenediamine)_3\cdot 10H_2O$ as a Synthon for the Generation of two New Antimonato Polyoxovanadates".*

„The New Water-Soluble Cluster Compound $\{Zn(en)_3\}_3[V_{15}Sb_6O_{42}(H_2O)]\cdot(ethylenediamine)_3\cdot 10H_2O$ as a Synthon for the Generation of two New Antimonato Polyoxovanadates”.

Veröffentlicht in *Chem. Eur. J.* **2018**, *24*, 5522.
DOI: 10.1002/chem.201705732

CHEMISTRY
A European Journal

www.chemeurj.org

A Journal of
ChemPubSoc Europe

2018-24/21

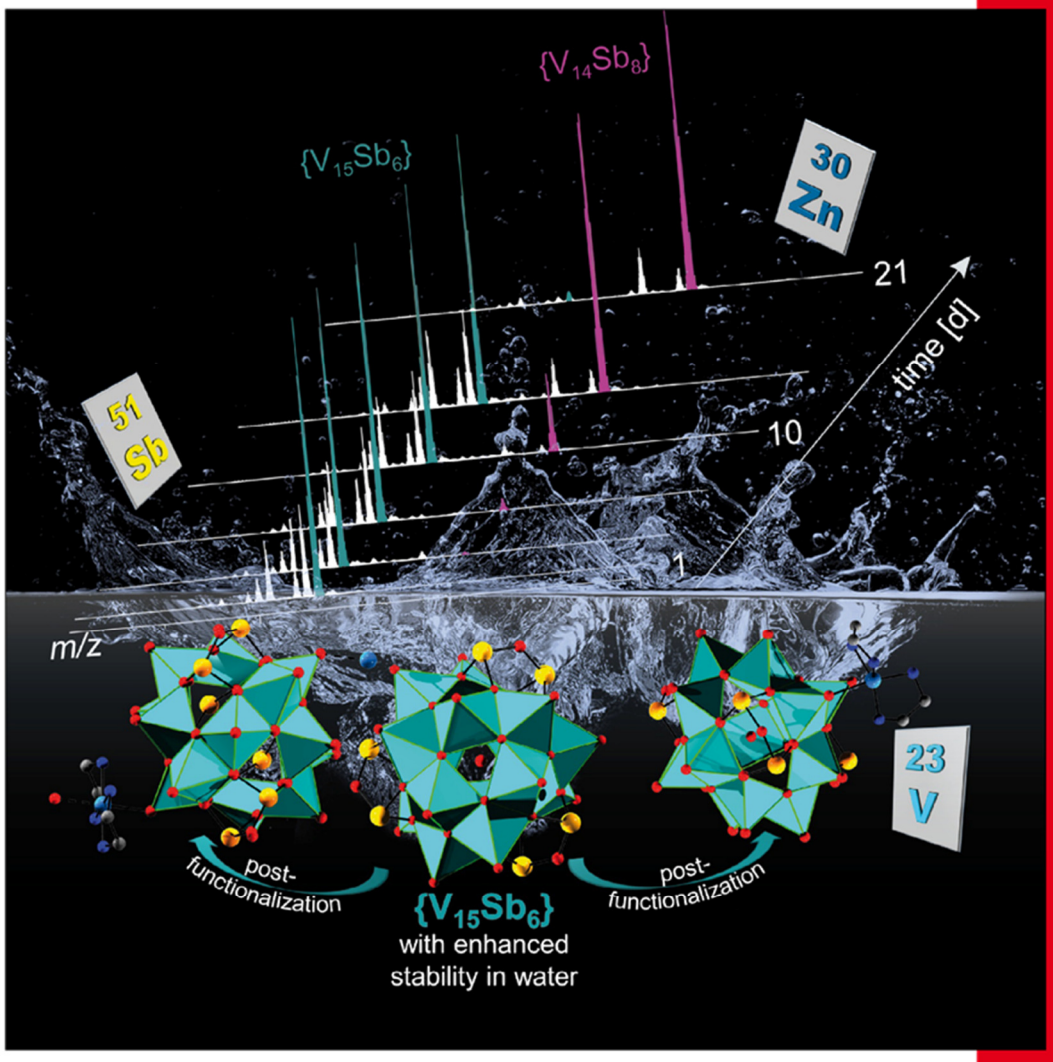

Cover Feature:
W. Bensch et al.
New Water-Soluble Cluster Compound {Zn(en)$_3$}$_3$[V$_{15}$Sb$_6$O$_{42}$(H$_2$O)]·(Ethylenediamine)$_3$·10 H$_2$O as a Synthon for the Generation of Two New Antimonato Polyoxovanadates

Supported by
ACES Asian Chemical Editorial Society

WILEY-VCH

ChemPubSoc Europe

DOI: 10.1002/chem.201705732

CHEMISTRY A European Journal Full Paper

Antimonato Polyoxovanadate Clusters

New Water-Soluble Cluster Compound {Zn(en)$_3$}$_3$[V$_{15}$Sb$_6$O$_{42}$(H$_2$O)]·(Ethylenediamine)$_3$·10 H$_2$O as a Synthon for the Generation of Two New Antimonato Polyoxovanadates

Lisa K. Mahnke,[a] Ulrike Warzok,[b] Mengxi Lin,[a] Christian Näther,[a] Christoph A. Schalley,[b] and Wolfgang Bensch*[a]

Abstract: A new antimonato polyoxovanadate {Zn(en)$_3$}$_3$[V$_{15}$Sb$_6$O$_{42}$(H$_2$O)]·3 en·10 H$_2$O (en = ethylenediamine) synthesized under hydrothermal conditions exhibits remarkable solubility in water. Electrospray ionization mass spectrometry (ESI-MS) investigations on an aqueous solution demonstrate that the cluster core remains fully intact for 72 h. At longer times, slow transformation into a {V$_{14}$Sb$_8$O$_{42}$} cluster is observed. The conversion reaches 50% after 14 days and is complete after approximately 20 days. The rate of this {V$_{15}$Sb$_6$}→{V$_{14}$Sb$_8$} cluster transformation is significantly increased in the presence of ammonium acetate. Applying the new compound as a synthon in the presence of 1,10-phenanthroline (phen) led to crystallization of {Zn(phen)$_3$}$_2$[Zn(en)$_2$V$_{15}$Sb$_6$O$_{42}$(H$_2$O)]·23 H$_2$O after a short reaction time, whereas addition of Sb$_2$O$_3$ led to fast crystallization of {(Zn(en)$_2$(H$_2$O)$_2$)(Zn(en)$_2$)}[Zn(en)$_2$V$_{15}$Sb$_6$O$_{42}$(H$_2$O)]·8.5 H$_2$O. In the crystal structure of {Zn(en)$_3$}$_3$[V$_{15}$Sb$_6$O$_{42}$(H$_2$O)]·3 en·10 H$_2$O, the en molecules are seen to be attached to the cluster anion through Sb–N bonds. In the structures of the two new compounds obtained, the [V$_{15}$Sb$_6$O$_{42}$(H$_2$O)]$^{6-}$ anions are expanded by Zn^{2+}-centered complexes through Zn–O–V bond formation.

Introduction

High-nuclearity heterometallic polyoxovanadates (POVs) containing main group semimetals such as As, Sb, Si, or Ge in the cluster shell are of interest due to their often intriguing magnetic and electronic properties.[1] Most high-nuclearity POVs can be structurally derived from the {V$_{18}$O$_{42}$} archetype cluster by replacing VO$_5$ square pyramids by one, two, or three E$_2$O$_5$ units (E = As, Sb) or E′$_2$O$_7$ moieties (E′ = Si, Ge).[2] If E = Sb (Sb-POVs), the three cluster anions [V$_{14}$Sb$_8$O$_{42}$]$^{4-}$ {V$_{14}$}, [V$_{15}$Sb$_6$O$_{42}$]$^{6-}$ {V$_{15}$}, or [V$_{16}$Sb$_4$O$_{42}$]$^{8-}$ {V$_{16}$}[2] can be synthesized. With regard to the magnetic properties, the {V$_{15}$} cluster is most interesting because the magnetic ground state is an $S = {}^1/_2$ spin state.[3] Heterometal POVs are usually synthesized under solvothermal conditions in basic solutions using simple vanadium compounds such as V$_2$O$_5$ or NH$_4$VO$_3$ in the presence of a suitable heteroatom precursor. The dissolved vanadium and heteroatom species then self-assemble to form the clusters.[4] This synthetic approach, however, does not allow for control of the nuclearity of the POV or the number of heteroatoms incorporated into the cluster shell. Moreover, solvothermal syntheses often require relatively long reaction times, typically between 5 and 14 days.

Focusing on Sb-POVs, compensation of the negative charges of the clusters can be achieved by ammonium ions[5–9] or transition metal complexes.[10–20] Also, several Sb-POVs exist that feature cluster anions expanded by transition-metal complexes, as exemplified by [V$_{16}$Sb$_4$O$_{42}$(H$_2$O){VO(dach)$_2$}$_4$],[21] {[Fe(dach)$_2$]$_3$[V$_{15}$Sb$_6$O$_{42}$(H$_2$O)]}·8 H$_2$O[22] (dach = *trans*-1,2-diaminocyclohexane), [{Ni(en)$_2$}$_2$V$_{14}$Sb$_8$O$_{42}$]·5.5 H$_2$O[18] (en = ethylenediamine), [Zn$_2$(dien)$_3$][{Zn(dien)}$_2$V$_{16}$Sb$_4$O$_{42}$(H$_2$O)]·4 H$_2$O, and [Zn$_2$(dien)$_2$]$_2$ [{Zn(dien)}$_2$V$_{14}$Sb$_8$O$_{42}$(H$_2$O)]·4 H$_2$O[15] (dien = diethylenetriamine).

Very recently, we discovered an Sb-POV exhibiting reasonably good solubility in water, namely {Ni(en)$_3$}$_3$-[V$_{15}$Sb$_8$O$_{42}$(H$_2$O)]· ≈ 15 H$_2$O[10] (**I**). Through time-dependent ESI-MS studies, we observed that the {V$_{15}$} cluster is gradually transformed into the {V$_{14}$} compound. The great potential of **I** as a synthon has been demonstrated by the preparation of {Ni(phen)$_3$}$_2$[{Ni(en)$_2$}V$_{15}$Sb$_6$O$_{42}$(H$_2$O)]·19 H$_2$O, [{Ni(en)$_2$}$_2$V$_{14}$Sb$_8$O$_{42}$]·5.5 H$_2$O, and {Ni(phen)$_3$}$_2$ [V$_{14}$Sb$_8$O$_{42}$]·phen·12 H$_2$O (phen = 1,10-phenanthroline).[10,11,23,24] With increasing reaction temperature and time, formation of the Sb-richer cluster anion is favored. In situ X-ray diffraction experiments evidenced that **I** is dissolved or amorphized within minutes, and that product formation sets in after a distinct induction period, leading to formation of the favored {V$_{14}$} cluster.[24]

[a] L. K. Mahnke, M. Lin, Prof. Dr. C. Näther, Prof. Dr. W. Bensch
Institut für Anorganische Chemie
Christian-Albrechts-Universität zu Kiel
Max-Eyth-Strasse 2, 24118 Kiel (Germany)
E-mail: wbensch@ac.uni-kiel.de

[b] U. Warzok, Prof. Dr. C. A. Schalley
Institut für Chemie und Biochemie, Freie Universität Berlin
Takustrasse 3, 14195 Berlin (Germany)

Supporting information and the ORCID number(s) for the author(s) of this article can be found under https://doi.org/10.1002/chem.201705732.

During our investigations of zinc-containing antimonato polyoxovanadates in hydrothermal aqueous en solutions, we discovered the new compound {Zn(en)$_3$}$_3$[V$_{15}$Sb$_6$O$_{42}$(H$_2$O)]·3 en·10 H$_2$O (**II**). Interestingly, the solubility of **II** in water is five times greater than that of **I**. ESI-MS experiments evidenced a remarkably different solution reactivity of **II** compared to that of **I**. Whereas the {V$_{15}$} core of **I** undergoes a relatively fast transformation into the {V$_{14}$} cluster, the anion of compound **II** is stable in water over several days. This finding motivated us to use **II** as a synthon for the preparation of new {V$_{15}$}-containing compounds. Herein, we report kinetic studies employing ESI-MS and compare the reactivities of **I** and **II** in aqueous solutions. The syntheses of the new compounds {Zn(phen)$_3$}$_2$[Zn(en)$_2$V$_{15}$Sb$_6$O$_{42}$(H$_2$O)]·23 H$_2$O (**III**) and {(Zn(en)$_2$(H$_2$O)$_2$)(Zn(en)$_2$)}[Zn(en)$_2$V$_{15}$Sb$_6$O$_{42}$(H$_2$O)]·8.5 H$_2$O (**IV**) are described and their crystal structures are discussed.

Results and Discussion

The title compound {Zn(en)$_3$}$_3$[V$_{15}$Sb$_6$O$_{42}$(H$_2$O)]·3 en·10 H$_2$O (**II**) was synthesized by the solvothermal reaction of NH_4VO_3, Sb_2O_3, and $ZnCl_2$ in an ethylenediamine/water mixture. A reaction time of 5 days afforded the product in 90.6% yield (based on V). The solubility of compound **II** in distilled water (5.75 g L^{-1}) is significantly higher than that of **I** (1.19 g L^{-1}[10]), as determined by a standard procedure based on UV/Vis spectrophotometry (Supporting Information, Figure S1).

The distinct solubility of **II** makes it an ideal starting material for the preparation of new Sb-POV compounds. This is exemplified by the formation of {Zn(phen)$_3$}$_2$[Zn(en)$_2$V$_{15}$Sb$_6$O$_{42}$(H$_2$O)]·23 H$_2$O (**III**) upon reaction of **II** with 1,10-phenanthroline and the formation of {(Zn(en)$_2$(H$_2$O)$_2$)(Zn(en)$_2$)}[Zn(en)$_2$V$_{15}$Sb$_6$O$_{42}$(H$_2$O)]·8.5 H$_2$O (**IV**) when **II** was reacted with Sb_2O_3. Both procedures proved to be very convenient; the reactions were performed in aqueous solution, reached completion within 24 h, and gave yields of 28 and 78%, respectively.

Interestingly, the new compounds **III** and **IV** contain an unchanged {V$_{15}$} cluster core, whereas post-functionalization of **I** in previous studies typically yielded products with {V$_{14}$}-type clusters.

The negative-mode ESI mass spectrum of a 60 μM aqueous solution obtained from crystals of compound **II** (**M** = V$_{15}$Sb$_6$O$_{42}$) recorded 5 min after sample preparation features signals attributable to the intact cluster ions [**M**·H$_2$O]$^{3-}$/[**M**·H·H$_2$O]$^{3-}$ and [**M**·H·H$_2$O]$^{2-}$/[**M**·2 H·H$_2$O]$^{2-}$ at *m/z* 728 and 1093, respectively (Figure 1 a). These cluster ions contain an encapsulated water molecule, as also shown by X-ray crystal structure analysis (see below). The mass spectrum also features a peak due to **M**$^{3-}$/[**M**·H]$^{3-}$ ions at *m/z* 722, which can be assigned to an empty cluster. In agreement with our earlier mass spectrometric study on compound **I**,[10] the [V$_{15}$Sb$_6$O$_{42}$]$^{6-}$ core undergoes two or three one-electron oxidations of V^{IV} to V^{V} during the ionization process, yielding triply- and quadruply-charged cluster ions, and these can form proton adducts for charge compensation. This process results in overlapping isotope patterns for all peaks. Furthermore, the intact cluster is present as its complex [**M**·Zn(en)·H$_2$O]$^{2-}$/[**M**·Zn(en)·H·H$_2$O]$^{2-}$, observable as a low-abundance signal at *m/z* 1155. Ten days after dissolution of **II**, a new signal at *m/z* 792 appeared in the mass spectrum, indicative of the formation of an Sb-enriched {V$_{14}$} cluster (**N** = V$_{14}$Sb$_8$O$_{42}$) in solution, appearing as [**N**·H$_2$O]$^{3-}$/[**N**·H·H$_2$O]$^{3-}$ ions (Figure 1 b). Net exchange of a VO unit by an Sb–O–Sb unit has also been observed for the well-studied Ni analogue **I**.[10]

However, the products obtained by post-functionalization of **I** and **II** differ in their cluster structures. To elucidate these diverging results, we investigated the time-dependent solution reactivities of compounds **I** and **II**, namely the {V$_{15}$Sb$_6$}→{V$_{14}$Sb$_8$} transformation reaction, in aqueous solution (Figures S2–S6). The previously reported {V$_{15}$}→{V$_{14}$} reaction of nickel compound **I** in water is relatively fast, giving 50% conversion after 110 h (Figure 2).[10] The corresponding reaction of the new compound **II** is clearly slower and reaches a conversion of 50% only after 330 h. This indicates a significantly in-

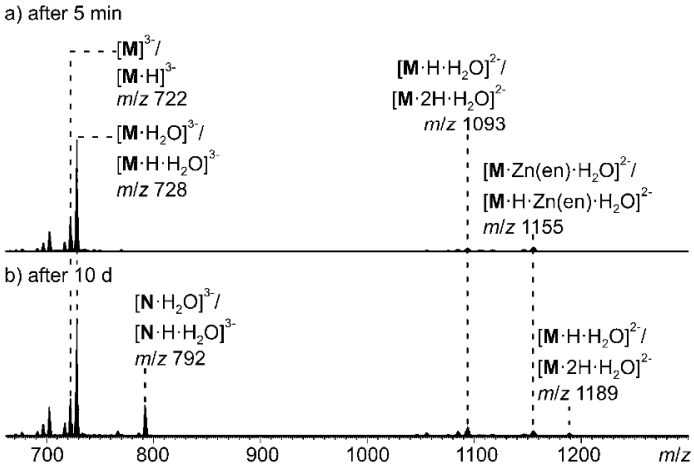

Figure 1. ESI-Q-TOF-HRMS of compound **II** (60 μM in H$_2$O) after a) 5 min and b) 10 days. **M** = V$_{15}$Sb$_6$O$_{42}$, **N** = V$_{14}$Sb$_8$O$_{42}$.

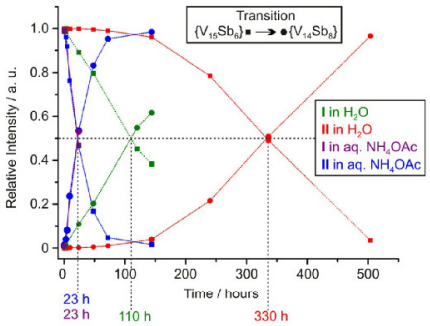

Figure 2. Time-dependent formation at 277 K of the {V$_{14}$} cluster core from the {V$_{15}$} cluster core for compounds **I** and **II** in aqueous solution and in aqueous ammonium acetate solution (1%), with the corresponding times at which 50% conversion was reached.

creased stability of the {V$_{15}$} core of **II** in aqueous solution and rationalizes why compounds **III** and **IV** can be selectively prepared by ligand-exchange reactions, during which the cluster core remains intact. When **I** and **II** were dissolved in aqueous ammonium acetate solution (1%), which acts as a buffer in the neutral pH range, the {V$_{15}$Sb$_6$}→{V$_{14}$Sb$_8$} transformation became very fast for both precursors **I** and **II**, resulting in a virtually identical time of 23 h to reach 50% conversion. No major degradation was observed within the evaluated reaction times. This finding encourages the use of additives such as ammonium acetate for future studies aimed at the systematic synthesis of {V$_{14}$} cluster compounds from the known {V$_{15}$} precursors. It should be noted that when **I** and **II** were dissolved in aqueous NH$_3$ solution (1%), both underwent complete degradation after approximately 1 day, and no {V$_{15}$Sb$_6$}→{V$_{14}$Sb$_8$} transformation was observed.

Compound **II** crystallizes in the chiral non-centrosymmetric monoclinic space group $P2_1$, with two formula units per unit cell (Table S1). All atoms are located in general positions, except for three oxygen atoms. Compounds **III** and **IV** crystallize in the centrosymmetric monoclinic space groups $C2/c$ and $P2_1/c$, respectively (Table S1). In the latter two compounds, several atoms are in special positions. The structures of **II**–**IV** feature the {V$_{15}$Sb$_6$O$_{42}$} cluster (approximate D_3 symmetry; Figure 3) consisting of 15 edge- and corner-sharing VO$_5$ square pyramids and three Sb$_2$O$_5$ handle-like units, which are constructed by corner-sharing of two SbO$_3$ trigonal pyramids with one water molecule in the middle of the cluster shell. The arrangement of the VO$_5$ polyhedra generates two hexagons of edge-sharing VO$_5$ pyramids (Figure 3 left, pink and green pyramids). The two hexagons are C_4-symmetrically connected by three VO$_5$ pyramids (Figure 3 left, blue pyramids). The geometric parameters are in full agreement with data reported in the literature for {V$_{15}$}-core-containing Sb-POVs (Tables S2–S6).[5–9,12–19,21,22,25,26]

Determination of the oxidation states by bond valence sum (BVS[27]) calculations indicated the presence of V^{IV} centers in all three compounds (Table S7), allowing formulation of the clusters as [V$^{IV}_{15}$Sb$^{III}_6$O$_{42}$]$^{6-}$. The presence of V^{IV} is supported by the characteristic V=O stretching vibration in the IR spectra (**II**: 974; **III**: 959, **IV**: 974 cm^{-1} (Figures S10–S12). The negative charges of the cluster anion in **II** are compensated by three unique Zn^{2+}-centered complexes. The Zn^{2+} cations are surrounded by three bidentate en ligands with typical Zn–N bond lengths and N–Zn–N angles (Tables S2, S5, and S6). The N–Zn–N angles indicate severe distortion of the octahedra. Two [Zn(en)$_3$]$^{2+}$ complexes are Λ-isomers (Zn(1) and Zn(2)) and the remaining complex forms the Δ-isomer (Zn(3)).[28] Interesting structural features in **II** are short Sb–N distances to the N atoms of all three unique en molecules (2.613(10)–2.656(13) Å), involving three of the six unique Sb atoms. These Sb–N distances are much shorter than the sum of the van der Waals radii of Sb and N (3.55 Å).[29–31] Comparably short Sb–N separations have previously been observed in several Sb-POVs (2.528–2.731 Å).[8,13,17,25] In a recent DFT-based investigation, we demonstrated that such Sb–N distances must be treated as chemical bonds.[20]

The Zn^{2+}-centered complexes and the cluster anions are arranged alternatingly along [010] and [001] (Figure 4), and each cluster is surrounded by eight complexes (Figure S13). Short distances between the N atoms of the en ligands and the O atoms of water molecules (2.772(19)–3.192(17) Å, Table S8) suggest hydrogen-bonding (HB) interactions.[32] Using the notation introduced by Infantes et al., the water molecules in **II** form C3

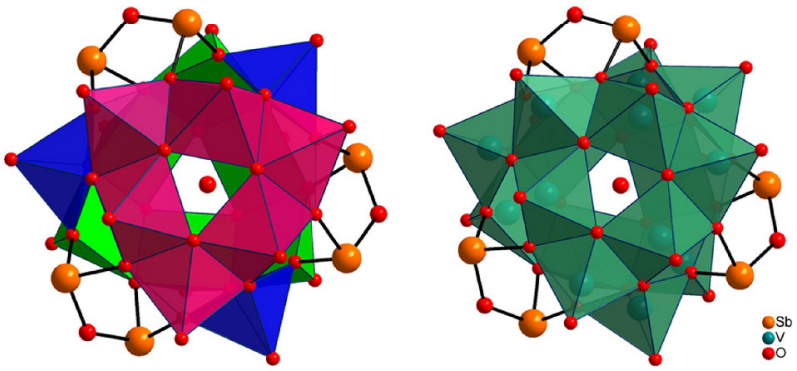

Figure 3. Polyhedral representation of the [V$_{15}$Sb$_6$O$_{42}$(H$_2$O)]$^{6-}$ cluster anion.

ChemPubSoc Europe

CHEMISTRY A European Journal Full Paper

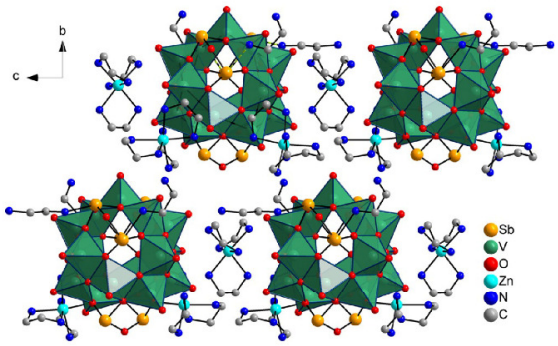

Figure 4. Compound **II**: View of four clusters with the corresponding charge-balancing counter ions. H atoms have been omitted for clarity.

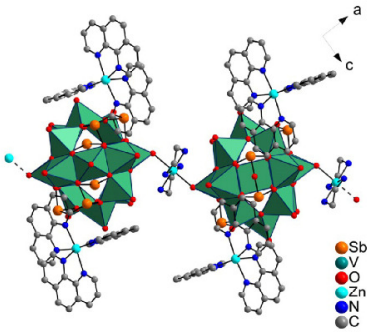

Figure 6. View of the 1D chain in compound **III** directed along [101] and charge-balancing $[Zn(phen)_3]^{2+}$ complexes. H atoms have been omitted for clarity.

and C6 chains connecting the cluster anions in a three-dimensional arrangement (Figure 5, Table S9).[33–35]

In the structure of **III**, $\{V_{15}\}$ clusters are connected to their nearest neighbors by a $[Zn(en)_2]^{2+}$ complex through O_{term}–Zn–O_{term} interactions to form a chain directed along [101] (Figure 6). The independent Zn^{2+} cation of $[Zn(en)_2]^{2+}$ is located in a special position and is bonded to N atoms of two symmetry-related bidentate en ligands (Zn–N bonds: 2.120(5) and 2.127(5) Å). The coordination environment is completed by bonds to terminal O atoms of adjacent cluster anions (Zn–O: 2.241(4) Å), thus leading to a distorted octahedral $[Zn(en)_2O_2]$ complex (Tables S3, S5, and S6). The bite angle for the en ligands connecting the cluster is 82.4(2)°. The corresponding angle of 97.6(2)° between these two en ligands is in line with literature data.[23,36–41] The second unique Zn^{2+} cation is in a distorted octahedral environment made up of three bidentate phen ligands (Tables S3, S5, and S6). The $[Zn(phen)_3]^{2+}$ complexes are located between the chains, thus generating a layer-like arrangement that extends in all crystallographic directions (Figure 7). A sandwich-type arrangement is observed between the phen ligands of the $[Zn(phen)_3]^{2+}$ complexes, indicative of π–π stacking interactions, which organize the complexes into strands. The C···C distances between adjacent phen ligands range from 3.588(9) to 3.918(11) Å (average: 3.813 Å,

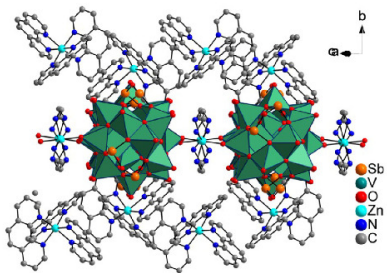

Figure 7. Compound **III**: Four cluster anions surrounded by $[Zn(phen)_3]^{2+}$ complexes and connected through $[Zn(en)_3]^{2+}$ bridges to 1D chains directed along [101]. H atoms have been omitted for clarity.

Figure S16, Table S3).[42] The water molecules are involved in HB interactions and form clusters, which can be identified as U^0 with one R6 ring according to Infantes et al.[31–33] The water cluster interacts with the anions through hydrogen bonds (O–O distances: 2.654(11)–2.900(11) Å; average: 2.771 Å) as well as with H atoms of the ligands of the Zn^{2+}-centered complexes (O···H–X distances: 2.274(4)–2.697(4) Å; average: 2.531 Å) (Figure 8, Tables S10–S12).

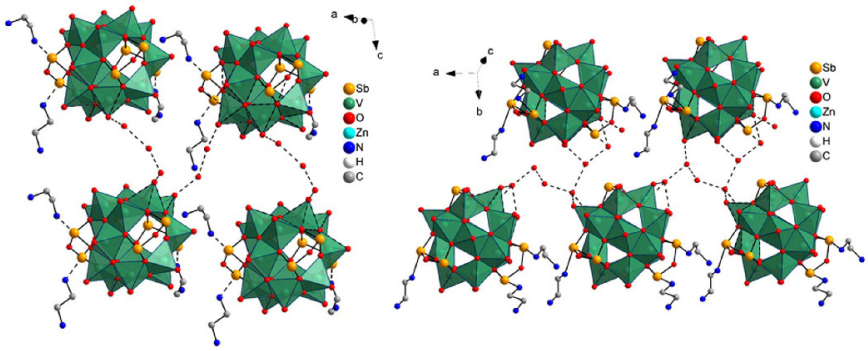

Figure 5. Compound **II**: View of the cluster anions connected by C3 (left) and C6 (right) water chains. O-O separations indicative of HB interactions are shown as dotted lines. Note that the Zn^{2+}-centered complexes are not displayed and H atoms have been omitted for clarity.

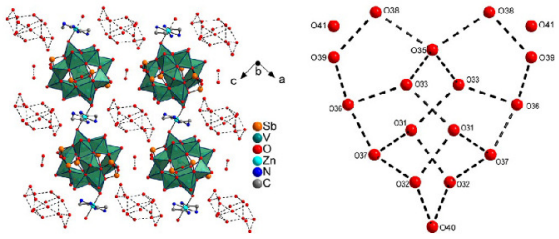

Figure 8. Left: View of the chains in the structure of **III** with water clusters. Right: U^0-water cluster with one R6 ring and R5 rings. Hydrogen atoms have been omitted for clarity.

In the structure of {(Zn(en)$_2$(H$_2$O)$_2$)(Zn(en)$_2$)}-[Zn(en)$_2$V$_{15}$Sb$_6$O$_{42}$(H$_2$O)]·8.5 H$_2$O (**IV**), the three unique Zn^{2+} cations are in different coordination environments. Zn(1) is surrounded by two en ligands (Zn–N bonds: 2.021(8)–2.118(9) Å; average: 2.056 Å) and one terminal O atom of the anion (Zn–O: 2.344(6) Å), resulting in a distorted trigonal bipyramid (Table S5).[41,43–45] Zn(2) is in a distorted octahedral environment comprising four N atoms of two en ligands and two O atoms of H$_2$O molecules, with geometric parameters in accordance with literature data (Tables S5 and S6).[45–47] The basal plane is formed by two N and two O atoms, and the apical positions are occupied by two N atoms. Zn(3) is surrounded by two en ligands (Zn–N bonds: 1.973(10)–2.018(9) Å; average: 2.003 Å) forming a distorted tetrahedron (N–Zn–N angles: 85.9(4)–128.0(4)°) (Figure 9; Tables S4–S6). All angles and bond lengths are in full agreement with literature data for Zn-containing POVs[14,15] and other zinc ethylenediamine complexes.[36–41,43–45,47,48]

Each [V$_{15}$Sb$_6$O$_{42}$(H$_2$O)]$^{6-}$ anion is surrounded by nine Zn^{2+}-centered complexes. Some H atoms bonded to N atoms of the en ligands are connected to O atoms of the anion by HB interactions (O···H–N distances: 2.007(7)–2.688(6) Å; average: 2.367 Å; Table S13). The clusters are arranged in rods along [001] and stacked in an ABAB fashion along [010] and [100]. The water molecules form a D4 chain (Figure S18, pink) and an R8 ring, including HB to one water ligand of the [Zn(en)$_2$(H$_2$O)$_2$]$^{2+}$ complex (Figure S18, yellow).[33–35,49]

The D4 and R8 water clusters join [Zn(en)$_2$V$_{15}$Sb$_6$O$_{42}$(H$_2$O)] moieties by HB to several terminal O atoms of the anions (Figure S18, dotted lines). Two unique Sb atoms have one O atom of a water molecule at distances shorter than 3 Å (Sb(3)-O(60): 2.788(26) Å; Sb(6)-O(52): 2.928(8) Å), indicating weak interactions when considering the sum of the van der Waals radii (3.52 Å[29–31]).

Conclusions

In summary, we have reported a new water-soluble hetero-polyoxovanadate (**II**), with Zn^{2+} complexes as charge-balancing units. We have examined the transformation of this precursor into two new hetero-polyoxovanadates that exhibit numerous fascinating structural features. Furthermore, the reactivity of **II** in solution has been studied by ESI-MS, which confirmed the increased stability of this compound in solution and a decelerated {V$_{15}$Sb$_6$}→{V$_{14}$Sb$_8$} transition reaction as compared to the earlier introduced hetero-polyoxovanadate (**I**), with nickel complexes as the counter ions. This finding elucidates the formation of compounds **III** and **IV**, which feature an intact {V$_{15}$Sb$_6$} cluster core after post-functionalization. In future work, we intend to explore the effects of additives on the transformation processes, as ammonium acetate was found to greatly accelerate the competing {V$_{15}$Sb$_6$}→{V$_{14}$Sb$_8$} transformation in solution.

CCDC 1587912, 1587913, and 1587914 contain the supplementary crystallographic data for this paper. These data can be obtained free of charge from The Cambridge Crystallographic Data Centre.

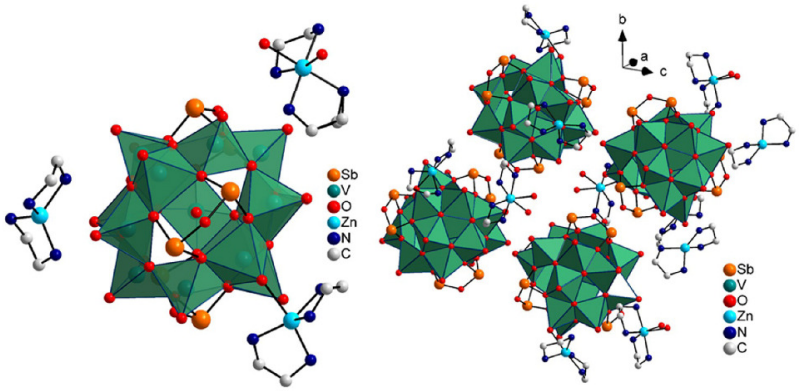

Figure 9. Left: View of the molecular structure of **IV** with the three unique charge-balancing complexes: [Zn(en)$_2$]$^{2+}$ connected to the cluster shell by a Zn–O bond, [Zn(en)$_2$]$^{2+}$, and [Zn(en)$_2$(H$_2$O)$_2$]$^{2+}$. Right: Four clusters (**IV**) with charge-balancing units. Note that only the major split position of the Zn(2) complex is shown and that H atoms have been omitted for clarity.

ChemPubSoc Europe

CHEMISTRY A European Journal Full Paper

Experimental Section

General

All chemicals, namely NH_4VO_3 (Merck, 99%), Sb_2O_3 (Merck, pure), $ZnCl_2$ (Merck, pure), 1,10-phenanthroline (ABCR, 99%), and ethylenediamine (Grüssing, 99%), were used as received without further purification. The studied compounds were prepared under solvothermal conditions in Duran® glass tubes (≈11 mL). The products were collected by filtration, washed with small amounts of distilled water and ethanol, and finally dried.

Synthesis and characterization

Synthesis of {Zn(en)$_3$}$_3$[V$_{15}$Sb$_6$O$_{42}$(H$_2$O)]·3 en·10 H$_2$O (II): NH_4VO_3 (0.1567 g, 1.34 mmol), Sb_2O_3 (0.0774 g, 0.265 mmol), and $ZnCl_2$ (0.0896 g, 0.657 mmol) were mixed with ethylenediamine (2.3 mL) and distilled H_2O (1.7 mL). After heating at 150 °C for 5 d, brown crystals were obtained. Yield based on V: 90.6%. Elemental analysis calcd (%) for $C_{24}H_{126}N_{24}O_{63}Sb_6V_{15}Zn_3$: C 8.36, H 3.68, N 9.74; found: C 8.09, H 3.45, N 9.20. EDX analysis gave a ratio of 15.24 (V) : 6.24 (Sb) : 3.02 (Zn).

Synthesis of {Zn(phen)$_3$}$_2$[Zn(en)$_2$V$_{15}$Sb$_6$O$_{42}$(H$_2$O)]·23 H$_2$O (III): II (0.1481 g, 0.045 mmol), 1,10-phenanthroline (0.0730 g, 0.405 mmol), and distilled water (4 mL) were heated at 150 °C for 24 h, whereupon dark-brown crystals were formed. Yield based on V: 78.5%. Elemental analysis calcd (%) for $C_{76}H_{94}N_{16}O_{57}Sb_6V_{15}Zn_3$: C 23.81, H 2.47, N 5.84; found: C 24.11, H 2.28, N 5.83. EDX analysis gave a ratio of 14.31 (V) : 6.15 (Sb) : 3.08 (Zn).

Synthesis of {(Zn(en)$_2$(H$_2$O)$_2$)(Zn(en)$_2$)}-[Zn(en)$_2$V$_{15}$Sb$_6$O$_{42}$(H$_2$O)]·8.5 H$_2$O (IV): II (0.1810 g, 0.055 mmol) and Sb_2O_3 (0.0481 g, 0.165 mmol) were mixed with distilled water (4 mL). After heating at 150 °C for 24 h, black to brown crystals were formed. Yield based on V: 28.0%. Elemental analysis calcd (%) for $C_{12}H_{70}N_{12}O_{53}Sb_6V_{15}Zn_3$: C 4.93, H 2.42, N 5.75; found: C 4.94, H 2.09, N 5.65. EDX analysis gave a ratio of 14.66 (V) : 6.09 (Sb) : 3.05 (Zn).

Single-crystal structure analysis

Data collections were performed using a STOE imaging plate diffraction system (IPDS-2) employing $Mo_{K\alpha}$ radiation ($\lambda = 0.71073$ Å). The crystal structures were solved with SHELXT[50,51] and refined against F^2 using SHELXL-2014.[50,51] All non-H atoms were refined anisotropically, except for some disordered water O atoms in **III**. The C–H and N–H H atoms of the en ligands coordinated to the Zn cations were positioned with idealized geometries and refined isotropically with $U_{iso}(H) = 1.2\ U_{eq}(C)$ using a riding model. In all of the compounds, the water molecules were disordered and refined using a split model. The N–H H atoms of the non-coordinating en ligands in compound **II** and the water H atoms in all of the compounds were not located, but were considered in the calculation of the molecular formulae and the molecular masses.

Mass spectrometry

Electrospray ionization quadrupole time-of-flight high-resolution mass spectrometric (ESI-Q-TOF-HRMS) experiments were performed with a Synapt G2-S HDMS instrument (Waters Co., Milford, MA, USA). The flow rate was set at 3–5 μL min^{-1}, the spray voltage at 1.6 kV, the sample cone voltage at 10 V, the source offset at 80 V, the nebulizer gas pressure at 6 bar, and the desolvation gas flow at 500 L h^{-1}. 60 μM solutions from crystalline samples **I** and **II** were prepared in H_2O, 1% aqueous NH_4OAc solution, and 1% aqueous NH_3 solution, respectively. Time-dependent measurements were conducted on samples kept at 4 °C, from which aliquots were taken and directly subjected to mass spectrometric analysis. All reaction times quoted therefore refer to reaction at 4 °C.

Acknowledgements

The authors thank the Land of Schleswig-Holstein and the Deutsche Forschungsgemeinschaft (priority program 1415 and CRC 1109) for financial support.

Conflict of interest

The authors declare no conflict of interest.

Keywords: cluster compounds · crystal structure · ESI-MS · solvothermal synthesis · water-soluble precursor

[1] a) S. Bertaina, S. Gambarelli, T. Mitra, B. Tsukerblat, A. Müller, B. Barbara, *Nature* **2008**, *453*, 203; b) C. J. Calzado, J. M. Clemente-Juan, E. Coronado, A. Gaita-Arino, N. Suaud, *Inorg. Chem.* **2008**, *47*, 5889; c) S. Cardona-Serra, J. M. Clemente-Juan, E. Coronado, A. Gaita-Ariño, N. Suaud, O. Svoboda, R. Bastardis, N. Guihéry, J. J. Palacios, *Chem. Eur. J.* **2015**, *21*, 763; d) J.-J. Chen, M. D. Symes, S.-C. Fan, M.-S. Zheng, H. N. Miras, Q.-F. Dong, L. Cronin, *Adv. Mater.* **2015**, *27*, 4649; e) K. K. Kasem, F. A. Schultz, *Can. J. Chem.* **1995**, *73*, 858.
[2] K. Y. Monakhov, W. Bensch, P. Kögerler, *Chem. Soc. Rev.* **2015**, *44*, 8443.
[3] P. Kögerler, B. Tsukerblat, A. Müller, *Dalton Trans.* **2010**, *39*, 21.
[4] C. Streb, "*Structure and Bonding in Molecular Vanadium Oxides: From Templates via Host–Guest Chemistry to Applications*" in *Structure and Bonding*, Springer, Heidelberg, **2017**, DOI: 10.1007/430 2017 2.
[5] X.-X. Hu, J.-Q. Xu, X.-B. Cui, J.-F. Song, T.-G. Wang, *Inorg. Chem. Commun.* **2004**, *7*, 264.
[6] R. Kiebach, C. Näther, W. Bensch, *Solid State Sci.* **2006**, *8*, 964.
[7] E. Antonova, A. Wutkowski, C. Näther, W. Bensch, *Solid State Sci.* **2011**, *13*, 2154.
[8] E. Antonova, C. Näther, P. Kögerler, W. Bensch, *Angew. Chem. Int. Ed.* **2011**, *50*, 764; *Angew. Chem.* **2011**, *123*, 790.
[9] R. Kiebach, C. Näther, P. Kögerler, W. Bensch, *Dalton Trans.* **2007**, 3221.
[10] M. Wendt, U. Warzok, C. Näther, J. van Leusen, P. Kögerler, C. A. Schalley, W. Bensch, *Chem. Sci.* **2016**, *7*, 2684.
[11] M. Wendt, C. Näther, W. Bensch, *Chem. Eur. J.* **2016**, *22*, 7747.
[12] E. Antonova, C. Näther, W. Bensch, *Dalton Trans.* **2012**, *41*, 1338.
[13] E. Antonova, C. Näther, W. Bensch, *CrystEngComm* **2012**, *14*, 6853.
[14] E. Antonova, C. Näther, P. Kögerler, W. Bensch, *Dalton Trans.* **2012**, *41*, 6957.
[15] Y. Gao, Z. Han, Y. Xu, C. Hu, *J. Cluster Sci.* **2010**, *21*, 163.
[16] H.-Y. Guo, X. Zhang, X.-B. Cui, Q.-S. Huo, J.-Q. Xu, *CrystEngComm* **2016**, *18*, 5130.
[17] H. Lühmann, C. Näther, P. Kögerler, W. Bensch, *Inorg. Chim. Acta* **2014**, *421*, 549.
[18] L. Yu, J.-P. Liu, J.-P. Wang, J.-Y. Niu, *Chem. Res. Chin. Univ.* **2009**, *25*, 426.
[19] L. Zhang, X. Zhao, J. Xu, T. Wang, *Dalton Trans.* **2002**, 3275.
[20] M. Rasmussen, C. Näther, J. van Leusen, P. Kögerler, L. Zhechkov, T. Heine, W. Bensch, *Inorg. Chem.* **2017**, *56*, 7120.
[21] A. Wutkowski, C. Näther, P. Kögerler, W. Bensch, *Inorg. Chem.* **2008**, *47*, 1916.
[22] A. Wutkowski, C. Näther, P. Kögerler, W. Bensch, *Inorg. Chem.* **2013**, *52*, 3280.
[23] M. Wendt, P. Polzin, J. van Leusen, C. Nather, P. Kögerler, W. Bensch, *Dalton Trans.* **2017**, *46*, 1618.
[24] M. Wendt, L. K. Mahnke, N. Heidenreich, W. Bensch, *Eur. J. Inorg. Chem.* **2016**, 5393.
[25] E. Antonova, C. Näther, P. Kögerler, W. Bensch, *Inorg. Chem.* **2012**, *51*, 2311.

[26] E. Antonova, B. Seidlhofer, J. Wang, M. Hinz, W. Bensch, *Chem. Eur. J.* **2012**, *18*, 15316.
[27] a) I. D. Brown, D. Altermatt, *Acta Crystallogr. B* **1985**, *41*, 244; b) M. O'Keefe, N. E. Brese, *J. Am. Chem. Soc.* **1991**, *113*, 3226.
[28] A. G. Mitchell, *J. Pharm. Pharm. Sci.* **1998**, *1*, 8.
[29] A. Bondi, *J. Phys. Chem.* **1964**, *68*, 441.
[30] A. Bondi, *J. Phys. Chem.* **1966**, *70*, 3006.
[31] M. Mantina, A. C. Chamberlin, R. Valero, C. J. Cramer, D. G. Truhlar, *J. Phys. Chem. A* **2009**, *113*, 5806.
[32] a) D. Braga, L. Maini, M. Polito, E. Tagliavini, F. Grepioni, *Coord. Chem. Rev.* **2003**, *246*, 53; b) J. Hernández-Paredes, R. C. Carrillo-Torres, O. Hernández-Negrete, R. R. Sotelo-Mundo, D. Glossman-Mitnik, H. E. Esparza-Ponce, M. E. Alvarez-Ramos, *J. Mol. Struct.* **2017**, *1141*, 53; c) M. Huš, T. Urbic, *J. Chem. Phys.* **2012**, *136*, 144305; d) G. A. Jeffrey, *An Introduction to Hydrogen Bonding*, Oxford University Press, New York, **1997**; e) I. Nobeli, S. L. Price, J. P. M. Lommerse, R. Taylor, *J. Comput. Chem.* **1997**, *18*, 2060; f) L. J. Prins, D. N. Reinhoudt, P. Timmerman, *Angew. Chem. Int. Ed.* **2001**, *40*, 2382; *Angew. Chem.* **2001**, *113*, 2446.
[33] L. Infantes, J. Chisholm, S. Motherwell, *CrystEngComm* **2003**, *5*, 480.
[34] L. Infantes, L. Fábián, W. D. S. Motherwell, *CrystEngComm* **2007**, *9*, 65.
[35] L. Infantes, S. Motherwell, *CrystEngComm* **2002**, *4*, 454.
[36] S. T. Hafeez, S. Ali, M. N. Tahir, M. Iqbal, K. S. Munawar, *J. Coord. Chem.* **2014**, *67*, 2479.
[37] S. T. Hafeez, M. N. Tahir, S. Ali, M. Iqbal, H. Gulab, K. S. Munawar, *J. Coord. Chem.* **2015**, *68*, 3636.
[38] A.-Y. Fu, D.-Q. Wang, D.-Z. Sun, *Acta Crystallogr. Sect. E* **2005**, *61*, m401 – m403.
[39] Ş. Işık, Y. Köysal, M. Yavuz, Z. Heren, L. Vurucu, *Acta Crystallogr. Sect. E* **2005**, *61*, m2066 – m2068.
[40] M.-T. Li, X.-C. Fu, X.-Y. Wang, C.-G. Wang, *Acta Crystallogr. Sect. E* **2007**, *63*, m1677 – m1677.
[41] S.-T. Zheng, Y.-M. Chen, J. Zhang, G.-Y. Yang, *Z. Anorg. Allg. Chem.* **2006**, *632*, 155.
[42] a) J. W. G. Bloom, S. E. Wheeler, *Angew. Chem. Int. Ed.* **2011**, *50*, 7847; *Angew. Chem.* **2011**, *123*, 7993; b) Y.-H. Chi, J.-M. Shi, H.-N. Li, W. Wei, E. Cottrill, N. Pan, H. Chen, Y. Liang, L. Yu, Y.-Q. Zhang, C. Hou, *Dalton Trans.* **2013**, *42*, 15559; c) S. Grimme, *Angew. Chem. Int. Ed.* **2008**, *47*, 3430; *Angew. Chem.* **2008**, *120*, 3478; d) J. Hilbert, C. Näther, W. Bensch, *Dalton Trans.* **2015**, *44*, 11542; e) S. L. Cockroft, J. Perkins, C. Zonta, H. Adams, S. E. Spey, C. M. R. Low, J. G. Vinter, K. R. Lawson, C. J. Urch, C. A. Hunter, *Org. Biomol. Chem.* **2007**, *5*, 1062; f) C. A. Hunter, K. R. Lawson, J. Perkins, C. J. Urch, *J. Chem. Soc. Perkin Trans. 2* **2001**, 651; g) C. Janiak, *J. Chem. Soc. Dalton Trans.* **2000**, 3885; h) C. R. Martinez, B. L. Iverson, *Chem. Sci.* **2012**, *3*, 2191; i) G. B. McGaughey, *J. Biol. Chem.* **1998**, *273*, 15458; j) M. J. Rashkin, M. L. Waters, *J. Am. Chem. Soc.* **2002**, *124*, 1860; k) A. L. Ringer, M. O. Sinnokrot, R. P. Lively, C. D. Sherrill, *Chem. Eur. J.* **2006**, *12*, 3821; l) M. O. Sinnokrot, C. D. Sherrill, *J. Phys. Chem. A* **2003**, *107*, 8377; m) M. O. Sinnokrot, E. F. Valeev, C. D. Sherrill, *J. Am. Chem. Soc.* **2002**, *124*, 10887.
[43] Y. Liu, R. Pan, J.-W. Cheng, H. He, B.-F. Yang, Q. Zhang, G.-Y. Yang, *Chem. Eur. J.* **2015**, *21*, 15732.
[44] L. Zhang, Z. Shi, G. Yang, X. Chen, S. Feng, *J. Solid State Chem.* **1999**, *148*, 450.
[45] S.-T. Zheng, J. Zhang, G.-Y. Yang, *Chem. Lett.* **2003**, *32*, 810.
[46] D. Sun, D.-F. Wang, F.-J. Liu, H.-J. Hao, N. Zhang, R.-B. Huang, L.-S. Zheng, *CrystEngComm* **2011**, *13*, 2833.
[47] J. Zhou, X. Liu, F. Hu, R. Chen, H. Zou, W. Fu, G. Liang, Y. Chen, *CrystEngComm* **2013**, *15*, 4593.
[48] a) Y. Qi, Y. Li, E. Wang, H. Jin, Z. Zhang, X. Wang, S. Chang, *Inorg. Chim. Acta* **2007**, *360*, 1841; b) Y. Qi, Y. Li, E. Wang, Z. Zhang, S. Chang, *Dalton Trans.* **2008**, 2335.
[49] a) S. Maheshwary, N. Patel, N. Sathyamurthy, A. D. Kulkarni, S. R. Gadre, *J. Phys. Chem. A* **2001**, *105*, 10525; b) K. Mizuse, J.-L. Kuo, A. Fujii, *Chem. Sci.* **2011**, *2*, 868; c) A. Wutkowski, C. Näther, W. Bensch, *Inorg. Chim. Acta* **2011**, *379*, 16; d) A. Yangui, W. Rekik, S. Elleuch, Y. Abid, *Acta Crystallogr. Sect. E* **2014**, *70*, m227.
[50] G. M. Sheldrick, *Acta Crystallogr. Sect. A* **2008**, *64*, 112.
[51] G. M. Sheldrick, *Acta Crystallogr. Sect. C* **2015**, *71*, 3.

Manuscript received: December 4, 2017
Version of record online: February 21, 2018

4.5. Die Publikation *„Rational Syntheses of Three New {$V_{14}Sb_8$}-Clusters Applying a Water Soluble High-Nuclearity Cluster as Synthon"*

In der Publikation wird über die rationale solvothermale Synthese von drei neuen Verbindungen mit dem {$V_{14}Sb_8O_{42}$}-Cluster berichtet: {$Zn(phen)_3$}$_2$[$V_{14}Sb_8O_{42}(H_2O)$]·0.5 phen·17 H_2O, [{$Zn(en)_2$}$_2$$V_{14}Sb_8O_{42}$]·7 H_2O und {$Fe(phen)_3$}$_2$[$V_{14}Sb_8O_{42}(H_2O)$]·11 H_2O. Als Edukt wurde der Precursor Zn-{$V_{15}Sb_6$} eingesetzt. Zuvor erzielte ESI-MS-Ergebnisse bei der Untersuchungen des Precursor Zn-{$V_{15}Sb_6$} zeigten, dass durch Zugabe von NH_4OAc die Bildung des Endproduktes beeinflusst werden kann. Daher konnte durch Einstellen des pH-Wertes die Kristallisation von Verbindungen mit dem {$V_{15}Sb_6O_{42}$}-Cluster vermieden und ausschließlich Produkte mit dem {$V_{14}Sb_8O_{42}$}-Cluster erhalten werden. Während der Transformation {$V_{15}Sb_6O_{42}$} → {$V_{14}Sb_8O_{42}$} sind, wie die Produkte zeigen, ebenfalls Ligandenaustausch und der Austausch ganzer Komplexeinheiten möglich, was neue Möglichkeiten für die Synthese neuer funktioneller Materialen bietet. In allen drei Verbindungen deuten kurze Sb···O-Abstände auf schwache Wechselwirkungen hin, was zur Ausbildung von Aggregaten mit höherer Dimensionalität führt. Die Kristallwassermoleküle sind über Wasserstoffbrückenbindungen zu unterschiedlichen Wasserclustern verbunden. Zusätzlich werden Wechselwirkungen zwischen den H_2O-Molekülen und dem Cluster sowie mit den Liganden der Übergangsmetallkomplexe gefunden.

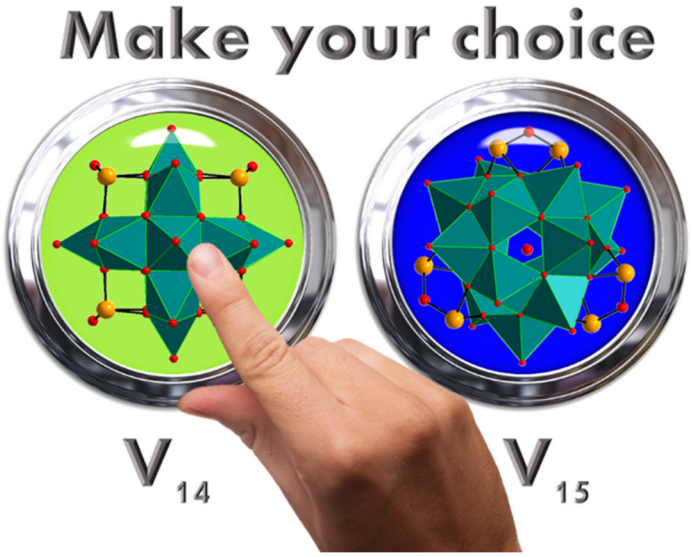

Abbildung 22: TOC Grafik der Publikation *„Rational Syntheses of Three New {$V_{14}Sb_8$}-Clusters Applying a Water Soluble High-Nuclearity Cluster as Synthon"*.

„Rational Syntheses of Three New {$V_{14}Sb_8$}-Clusters Applying a Water Soluble High-Nuclearity Cluster as Synthon"

Veröffentlicht in *Cryst. Growth Des.* **2018**, *18*, 6100.
DOI: 10.1021/acs.cgd.8b00987

CRYSTAL GROWTH & DESIGN

Article

Cite This: *Cryst. Growth Des.* 2018, 18, 6100–6106

pubs.acs.org/crystal

Rational Syntheses of Three New {$V_{14}Sb_8$} Clusters Applying a Water-Soluble High-Nuclearity Cluster as Synthon

Lisa K. Mahnke, Michael Wendt, Christian Näther, and Wolfgang Bensch*

Institut für Anorganische Chemie, Christian-Albrechts-Universität zu Kiel, Max-Eyth-Straße 2, 24118 Kiel, Germany

Supporting Information

ABSTRACT: We report the rational solvothermal syntheses and crystal structures of three new antimonato-polyoxovanadates, $\{Zn(phen)_3\}_2[V_{14}Sb_8O_{42}(H_2O)]\cdot 0.5\ phen\cdot 17\ H_2O$ (**1**), $[\{Zn(en)_2\}_2V_{14}Sb_8O_{42}]\cdot 7\ H_2O$ (**2**), and $\{Fe(phen)_3\}_2[V_{14}Sb_8O_{42}(H_2O)]\cdot 11\ H_2O$ (**3**), using the water-soluble $\{Zn(en)_3\}_3[V_{15}Sb_6O_{42}(H_2O)]\cdot 3en\cdot 10H_2O$ as synthon. The solvothermal reactions are fast and product formation is finished within 24 h. Adjustment of the pH value by application of an ammonia buffer avoided crystallization of the $\{V_{15}Sb_6O_{42}\}$ core containing products. In the structure of **1**, the en ligands of the starting compound are in situ exchanged by phen molecules. In **2**, one en ligand of the $[Zn(en)_3]^{2+}$ complexes of the educt is emitted under the reaction conditions, leading to crystallization of a layered structure formed by V−O−Zn−O bonds. Finally, in compound **3**, the initially Zn^{2+}-centered complexes are exchanged in situ by Fe^{2+}-centered complexes with phen ligands. In all three structures, short intercluster Sb···O separations indicate weak interactions, leading to aggregates of higher dimensionality. The crystal water molecules are connected by intermolecular hydrogen bonds, leading to the formation of different types of water clusters. In addition, the water molecules are involved in hydrogen bonding to the cluster anions and ligands of the transition metal complexes.

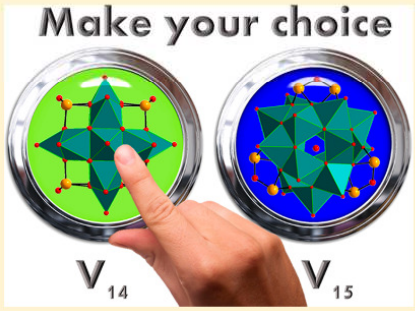

INTRODUCTION

The properties of polyoxovanadates (POVs) and hetero-metal modified POVs are discussed in the areas like (photo-[1−3]) catalytically,[4,5] magnetically,[5−7] or physiological[8,9] applications or as new anode materials in batteries,[10] in visible light driven dye degradation,[2] in green catalysis,[3] and as absorbents in water filters.[11] Traditionally, most POVs and hetero-POVs are synthesized under solvothermal conditions using multiple starting materials being reacted under solvothermal conditions at high pH values for several days or even weeks. In addition, which cluster anions are formed cannot be predicted and very often the product contains appreciable amounts of side phases.[12−35] Due to the large number of synthesis parameters (solvent, temperature, pressure, pH value, nature of educts, etc.), the preparation of new hetero-metal containing POVs is based on the trial-and-error approach. The preparation of new Sb-POVs was restricted to the serendipitous solvothermal approach without any influence on the crystallized product or avoidance of side products. Hence, the chemistry of such POVs is very different compared to polyoxomolybdates or polyoxotungstates where a variety of high-nuclearity precursors are available which can be used under ambient conditions for generation of new compounds.[34]

Very recently, we prepared two new precursors which are soluble in water, namely, $\{Ni(en)_3\}_3[V_{15}Sb_6O_{42}(H_2O)_x]\cdot\sim 15H_2O$[36] (Ni-$\{V_{15}Sb_6\}$) and $\{Zn(en)_3\}_3[V_{15}Sb_6O_{42}(H_2O)]\cdot 3en\cdot 10H_2O$[37] (Zn-$\{V_{15}Sb_6\}$) (en = ethylenediamine). The ESI MS (electrospray ionization mass spectroscopy) investigations of Ni-$\{V_{15}Sb_6\}$ evidenced that the transformation to an antimony richer cluster, namely, $\{V_{14}Sb_8O_{42}\}$, occurs at room temperature within a short time period;[36] i.e., transformation starts after about 24 h. Therefore, using Ni-$\{V_{15}Sb_6\}$ as synthon mainly compounds with the $\{V_{14}Sb_8\}$ cluster could be prepared.[38,39] In contrast, ESI MS characterization of Zn-$\{V_{15}Sb_6\}$ demonstrated an unexpected stability in water for at least 72 h, and the $\{V_{15}Sb_6\}$ cluster is the main product in solution over a large time span.[37] The transformation to the $\{V_{14}Sb_8O_{42}\}$ cluster reaches only 50% after 14 days and is completed after ca. 20 days. But interestingly, adjustment of the pH value between 8.5 and 9.5 by addition of NH_4OAc to the aqueous solution of Zn-$\{V_{15}Sb_6\}$ leads to an *in situ* transformation of the $\{V_{15}Sb_6\}$ moiety into the V-poorer $\{V_{14}Sb_8\}$ shell within 72 h at room temperature and within 24 h at 150 °C.[37] Hence, adjusting the pH value allows directed selection of the dominating cluster shell in solution according to ESI MS experiments. This observation encouraged us performing syntheses with pH values between 8.5 and 9.5, and successfully synthesized and characterized the new compounds $\{Zn(phen)_3\}_2[V_{14}Sb_8O_{42}(H_2O)]\cdot 0.5\ phen\cdot 17\ H_2O$ (**1**), $[\{Zn(en)_2\}_2V_{14}Sb_8O_{42}]\cdot 7\ H_2O$ (**2**), and $\{Fe(phen)_3\}_2[V_{14}Sb_8O_{42}(H_2O)]\cdot 11\ H_2O$ (**3**).

Received: June 28, 2018
Revised: August 3, 2018
Published: August 20, 2018

DOI: 10.1021/acs.cgd.8b00987
Cryst. Growth Des. 2018, 18, 6100–6106

„Rational Syntheses of Three New {$V_{14}Sb_8$}-Clusters Applying a Water Soluble High-Nuclearity Cluster as Synthon"

EXPERIMENTAL SECTION

Materials and Reagents. All chemicals, NH_4VO_3 (Merck, 99%), Sb_2O_3 (Merck, pure), $ZnCl_2$ (Merck, pure), $FeCl_2{\cdot}4H_2O$ (fluka, pure), 1,10-phenanthroline (phen) (abcr, 99%), ethylenediamine (en) (Grüssing, 99%), and NH_4Cl (Grüssing, purum 99.5%), were used as received without further purification. The compounds have been prepared under solvothermal conditions in DURAN glass tubes (volume ∼ 11 mL). The precursor $\{Zn(en)_3\}_3[V_{15}Sb_6O_{42}(H_2O)]{\cdot}3en{\cdot}15H_2O$ ($Zn\{V_{15}Sb_6\}$) was synthesized using the published protocol.[37] The products were filtered off and were washed with distilled water and ethanol. All compounds were obtained by reacting the slurries at 150 °C for 1 day.

Synthesis of $\{Zn(phen)_3\}_2[V_{14}Sb_8O_{42}]{\cdot}0.5phen{\cdot}18H_2O$ (1). 0.1480 g (0.045 mmol) of $\{Zn(en)_3\}_3[V_{15}Sb_6O_{42}(H_2O)]{\cdot}3en{\cdot}15H_2O$[37] (Zn-$\{V_{15}Sb_6\}$), 0.0727 g of 1,10-phenanthroline (0.403 mmol), and 0.0060 g (0.110 mmol) of NH_4Cl were mixed with 4 mL of dist. H_2O. Brown crystals were obtained with a yield of ca. 88% based on V. Elemental analysis: C: 24.32, H: 1.71, N: 4.86%; calc.-$8H_2O$ ($C_{78}H_{72}N_{13}O_{52}Sb_8V_{14}Zn_2$): C: 24.39, H: 1.89, N: 4.74%. EDX analysis, ratio: 14.14 (V):7.53 (Sb):2.10 (Zn). Note: **1** can also be prepared using NH_4VO_3, Sb_2O_3, $Zn(NO_3)_2{\cdot}6H_2O$, 1,10-phenanthroline, methylamine, and water within 7 days at T = 150 °C (for more information, see the Supporting Information).

Synthesis of $[\{Zn(en)_2\}_2V_{14}Sb_8O_{42}]{\cdot}7H_2O$ (2). 0.1480 g (0.045 mmol) of Zn-$\{V_{15}Sb_6\}$ and 0.0060 g (0.110 mmol) of NH_4Cl were mixed with 4 mL of dist. H_2O. Brown to black crystals crystallized with a yield based on V of 35%. Elemental analysis: C: 4.02, H: 1.79, N: 4.40%; calc.-$4H_2O$ ($C_8H_{38}N_8O_{45}Sb_8V_{14}Zn_2$): C: 3.45, H: 1.38, N: 4.02%. EDX analysis, ratio: 14.28 (V):7.72 (Sb):2.05 (Zn).

Synthesis of $\{Fe(phen)_3\}_2[V_{14}Sb_8O_{42}(H_2O)]{\cdot}phen{\cdot}11\ H_2O$ (3). 0.1480 g (0.045 mmol) of Zn-$\{V_{15}Sb_6\}$, 0.0319 g (0.160 mmol) of $FeCl_2{\cdot}4\ H_2O$, 0.0727 g of 1,10-phenanthroline (0.403 mmol), and 0.0060 g (0.110 mmol) of NH_4Cl were mixed with 4 mL of dist. H_2O, which leads to the formation of red crystals with a yield based on V of 55%. Elemental analysis: C: 25.53, H: 2.57, N: 5.61%; calc.-$3H_2O$ ($C_{84}H_{72}Fe_2N_{14}O_{50}Sb_8V_{14}$): C: 26.03, H: 1.87, N: 5.06%. EDX analysis, ratio: 14.03 (V):8.50 (Sb):1.98 (Fe).

Please note: The compound can also be synthesized applying NH_4VO_3, Sb_2O_3, $FeCl_2{\cdot}4H_2O$, 1,10-phenanthroline, diethylenetriamine, and water within 7 days at T = 150 °C (for more information, see the Supporting Information).

IR spectra were measured from 400 to 4000 cm^{-1} using a Genesis FTIRTM spectrometer (ATI Mattson) at room temperature. CHN analyses were performed with an EA Elemental Analyzer (EURO VECTOR Instruments). EDX analyses were done with an Environmental Scanning Electron Microscope ESEM XL30 (Philips) equipped with an EDX detector.

X-ray diffraction. The X-ray powder patterns were recorded using a STADI-P diffractometer in transmission geometry with Cu–Kα_1 radiation (STOE, λ = 1.540598 Å, Ge(111) monochromator) with a Mythen 1K detector. The powder patterns of the compounds are compared with those calculated with single crystal structural data demonstrating the phase purity of the materials (Figures S1–S3).

Single Crystal Structure Determination. Data collections have been performed with a STOE Imaging Plate Diffraction System (IPDS-1) with Mo–Kα radiation (λ = 0.71073 Å). A numerical absorption correction was performed for all structures (see Tables S1–S4). The crystal structures have been solved with SHELXS-97 and refined against F^2 using SHELXL-2014.[40,41]

Most of the non-hydrogen atoms were refined anisotropically. The C-H H atoms were positioned with idealized geometry and refined using a riding model. The O-H H atoms in **1** and **3** were not located during structure refinements, but they are considered in the calculation of the formula and the molecular weight. The positions of two O atoms in the structure of **3** are half-occupied. In the structure of **2**, the O-H H atoms of three water molecules atoms were located in Fourier difference maps, their bond lengths were set to ideal values, and afterward they were refined using a riding model. The fourth water position is only half-occupied, and the H atoms could not be located but were considered in the calculation of the molecular formula and the molecular weight.

One phen ligand is disordered in **1** around a center of inversion and was refined isotropically with half occupancy using restraints. Various water atoms are disordered, and their positions are not fully occupied. They were only refined isotropically using a split model. The crystal investigated was non-merohedral twinned. Both individuals were indexed separately, and from their orientation matrix, the twin matrix was calculated. Afterward, the structure was refined using the data in HKLF-5 format (BASF parameter: 0.1080(8)). Therefore, equivalent reflections were merged before the HKLF-5 file was generated. To avoid errors because of twinning, the absorption correction was performed using data, in which the overlapping reflections were removed.

Selected crystallographic data and the results of refinements are summarized in the Supporting Information (Tables S1–S4).

CCDC 1852015 (**1**), CCDC 1852016 (**2**), and CCDC 1852017 (**3**) contain the supplementary crystallographic data for this paper.

RESULTS AND DISCUSSION

Synthetic Aspects. Recently, we applied $\{Ni(en)_3\}_3[V_{15}Sb_6O_{42}(H_2O)_x]{\cdot}{\sim}15H_2O$ as starting material for the preparation of new Sb-POVs and obtained compounds containing the $\{V_{14}Sb_8\}$ cluster shell.[38,39] The formation of the V-poorer cluster anion could be understood on the basis of results of ESI MS experiments demonstrating a relatively fast conversion $\{V_{15}Sb_6\} \rightarrow \{V_{14}Sb_8\}$.[36] Such transformation took much more time for Zn-$\{V_{15}Sb_6\}$, and the transformation velocity could be significantly enhanced by adjusting the pH value in the window 8.5–9.5. An important difference between aqueous solutions of Zn-$\{V_{15}Sb_6\}$ and Ni-$\{V_{15}Sb_6\}$ is the pH value: for the former precursor, pH ≈ 10.5 was measured, while, for the latter, pH ≈ 9.8, which is near the pH value range necessary for the conversion of the cluster anion in the starting material. According to these observations, the pH value of the solution seems to play a product determining role. It should be also noted that, in contrast to syntheses performed with multiple starting materials, the yield is high using either Zn-$\{V_{15}Sb_6\}$ or Ni-$\{V_{15}Sb_6\}$, and mainly phase pure samples are obtained.

Crystal Structures. All compounds crystallize in the centrosymmetric monoclinic space group $P2_1/n$ with four (**1** and **3**) or two (**2**) formula units per unit cell (Table S4).

In all three structures, eight VO_5 square pyramids share common edges to form an eight-membered ring. Two triads of edge-sharing VO_5 polyhedra are located above and below this ring. These triads are either parallel (β-isomer of the $\{V_{14}Sb_8O_{42}\}$ cluster) (Figure 1, right) or rotated against each other by 90° (α-isomer) (Figure 1, left). The niches of the cluster anion generated by the arrangement of the VO_5

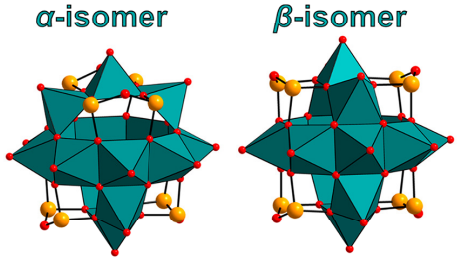

Figure 1. Polyhedral view of the α-isomer (left) and the β-isomer of the $\{V_{14}Sb_8O_{42}\}$ cluster (right). (color code: red: O, orange: Sb, green: VO_5 square pyramids).

DOI: 10.1021/acs.cgd.8b00987
Cryst. Growth Des. 2018, 18, 6100–6106

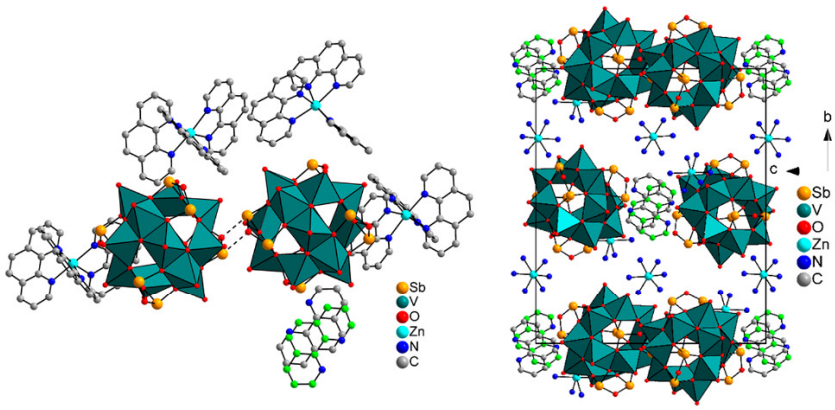

Figure 2. View of the structure of compound **1**. Left: arrangement of two anions with surrounding $[Zn(phen)_3]^{2+}$ complexes and a disordered phen molecule; the dashed lines indicate intercluster Sb···O interactions (H atoms are omitted for clarity). Right: packing of $[V_{14}Sb_8O_{42}]^{4-}$ clusters with view along *a*-axis (C atoms of the complexes and H atoms are omitted for clarity).

polyhedra are occupied by Sb_2O_5 handles formed by corner-sharing of two SbO_3 moieties. The cluster anion in compounds **1** and **3** feature the D_{2d}-symmetric α-isomer (Figure 1, left), and the D_{2h}-symmetric β-isomer is observed in the structure of **2** (Figure 1, right).

The terminal V=O bonds are characteristic for the VO_5 square pyramids with averages of 1.603 Å for **1**, 1.608 Å for **2**, and 1.607 Å for **3**. These V^{IV}=O groups lead to a strong absorption in the IR spectra which are located at 971−981 cm^{-1} for the title compounds (Figure S4).[12−16,18−29,36−38,42,43] All longer V−O bonds (Tables S1−S3) are in agreement with literature data and scatter around 2 Å.[12−16,18−29,36−38,42,43] The Sb−O bond lengths (Tables S1−S3) (**1**: average: 1.951 Å; **2**: average: 1.961 Å; **3**: average: 1.952 Å) are typical for Sb^{III}−O^{2-} and match well with those reported for other Sb-POVs.[12−16,18−29,36−38,42,43] The oxidation states of V and Sb were determined by the bond valence sum (BVS) method, resulting in +IV for V centers and +III for Sb (Table S5).[44−46] The V−V separations are between 2.774 and 3.112 Å (**1**: average: 2.990 Å; **2**: average: 2.981 Å; **3**: average: 2.988 Å) and are typical for Sb-POVs.[12−16,18−29,36−38,42,43]

In the structure of **1**, the $[V_{14}Sb_8O_{42}]^{4-}$ cluster is surrounded by two crystallographically independent $[Zn(phen)_3]^{2+}$ complexes (Figure 2); i.e., the en ligands of the complex in the starting material are *in situ* exchanged by phen molecules. The geometric parameters of the complex (Table S1) are in agreement with data reported in the literature. The octahedral Zn^{2+}-centered complexes are moderately distorted as evidenced by the Zn−N bonds and N−Zn−N angles (Table S1), which is also in agreement with literature data.[47−51] The angles between the almost planar phen ligands are in the range of 74.2−88.1° (average: 82.6°). Along [010], mixed layers composed of $[V_{14}Sb_8O_{42}]^{4-}$ anions and phen molecules alternate with layers containing Zn^{2+}-centered complexes (Figure 2, right). Along [001], phen molecules and cluster anions alternate, while, in the adjacent layer, only $[Zn(phen)_3]^{2+}$ complexes are located. Water molecules are joined through H bonding interactions to form a water cluster and are connected to N atoms of the disordered phen molecule (Table S6, Figure S5). Following the nomenclature of Infantes et al., the water molecules with fully occupied crystallographic positions form a C8 chain (Table S6, Figure S5).[52,53] Two adjacent $[V_{14}Sb_8O_{42}]^{4-}$ anions are oriented "face-to-face" which leads to a short Sb−O distance of 2.619(5) Å (Figure 2, left), which is much smaller than the sum of their van der Waals radii (3.52 Å[54−56]), indicating at least weak Sb−O bonding interactions. The phen ligands of the complexes are arranged to form π−π stacking (Figure S6) with intermolecular distances of 3.380(17)−3.381(9) Å for T-shaped orientation and 3.384(2) and 3.530(9) Å for sandwich type π−π stacking (average: 3.419 Å). According to literature reports,[57−66] such short intermolecular separations are typical for interactions with energies in the kcal·mol^{-1} range.

In the structure of **2**, each β-{$V_{14}Sb_8O_{42}$} cluster is linked via four O_{term}−Zn^{2+}−O_{term} bonds (Zn−O: 2.202(4) and 2.204(4) Å), generating a layer within the (101) plane (Figure 3). The

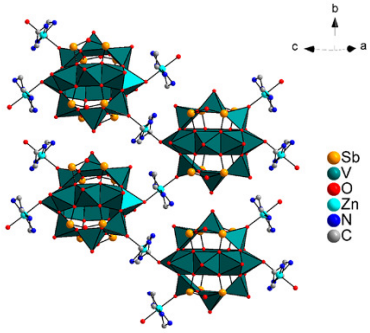

Figure 3. View of the cluster anions connected by Zn^{2+}-centered complexes in **2** forming a layer in the (101) plane (H atoms are not displayed for clarity).

Zn^{2+} cation is surrounded by two en ligands and two terminal O^{2-} atoms of VO_5 polyhedra, yielding a slightly distorted {$Zn(en)_2O_2$} octahedron. The geometric parameters (Table S2) of this polyhedron are in accordance with literature data.[48,67−71] A short intramolecular N···O separation between one cluster oxygen and N-H atom of the en ligands indicates hydrogen bonding interaction (Figure 4, left). Between N-H atoms of the en ligands and H_2O molecules, H bonds are also observed (Table S7).

DOI: 10.1021/acs.cgd.8b00987
Cryst. Growth Des. 2018, 18, 6100−6106

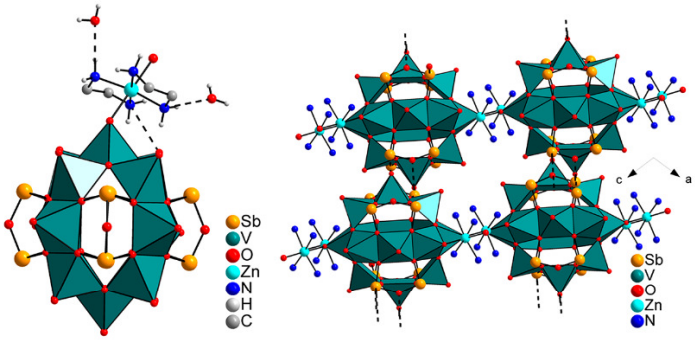

Figure 4. View of the $\{V_{14}Sb_8O_{42}\}$ cluster in the structure of **2** with intramolecular H bonds and N-H···O bonds (left, only water and N-H H atoms are displayed); right: the three-dimensional network generated by weak intercluster Sb···O interactions.

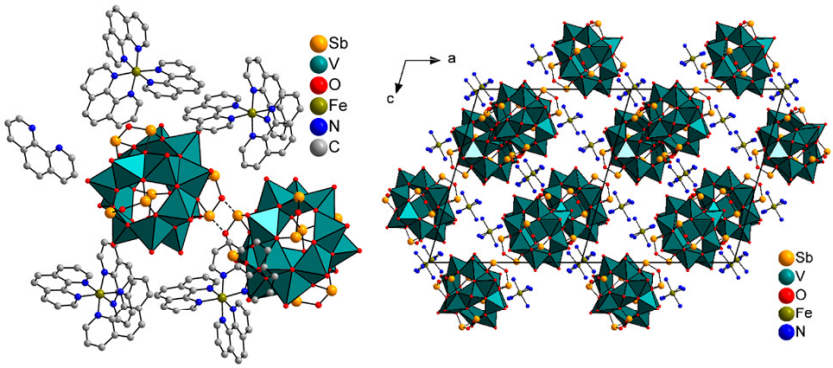

Figure 5. Left: two cluster anions in the structure of **3** joined by weak Sb···O interactions, four $[Fe(phen)_3]^{2+}$ complexes, and one phen molecule (H atoms have been omitted for clarity). Right: packing of cations and anions in the structure of **3** (C and H atoms have been omitted for clarity).

Three Sb−O separations < 3 Å (2.668(4)−2.959(4) Å) indicate weak intercluster interactions, and taking theses interactions into account, a three-dimensional network is generated (Figure 4, right) with pores along [010] (Figure 4, right). Crystal water molecules are involved in hydrogen bonds with oxygen atoms of the anion and N atoms of the complexes (Figure S7).[72,73]

During the synthesis of **3**, the $[Zn(en)_3]^{2+}$ complexes of Zn-$\{V_{15}Sb_6\}$ are exchanged by Fe^{2+}-centered complexes. The structure of **3** contains the α-$\{V_{14}Sb_8O_{42}\}$ cluster which is surrounded by two crystallographically independent $[Fe(phen)_3]^{2+}$ complexes (Figure 5, left). The Fe−N bond lengths as well as the N−Fe−N angles match well with those reported for Fe^{2+}-centered phen complexes[74−78] and indicate a moderate distortion of the octahedra. Adjacent $\{V_{14}Sb_8O_{42}\}$ moieties are connected via weak Sb−O bonds (Sb−O: 2.645(3) Å) to form a dimer (Figure 5, left).

Like in the structure of **1**, the phen ligands are arranged to form $\pi-\pi$ interactions with distances between 3.542(9) Å and 3.701(6) Å for the T-shaped type (average: 3.622 Å) and 3.336(6)−3.861(5) Å (average: 3.610 Å) for the sandwich-type (Table S8, Figure S8).[57−63] The angles between the planes of the phen molecules are between 79.8° and 88.9° (average: 85.6°).

The crystal water molecules form a C5 chain with O−O distances between 2.864(6) Å and 2.923(19) Å (average: 2.860 Å) (Figure S9).[52,53,79,80] Furthermore, the H_2O molecules interact with the anionic clusters via short O_3Sb···O distances of 2.874(6)−3.129(8) Å (average: 3.031 Å; Figure S9, yellow dotted lines) and with O_4V-O···O distances from 2.768(7) Å to 2.947(7) Å (average: 2.877 Å; Figure S9, red dotted lines).

■ CONCLUSION

In the past years, many Sb-POV compounds were successfully synthesized using multiple sources as starting materials. As a drawback, most of the products were not phase pure and often the compounds were obtained in low yields, which made elaborate synthesis parameter optimization necessary for receiving enough material for further characterizations. Here, we demonstrated the large synthetic potential of the water-soluble precursor Zn-$\{V_{15}Sb_6\}$ for the directed generation of new V-poorer Sb-POVs obtained in high yield at short reaction times and as phase pure materials. If the pH value is adjusted between 8.5 and 9.5 using a buffer, only $\{V_{14}Sb_8\}$ clusters containing compounds crystallize, while higher pH values (>10) afford formation of compounds comprising the $\{V_{15}Sb_6\}$ cluster core. Compared to syntheses of Sb-POVs using multiple sources as starting material, the reaction time is drastically reduced to hours instead of days or weeks. For the preparation of new compounds, only water is needed because reducing molecules like, e.g., amines, are not required. Furthermore, the pronounced pH dependence decides which cluster is formed in the product, which allows rational planning

DOI: 10.1021/acs.cgd.8b00987
Cryst. Growth Des. 2018, 18, 6100−6106

of a synthesis and the so-called "black box" approach can be avoided. Furthermore, the results presented here demonstrate that ligands can be exchanged or even complex cations. All of these findings open new opportunities for the selective preparation of Sb-POV compounds exhibiting unusual structural features, chemical compositions, and properties which cannot be synthesized without screening a large parameter set in time-consuming ways.

■ ASSOCIATED CONTENT

Supporting Information

The Supporting Information is available free of charge on the ACS Publications website at DOI: 10.1021/acs.cgd.8b00987.

Additional tables with selected bond lengths and angles and bond valence sum analyses, images of the structures, powder patterns, IR spectra and assignments of the V=O infrared absorption bands of all three compounds, $\pi-\pi$ interactions and interactions between water molecules (PDF)

Accession Codes

CCDC 1852015−1852017 contain the supplementary crystallographic data for this paper. These data can be obtained free of charge via www.ccdc.cam.ac.uk/data_request/cif, or by emailing data_request@ccdc.cam.ac.uk, or by contacting The Cambridge Crystallographic Data Centre, 12 Union Road, Cambridge CB2 1EZ, UK; fax: +44 1223 336033.

■ AUTHOR INFORMATION

Corresponding Author

*E-mail: wbensch@ac.uni-kiel.de.

ORCID

Christian Näther: 0000-0001-8741-6508

Author Contributions

The manuscript was written through contributions of all authors. All authors have given approval to the final version of the manuscript.

Notes

The authors declare no competing financial interest.

■ ACKNOWLEDGMENTS

The authors thank the State Schleswig-Holstein for financial support.

■ REFERENCES

(1) Zhang, H.-M.; Yang, J.; Kan, W.-Q.; Liu, Y.-Y.; Ma, J.-F. Photocatalytic Properties and Luminescent Sensing for Cr^{3+} Cations of Polyoxovanadates-Based Inorganic−Organic Hybrid Compounds with Multiple Lewis Basic Sites. *Cryst. Growth Des.* **2016**, *16*, 265−276.

(2) Li, X.; Yang, L.; Qin, C.; Liu, F.-H.; Zhao, L.; Shao, K.-Z.; Su, Z.-M. POM-based inorganic−organic hybrid compounds: Synthesis, structures, highly-connected topologies and photodegradation of organic dyes. *RSC Adv.* **2015**, *5*, 59093−59098.

(3) Li, S.; Yu, X.; Zhang, G.; Ma, Y.; Yao, J.; Keita, B.; Louis, N.; Zhao, H. Green chemical decoration of multiwalled carbon nanotubes with polyoxometalate-encapsulated gold nanoparticles: Visible light photocatalytic activities. *J. Mater. Chem.* **2011**, *21*, 2282−2287.

(4) Wang, C.; Bu, X.; Ma, J.; Liu, C.; Chou, K.; Wang, X.; Li, Q. Wells−Dawson type $Cs_{5.5}H_{0.5}P_2W_{18}O_{62}$ based Co/Al_2O_3 as binfunctional catalysts for direct production of clean-gasoline fuel through Fischer−Tropsch synthesis. *Catal. Today* **2016**, *274*, 82−87.

(5) Campbell, M. L.; Sulejmanovic, D.; Schiller, J. B.; Turner, E. M.; Hwu, S.-J.; Whitehead, D. C. Room-temperature catalytic oxidation of alcohols with the polyoxovanadate salt $Cs_5(V_{14}As_8O_{42}Cl)$. *Catal. Sci. Technol.* **2016**, *6*, 3208−3213.

(6) Cardona-Serra, S.; Clemente-Juan, J. M.; Coronado, E.; Gaita-Ariño, A.; Suaud, N.; Svoboda, O.; Bastardis, R.; Guihéry, N.; Palacios, J. J. Electrically Switchable Magnetic Molecules: Inducing a Magnetic Coupling by Means of an External Electric Field in a Mixed-Valence Polyoxovanadate Cluster. *Chem.—Eur. J.* **2015**, *21*, 763−769.

(7) Bertaina, S.; Gambarelli, S.; Mitra, T.; Tsukerblat, B.; Müller, A.; Barbara, B. Quantum oscillations in a molecular magnet. *Nature* **2008**, *453*, 203−206.

(8) Rhule, J. T.; Hill, C. L.; Judd, D. A.; Schinazi, R. F. Polyoxometalates in Medicine. *Chem. Rev.* **1998**, *98*, 327−358.

(9) Hasenknopf, B. Polyoxometalates: introduction to a class of inorganic compounds and their biomedical applications. *Front. Biosci., Landmark Ed.* **2005**, *10*, 275−287.

(10) Chen, J.-J.; Symes, M. D.; Fan, S.-C.; Zheng, M.-S.; Miras, H. N.; Dong, Q.-F.; Cronin, L. High-Performance Polyoxometalate-Based Cathode Materials for Rechargeable Lithium-Ion Batteries. *Adv. Mater.* **2015**, *27*, 4649−4654.

(11) Herrmann, S.; de Matteis, L.; de la Fuente, J. M.; Mitchell, S. G.; Streb, C. Removal of Multiple Contaminants from Water by Polyoxometalate Supported Ionic Liquid Phases (POM-SILPs). *Angew. Chem., Int. Ed.* **2017**, *56*, 1667−1670.

(12) Antonova, E.; Näther, C.; Bensch, W. Antimonato polyoxovanadates with structure directing transition metal complexes: pseudopolymorphic $\{Ni(dien)_2\}_3[V_{15}Sb_6O_{42}(H_2O)]\cdot nH_2O$ compounds and $\{Ni(dien)_2\}_4[V_{16}Sb_4O_{42}(H_2O)]$. *Dalton Trans* **2012**, *41*, 1338−1344.

(13) Antonova, E.; Näther, C.; Bensch, W. Assembly of $[V_{15}Sb_6O_{42}(H_2O)]^{6-}$ cluster shells into higher dimensional aggregates via weak Sb···N/Sb···O intercluster interactions and a new polyoxovanadate with a discrete $[V_{16}Sb_4O_{42}(H_2O)]^{8-}$ cluster shell. *CrystEngComm* **2012**, *14*, 6853−6860.

(14) Antonova, E.; Näther, C.; Kögerler, P.; Bensch, W. Organic functionalization of polyoxovanadates: Sb-N bonds and charge control. *Angew. Chem., Int. Ed.* **2011**, *50*, 764−767.

(15) Antonova, E.; Näther, C.; Kögerler, P.; Bensch, W. A C_2-symmetric antimonato polyoxovanadate cluster $[V_{16}Sb_4O_{42}(H_2O)]^{8-}$ derived from the $\{V_{18}O_{42}\}$ archetype. *Dalton Trans* **2012**, *41*, 6957−6962.

(16) Antonova, E.; Näther, C.; Kögerler, P.; Bensch, W. Expansion of antimonato polyoxovanadates with transition metal complexes: $(Co(N_3C_5H_{15})_2)_2[\{Co(N_3C_5H_{15})_2\}V_{15}Sb_6O_{42}(H_2O)]\cdot 5H_2O$ and $(Ni(N_3C_5H_{15})_2)_2[\{Ni(N_3C_5H_{15})_2\}V_{15}Sb_6O_{42}(H_2O)]\cdot 8H_2O$. *Inorg. Chem.* **2012**, *51*, 2311−2317.

(17) Antonova, E.; Seidlhofer, B.; Wang, J.; Hinz, M.; Bensch, W. Controlling nucleation and crystal growth of a distinct polyoxovanadate cluster: an in situ energy dispersive X-ray diffraction study under solvothermal conditions. *Chem.—Eur. J.* **2012**, *18*, 15316−15322.

(18) Antonova, E.; Wutkowski, A.; Näther, C.; Bensch, W. New antimonato polyoxovanadates based on the $[V_{14}{}^{IV}Sb_8{}^{III}O_{42}(H_2O)]^{4-}$ cluster type. *Solid State Sci.* **2011**, *13*, 2154−2159.

(19) Gao, Y.; Han, Z.; Xu, Y.; Hu, C. pH-Dependent Assembly of Two Novel Organic−inorganic Hybrids Based on Vanadoantimonate Clusters. *J. Cluster Sci.* **2010**, *21*, 163−171.

(20) Guo, H.-Y.; Zhang, X.; Cui, X.-B.; Huo, Q.-S.; Xu, J.-Q. Vanadoantimonates: From discrete clusters to high dimensional aggregates. *CrystEngComm* **2016**, *18*, 5130−5139.

(21) Hu, X.-X.; Xu, J.-Q.; Cui, X.-B.; Song, J.-F.; Wang, T.-G. A novel one-dimensional framework material constructed from antimony-substituted polyoxovanadium clusters: $[(C_2N_2H_{10})_2\beta\text{-}\{Sb^{III}{}_8V^{IV}{}_{14}O_{42}(H_2O)\}](C_2N_2H_8)\cdot 4H_2O$. *Inorg. Chem. Commun.* **2004**, *7*, 264−267.

(22) Kiebach, R.; Näther, C.; Bensch, W. $[C_6H_{17}N_3]_4[Sb_4V_{16}O_{42}]\cdot 2H_2O$ and $[NH_4]_4[Sb_8V_{14}O_{42}]\cdot 2H_2O$— the first isolated Sb derivates of the $[V_{18}O_{42}]$ family. *Solid State Sci.* **2006**, *8*, 964−970.

(23) Kiebach, R.; Näther, C.; Kögerler, P.; Bensch, W. $[V^{IV}{}_{15}Sb^{III}{}_6O_{42}]^{6-}$: an antimony analogue of the molecular magnet $[V_{15}As_6O_{42}(H_2O)]^{6-}$. *Dalton Trans* **2007**, 3221−3223.

(24) Lühmann, H.; Näther, C.; Kögerler, P.; Bensch, W. Solvothermal synthesis and crystal structure of a heterometal-bridged {$V_{15}Sb_6$} dimer: $[Ni_2(tren)_3(V_{15}Sb_6O_{42}(H_2O)_{0.5})]_2[Ni(trenH)_2]\cdot H_2O$. *Inorg. Chim. Acta* **2014**, *421*, 549−552.
(25) Rasmussen, M.; Näther, C.; van Leusen, J.; Kögerler, P.; Zhechkov, L.; Heine, T.; Bensch, W. Covalent Co-O-V and Sb-N Bonds Enable Polyoxovanadate Charge Control. *Inorg. Chem.* **2017**, *56*, 7120−7126.
(26) Wutkowski, A.; Näther, C.; Kögerler, P.; Bensch, W. Antimonato polyoxovanadate based three-dimensional framework exhibiting ferromagnetic exchange interactions: synthesis, structural characterization, and magnetic investigation of $\{[Fe(C_6H_{14}N_2)_2]_3[V_{15}Sb_6O_{42}(H_2O)]\}\cdot 8H_2O$. *Inorg. Chem.* **2013**, *52*, 3280−3284.
(27) Wutkowski, A.; Näther, C.; Kögerler, P.; Bensch, W. $[V_{16}Sb_4O_{42}(H_2O)\{VO(C_6H_{14}N_2)_2\}_4]$: a terminal expansion to a polyoxovanadate archetype. *Inorg. Chem.* **2008**, *47*, 1916−1918.
(28) Yu, L.; Liu, J.-p.; Wang, J.-p.; Niu, J.-y. Hydrothermal Synthesis and Crystal Structure of a New 2D Layer Compound $[(Ni(en)_2)_2Sb_8V_{14}O_{42}]\ 5.5H_2O$. *Chem. Res. Chin. Univ.* **2009**, *25*, 426−429.
(29) Zhang, L.; Zhao, X.; Xu, J.; Wang, T. A novel two-dimensional structure containing the first antimony-substituted polyoxovandium clusters: $[\{Co(en)_2\}_2Sb^{III}{}_8V^{IV}{}_{14}O_{42}(H_2O)]\ 6H_2O$. *Dalton Trans* **2002**, 3275−3276.
(30) Anjass, M. H.; Kastner, K.; Nägele, F.; Ringenberg, M.; Boas, J. F.; Zhang, J.; Bond, A. M.; Jacob, T.; Streb, C. Stabilization of Low-Valent Iron(I) in a High-Valent Vanadium(V) Oxide Cluster. *Angew. Chem., Int. Ed.* **2017**, *56*, 14749−14752.
(31) Lechner, M.; Kastner, K.; Chan, C. J.; Güttel, R.; Streb, C. Aerobic Oxidation Catalysis by a Molecular Barium Vanadium Oxide. *Chem.—Eur. J.* **2018**, *24*, 4952−4956.
(32) Schwarz, B.; Forster, J.; Goetz, M. K.; Yücel, D.; Berger, C.; Jacob, T.; Streb, C. Visible-Light-Driven Water Oxidation by a Molecular Manganese Vanadium Oxide Cluster. *Angew. Chem., Int. Ed.* **2016**, *55*, 6329−6333.
(33) Seliverstov, A.; Streb, C. A new class of homogeneous visible-light photocatalysts: Molecular cerium vanadium oxide clusters. *Chem.—Eur. J.* **2014**, *20*, 9733−9738.
(34) Streb, C. Structure and Bonding in Molecular Vanadium Oxides: From Templates via Host−Guest Chemistry to Applications. In *Polyoxometalate-Based Assemblies and Functional Materials*; Song, Y.-F., Ed.; Structure and Bonding; Springer International Publishing: Cham, 2018; pp 1−17.
(35) Tucher, J.; Peuntinger, K.; Margraf, J. T.; Clark, T.; Guldi, D. M.; Streb, C. Template-dependent photochemical reactivity of molecular metal oxides. *Chem.—Eur. J.* **2015**, *21*, 8716−8719.
(36) Wendt, M.; Warzok, U.; Näther, C.; van Leusen, J.; Kögerler, P.; Schalley, C. A.; Bensch, W. Catalysis of "outer-phase" oxygen atom exchange reactions by encapsulated "inner-phase" water in {$V_{15}Sb_6$}-type polyoxovanadates. *Chem. Sci.* **2016**, *7*, 2684−2694.
(37) Mahnke, L. K.; Warzok, U.; Lin, M.; Näther, C.; Schalley, C. A.; Bensch, W. New Water-Soluble Cluster Compound $\{Zn(en)_3\}_3[V_{15}Sb_6O_{42}(H_2O)]\cdot(Ethylenediamine)_3\cdot 10\ H_2O$ as a Synthon for the Generation of Two New Antimonato Polyoxovanadates. *Chem.—Eur. J.* **2018**, *24*, 5522.
(38) Wendt, M.; Näther, C.; Bensch, W. High Nuclearity Antimonato-Polyoxovanadate Cluster $\{V_{15}Sb_6O_{42}\}$ as a Synthon for the Solvothermal in situ Generation of alpha- and beta-$\{V_{14}Sb_8O_{42}\}$ Isomers. *Chem.—Eur. J.* **2016**, *22*, 7747−7751.
(39) Wendt, M.; Mahnke, L. K.; Heidenreich, N.; Bensch, W. Nucleation and Crystal Growth of a $\{V_{14}Sb_8O_{42}\}$ Cluster from a $\{V_{15}Sb_6O_{42}\}$ Polyoxovanadate: In Situ XRD Studies. *Eur. J. Inorg. Chem.* **2016**, *2016*, 5393−5398.
(40) Sheldrick, G. M. A short history of SHELX. *Acta Crystallogr., Sect. A: Found. Crystallogr.* **2008**, *64*, 112−122.
(41) Sheldrick, G. M. Crystal structure refinement with SHELXL. *Acta Crystallogr., Sect. C: Struct. Chem.* **2015**, *71*, 3−8.
(42) Mahnke, L. K.; Kondinski, A.; Warzok, U.; Näther, C.; van Leusen, J.; Schalley, C. A.; Monakhov, K. Y.; Kögerler, P.; Bensch, W. Configurational Isomerism in Polyoxovanadates. *Angew. Chem., Int. Ed.* **2018**, *57*, 2972−2975.
(43) Wendt, M.; Polzin, P.; van Leusen, J.; Näther, C.; Kögerler, P.; Bensch, W. In situ ligand exchange-mediated 0D/1D transformation of a polyoxovanadate. *Dalton Trans* **2017**, *46*, 1618−1623.
(44) Brown, I. D.; Altermatt, D. Bond-valence parameters obtained from a systematic analysis of the Inorganic Crystal Structure Database. *Acta Crystallogr., Sect. B: Struct. Sci.* **1985**, *41*, 244−247.
(45) O'Keefe, M.; Brese, N. E. Atom sizes and bond lengths in molecules and crystals. *J. Am. Chem. Soc.* **1991**, *113*, 3226−3229.
(46) Palenik, R. C.; Abboud, K. A.; Palenik, G. J. Bond valence sums and structural studies of antimony complexes containing Sb bonded only to O ligands. *Inorg. Chim. Acta* **2005**, *358*, 1034−1040.
(47) Wang, C.; Zhou, G.; Zhang, Z.; Zhu, D.; Xu, Y. Hydrothermal synthesis, characterization, and luminescence of two new arsenic−vanadium compounds with a γ-$[As_8V_{14}O_{42}(H_2O)]^{4-}$ anion. *J. Coord. Chem.* **2011**, *64*, 1198−1206.
(48) Guo, H.-Y.; Zhang, T.-T.; Lin, P.-H.; Xiao-Zhang, X.-Z.; Cui, X.-B.; Huo, Q.-S.; Xu, J.-Q. Preparation, structure and characterization of a series of vanadates. *CrystEngComm* **2017**, *19*, 265−275.
(49) Chen, H.; Xu, X.-y.; Gao, J.; Yang, X.-j.; Lu, L.-d.; Wang, X. *Huaxue Shiji*; **2006**, *28*, 478−480.
(50) Wei, Y.; Yuan, C.; Yang, P. Tris(1,10-phenanthroline-κ2N,N′)zinc(II) bis(perchlorate) ethanol solvate monohydrate. *Acta Crystallogr., Sect. E: Struct. Rep. Online* **2004**, *60*, m1686−m1688.
(51) Yi, Z.-H.; Cui, X.-B.; Zhang, X.; Yu, J.-H.; Lu, J.; Xu, J.-Q.; Yang, G.-D.; Wang, T.-G.; Yu, H.-H.; Duan, W.-J. Hydrothermal syntheses and structural characterizations of organic-inorganic hybrid materials of the M(II)-ligand/vanadium oxide system (M(II) = Mn(II), Cu(II) and Zn(II); ligand = 2,2'-bipyridine and 1,10-phenanthroline). *Dalton Trans* **2007**, 2115−2120.
(52) Infantes, L.; Chisholm, J.; Motherwell, S. Extended motifs from water and chemical functional groups in organic molecular crystals. *CrystEngComm* **2003**, *5*, 480.
(53) Infantes, L.; Motherwell, S. Water clusters in organic molecular crystals. *CrystEngComm* **2002**, *4*, 454.
(54) Bondi, A. van der Waals Volumes and Radii. *J. Phys. Chem.* **1964**, *68*, 441−451.
(55) Bondi, A. van der Waals Volumes and Radii of Metals in Covalent Compounds. *J. Phys. Chem.* **1966**, *70*, 3006−3007.
(56) Mantina, M.; Chamberlin, A. C.; Valero, R.; Cramer, C. J.; Truhlar, D. G. Consistent van der Waals radii for the whole main group. *J. Phys. Chem. A* **2009**, *113*, 5806−5812.
(57) Bloom, J. W. G.; Wheeler, S. E. Taking the Aromaticity out of Aromatic Interactions. *Angew. Chem., Int. Ed.* **2011**, *50*, 7847.
(58) Chi, Y.-H.; Shi, J.-M.; Li, H.-N.; Wei, W.; Cottrill, E.; Pan, N.; Chen, H.; Liang, Y.; Yu, L.; Zhang, Y.-Q.; et al. pi-pi stacking, spin density and magnetic coupling strength. *Dalton Trans* **2013**, *42*, 15559−15569.
(59) Grimme, S. Do Special Noncovalent π−π Stacking Interactions Really Exist? *Angew. Chem., Int. Ed.* **2008**, *47*, 3430−3434.
(60) Hilbert, J.; Näther, C.; Bensch, W. Utilization of mixtures of aromatic N-donor ligands of different coordination ability for the solvothermal synthesis of thiostannate containing molecules. *Dalton Trans* **2015**, *44*, 11542−11550.
(61) Janiak, C. A critical account on π−π stacking in metal complexes with aromatic nitrogen-containing ligands. *J. Chem. Soc., Dalton Trans.* **2000**, 3885−3896.
(62) Martinez, C. R.; Iverson, B. L. Rethinking the term "pi-stacking". *Chem. Sci.* **2012**, *3*, 2191.
(63) Ringer, A. L.; Sinnokrot, M. O.; Lively, R. P.; Sherrill, C. D. The effect of multiple substituents on sandwich and T-shaped pi-pi interactions. *Chem.—Eur. J.* **2006**, *12*, 3821−3828.
(64) Grimme, S. Density functional theory with London dispersion corrections. *WIREs Comput. Mol. Sci.* **2011**, *1*, 211−228.
(65) Grimme, S.; Antony, J.; Ehrlich, S.; Krieg, H. A consistent and accurate ab initio parametrization of density functional dispersion correction (DFT-D) for the 94 elements H-Pu. *J. Chem. Phys.* **2010**, *132*, 154104.

DOI: 10.1021/acs.cgd.8b00987
Cryst. Growth Des. 2018, 18, 6100−6106

(66) Goerigk, L.; Kruse, H.; Grimme, S. Benchmarking density functional methods against the S66 and S66×8 datasets for non-covalent interactions. *ChemPhysChem* **2011**, *12*, 3421−3433.
(67) Hafeez, S. T.; Ali, S.; Tahir, M. N.; Iqbal, M.; Munawar, K. S. One-pot synthesis, structural elucidation, DNA binding and alkaline phosphatase inhibition studies of zinc(II) complexes with 4-nitrocinnamic acid and ethylenediamine. *J. Coord. Chem.* **2014**, *67*, 2479−2495.
(68) Khan, M. I.; Yohannes, E.; Doedens, R. J. A novel series of materials composed of arrays of vanadium oxide container molecules, $V_{18}O_{42}(X)$ (X = H_2O, Cl^-, Br^-): Synthesis and characterization of $M_2(H_2N(CH_2)_2NH_2)_5(M(H_2N(CH_2)_2NH_2)_2)_2V_{18}O_{42}(X)$. $9H_2O$ (M = Zn, Cd). *Inorg. Chem.* **2003**, *42*, 3125−3129.
(69) Qi, Y.; Li, Y.; Qin, C.; Wang, E.; Jin, H.; Xiao, D.; Wang, X.; Chang, S. From Chain to Network: Design and Analysis of Novel Organic−Inorganic Assemblies from Organically Functionalized Zinc-Substituted Polyoxovanadates and Zinc Organoamine Subunits. *Inorg. Chem.* **2007**, *46*, 3217−3230.
(70) Zheng, S.-T.; Chen, Y.-M.; Zhang, J.; Yang, G.-Y. Two New Polyoxovanadate-supported Transition Metal Complexes: $[Zn(en)_2]$-$[Zn(en)_2(H_2O)_2][\{Zn(en)(enMe)\}As_6V_{15}O_{42}(H_2O)]\cdot 4H_2O$ and $[Zn_2(enMe)_2(en)_3][\{Zn(enMe)_2\}As_6V_{15}O_{42}(H_2O)]\cdot 4H_2O$. *Z. Anorg. Allg. Chem.* **2006**, *632*, 155−159.
(71) Zheng, S.-T.; Zhang, J.; Yang, G.-Y. $[\{\{Zn(en)_2\}_2As_6V_{15}O_{42}(H_2O)\}_2\{Zn(en)_2\}]\cdot 2Hen\cdot 3H_2O$. The First Dimeric Arsenic-Vanadium Cluster Linked by $Zn(en)_2$ Complex Bridge. *Chem. Lett.* **2003**, *32*, 810−811.
(72) Huš, M.; Urbic, T. Strength of hydrogen bonds of water depends on local environment. *J. Chem. Phys.* **2012**, *136*, 144305.
(73) Jeffrey, G. A. *An Introduction to Hydrogen Bonding*; Topics in Physical Chemistry; Oxford University Press: New York, 1997.
(74) Avdeeva, V. V.; Vologzhanina, A. V.; Goeva, L. V.; Malinina, E. A.; Kuznetsov, N. T. Boron Cluster Anions $[B_nH_n]^{2-}$ (n = 10, 12) in Reactions of Iron(II) and Iron(III) Complexation with 2, 2′-Bipyridyl and 1, 10-Phenanthroline. *Z. Anorg. Allg. Chem.* **2014**, *640*, 2149−2160.
(75) De, A.; Garai, M.; Yadav, H. R.; Choudhury, A. R.; Biswas, B. Catalytic promiscuity of an iron(II)-phenanthroline complex. *Appl. Organomet. Chem.* **2017**, *31*, e3551.
(76) Huang, M.-Q.; Chen, Y.-P.; Huang, M.-M.; Wei, W.-J.; Sun, Y.-Q.; Lin, H.-Y. The Study on Isomer of $[V_{16}O_{38}Cl]^{4-}$ Cluster and a Mixed-Valent Polyoxovanadate Based on a New Topology. *J. Cluster Sci.* **2017**, *28*, 2795−2807.
(77) Liu, H.; Wang, J.; Li, Y.; Jian, F. Synthesis and Crystal Structure of the Heteronuclear Decavanadates Complex: $[Fe(phen)_3]_2\cdot[V_{10}O_{28}]\cdot 15H_2O$. *J. Chem. Crystallogr.* **2011**, *41*, 1254−1257.
(78) Xiao, L.-N.; Xu, J.-N.; Hu, Y.-Y.; Wang, L.-M.; Wang, Y.; Ding, H.; Cui, X.-B.; Xu, J.-Q. Synthesis and characterizations of the first $V_{16}O_{39}Cl^{6-}$ ($V_{16}O_{39}$) polyanion. *Dalton Trans* **2013**, *42*, 5247−5251.
(79) Infantes, L.; Fábián, L.; Motherwell, W. D. S. Organic crystal hydrates: What are the important factors for formation. *CrystEngComm* **2007**, *9*, 65−71.
(80) Mizuse, K.; Kuo, J.-L.; Fujii, A. Structural trends of ionized water networks: Infrared spectroscopy of watercluster radical cations $(H_2O)^{n+}$ (n = 3−11). *Chem. Sci.* **2011**, *2*, 868−876.

DOI: 10.1021/acs.cgd.8b00987
Cryst. Growth Des. 2018, 18, 6100−6106

4.6. Die Publikation *„Soluble Hetero-Polyoxovanadates and Their Solution Chemistry Analyzed by Electrospray Ionization Mass Spectrometry"*

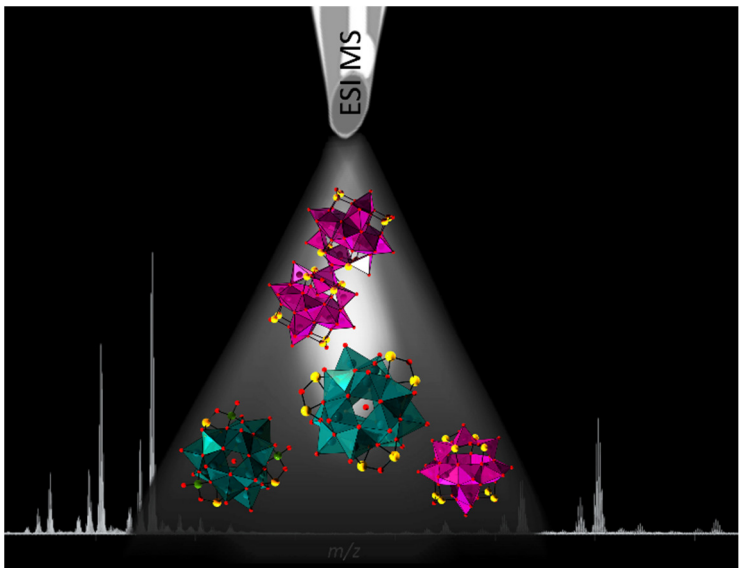

Abbildung 23: TOC Grafik des Minireview *„Soluble Hetero-Polyoxovanadates and Their Solution Chemistry Analyzed by Electrospray Ionization Mass Spectrometry"*

In dem Minireview wird ein Überblick über die synthetischen Möglichkeiten geboten, wenn wasserlösliche Vorläuferverbindungen für die Präparation neuer Polyoxometallate (POM) eingesetzt werden. Zusätzlich wird die Chemie von Polyoxovanadaten (POVs) in wässrigen Lösungen diskutiert. Polyoxometallate stellen eine einzigartige Verbindungsklasse dar und in der Literatur wird über viele interessante Eigenschaften berichtet. In einigen Anwendungsbereichen sind bereits viel versprechende Resultate erzielt worden. Allerdings ist die rationale Synthese von POMs nur eingeschränkt möglich und in den meisten Fällen werden POMs durch Variation der Syntheseparameter erhalten. Gerade im Bereich der POVs ist bisher nur wenig über die Chemie in wässrigen Medien bekannt. Mit ESI-MS-Untersuchungen konnten wichtige Erkenntnisse in diesem Bereich der POM-Chemie erzielt werden. Nach einer Einleitung in die Chemie der POMs und im Speziellen der POVs bezüglich der Synthesebedingungen und des strukturellen Aufbaus, werden Beispiele von mit ESI-MS charakterisierten POMs diskutiert, wobei deren Reaktivität in Lösung im Mittelpunkt steht. Anschließend werden die Untersuchungen der Arbeitsgruppe BENSCH in Kooperation mit der Arbeitsgruppe SCHALLEY in Bezug auf lösliche antimonsubstituierte Polyoxovanadate detailliert diskutiert.

Veröffentlicht in *Chem. Eur. J.* **2019**, *25*, 1405.
DOI: 10.1002/chem.201803291

ChemPubSoc Europe

DOI: 10.1002/chem.201803291

CHEMISTRY A European Journal Minireview

Polyoxometalates

Soluble Hetero-Polyoxovanadates and Their Solution Chemistry Analyzed by Electrospray Ionization Mass Spectrometry

Ulrike Warzok,*[a] Lisa K. Mahnke,[b] and Wolfgang Bensch*[b]

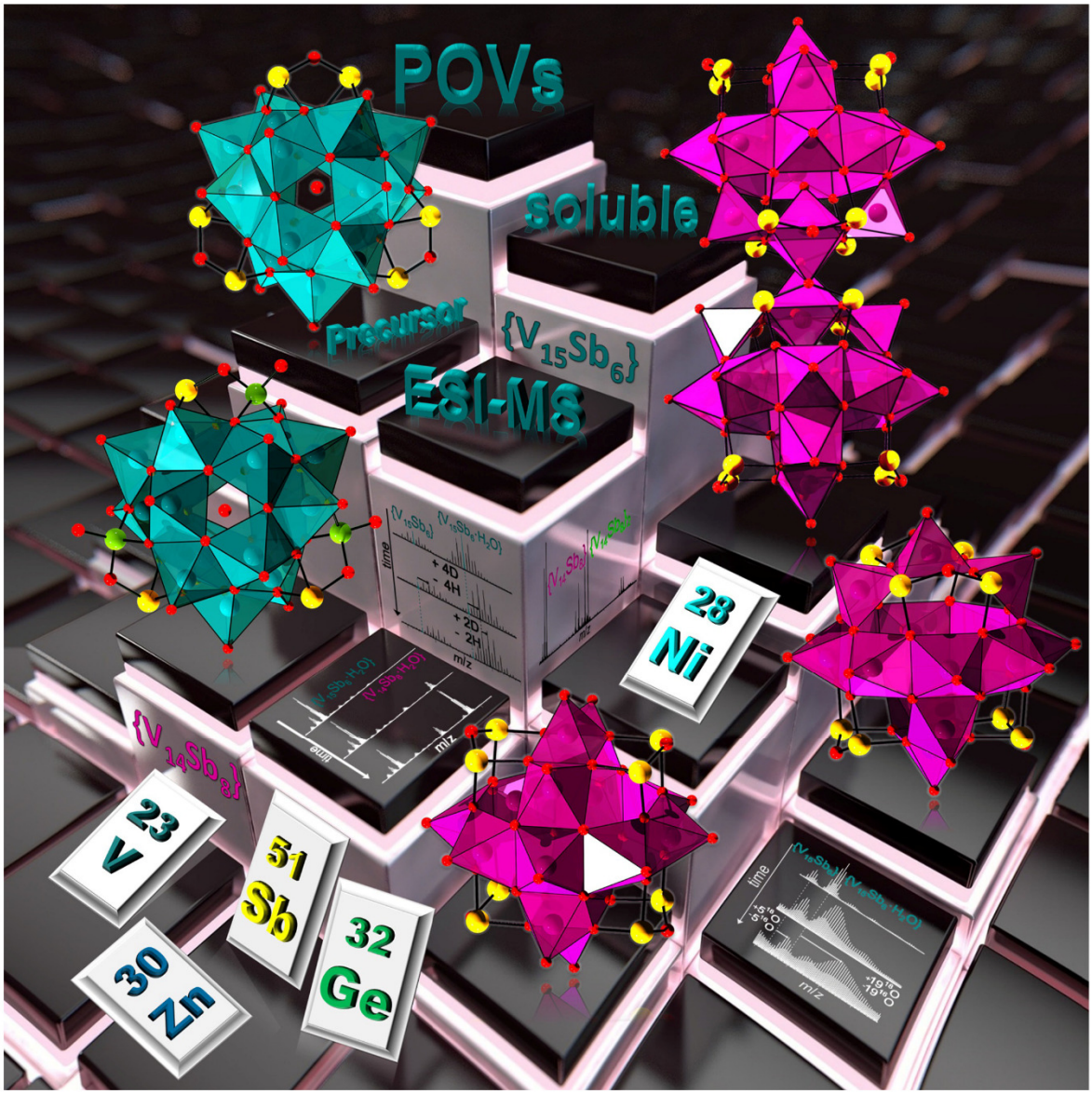

ChemPubSoc Europe

CHEMISTRY A European Journal Minireview

Abstract: Polyoxometalates (POMs) are an intriguing class of compounds due to their tremendous structural variety and the wide spectrum of resulting properties, which make them interesting for applications in fields such as catalysis, material science or nanotechnology. Their ability to form large supramolecular architectures by self-assembly offers an entry to complex, functional systems. After an introduction into the structure and synthesis of POMs of the early transition metals, recently discovered water-soluble antimonato polyoxovanadates (Sb-POVs) and the investigation of their chemical reactivity are discussed. Electrospray ionization mass spectrometry (ESI-MS) is presented as an analytical technique suitable to investigate the structure of complex POM assemblies in solution and to probe the underlying reactivity and formation mechanisms. This Minireview highlights the first studies on the soluble Sb-POVs and how the knowledge of their reactivity obtained by ESI-MS has fostered the syntheses of numerous novel Sb-POV compounds.

1. Introduction

Polyoxometalates (POMs) of the early transition metals (vanadium, niobium, molybdenum, tungsten and tantalum) have been studied over the last decades for the generation of complex, functional molecular architectures. The process normally leading to higher-order structures is the self-assembly of building blocks, often consisting of preformed smaller clusters, into stable and structurally well-defined aggregates.[1–3] In general, POM compounds consist of the polyoxoanions of the early transition metals and include a huge number of structurally fascinating and interesting materials.[4,5] Furthermore, the formation of so-called polyoxo-nobel-metalates which include palladium, platinum or gold, has been demonstrated.[6] This field of research is also steadily growing, but is beyond the scope of this review. Early transition metals can form M=O double bonds in contrast to most other metals. These promote the *trans*-effect and in turn favor the self-assembly of molecular polyoxometalates by condensation reactions over the formation of infinite, bulk oxides. This yields discrete, often concave or even cage-like structures because the double bonds are directed outwards and virtually seal off the cluster from further aggregation.[5] The early transition metals of Groups 5 and 6 can adopt their highest oxidation state +5 or +6. Furthermore, they exhibit the appropriate charge density and charge-to-ionic-radius ratio to form the structurally determining M=O double bonds with strongly π-donating oxo ligands.[4,7,8] The resulting coordination polyhedra range from tetrahedra (coordination number 4) to pentagonal bipyramids (coordination number 7), which enables generation of a great structural variety.

POMs cover a broad spectrum of interesting properties related to their size and shape, their redox behavior, magnetic and photochemical characteristics. Possible applications range from catalysis, molecular electronics, material science and medicine to molecular magnets, nanosensors and nanoreactors, for small molecule-uptake and storage, as well as for battery research and artificial cell models.[5,8,9] The scientific interest to integrate preformed POM clusters into complex molecular architectures by hierarchical self-assembly in solution is steadily growing and will likely lead to an increasing number of sophisticated structures with intriguing properties and functionalities.[10]

Although the number of POMs exhibiting fascinating and unusual structures is enormous, comparably little is known about the reactions and mechanisms in solution occurring during the formation processes of POMs. Comprehensive insights into the structure and reactivity of POMs in solution can be obtained by a number of different analytical techniques. Electrospray ionization mass spectrometry (ESI-MS), in particular, has proven to be a versatile tool for investigating the reactions in solution. In combination with state-of-the-art mass spectrometric techniques, as well as with the fast-emerging ion-mobility mass spectrometry (IM-MS), the structure of new POM architectures and their reactivity in gas phase and solution can be elucidated.

Prior to 2016, antimonato polyoxovanadates (Sb-POVs) have only been accessible under drastic solvothermal conditions. Due to the absence of well-soluble precursors, the discovery process of new compounds relayed solely on serendipity, rather than rational synthesis. The solution and gas-phase chemistry of Sb-POVs was virtually unexplored, which left fundamental questions concerning their formation mechanisms, stability and host–guest chemistry unanswered. This lack of knowledge could, to some extent, account for the relatively slow progress to generate more complex, functional assemblies from polyoxovanadates, as compared to the other members of the POM classes. With the emergence of the first water-soluble Sb-POV compounds, this drawback might be compensated in the future.

In this Minireview, we will give a short introduction into the structure and synthesis of POMs of the early transition metals, in general, and Sb-POVs, in particular. Selected examples of complex POM assemblies are presented and how mass spectrometry can be employed to investigate their structure and reactivity. Furthermore, we highlight the first studies on soluble Sb-POVs compounds and how the knowledge of their reac-

[a] *Dr. U. Warzok*
Institut für Chemie und Biochemie, Freie Universität Berlin
Takustr. 3, 14195 Berlin (Germany)
E-mail: ulrike.warzok@fu-berlin.de

[b] *L. K. Mahnke, Prof. Dr. W. Bensch*
Institut für Anorganische Chemie
Christian-Albrechts-Universität zu Kiel
Max-Eyth-Straße 2, 24118 Kiel (Germany)
E-mail: wbensch@ac.uni-kiel.de

The ORCID identification numbers for the authors of this article can be found under https://doi.org/10.1002/chem.201803291.

ChemPubSoc Europe

CHEMISTRY A European Journal Minireview

tivity obtained by ESI-MS has fostered the syntheses of numerous novel Sb-POV compounds.

2. Polyoxometalate Structures

2.1. General aspects

Polyoxometalates (POMs) are often formed in acidic aqueous solutions by combined hydrolysis and condensation reactions and can thereby self-assemble to cluster anions of high nuclearity.[7] Although the first example of a molybdenum POM $[PMo_{12}O_{40}]^{3-}$ was already reported by Berzelius in 1826,[11] only the development of X-ray diffraction methods in the early 20th century allowed the full analytical characterization by Keggin in 1933.[12] This POM belongs to the group of the well-known Keggin anions with the general formula $[XM_{12}O_{40}]^{n-}$ (with M = Mo, W and X = for example: PO_4^{3-}, SiO_4^{2-} and SO_4^{2-}). This cluster type consists of octahedral MO_6 units which condense to edge-linked trigonal M_3O_{13} units. Four of these so-called triads self-assemble around the templating phosphate anion by corner sharing, forming the $[PMo_{12}O_{40}]^{3-}$ Keggin anion (Figure 1).[4,7,13]

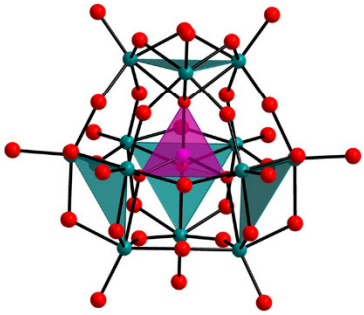

Figure 1. Archetypal $[XMo_{12}O_{40}]^{3-}$ Keggin anion formed by self-assembly from four triads, edge-linked trigonal $\{M_3O_{13}\}$ units (turquoise), around a templating heteroanion X (purple).

Since the discovery and structural characterization of the first POMs, the diversity of chemical compositions and cluster geometries has been steadily growing. POMs in general include a vast number of possible crystal structures and may incorporate different heteroatoms, additional heterometallic centers, as well as organic cations or ligands. Hence, their classification is mostly only possible in broad categories.[4]

Isopolyanions are high-nuclearity metal-oxide clusters, such as the Lindqvist $[M_6O_{19}]^{n-}$ anion, which are composed of only one transition-metal element and no further heteroatoms (Figure 2a). They are less stable and more reactive than their heteroatom-based siblings. Heteropolyanions contain main-group heteroanions such as sulfate, phosphate, silicate, germanate, arsenate or antimonate, which can act as templates for their formation. Furthermore, they may contain more than one type of (transition) metal cation. This class of POMs often forms very stable compounds and is the most widely explored subset of

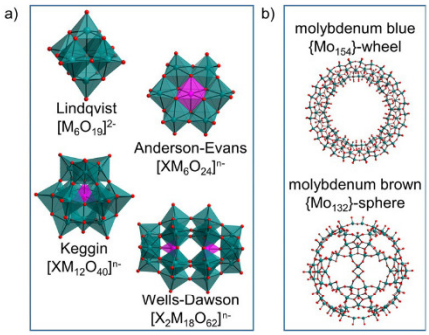

Figure 2. Structures of the classical polyoxometalates.

Ulrike Warzok received her Master of Science in Chemistry from Freie Universität Berlin. She completed her Master thesis with Prof. Dr. H.-U. Reissig in 2014, working on the synthesis of new prodigiosin derivatives. For her doctoral studies, she joined the group of Prof. Dr. C. A. Schalley at Freie Universität Berlin to investigate the structure and reactivity of supramolecular capsules and polyoxometalates by mass spectrometry and ion mobility. Since finishing her PhD in 2018, she is currently working on POMs in the same group and will soon join the groups of Prof. F. D. Toste and Prof. K. N. Raymond at UC Berkeley as a postdoctoral fellow of the Alexander-von-Humboldt Foundation to work on supramolecular catalysis.

Lisa Katharina Mahnke received her Bachelor of Science degree in 2014 and Master of Science in 2016 in Chemistry from the Christian-Albrechts-University of Kiel (Germany). She worked on the synthesis and characterization of new polyoxovanadates in the working group of Prof. Dr. Wolfgang Bensch. Also in 2016, she started her PhD thesis in the same group with focus on transformation reactions of soluble heteroatom-based-polyoxovanadate synthons.

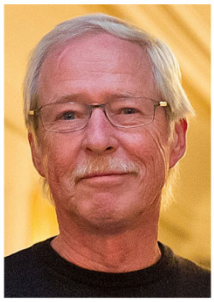

Wolfgang Bensch received his Dr. rer. nat. in 1983 at the Ludwig-Maximilians-University of Munich (Germany) under the supervision of Prof. Dr. Eberhard Amberger working on vanadium-chalkogenides. He was a postdoctoral fellow at the University of Zurich (Switzerland) in the working group of Prof. Dr. Oswald and joined the Siemens company in 1986. From 1990–1993, he habilitated at the Johann Wolfgang Goethe University in Frankfurt (Germany) in the working group of Prof. Dr. Schlögl and was appointed as full professor for Inorganic Solid State Chemistry at the Christian-Albrechts-University of Kiel (Germany) in 1997.

ChemPubSoc Europe

CHEMISTRY A European Journal Minireview

POM clusters. It includes notable examples like Anderson–Evans $[XM_6O_{24}]^{n-}$, the above-mentioned Keggin $[XM_{12}O_{40}]^{n-}$ and Wells–Dawson $[X_2M_{18}O_{62}]^{n-}$ clusters (Figure 2a). Their preparation is relatively facile and they exhibit interesting catalytic and electronic behavior.[14] The third category of POMs involves gigantic cluster geometries, which are formed by self-assembly in simple one-pot procedures to form molybdenum blue or molybdenum brown-type clusters. These large concave architectures can reach an impressive size of 154 Mo atoms incorporated in Mo-blue wheels or 132 Mo centers within Mo-brown spheres (Figure 2b). They were first characterized by Müller et al. in 1995 and are formed under highly reducing conditions from simple metal precursors in combination with a variety of additional ligands.[4,13,14,15]

2.2. Synthesis

Approaches for the synthesis of POMs are characterized by one-pot procedures and involve pH-dependent formation of different metalate species, mostly starting from small metal-containing precursors—often hydroxide complexes—in acidic aqueous or non-aqueous media. However, the synthetic principals are still rather empirical and based on trial and error, due to the unknown self-assembly steps and various intermediates that can be involved in the formation of the final products. Usually, systematic variations of reaction parameters like pH value, concentration, type of metal source, reaction temperature and pressure, if solvothermal conditions are used, are the only way to influence the chemical composition, crystal structure and the related properties. The discovery of new compounds is, nevertheless, mostly serendipitous. Moreover, the type and concentration of the potentially employed reducing agent and heteroatom source, as well as the choice of templating anions or additional ligands have major effects on the final cluster geometry and composition.[4,8] The synthetic strategies vary from rational hydrolytic assembly, hydrothermal or solvothermal methods, post-functionalization or partial decomposition of a parent cluster. By the addition of small amounts of water to a non-aqueous solution of the precursor compound, the rational hydrolytic assembly takes place in a stepwise and controlled manner. The synthesis of POMs by hydrothermal or solvothermal methods allows the usage of poorly soluble oxides under increased temperature and pressure. The surface reactivity of a preassembled cluster can lead to new compounds by post-functionalization, thereby forming more extended assemblies from larger building blocks.[16] Another synthetic strategy has become essential in current research. The design and creation of lacunary structures which exhibit vacant positions occurs over partial decomposition of parent clusters, for example, by careful hydrolysis under basic conditions. The vacant positions can be filled by additional cations, used as connection points to crosslink different POM clusters with each other to more enlarged architectures and such materials can be used in new and promising applications.[4,8,17] This is particularly useful for the generation of large supramolecular POM assemblies. Here, the building blocks should possess a certain degree of preorganization to obtain architectures with well-defined geometries and the desired chemical properties.[1,2,5,18]

2.3. Polyoxovanadates

Polyoxovanadates (POVs) represent a special subcategory in the group of POMs. Vanadium is stable in different oxidations states and can build mixed-valent metal-oxide clusters (oxidation states +IV, +V, mixed +IV/+V or even +III). The geometry of the cation-based polyhedra ranges from tetrahedral over square pyramidal to octahedral and even trigonal bipyramidal coordination is possible. By contrast, Mo- and W-containing POMs form predominantly MoO_6 and WO_6 octahedra. The larger structural diversity of VO_x units results in a wide variety of high- and low-nuclearity cluster motifs.[19] Hence, POVs have found application in the fields of catalysis, sol-gel chemistry, gas sensing, geochemistry, sorption and intercalated layered materials, surface- and nano-sciences, as well as secondary electrode materials for advanced lithium ion batteries and vanadium redox-flow batteries.[19,20,21] They are also in the focus of scientific interest as possible single-molecular magnets because they can be magnetically functionalized.[19] The structural flexibility and the resulting electronic and electrochemical properties of the POVs could be harnessed by Streb and coworkers who presented the conversion of methanol to formaldehyde by visible light-driven photoredox catalysis. In their study, a thermally labile $[V_4O_{12}]^{4-}$ cluster rearranges to a pentanuclear $[V_5O_{14}]^{3-}$ cluster, which exhibits an absorption maximum in the visible-light range and acts as a photooxidant. The reduced cluster species condensates to the two-electron reduced species $[V^{IV}_2V^{V}_8O_{26}]^{4-}$, which can be reoxidized with molecular oxygen or hydrogen peroxide (Figure 3).[21]

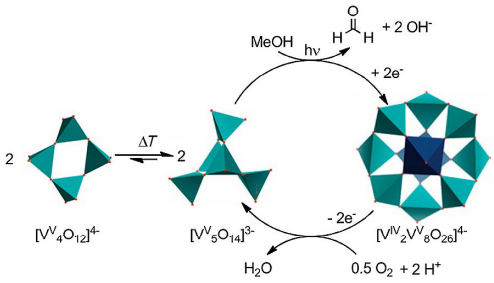

Figure 3. Streb's catalytic photooxidation of methanol to formaldehyde by a POV cluster. Color code: $[V^{V}O_4]$ tetrahedra in cyan, $[V^{IV}O_5]$ square pyramids in dark blue. Reprinted and adapted with permission from ref. [21] (Copyright 2013, Royal Society of Chemistry).

The decavanadate ion $[V_{10}O_{28}]^{6-}$ is one of the most studied isopolyanions of POVs. The structure is composed of VO_6 octahedra sharing common edges and was first reported in 1956 by Rossotti and Rossotti.[22] The decavanadate ion is formed over a wide pH range of 3–8 and is thermodynamically favored in this range compared to other vanadate species.[7,19,23] Hence,

ChemPubSoc Europe

CHEMISTRY A European Journal Minireview

structural diversity for new POV compounds cannot be achieved by syntheses under acidic or weakly basic conditions, as common for Mo- and W-POMs, but rather under reducing conditions in basic media.[7,23]

A prominent example of the isopolyanionic family of vanadium obtained under such conditions is the "fully reduced" archetype $[V^{IV}_{18}O_{42}]^{12-}$, first reported by Johnson and Schlemper in 1978.[24] The cluster is constructed of 18 edge-sharing VO_5 square pyramids, adopting idealized T_d and D_{4d} symmetries.[7,19] Based on this archetype, structures of heteroatom-substituted POVs can be described easily. It is possible to functionalize POVs by the integration of heteroelements, like Si, Ge, As or Sb, into the cluster structure (hetero-POVs). Many hetero-POVs can be described using the archetypal $[V^{IV}_{18}O_{42}]^{12-}$ structure by the formal replacement of two, three or four VO_5 square pyramids by two, three or four E_2O_x groups (rarer $E_2O_xS_2$) with E = Si, Ge, As, Sb and $x = 5$ or 7. Electronic and magnetic properties of the clusters can be modulated or modified by the chemical nature and number of incorporated heteroatoms, respectively. They influence the redox potentials and the steric, as well as electronic environment around the terminal V=O groups.

2.4. Antimonato polyoxovanadates

The hetero-POV chemistry of arsenato- and antimonato-POVs is well developed due to the highly interesting magnetic properties and the possibly occurring spin-frustration, as well as their potential redox activities. The integration of heteroelement-atoms like antimony allows the tuning of electronic and magnetic properties.[19] Also, other compound properties and their chemical behavior are characterized by the lone electron pairs of As^{III} and Sb^{III}. They lead to a steric hindrance around the heteroatom and can act as potential bonding partners.[19] The known Sb-POVs can be described with the archetypal $\{V_{18}O_{42}\}$ by formal substitution of two, three or four VO_5 pyramids by two, three or four handle-like Sb_2O_5 moieties resulting in the most common $\{V_{16}Sb_4O_{42}\}$-,[25–29] $\{V_{15}Sb_6O_{42}\}$-[25,27,30–35] and $\{V_{14}Sb_8O_{42}\}$-types[28–30,32,36–39] (Figure 4).

Depending on the arrangement of the vanadium skeleton, different structural isomers exist, whereas numerous more are imaginable and density functional theory calculations confirm their feasibility.[19,39,40] During the past decades, Sb-POVs were only accessible under hydrothermal or solvothermal conditions with low-molecular vanadium sources like V_2O_5, NH_4VO_3, $NaVO_3$ and $VOSO_4$ or even vanadium halides. Long reaction times, often high temperatures and usually high pH values for reductive reaction conditions needed to be applied because no soluble heteroatom-containing precursor with higher nuclearity was accessible for post-functionalization. The synthesis of new compounds has so far been highly serendipitous and the complexity of obtained reaction products was rather limited compared to other classes of POMs.[19]

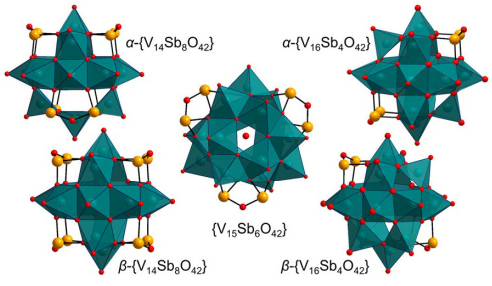

Figure 4. Experimentally observed fully-reduced Sb-POVs. Color code: V in turquoise, O in red, Sb in orange, $V^{IV}O_5$ as green polyhedra.

3. High-Nuclearity POM Structures in Solution

The usage of prebuild synthons in the preparation of polyoxometalates has gained increasing interest because high nuclearity clusters have already demonstrated an immense range of promising properties, as mentioned above. In this regard, the assembly of POM substructures to form larger and highly ordered architectures is especially interesting, but also challenging.[10,41]

Luban and co-workers presented an intriguing example of a well-ordered assembly from a total of 13 substructures.[42] They combined a supramolecular templating effect and a kinetic competition approach to selectively generate the complex $\{Mn_{40}W_{224}\}$ polyanionic architecture **1**, which was characterized by single-crystal structure determination (Figure 5a). From the structure of the compound and the knowledge of the synthetic procedure, the authors proposed a hypothesis for an assembly mechanism: The initial $\{P_2W_{18}\}$ Dawson-type precursor transforms in solution to a $\{P_8W_{48}\}$ macrocycle and, in combination with a manganese building block, to Mn-containing $\{P_2W_{14}Mn_4\}$ and $\{P_2W_{15}Mn_3\}$ Dawson-type clusters (Figure 5b). These reactions proceed via a common $\{P_2W_{12}\}$ intermediate. The $\{P_8W_{48}\}$ macrocycle then templates the formation of the superstructure by the formation of Mn–O=W bridges between the subunits. The final assembly contains four identical trimeric Dawson-type clusters, which encapsulate the central $\{P_8W_{48}\}$ ring. Although the complexity of the resulting POM architecture is impressive, its formation mechanism and the underlying driving forces remain rather vague. More detailed knowledge on the reactivity of the single building blocks and transient intermediates in solution would be valuable for an extension of the assembly process to other supramolecular POM compounds.

3.1. Electrospray ionization mass spectrometry for the characterization of POMs

The analysis of POMs is becoming increasingly challenging, as they grow steadily in size and complexity. In this regard, ESI enables their analysis by MS because this soft ionization technique allows the transfer of large, non-covalently bound complexes into the gas phase with only minor or no fragmentation. Consequently, ESI-MS has become one of the standard methods for the analysis of POMs and numerous impressive assemblies could be detected and investigated.

ChemPubSoc Europe

CHEMISTRY A European Journal Minireview

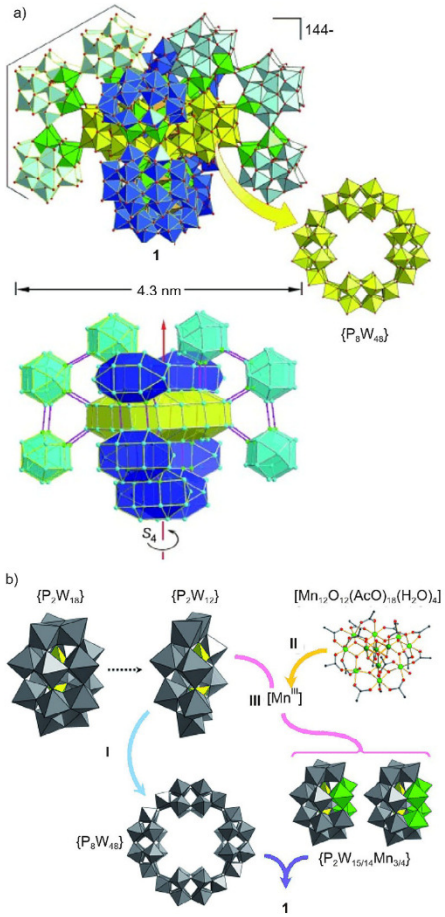

Figure 5. a) Structure of the $\{Mn_{40}W_{224}\}$ cluster **1** consisting of an encapsulated $\{P_8W_{48}\}$ macrocycle (yellow) and 12 corner-sharing Dawson-type clusters (green and blue) with stabilizing Mn–O=W bonds (violet, lower picture); b) proposed self-assembly mechanism. Color code: WO_x-polyhedra in grey, MnO_6-polyhedra in green, PO_4-polyhedra in yellow. Reprinted and adapted with permission from ref. [42] (Copyright 2011 Wiley-VCH Verlag GmbH & Co. KGaA, Weinheim).

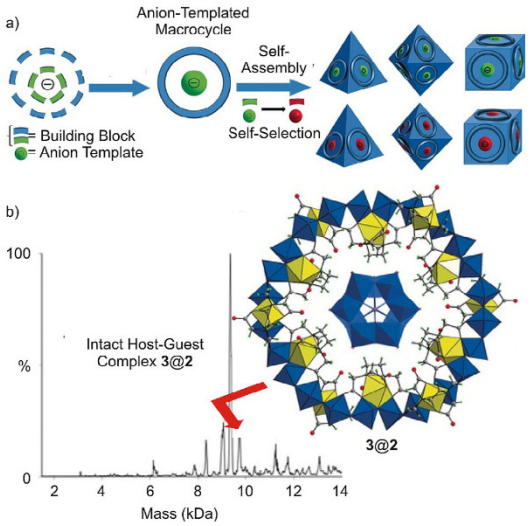

Figure 6. Cronin's cluster-of-clusters architectures. a) Schematic representation of the dynamic assembly of the anion-templated macrocycle, followed by cluster-of-clusters assembly; b) Polyhedral representation of the crystal structure of the host-guest complex **3@2** of macrocycle and template cluster $\{Mo_{12}O_{36}(HPO_3)_2$ with deconvoluted neutral ESI mass spectrum showing host-guest complex **3@2** in water. Color code: MoO_x-polyhedra in blue, FeO_x-polyhedra in yellow. Reprinted and adapted from ref. [47].

Besides the simple analytical characterization of compounds by determining the exact mass and charge state of an ion to obtain its stoichiometry, mass spectrometry offers a variety of experiments to elucidate more complex structural aspects, reactivity and thermochemistry. When ions are transferred into a region of high vacuum, they lose their solvation shell and do not interact with each other due to charge repulsion. This enables the study of isolated ions and their intrinsic properties without the influence of the surrounding system. Mass spectrometry, thereby, functions complementary to methods such as NMR spectroscopy or X-ray crystal structure analysis.[43]

The group of Cronin has shown a variety of impressive architectures that could be analyzed with ESI-MS.[44–46] Recently, they presented the assembly of several POM cluster-of-clusters architectures based on a $\{Mo_{24}Fe_{12}\}$ macrocycle **2**, which forms around a templating anion (Figure 6a).[47] In the case of $\{Mo_{12}O_{36}(HPO_3)_2\}$ as the template cluster anion **3**, the intact host–guest complex **3@2** of macrocycle and template could be detected by ESI-MS (Figure 6b).

A very recent example for an impressive supramolecular architecture containing several POMs was presented by Wang and co-workers in 2017. They demonstrated the formation of the host-guest complex $\{As_4Cu_4[Cu(H_2O)]_{12}\}@\{Nb_7O_{22}\}_4$ **4** (Figure 7a).[48] A one-pot reaction starting from the Lindqvist-type $\{Nb_6O_{19}\}$ cluster, as well as homonuclear copper and arsenic precursors in basic aqueous medium led to the stepwise self-assembly of the complex as evidenced by single-crystal X-ray structure analysis.

The initial extension of the $\{Nb_6O_{19}\}$ to a $\{Nb_7O_{22}\}$ cluster core is crucial for the formation of the tetrahedral, concave $\{Nb_7O_{22}\}_4$ host framework and for the encapsulation of the guest because it enables the formation of oxo-bridges between host and guest molecules (Figure 7b). The in situ formed tetrameric $\{As_4Cu_{16}\}$ guest cluster features an interesting high-nuclearity magnetic core that is stabilized within the $\{Nb_7O_{22}\}_4$ framework. The presence of the intact assembly in solution was evidenced by ESI-MS measurements showing two prominent peak envelopes for cluster anions of different charge states. Furthermore, the compound is stable over a wide pH range in basic aqueous solution. Only at pH values lower than 8 or larger than 12.2, the decomposition of the cluster was observed with ESI-MS (Figure 7c).

ChemPubSoc Europe

CHEMISTRY A European Journal Minireview

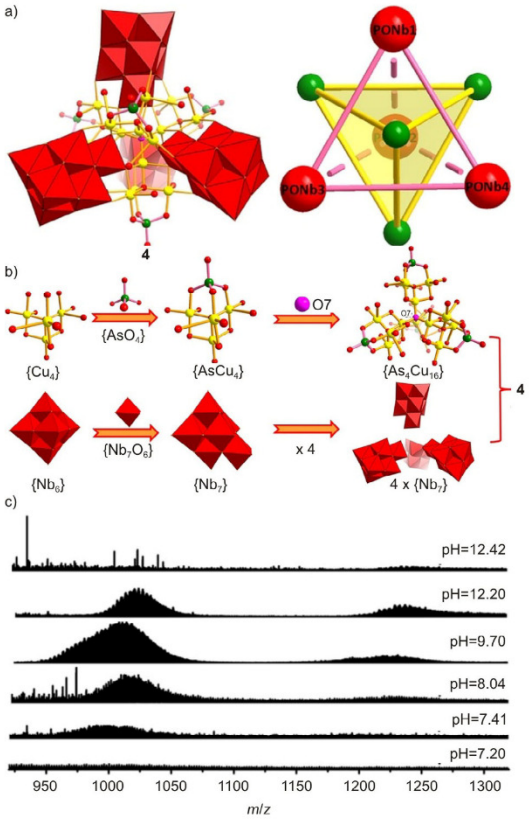

Figure 7. Wang's host-guest complex $\{As_4Cu_{16}\}@\{Nb_7\}_4$ **4**. a) Polyhedral/ball-and-stick view of compound **4** and ball-and-stick view of the linking model of arsenic atoms and PONbs. b) Self-assembly of the $\{As_4Cu_{16}\}$ cluster and the tetrameric $\{Nb_7\}$ host which form the host-guest complex **4**; Color code: NbO_6 as red octahedra, Cu in yellow, As in green, O in red, $\{Nb_7\}$ in red, $\{As_4Cu_{16}\}$ in green. c) ESI-MS spectra of **4** in aqueous solution at different pH values. Reprinted and adapted with permission from ref. [48] (Copyright 2017 Wiley-VCH Verlag GmbH & Co. KGaA, Weinheim).

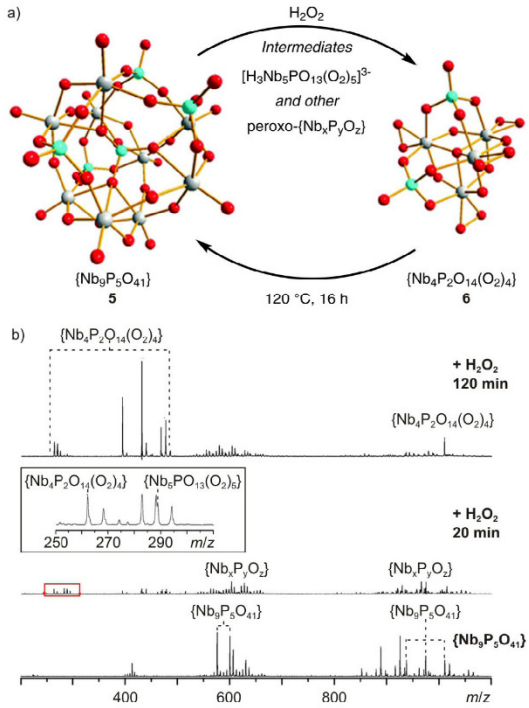

Figure 8. Casey's $\{Nb_9P_5O_{41}\}$ cluster reacts reversibly with hydrogen peroxide. a) interconversion of compounds **5** and **6**. Color code: Nb in gray, P in green, O in red. b) ESI-MS spectra of solution of **5** and after addition of H_2O_2. The inset shows more detailed peak assignments. Reprinted and adapted with permission from ref. [52] (Published by The Royal Society of Chemistry).

3.2. Elucidating the solution reactivity of POMs by ESI-MS

An integral aspect of the research concerned with the assembly of POM architectures is the investigation of their reactivity in solution. This comprises the tasks to unravel their formation mechanism or to investigate their kinetic and thermodynamic stability in solution, as well as the elucidation of possible stimuli-induced reactions.

NMR spectroscopy is not practical for most POMs because commonly incorporated metals are usually not well-suited for such experiments and the cost of ^{17}O-enriched water limits its use for the synthesis of isotopically labelled POMs.[49] ESI-MS is thus the most suitable and straightforward technique for the solution investigations for these types of compounds.[45,50] Especially when the formation of different isomers, short-lived reaction intermediates or products of low abundance complicate the analysis.[51]

Casey and Son presented a Keggin-like pentaphosphate niobate polyoxometalate cluster $\{Nb_9P_5O_{41}\}$ **5**, which incorporates a central phosphate and four additional phosphates in the outer layer of the cluster (Figure 8a, left side).[52] The compound is soluble in water and stable in the pH range from 3 to 12, as shown by ESI-MS experiments. Furthermore, they demonstrated the conversion of **5** into the smaller $\{Nb_4P_2O_{14}(O_2)_4\}$ peroxo-cluster **6** upon reaction with hydrogen peroxide in solution. This process could be reversed by hydrothermal treatment of a solution of **6** (Figure 8a). By performing time-dependent ESI-MS measurements on the reaction of **5** with hydrogen peroxide, they observed the formation of peroxo-$\{Nb_9P_5\}$ or similar peroxo-Keggin-like side products. Additionally, the formation of a $[H_3Nb_5PO_{13}(O_2)_5]^{3-}$ intermediate was observed at the beginning, which vanished over the course of the reaction. Cluster **6** was then formed selectively (Figure 8b).

In addition to the straightforward monitoring of the species in the reaction mixture over time or to applying different reaction conditions to study the formation mechanism and the dynamics of POMs in solution,[46,52,53,54] the exchange of building blocks is often investigated.[55] In the case of POM clusters, exchange experiments are commonly performed as isotopic labeling studies.[56,57] Dosing of small amounts of a suitable labeling reagent, often $H_2{}^{18}O$, or dissolution of the cluster in the reagent makes it possible to observe the exchange of oxygen atoms in an oxo-cluster by the shift and broadening of its isotopic pattern. Information on the structural features and the ki-

netic stability of different positions can be deduced from such patterns.[58,59] In this regard, ESI-MS can very often be used to obtain quantitative or at least semi-quantitative results if structurally similar complexes of the same charge state are regarded. The synthesis of new POMs often occurs by template-induced post-functionalization or rearrangement processes of a substrate cluster into another one. To rationalize and explore these processes, ESI-MS is commonly applied.[45,46,48,50,54,57,60,61]

Cronin and co-workers presented the oscillatory guest-exchange process driven by competing redox processes in a POM capsule system (Figure 9a).[62] Using ESI-MS, EPR und UV/

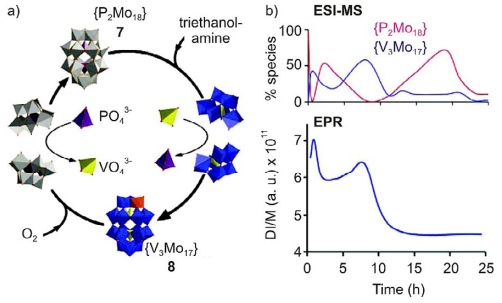

Figure 9. a) Redox-driven guest-exchange reaction interconverting $\{P_2Mo_{18}\}$ **7** into $\{V_3Mo_{17}\}$ **8** by dissociation of the $\{P_2Mo_{18}\}$ capsule **7** into two $\{PMo_9\}$ halves. Color code: MoO_x-polyhedra in gray/blue, VO_4-polyhedra in lime, PO_4-polyhedra in purple. b) Amounts of the $\{P_2Mo_{18}\}$ and $\{V_3Mo_{17}\}$ capsules **7** and **8** in the reaction mixture over time as observed using ESI-MS and EPR indicating oscillation of the reactive system. Reprinted and adapted with permission from ref. [62] (Copyright 2012, American Chemical Society).

Vis spectroscopy, they could demonstrate that the addition of ammonium vanadate and triethanolamine to their system resulted in six complete oscillations (Figure 9b). The Dawson-type $\{P_2Mo_{18}\}$ capsule **7** bearing two encapsulated phosphate guests converts into the $\{V_3Mo_{17}\}$ capsule **8** with two vanadate guests and one vanadium incorporated into the cluster shell. They postulated a reaction mechanism that involves the opening and closing of the cluster capsules, which is driven by a competition between reductive and oxidative processes.

3.3. Gas-phase reactivity and ion mobility

In addition to the compositional analysis of solutions by ESI-MS, mass spectrometry offers the opportunity to investigate isolated ions in more detail in the gas phase. Tandem mass spectrometry is a technique to probe the structure and intrinsic reactivity of a complex without the influence of a solvent. Such an experiment generally involves the mass selection of the ion of interest, its activation, for example, by collision-induced dissociation (CID) with inert gas molecules, and the resulting gas-phase fragmentation, followed by mass analysis and detection of the resulting product ions.[63] The obtained fragmentation patterns can be related to the relative energy demand of competing reactions which in turn elucidates structural details of the investigated complexes because their reactivity is commonly closely related to their structural and energetic features. CID tandem MS can also be used for the analysis of POMs, often in combination with isotopic labeling of the analyte prior to the experiment.[45,50,60] The fragmentation of the parent cluster may lead to product ions with the same or similar stoichiometries, as observed for solution-phase species, and can thereby give information about formation mechanisms in solution.[64] However, this approach cannot be applied to all systems as the sequence of bond cleavages, starting typically with the weakest bonds, does not necessarily resemble the order of assembly. Rather, reactions in the gas phase can provide valuable information on the intrinsic properties of the analyte if reactions are observed that do not occur in solution.[59,65]

A gas-phase technique currently gaining immense attention is ion mobility mass spectrometry (IM-MS). This method is used to separate ions not only based on their *m/z*, but also by their size and shape. In a standard IM-MS experiment, ions are guided by a weak electric field through an ion mobility cell filled with an inert buffer gas. More extended ions undergo a larger number of collisions with the buffer gas than compact ions of the same *m/z* and are thereby decelerated during their migration. As a result, these more extended ions leave the cell after longer drift times.[66] The intrinsic physical property related to size and shape relevant for these experiments is the collision-cross section (CCS). The characteristic CCS of an ion offers structural information, such as its connectivity, configuration, conformational dynamics and topology, and can be compared to values based on theoretical calculation, NMR experiments or X-ray crystallography. It can be used for the differential separation of ions in a complex mixture prior to their mass analysis and is very valuable because it does not only provide ensemble-averaged information, but rather for each single species.[66]

The scientific interest in harnessing IM-MS for the investigation of complex molecular systems is steadily growing because it provides the opportunity to observe and monitor for example, self-assembly and self-sorting processes of supramolecular architectures, the formation of host-guest complexes or gas-phase reactions.[67] In the field of POM, IM-MS is frequently used to separate and analyze complex product mixtures after self-assembly processes.[47] A growing number of examples has been published in which IM-MS was utilized as a supporting analytical method besides X-ray crystal structure analysis and NMR spectroscopy to confirm the formation of POMs.[68] Employing IM-MS even for the major part of the analysis of their POM assemblies, Cronin and co-workers have published studies on the structural elucidation by IM-MS in cases, for which no X-ray crystal structures could be obtained.[69] For example, they presented an IM-MS study in which the hierarchical self-assembly of an icosahedral nanoscale Keplerate cluster **9** was shown.[70] Twelve pentagonal $\{Mo^{V}Mo^{IV}_5\}$ building blocks are connected by thirty Fe^{III} centers and form an overall $\{Mo_{72}Fe_{30}O_{252}\}$ shell around an encapsulated Keggin-type $\{SiMo_{12}O_{40}\}$ cluster (Figure 10, inset).[71]

In addition to the intact Keplerate nanocluster **9**, higher-order supramolecular structures were observed in the gas phase for the first time. The different oligomers could be resolved by IM-MS. The group proposed similar gas-phase struc-

ChemPubSoc Europe

CHEMISTRY A European Journal Minireview

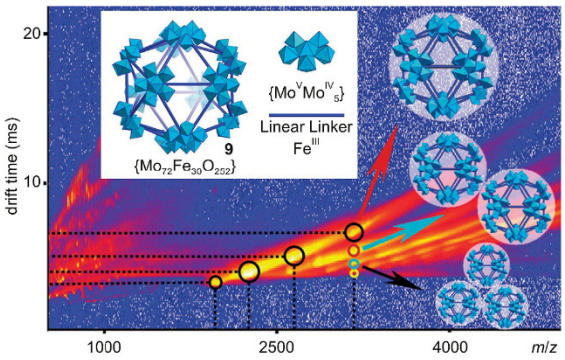

Figure 10. Cronin's supramolecular assembly of Keplerate clusters. 2D-IM-MS plot resolves intact cluster ions (black circles) and oligomeric assemblies (red, blue and yellow circles). Inset: schematic representation of Keplerate cluster structure **9** and building blocks. Reprinted and adapted with permission from ref. [70] (Copyright 2013, Royal Society of Chemistry).

tures to those observed earlier for these so-called Keplerate "blackberries" in solution and in the solid state (Figure 10).

4. Reactivity of Sb-POVs

4.1. Reactivity of the $\{V_{15}Sb_6O_{42}\}$-type polyoxovanadates

In general, the solution chemistry of antimonato polyoxovanadate clusters has been only poorly understood until recently due to the lack of soluble species. Their preparation was consequently restricted to the highly serendipitous solvothermal method with low-nuclearity precursors. Furthermore, fundamental questions concerning their formation mechanisms, stabilities and host-guest chemistry were left unanswered.

In 2016, we introduced four novel compounds with the composition of $\{M(en)_3\}_3[V_{15}Sb_6O_{42}(H_2O)_x]\cdot n\,H_2O$ ($n \approx 15$ or 28; $x = 0$, 1; M = Ni^{II}, Co^{II}, Fe^{II}; en = ethylenediamine) and identified compound **10** with M = Ni^{II} (Ni-$\{V_{15}Sb_6\}$) as the first water-soluble member of the Sb-POV class.[33] All four compounds were obtained by solvothermal synthesis and consist of the known $[V_{15}Sb_6O_{42}(H_2O)_x]^{6-}$ ($x = 0$, 1) cluster and isolated, charge-compensating $\{M(en)_3\}^{2+}$ complexes. The unusually high water solubility of **10** enabled us to study the structure of the $\{V_{15}Sb_6O_{42}\}$ cluster in solution and its reactivity, both in solution and in the gas phase.

ESI-MS measurements showed that the $\{V_{15}Sb_6O_{42}\}$ cluster stays intact upon dissolution of the Ni-$\{V_{15}Sb_6\}$ **10** in water. Interestingly, a series of ions was observed in the corresponding mass spectrum, which belong to water-free and water-containing complexes of the cluster (see for example, Figure 11 b, top spectrum).

It was proposed that the water-containing complex could correspond to one of the following three structures: 1) a solvent adduct, which is formed due to incomplete desolvation, 2) a cluster in which the water has opened one of the oxo bridges, resulting in two free M-OH groups or 3) a host-guest complex with the water molecule residing inside the closed

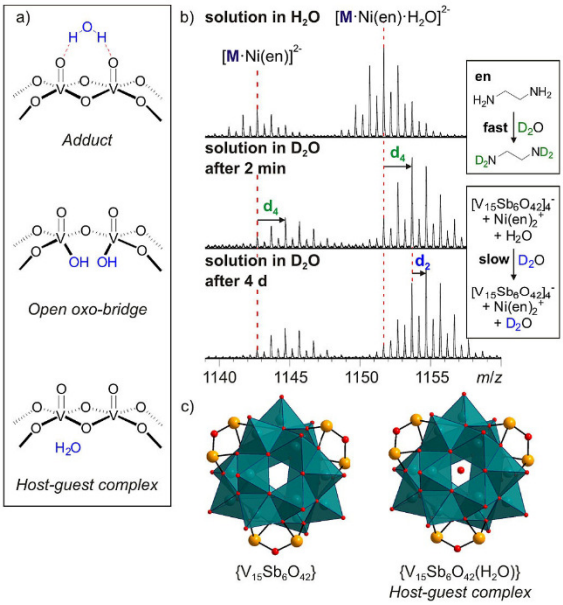

Figure 11. a) Possible structures of the $\{V_{15}Sb_6O_{42}\}$ clusters in water as observed by ESI-MS. b) ESI-MS spectra of a solution H/D exchange experiment performed on **10**. c) Solution contains a water-free and a water-encapsulating $\{V_{15}Sb_6O_{42}\}$ cluster core as distinct species. **M** = $\{V_{15}Sb_6O_{42}\}$. Color code: V in turquoise, Sb in orange, O in red. Reprinted and adapted with permission from ref. [33] (Published by The Royal Society of Chemistry).

cluster cavity (Figure 11 a). A time-dependent H/D exchange experiment in solution performed on **10** demonstrated significantly slower exchange for the water protons than for the amine protons of the attached ethylenediamine ligand (Figure 11 b). For the first two possible structures, fast exchange and no significant difference between the proton types would be expected. Therefore, we concluded that the cluster core is present in solution as two distinct solution species: a closed, cage-like cluster with a single water molecule encapsulated within its cavity and a closed, cage-like cluster with an empty cavity (Figure 11 c).[33]

These findings provided the basis for a reevaluation of some unassigned remaining electron density in the crystal structure of **10** obtained during the working process, which then confirmed the presence of an encapsulated water molecule in part of the cluster shells. This underlines the importance of ESI-MS for structural analysis of clusters in combination with X-ray crystal structure analysis.

Tandem MS experiments revealed an intriguing gas-phase reactivity of the $\{V_{15}Sb_6O_{42}\}$ cluster. Collision-induced dissociation (CID) of the water-encapsulating cluster resulted in the loss of the guest molecule, while leaving the host structure intact as an empty cluster core (Figure 12 a,b). This gas-phase fragmentation indicates a significant influence of the guest onto the reactivity of the cluster host because it was rationalized that the water participates in the reaction mechanism. It could open an oxo-bridge upon attack on a vanadium ion from the inside of the cavity. After proton transfer steps, the

ChemPubSoc Europe

CHEMISTRY A European Journal Minireview

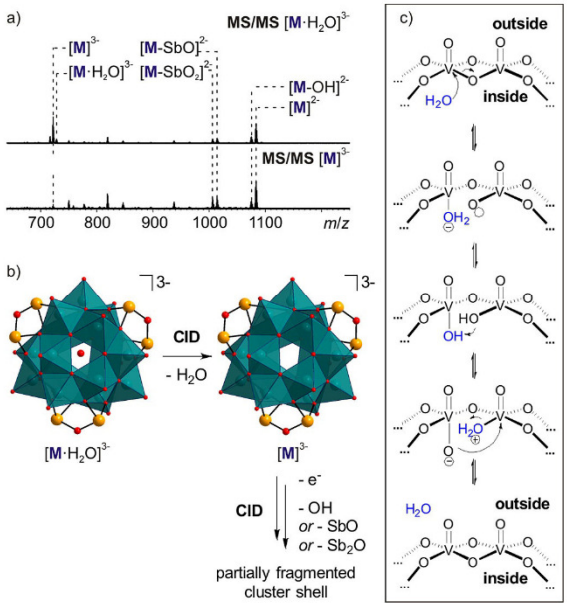

Figure 12. a) CID tandem MS experiment performed on water-free cluster ions $[\mathbf{M}]^{3-}$ and water-encapsulating cluster ions $[\mathbf{M}{\cdot}H_2O]^{3-}$; b) observed fragmentation pathway includes prominent loss of encapsulated water from intact cluster core; c) proposed mechanism for loss of inner-phase water resulting in an intact cluster core by participation of the guest itself. M = $\{V_{15}Sb_6O_{42}\}$. Color code: V in turquoise, Sb in orange, O in red. Reprinted and adapted with permission from ref. [33] (Published by The Royal Society of Chemistry).

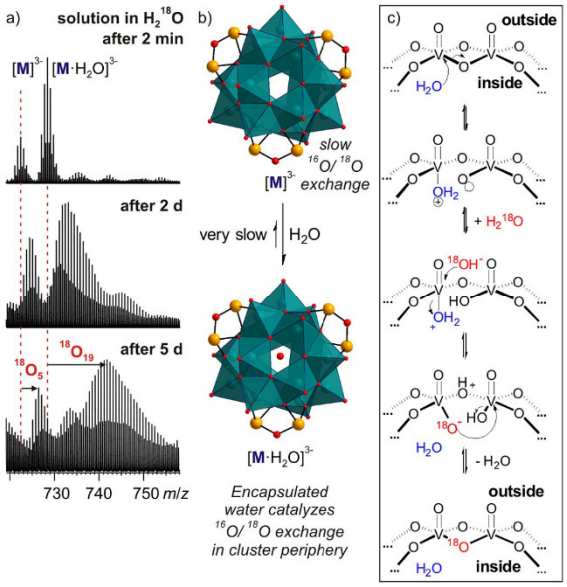

Figure 13. a) ESI-MS spectra of $^{16}O/^{18}O$ exchange experiment performed on **10** in solution; b) different $^{16}O/^{18}O$ exchange rates observed for water-free and water-encapsulating cluster core, encapsulated inner-water catalyzes the exchange; c) proposed mechanism for the $^{16}O/^{18}O$ exchange reaction under catalysis of the guest water molecule within the cluster. M = $\{V_{15}Sb_6O_{42}\}$. Color code: V in turquoise, Sb in orange, O in red. Reprinted and adapted with permission from ref. [33] (Published by The Royal Society of Chemistry).

oxo-bridge is reformed with the water molecule as the leaving group on the outside of the cage (Figure 12c).[33] The influence of the cluster's inner-phase on its outer-phase reactivity became even more evident when the $^{16}O/^{18}O$ isotope-exchange in solution was investigated. Cluster cages with an encapsulated water molecule exhibited a significantly faster oxygen-atom exchange in the cluster periphery than those with an empty cavity (Figure 13a,b). The proposed mechanism accounting for this effect of different exchange rates proceeds through similar initial steps as the gas-phase fragmentation mechanism.

The acceleration of the exchange is achieved by the initial opening of an oxo-bridge by the inner-phase water, which is not facilitated in case of the empty clusters. In the following, the exchange step and the closing of the oxo-bridge occur to regenerate the intact cluster cage, similar to the gas-phase reaction. However, the loss of the encapsulated water in solution is, in contrast to the gas phase, neither favored by entropy (exclusion volume inside the cavity) nor enthalpy (nonsolvated inner surface of the cluster). Hence, the retention of the guest inside the cluster is favored and sustains the catalysis of the oxygen exchange in the cluster's periphery (Figure 13c).[33]

These results display the first reported example in polyoxovanadate chemistry for the transduction of inner-phase reactivity of an encapsulated guest molecule into changes in the

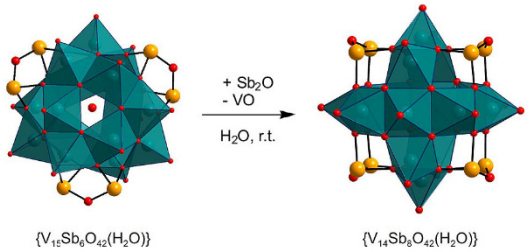

Figure 14. ESI-MS experiments gave first evidence for a selective $\{V_{15}Sb_6O_{42}\} \rightarrow \{V_{14}Sb_8O_{42}\}$ cluster transition in solution at ambient conditions. Color code: V in turquoise, Sb in orange, O in red.

outer-phase reactivity of the cluster cage. Its significance became obvious when we discovered that the Sb-richer $\{V_{14}Sb_8O_{42}\}$ cluster is selectively formed from the $\{V_{15}Sb_6O_{42}\}$ precursor **10** in solution at ambient condition and over the course of days (Figure 14). A formal exchange of a VO against an Sb–O–Sb unit occurred, which could be detected by ESI-MS.[33] This rearrangement reveals an astonishing reactivity because all compounds with a $\{V_{14}Sb_8O_{42}\}$ cluster core known until then were prepared under solvothermal conditions from mononuclear single-source precursors.

The ESI-MS investigations indicated that the $\{V_{15}Sb_6O_{42}\} \rightarrow \{V_{14}Sb_8O_{42}\}$ transformation could be accelerated by the addition

ChemPubSoc Europe

CHEMISTRY A European Journal Minireview

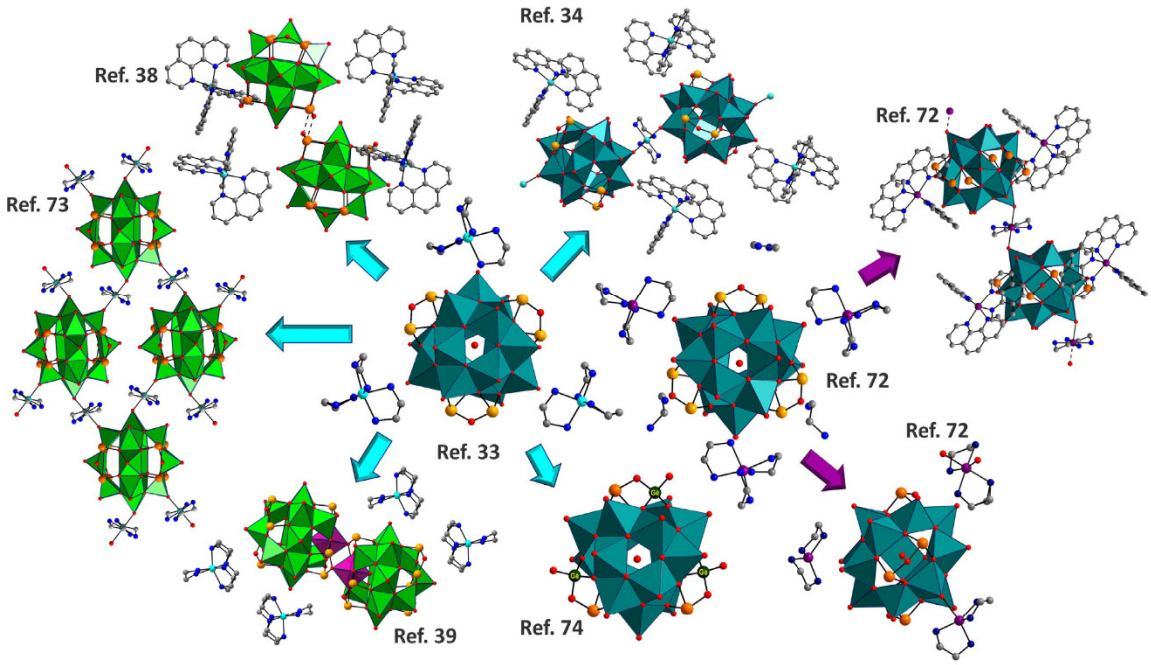

Scheme 1. Overview Sb-POV obtained by post-functionalization of soluble precursors **10** and **12**. Color code: $\{V_{14}Sb_8O_{42}\}$-cluster VO_5-polyhedra in green, $\{V_{15}Sb_6O_{42}\}$-cluster VO_5-polyhedra: turquoise, Sb: orange, O: red, Ni: light blue, Zn: purple, VO_6-octahedra: purple).

of ammonium additives.[72] Under stirring conditions, the transformation could reach full conversion after only 4 h at 150 °C, resulting in formation of $[\{Ni(en)_2\}_2V_{14}Sb_8O_{42}]\cdot 5.5H_2O$[36] featuring the β-isomer of the $\{V_{14}Sb_8O_{42}\}$ moiety.[73] This fast reaction progress allowed investigation of the conversion by in situ-XRD experiments at the DESY (German Electron Synchotron) facility in Hamburg. The kinetic evaluation of the data demonstrated that the rate-limiting step is the nucleation process (Avrami A3 kinetics).

No crystalline intermediates have been observed. The nucleation phase is heterogeneous and the crystallization was shown to be temperature-dependent. The in situ investigations of this transformation reaction demonstrated very low activation energies for nucleation (ca. 34.4 kJ mol^{-1}) and crystal growth (ca. 43.8 kJ mol^{-1}), which are in the range of metal–organic frameworks (50–140 kJ mol^{-1}), thiostannates (ca. 42 kJ mol^{-1}), thioantimonates (ca. 70 kJ mol^{-1}) or zeolites (40–100 kJ mol^{-1}).[73]

4.2. Post-functionalization of $\{V_{15}Sb_6O_{42}\}$-type POVs

The insights gained when studying the reactivity of the $\{V_{15}Sb_6O_{42}\}$ cluster in compound **10** have proven to be highly valuable for the further development of Sb-POV chemistry. The versatility of this high-nuclearity precursor was demonstrated in a number of post-functionalization reactions, thereby broadening the field of new Sb-POVs (Scheme 1).[34,38,73] The use of this new precursor has enabled the increase in structural complexity of the obtained cluster products, which have partially undergone the $\{V_{15}Sb_6O_{42}\}\rightarrow\{V_{14}Sb_8O_{42}\}$ transformation after short reaction times. Different configurational isomers of the $\{V_{14}Sb_8O_{42}\}$ cluster (α-$\{Ni(phen)_3\}_2[V_{14}Sb_8O_{42}]\cdot 12H_2O$ and β-$[\{Ni(en)_2\}_2V_{14}Sb_8O_{42}]\cdot 5.5H_2O$)[38] were obtained under mild conditions as compared to regular solvothermal syntheses. In addition, it was also possible to prepare a post-functionalized compound, namely $\{Ni(phen)_3\}_3[\{Ni(en)_2\}V_{15}Sb_6O_{42}]\cdot 19H_2O$, with an unchanged cluster core from compound **10** within 24 hours reaction time.[34]

Moreover, the Ni-$\{V_{15}Sb_6\}$ **10** proved to be a suitable precursor for an interesting supramolecular Sb-POV architecture. The reaction of this compound with cyclen in aqueous solution yields $\{Ni(cyclen)(en)\}_2[V_{14}Sb_8O_{42}(H_2O)]\cdot\approx 10H_2O$ (**11**) after a short reaction time.[39] The compound has undergone a ligand metathesis and the $\{V_{15}Sb_6O_{42}\}\rightarrow\{V_{14}Sb_8O_{42}\}$ transformation. Furthermore, the cluster core is present as the configurational α_1*-isomer of the previously observed α-$\{V_{14}Sb_8O_{42}\}$ cluster, featuring an inverted orientation of one of the edge-sharing VO_5 pyramids toward the center of the cage. This is the first example for configurational isomerism in hetero-POV chemistry. The cluster cavity is sufficiently large to accommodate both the inwards-oriented oxygen atom of the VO_5 pyramid and an additional H_2O guest, which forms strong hydrogen bonds to this oxygen atom (Figure 15, left). This arrangement generates an accessible open coordination site at this VO_5 pyramid, which is saturated by a neighboring cluster by supramolecular Sb–O···V and Sb–O···Sb contacts. The α_1*-$\{V_{14}Sb_8O_{42}\}$ cages hence form unprecedented dimeric structures in the solid state (Figure 15, right).

ChemPubSoc Europe

CHEMISTRY A European Journal Minireview

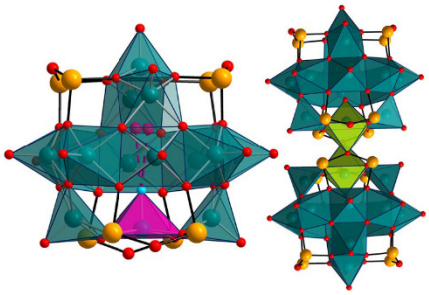

Figure 15. Polyhedral representation of α*-{$V_{14}Sb_8O_{42}$} cluster and its dimer in compound **11**. Color code: VO_5 as turquoise polyhedra, Sb in yellow, O in red, inward-oriented VO_5 pyramid in purple, distorted VO_6 octahedral in green.

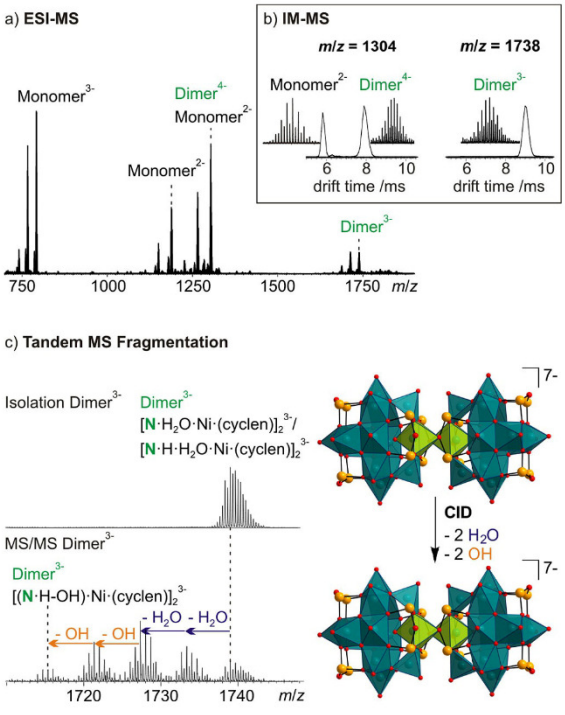

Figure 16. a) ESI-MS spectrum of **11**; b) IM-MS experiment for peaks at *m/z* 1304 and 1738 with corresponding arrival-time distributions and resolved isotopic patterns; c) CID tandem MS experiment performed on dimeric cluster ion with observed fragmentation pathway yielding a still-intact dimeric cluster. Color code: VO_5 as turquoise polyhedra, Sb in yellow, O in red, inward-oriented VO_5 pyramid in purple, distorted VO_6 octahedral in green.

ESI-MS studies performed on compound **11** revealed the presence of both the intact α_1*-{$V_{14}Sb_8O_{42}$} cluster ion and the dimer in solution (Figure 16a). Ions with partially overlapping isotope patterns could be unambiguously assigned by employing ion mobility for their separation in the gas phase prior to detection. The obtained arrival-time distributions for ions derived from dimeric cluster complexes feature narrow and Gaussian-shaped peaks indicating well-defined gas phase structures (Figure 16b). These results demonstrate the specific non-covalent interaction between two cluster cores of the α_1*-{$V_{14}Sb_8O_{42}$} isomer even in water. Time-dependent ESI-MS experiments showed that the {$V_{15}Sb_6O_{42}$}→α_1*-{$V_{14}Sb_8O_{42}$} transformation and the formal α_1*-{$V_{14}Sb_8O_{42}$}→[α_1*-{$V_{14}Sb_8O_{42}$}]$_2$ dimerization have been completed after the initial heating period of the reaction mixture, prior to product crystallization.

Interestingly, a CID tandem MS experiment performed on an ion derived from a dimeric cluster complex revealed a remarkable binding energy connecting the two α_1* monomers also in the gas phase. Although the very prominent cleavage of the dimeric ion into monomers is clearly favored by the reduction of charge repulsion, the characteristic loss of neutral water and hydroxyl radicals from the dimer ions yielding still-intact dimeric product ions was also observed (Figure 16c).[39]

These results emphasize the value of the soluble Sb-POV precursor **10** and the knowledge about its solution reactivity for the synthesis of complex new Sb-POV compounds. It also demonstrates that an array of small, yet cooperative effects including the changes to the counter-cation-ligand environment and the intramolecular noncovalent interaction between cluster-cage dimers can drive the formation of the high-energy configurational α_1*-{$V_{14}Sb_8O_{42}$} isomer. The analysis of this fascinating new compound highlights the ability of mass spectrometry to provide detailed structural insights into hierarchical self-assembly phenomena of Sb-POVs in solution.

The power of the Ni-{$V_{15}Sb_6$} **10** as a synthon has also been demonstrated by the reaction with GeO_2, which resulted in a mixed antimonato-germanato polyoxovanadate, namely {Ni(en)$_3$}$_3$[$V_{15}Sb_3Ge_3O_{42}$(OH)$_3$(H_2O)]·≈9H_2O.[74] In this mixed heteroatom POV, Sb and Ge occupy distinct positions that might have been formed by partial transformation (Figure 17). This

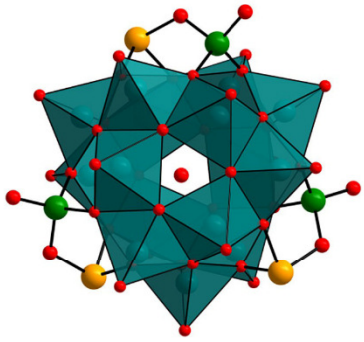

Figure 17. Polyhedral and ball-and-stick representation of the mixed antimonato-germanato polyoxovanadate in compound {Ni(en)$_3$}$_3$[$V_{15}Sb_3Ge_3O_{42}$(OH)$_3$(H_2O)]≈9H_2O. Color code: VO_5 as turquoise polyhedral, O in red, Sb in orange, Ge in green.

new category of POVs had not yet been reported at the time and might feature new and promising properties.

A second water-soluble Sb-POV, namely {Zn(en)$_3$}$_3$[$V_{15}Sb_6O_{42}$(H_2O)]·3 en·10H_2O **12** (Zn-{$V_{15}Sb_6$}) was synthesized by our group using solvothermal synthesis starting

ChemPubSoc Europe

CHEMISTRY A European Journal Minireview

from low-nuclearity materials.[72] It exhibits a significantly increased solubility in water compared to the water-soluble Ni-$\{V_{15}Sb_6\}$ precursor **10** and enabled the synthesis of two new Sb-POV compounds, $\{Zn(phen)_3\}_2[Zn(en)_2V_{15}Sb_6O_{42}(H_2O)]\cdot 23\,H_2O$ **13** and $\{(Zn(en)_2(H_2O)_2)(Zn(en)_2)\}[Zn(en)_2V_{15}Sb_6O_{42}(H_2O)]\cdot 8.5\,H_2O$ **14**, by very convenient post-functionalization procedures in a short reaction time of 24 hours at 150 °C. Interestingly, all new compounds **12**–**14** contain the $\{V_{15}Sb_6O_{42}\}$ cluster core with an encapsulated water molecule inside the cavity as a common motif. In all of them, strong interactions between the cluster and the ethylenediamine ligand or one of the $[Zn(en)_2]^{2+}$ complexes are present that underline the potential of Sb-POVs to form complex structures by supramolecular interactions (Scheme 1).

Compound **12** features a close interaction between one nitrogen atom of all three ethylenediamine molecules and three of the Sb atoms with Sb–N distances significantly shorter than the sum of their van der Waals radii. As was shown recently, such short Sb–N distances must be treated as covalent bonds with a strength comparable to a Sb–O bond.[35] In the structure of **13**, $\{V_{15}Sb_6O_{42}\}$ clusters are connected to their next neighbors by $[Zn(en)_2]^{2+}$ complexes forming a chain along [101]. These chains are surrounded by $[Zn(phen)_3]^{2+}$ complexes which interact with each other in a sandwich-type arrangement of π-π interactions. $(\{Zn(en)_2(H_2O)_2\}\{Zn(en)_2\})[Zn(en)_2V_{15}Sb_6O_{42}(H_2O)]\cdot 8.5\,H_2O$ **14** contains three different Zn^{2+} complexes in different coordination geometries. One of these Zn^{2+} cations is connected to the cluster by a Zn–O bond and exhibits a distorted trigonal bipyramidal environment.

We found by time-dependent ESI-MS experiments that the Zn-$\{V_{15}Sb_6\}$ compound **12** exhibits very similar properties in solution as the earlier investigated Ni-$\{V_{15}Sb_6\}$ compound **10**, with the main difference being the significantly prolonged reaction time under ambient conditions for the $\{V_{15}Sb_6O_{42}\}\rightarrow\{V_{14}Sb_8O_{42}\}$ transformation with 330 hours compared to, respectively, 110 hours after which 50% conversion is reached. This enabled the rational and selective formation of compounds, which all feature an intact and unchanged $\{V_{15}Sb_6O_{42}\}$ cluster core.[34,38,73] Furthermore, the rate of the $\{V_{15}Sb_6O_{42}\}\rightarrow\{V_{14}Sb_8O_{42}\}$ cluster transformation significantly increases for both compounds in the same manner, when ammonium acetate was added to the solution, with a time of 23 hours after which 50% conversion was reached.

These results indicate that the reactivity of the cluster cage is not only determined by the encapsulated water molecule, but also by the surrounding cationic metal complex, ligand environment, as well as additives and the pH value. It also encourages further exploration of the influence of these parameters for the rational application in antimonato polyoxovanadate chemistry.

5. Summary and Outlook

The majority of hetero-POV-studies have so far focused on the synthesis of new compounds applying starting materials like NH_4VO_3, V_2O_5 or even $\{V_{10}O_{28}\}$ with oxides as heteroatom sources. Taking advantage of the discovered soluble high-nuclearity Sb-POV precursors will likely lead to an expansion of the structural diversity of this compound class towards higher-order species. A more detailed mechanistic investigation of the $\{V_{15}Sb_6O_{42}\}\rightarrow\{V_{14}Sb_8O_{42}\}$ cluster rearrangement in solution, for which the understanding is still only rudimentary, would be highly interesting. It might open pathways to unexplored, more complex structures by, for example, intercepting reaction intermediates when introducing interlinking ligands or additional cluster types. Initial results indicated a strong influence of additives like ammonium acetate on the solution reactivity of the $\{V_{15}Sb_6O_{42}\}$ cluster independent of the counter ion. This approach could be extended to other additives and might result in the formation of still unobserved, but theoretically predicted cluster cages. In this regard, it might be possible to exchange the encapsulated guest within the cluster cavity from water to another guest molecules or ions. The possible template effect on structure and reactivity of the resulting species would certainly be fascinating. The formation of the $\{V_{15}Ge_3Sb_3O_{45}\}$ indicated impressively which currently unpredicted cluster constellations in polyoxovanadate chemistry might be possible by usage of prebuild synthon-like structures. The preparation and investigation of other mixed-heteroatom-POVs might lead to new innovative properties of such a compound class. Nevertheless, the understanding of the formation and, in this case, the transformation of the soluble precursors is necessary for a potentially planned rational synthesis. Insight into fundamental questions connected to the self-assembly of these new Sb-POVs might lead to the designed synthesis of problem-tailored compounds. The control over topology and structure of the synthesized polyoxovanadates could enable the design of multifunctional materials. The first promising attempts in the direction of understanding the formation of Sb-POVs have been made by ESI-MS under ambient and in situ X-ray investigations under hydrothermal conditions to gain insights into the dominating influences on the formation. Although the first steps are made, several challenges and questions remain to be solved. In this context, mass spectrometry and ion mobility will likely serve as probes for the elucidation of solution reactivity and the identification of new products or possible intermediates. This will increase the understanding of the building of Sb-POVs and maybe even other POVs or Group 5 polyoxometalates. These methods can provide rational guidelines for the synthesis of new compounds with unprecedented structures and architectures, as was already successfully done in the work discussed here.

Acknowledgements

This work was supported by the Deutsche Forschungsgemeinschaft DFG (CRC 1109) and the State of Schleswig-Holstein.

Conflict of interest

The authors declare no conflict of interest.

ChemPubSoc Europe

CHEMISTRY A European Journal Minireview

Keywords: antimonato polyoxovanadates · ESI-MS · polyoxometalates · post-functionalization · solution reactivity

[1] D.-L. Long, E. Burkholder, L. Cronin, *Chem. Soc. Rev.* **2007**, *36*, 105 – 121.
[2] D.-L. Long, R. Tsunashima, L. Cronin, *Angew. Chem. Int. Ed.* **2010**, *49*, 1736 – 1758; *Angew. Chem.* **2010**, *122*, 1780 – 1803.
[3] H. N. Miras, D.-L. Long, L. Cronin in *Advances in Inorganic Chemistry* (Eds. R. v. Eldik, L. Cronin), Elsevier, Amsterdam, **2017**, 1 – 28.
[4] M. Hutin, M. H. Rosnes, D.-L. Long, L. Cronin in *Comprehensive Inorganic Chemistry II*, (Eds. J. Reedijk, K. Poeppelmeier), Elsevier, Amsterdam, **2013**, 241 – 269.
[5] M. T. Pope, A. Müller (Eds.) *Polyoxometalate Chemistry From Topology via Self-Assembly to Applications*, Kluwer Academic Publishers, Dordrecht, **2002**.
[6] a) N. V. Izarova, M. T. Pope, U. Kortz, *Angew. Chem. Int. Ed.* **2012**, *51*, 9492 – 9510; *Angew. Chem.* **2012**, *124*, 9630 – 9649; b) Z. Lang, P. Yang, Z. Lin, L. Yan, M.-X. Li, J. J. Carbó, U. Kortz, J. M. Poblet, *Chem. Sci.* **2017**, *8*, 7862 – 7872; c) P. Yang, H. Li, T. Ma, F. Haso, T. Liu, L. Fan, Z. Lin, C. Hu, U. Kortz, *Chem. Eur. J.* **2018**, *24*, 2466 – 2473; d) P. Yang, Y. Xiang, Z. Lin, Z. Lang, P. Jiménez-Lozano, J. J. Carbó, J. M. Poblet, L. Fan, C. Hu, U. Kortz, *Angew. Chem. Int. Ed.* **2016**, *55*, 15766 – 15770; *Angew. Chem.* **2016**, *128*, 15998 – 16002.
[7] C. Streb in *Structure and Bonding* (Ed. D. M. P. Mingos), Springer, Berlin, **2017**, 1 – 17.
[8] H. N. Miras, L. Vilà-Nadal, L. Cronin, *Chem. Soc. Rev.* **2014**, *43*, 5679 – 5699.
[9] a) C. Boskovic, *Acc. Chem. Res.* **2017**, *50*, 2205 – 2214; b) D. E. Katsoulis, *Chem. Rev.* **1998**, *98*, 359 – 388; c) M. Ammam, *J. Mater. Chem. A* **2013**, *1*, 6291 – 6312.
[10] M. C. Pierre Gouzerh, *l'actualité chimique* **2006**, *298*, 1 – 14.
[11] J. J. Berzelius, *Ann. Phys.* **1826**, *82*, 369 – 392.
[12] J. F. Keggin, *Nature* **1933**, *131*, 908 – 909.
[13] J. J. Borrás-Almenar, E. Coronado, A. Müller, M. Pope (Eds.) *NATO Science Series*, Springer, Dordrecht, **2003**.
[14] S.-S. Wang, G.-Y. Yang, *Chem. Rev.* **2015**, *115*, 4893 – 4962.
[15] a) W. Xuan, R. Pow, D.-L. Long, L. Cronin, *Angew. Chem. Int. Ed.* **2017**, *56*, 9727 – 9731; *Angew. Chem.* **2017**, *129*, 9859 – 9863; b) M. T. Pope, A. Müller, *Angew. Chem. Int. Ed. Engl.* **1991**, *30*, 34 – 48; *Angew. Chem.* **1991**, *103*, 56 – 70; c) R. Pütt, A. Kondinski, K. Monakhov, *Chem. Unserer Zeit* **2018**, ##https://doi.org/10.1002/ciuz.201800818.
[16] a) R. J. Errington in *Polyoxometalate Chemistry From Topology via Self-Assembly to Applications* (Eds. M. T. Pope, A. Müller), Springer, Berlin, **2001**, 7 – 22; b) A. Müller, S. K. Das, P. Kögerler, H. Bögge, M. Schmidtmann, A. X. Trautwein, V. Schünemann, E. Krickemeyer, W. Preetz, *Angew. Chem. Int. Ed.* **2000**, *39*, 3413 – 3417; *Angew. Chem.* **2000**, *112*, 3555 – 3559.
[17] a) N. I. Gumerova, A. Rompel, *Nat. Chem. Rev.* **2018**, *2*, 0112; b) L. Vilà-Nadal, L. Cronin, *Nat. Rev. Mater.* **2017**, *2*, 17054.
[18] a) B. Li, W. Li, H. Li, L. Wu, *Acc. Chem. Res.* **2017**, *50*, 1391 – 1399; b) C.-H. Zhan, R. S. Winter, Q. Zheng, J. Yan, J. M. Cameron, D.-L. Long, L. Cronin, *Angew. Chem. Int. Ed.* **2015**, *54*, 14308 – 14312; *Angew. Chem.* **2015**, *127*, 14516 – 14520.
[19] K. Y. Monakhov, W. Bensch, P. Kögerler, *Chem. Soc. Rev.* **2015**, *44*, 8443 – 8483.
[20] a) J. L. Ferreira da Silva, M. Fátima Minas da Piedade, M. Teresa Duarte, *Inorg. Chim. Acta* **2003**, *356*, 222 – 242; b) J. M. Breen, W. Schmitt, *Angew. Chem. Int. Ed.* **2008**, *47*, 6904 – 6908; *Angew. Chem.* **2008**, *120*, 7010 – 7014; c) J. Tucher, K. Peuntinger, J. T. Margraf, T. Clark, D. M. Guldi, C. Streb, *Chem. Eur. J.* **2015**, *21*, 8716 – 8719; d) M. Lechner, K. Kastner, C. J. Chan, R. Güttel, C. Streb, *Chem. Eur. J.* **2018**, *24*, 4952 – 4956; e) M. H. Anjass, K. Kastner, F. Nägele, M. Ringenberg, J. F. Boas, J. Zhang, A. M. Bond, T. Jacob, C. Streb, *Angew. Chem. Int. Ed.* **2017**, *56*, 14749 – 14752; *Angew. Chem.* **2017**, *129*, 14944 – 14947; f) F. Carn, M. Djabourov, T. Coradin, J. Livage, N. Steunou, *J. Phys. Chem. B* **2008**, *112*, 12596 – 12605.
[21] J. Forster, B. Rösner, M. M. Khusniyarov, C. Streb, *Chem. Commun.* **2011**, *47*, 3114 – 3116.
[22] F. J. C. Rossotti, H. Rossotti, *Acta Chem. Scand.* **1956**, *10*, 957 – 984.
[23] J. Livage, *Materials* **2010**, *3*, 4175 – 4195.
[24] G. K. Johnson, E. O. Schlemper, *J. Am. Chem. Soc.* **1978**, *100*, 3645 – 3646.
[25] E. Antonova, C. Näther, W. Bensch, *CrystEngComm* **2012**, *14*, 6853 – 6859.
[26] a) E. Antonova, C. Näther, P. Kögerler, W. Bensch, *Dalton Trans.* **2012**, *41*, 6957 – 6962; b) A. Wutkowski, C. Näther, P. Kögerler, W. Bensch, *Inorg. Chem.* **2008**, *47*, 1916 – 1918.
[27] E. Antonova, C. Näther, W. Bensch, *Dalton Trans.* **2012**, *41*, 1338 – 1344.
[28] R. Kiebach, C. Näther, W. Bensch, *Solid State Sci.* **2006**, *8*, 964 – 970.
[29] Y. Gao, Z. Han, Y. Xu, C. Hu, *J. Cluster Sci.* **2010**, *21*, 163 – 171.
[30] H.-Y. Guo, X. Zhang, X.-B. Cui, Q.-S. Huo, J.-Q. Xu, *CrystEngComm* **2016**, *18*, 5130 – 5139.
[31] a) H. Lühmann, C. Näther, P. Kögerler, W. Bensch, *Inorg. Chim. Acta* **2014**, *421*, 549 – 552; b) E. Antonova, C. Näther, P. Kögerler, W. Bensch, *Inorg. Chem.* **2012**, *51*, 2311 – 2317; c) A. Wutkowski, C. Näther, P. Kögerler, W. Bensch, *Inorg. Chem.* **2013**, *52*, 3280 – 3284; d) R. Kiebach, C. Näther, P. Kögerler, W. Bensch, *Dalton Trans.* **2007**, 3221 – 3223.
[32] E. Antonova, C. Näther, P. Kögerler, W. Bensch, *Angew. Chem. Int. Ed.* **2011**, *50*, 764 – 767; *Angew. Chem.* **2011**, *123*, 790 – 793.
[33] M. Wendt, U. Warzok, C. Näther, J. van Leusen, P. Kögerler, C. A. Schalley, W. Bensch, *Chem. Sci.* **2016**, *7*, 2684 – 2694.
[34] M. Wendt, P. Polzin, J. van Leusen, C. Näther, P. Kögerler, W. Bensch, *Dalton Trans.* **2017**, *46*, 1618 – 1623.
[35] M. Rasmussen, C. Näther, J. van Leusen, P. Kögerler, L. Zhechkov, T. Heine, W. Bensch, *Inorg. Chem.* **2017**, *56*, 7120 – 7126.
[36] L. Yu, J.-p. Liu, J.-p. Wang, J.-Y. Niu, *Chem. Res. Chin. Univ.* **2009**, *25*, 426 – 429.
[37] a) L. Zhang, X. Zhao, J. Xu, T. Wang, *J. Chem. Soc. Dalton Trans.* **2002**, *146*, 3275 – 3276; b) E. Antonova, A. Wutkowski, C. Näther, W. Bensch, *Solid State Sci.* **2011**, *13*, 2154 – 2159; c) X.-X. Hu, J.-Q. Xu, X.-B. Cui, J.-F. Song, T.-G. Wang, *Inorg. Chem. Commun.* **2004**, *7*, 264 – 267; d) H.-Y. Guo, X. Zhang, L.-N. Xiao, X.-B. Cui, *Dalton Trans.* **2017**, *46*, 8022 – 8026.
[38] M. Wendt, C. Näther, W. Bensch, *Chem. Eur. J.* **2016**, *22*, 7747 – 7751.
[39] L. Mahnke, A. Kondinski, U. Warzok, C. Näther, J. van Leusen, C. Schalley, K. Y. Monakhov, P. Kögerler, W. Bensch, *Angew. Chem. Int. Ed.* **2018**, *57*, 2972 – 2975; *Angew. Chem.* **2018**, *130*, 3024 – 3028.
[40] A. Kondinski, T. Heine, K. Y. Monakhov, *Inorg. Chem.* **2016**, *55*, 3777 – 3788.
[41] Y.-L. Wu, X.-X. Li, Y.-J. Qi, H. Yu, L. Jin, S.-T. Zheng, *Angew. Chem. Int. Ed.* **2018**, *57*, 8572 – 8576; *Angew. Chem.* **2018**, *130*, 8708 – 8712.
[42] X. Fang, P. Kögerler, Y. Furukawa, M. Speldrich, M. Luban, *Angew. Chem. Int. Ed.* **2011**, *50*, 5212 – 5216; *Angew. Chem.* **2011**, *123*, 5318 – 5322.
[43] B. Baytekin, H. T. Baytekin, C. A. Schalley, *Org. Biomol. Chem.* **2006**, *4*, 2825 – 2841.
[44] H. N. Miras, E. F. Wilson, L. Cronin, *Chem. Commun.* **2009**, 1297 – 1311.
[45] H. N. Miras, L. Cronin in *New Strategies in Chemical Synthesis and Catalysis* (Ed. B. Pignataro), Wiley-VCH, Weinheim, **2012**, 1 – 32.
[46] J. M. Cameron, L. Vilà-Nadal, R. S. Winter, F. Iijima, J. C. Murillo, A. Rodríguez-Fortea, H. Oshio, J. M. Poblet, L. Cronin, *J. Am. Chem. Soc.* **2016**, *138*, 8765 – 8773.
[47] W. Xuan, A. J. Surman, Q. Zheng, D.-L. Long, L. Cronin, *Angew. Chem. Int. Ed.* **2016**, *55*, 12703 – 12707; *Angew. Chem.* **2016**, *128*, 12895 – 12899.
[48] L. Li, K. Dong, P. Ma, C. Zhang, J. Niu, J. Wang, *Chem. Eur. J.* **2017**, *23*, 16957 – 16960.
[49] a) E. M. Villa, C. A. Ohlin, J. R. Rustad, W. H. Casey, *J. Am. Chem. Soc.* **2009**, *131*, 16488 – 16492; b) J. R. Black, M. Nyman, W. H. Casey, *J. Am. Chem. Soc.* **2006**, *128*, 14712 – 14720; c) E. M. Villa, C. A. Ohlin, W. H. Casey, *J. Am. Chem. Soc.* **2010**, *132*, 5264 – 5272; d) S. Kuwajima, Y. Kikukawa, Y. Hayashi, *Chem. Asian J.* **2017**, *12*, 1909 – 1914.
[50] C. A. Ohlin, *Chem. Asian J.* **2012**, *7*, 262 – 270.
[51] a) F. W. McLafferty, *Science* **1981**, *214*, 280 – 287; b) D. P. Weimann, M. Kogej, C. A. Schalley in *Analytical Methods in Supramolecular Chemistry* (Ed. C. A. Schalley), Wiley-VCH, Weinheim, **2012**, 129 – 196.
[52] J.-H. Son, W. H. Casey, *Chem. Commun.* **2015**, *51*, 12744 – 12747.
[53] a) R. S. Winter, D.-L. Long, L. Cronin, *Inorg. Chem.* **2015**, *54*, 4151 4155; b) J.-H. Son, W. H. Casey, *Dalton Trans.* **2015**, *44*, 20330 – 20333; c) C. A. Ohlin, E. M. Villa, J. C. Fettinger, W. H. Casey, *Angew. Chem. Int. Ed.* **2008**, *47*, 8251 – 8254; *Angew. Chem.* **2008**, *120*, 8375 – 8378; d) J. R. Rustad, W. H. Casey, *Nat. Mater.* **2012**, *11*, 223 – 226; e) B. Schwarz, C. Streb, *Dalton Trans.* **2015**, *44*, 4195 – 4199.
[54] P. Bussian, F. Sobott, B. Brutschy, W. Schrader, F. Schüth, *Angew. Chem. Int. Ed.* **2000**, *39*, 3901 – 3905; *Angew. Chem.* **2000**, *112*, 4065 – 4069.

ChemPubSoc Europe

CHEMISTRY A European Journal Minireview

[55] a) A. Spyratou, S. Clifford, X. Melich, C. Deville, M. Tissot, G. Bonvin, P. Perrottet, A. Williams, *Aust. J. Chem.* **2009**, *62*, 1291 – 1299; b) H.-L. Zheng, X.-L. Chen, T. Li, Z. Yin, Y. Zhang, M. Kurmoo, M.-H. Zeng, *Chem. Eur. J.* **2018**, *24*, 7906 – 7912.

[56] a) M. N. Jackson, M. K. Kamunde-Devonish, B. A. Hammann, L. A. Wills, L. B. Fullmer, S. E. Hayes, P. H.-Y. Cheong, W. H. Casey, M. Nyman, D. W. Johnson, *Dalton Trans.* **2015**, *44*, 16982 – 17006; b) W. H. Casey, *Environ. Chem.* **2015**, *12*, 1 – 19.

[57] K. Eggers, T. Eichner, J. Woenckhaus, *Int. J. Mass Spectrom.* **2005**, *244*, 72 – 75.

[58] a) C. A. Ohlin, R. Brimblecombe, L. Spiccia, W. H. Casey, *Dalton Trans.* **2009**, 5278 – 5280; b) S. A. Pelster, B. Weimann, B. B. Schaack, W. Schrader, F. Schuth, *Angew. Chem. Int. Ed.* **2007**, *46*, 6674 – 6677; *Angew. Chem.* **2007**, *119*, 6794 – 6797; c) R. Tagore, H. Chen, R. H. Crabtree, G. W. Brudvig, *J. Am. Chem. Soc.* **2006**, *128*, 9457 – 9465; d) A. F. Panasci, J. G. McAlpin, C. A. Ohlin, S. Christensen, J. C. Fettinger, R. D. Britt, J. R. Rustad, W. H. Casey, *Geochim. Cosmochim. Acta* **2012**, *78*, 18 – 27; e) P. P. Pescarmona, M. E. Raimondi, J. Tetteh, B. McKay, T. Maschmeyer, *J. Phys. Chem. A* **2003**, *107*, 8885 – 8892.

[59] P. Roesch, U. Warzok, M. Enke, R. Müller, C. Schattenberg, C. A. Schalley, M. Kaupp, T. Braun, P. Wittwer, *Chem. Eur. J.* **2017**, *23*, 13964 – 13972.

[60] Q. Jia, J. Cao, Y. Duan, C. Hu, *Dalton Trans.* **2015**, *44*, 553 – 559.

[61] a) M. Martin-Sabi, R. S. Winter, C. Lydon, J. M. Cameron, D.-L. Long, L. Cronin, *Chem. Commun.* **2016**, *52*, 919 – 921; b) J.-H. Son, W. H. Casey, *Chem. Commun.* **2015**, *51*, 1436 – 1438; c) Q. Zheng, L. Vilà-Nadal, C. Busche, J. S. Mathieson, D.-L. Long, L. Cronin, *Angew. Chem. Int. Ed.* **2015**, *54*, 7895 – 7899; *Angew. Chem.* **2015**, *127*, 8006 – 8010.

[62] H. N. Miras, M. Sorus, J. Hawkett, D. O. Sells, E. J. L. McInnes, L. Cronin, *J. Am. Chem. Soc.* **2012**, *134*, 6980 – 6983.

[63] P. Kebarle, U. H. Verkerk in *Electrospray and MALDI Mass Spectrometry* (Ed. R. B. Cole), Wiley, Hoboken, **2010**, 1 – 48.

[64] a) H. N. Miras, D. Stone, D.-L. Long, E. J. L. McInnes, P. Kögerler, L. Cronin, *Inorg. Chem.* **2011**, *50*, 8384 – 8391; b) L. Vilà-Nadal, S. G. Mitchell, A. Rodríguez-Fortea, H. N. Miras, L. Cronin, J. M. Poblet, *Phys. Chem. Chem. Phys.* **2011**, *13*, 20136 – 20145; c) L. Vilà-Nadal, E. F. Wilson, H. N. Miras, A. Rodríguez-Fortea, L. Cronin, J. M. Poblet, *Inorg. Chem.* **2011**, *50*, 7811 – 7819.

[65] a) L. Miersch, M. Schlesinger, R. W. Troff, C. A. Schalley, T. Rüffer, H. Lang, D. Zahn, M. Mehring, *Chem. Eur. J.* **2011**, *17*, 6985 – 6990; b) D. Sattler, M. Schlesinger, M. Mehring, C. A. Schalley, *ChemPlusChem* **2013**, *78*, 1005 – 1014.

[66] F. Lanucara, S. W. Holman, C. J. Gray, C. E. Eyers, *Nat. Chem.* **2014**, *6*, 281 – 294.

[67] a) E. S. Baker, J. E. Bushnell, S. R. Wecksler, M. D. Lim, M. J. Manard, N. F. Dupuis, P. C. Ford, M. T. Bowers, *J. Am. Chem. Soc.* **2005**, *127*, 18222 – 18228; b) J.-F. Greisch, K. Y. Amsharov, J. Weippert, P. Weis, A. Böttcher, M. M. Kappes, *J. Am. Chem. Soc.* **2016**, *138*, 11254 – 11263.

[68] J. W. Purcell, H. N. Miras, D.-L. Long, P. Markopoulou, L. Cronin, *Chem. Eur. J.* **2017**, *23*, 9683 – 9689.

[69] L. G. Christie, A. J. Surman, R. A. Scullion, F. Xu, D.-L. Long, L. Cronin, *Angew. Chem. Int. Ed.* **2016**, *55*, 12741 – 12745; *Angew. Chem.* **2016**, *128*, 12933 – 12937.

[70] P. J. Robbins, A. J. Surman, J. Thiel, D.-L. Long, L. Cronin, *Chem. Commun.* **2013**, *49*, 1909 – 1911.

[71] A. M. Todea, J. Szakács, S. Konar, H. Bögge, D. C. Crans, T. Glaser, H. Rousselière, R. Thouvenot, P. Gouzerh, A. Müller, *Chem. Eur. J.* **2011**, *17*, 6635 – 6642.

[72] L. K. Mahnke, U. Warzok, M. Lin, C. Näther, C. A. Schalley, W. Bensch, *Chem. Eur. J.* **2018**, *24*, 5522 – 5528.

[73] M. Wendt, L. K. Mahnke, N. Heidenreich, W. Bensch, *Eur. J. Inorg. Chem.* **2016**, *2016*, 5393 – 5398.

[74] M. Wendt, L. K. Mahnke, C. Näther, J. van Leusen, P. Kögerler, W. Bensch, *Dalton Trans.* **2018**, *47*, 6672 – 6674.

Manuscript received: June 28, 2018
Accepted manuscript online: August 6, 2018
Version of record online: November 26, 2018

5. Zusammenfassung und Ausblick

Während der Doktorarbeit konnte die neue wasserlösliche und im Vergleich zur analogen Ni-Verbindung (Ni-{$V_{15}Sb_6$}) deutlich stabilere Verbindung {$Zn(en)_3$}$_3$[$V_{15}Sb_6O_{42}(H_2O)$] · 3 en · 10 H_2O (Zn-{$V_{15}Sb_6$}) hergestellt werden. ESI-MS-Untersuchungen belegen, dass Zn-{$V_{15}Sb_6$} in wässriger Lösung mindestens 72 Stunden stabil ist. Die Transformation zum {$V_{14}Sb_8O_{42}$}-Cluster erreicht erst nach 14 Tagen 50 %, während der Ni-{$V_{15}Sb_6$} bereits nach ca. fünf Tagen zu 50 % umgewandelt ist. Die Löslichkeit in Wasser wurde für beide Precursoren mit UV/Vis-Spektroskopie bestimmt und die Löslichkeit von Zn-{$V_{15}Sb_6$} ist viermal so hoch verglichen mit der von Ni-{$V_{15}Sb_6$}. Die im Vergleich zu Ni-{$V_{15}Sb_6$} deutlich verbesserte Stabilität erklärt auch, dass in Reaktionsprodukten oft der {$V_{15}Sb_6O_{42}$}-Cluster beobachtet wird, wie z. B. bei der Synthese der beiden neuen Verbindungen {($Zn(en)_2(H_2O)_2$)($Zn(en)_2$)}[{$Zn(en)_2$}$V_{15}Sb_6O_{42}(H_2O)$] · 8.5 H_2O und {$Zn(phen)_3$}$_2$[$Zn(en)_2V_{15}Sb_6O_{42}(H_2O)$] · 23 H_2O.

Der Einsatz der Precursoren bietet völlig neue synthetische Perspektiven zur Herstellung von Hetero-POVs. Besonders vorteilhaft ist, dass die Reaktionen deutlich schneller sind und dass mildere Bedingungen angewendet werden können. Um die Umwandlung des Synthons Ni-{$V_{15}Sb_6$} in die Verbindung [{$Ni(en)_2$}$_2V_{14}Sb_8O_{42}$]·5.5 H_2O besser zu verstehen, wurden *in situ* Röntgenbeugungsexperimente durchgeführt. Die Ergebnisse dieser Untersuchungen geben Hinweise darauf, dass das Edukt schnell amorphisiert oder aufgelöst wird und nach einer temperaturabhängigen Induktionszeit das Produkt gebildet wird. Der Einsatz von NH_4VO_3 hat die Bildung des Produktes signifikant beschleunigt, was für Röntgenbeugungsexperimente unter *in situ* Bedingungen notwendig ist. Das Produkt wird bei allen Temperaturen über heterogene Nukleation gebildet. Die niedrigen Aktivierungsenergien für Nukleation und Kristallisation zeigen, dass noch ein großes Potential für weitere Postfunktionalisierungsreaktionen vorhanden ist.

Mit Ni-{$V_{15}Sb_6$} konnte das α*-{$V_{14}Sb_8O_{42}$}-Isomer in der Verbindung {$Ni(en)(cyclen)$}$_2$[$V_{14}Sb_8O_{42}(H_2O)$]·*ca.*10 H_2O erhalten werden. In der Struktur ist die Spitze einer {VO_5}-Pyramide in die Clustermitte gerichtet, was zuvor noch nie beobachtet wurde. Zwischen zwei benachbarten Clustern werden sehr kurze Sb-O···V-

sowie Sb-O···Sb-Abstände gefunden, welche als kovalente Bindungen angesehen werden müssen. Über diese Bindungen wird ein Dimer ausgebildet und die $\{VO_5\}$-Pyramide zu einem verzerrten Oktaeder erweitert. Mit ESI-MS-Untersuchungen konnte nachgewiesen werden, dass das Dimer schon in der wässrigen Lösung gebildet wird und nicht erst während der Kristallisationsphase. Mit DFT-Rechnungen konnten Hinweise erhalten werden, dass noch weitere konfigurationelle Isomere zugänglich sein sollten und dass deren Bildung weniger energieaufwendig sein könnte als die des α*-Isomers.

Die Verbindung $\{Ni(en)_3\}_3[V_{15}Sb_3Ge_3O_{42}(OH)_3(H_2O)]\cdot\approx 9\ H_2O$ ist ein sehr seltenes Beispiel für POVs mit zwei verschiedenen Heteroatomen. Diese Verbindung konnte bei der Reaktion von Ni-$\{V_{15}Sb_6\}$ mit GeO_2 durch *in situ* Austausch von drei SbO_3-Pyramiden durch drei GeO_4-Tetraeder synthetisiert werden. Ein wesentlicher struktureller Unterschied zu anderen Sb/Ge-POVs ist, dass die Heteroatompositionen geordnet besetzt sind, während in den anderen Sb/Ge-POVs eine Mischbesetzung gefunden wird.

Mit den Erkenntnissen der ESI-MS-Untersuchungen wässriger Lösungen des Zn-$\{V_{15}Sb_6\}$ Precursors war die rational geplante Synthese von $\{V_{14}Sb_8O_{42}\}$-Clustern durch gezieltes Einstellen des pH-Wertes möglich. Bei einem pH-Wert größer 9.5 wird bevorzugt der $\{V_{15}Sb_6O_{42}\}$-Cluster gebildet, während bei pH < 9.5 der $\{V_{14}Sb_8O_{42}\}$-Cluster gebildet wird. Dieses Verhalten wurde ausgenutzt, um die Verbindungen $\{Zn(phen)_3\}_2[V_{14}Sb_8O_{42}(H_2O)]\cdot 0.5\ phen\cdot 17\ H_2O$, $[\{Zn(en)_2\}_2V_{14}Sb_8O_{42}]\cdot 7\ H_2O$ und $\{Fe(phen)_3\}_2[V_{14}Sb_8O_{42}(H_2O)]\cdot 11\ H_2O$ herzustellen. Bemerkenswert ist, dass nicht nur die Synthese der Sb-reicheren Cluster gelingt, sondern auch dass sowohl Liganden als auch Komplexe ausgetauscht werden können.

Die Ergebnisse der Synthesen mit löslichen Vorläuferverbindungen wurden in einem Minireview-Artikel zusammengefasst, in dem ein besonderer Schwerpunkt auf die Leistungsfähigkeit ESI-MS-basierter Charakterisierungen von POV-Lösungen gelegt wurde.

Die Integration von Lanthanoiden, die aufgrund ihrer magnetischen und lumineszierenden Eigenschaften von großem Interesse sind, wäre ein sehr interessantes zukünftiges Themengebiet. Erste Untersuchungen haben bereits stattgefunden, jedoch

muss die richtige Synthesestrategie bzw. der richtige Ligand gefunden werden, der die Lanthanoide unter hydrothermalen Bedingungen und bei pH-Werten > 8 stabilisiert.

Die Integration von Heteroatomen wie Sn in POVs ist nach wie vor nicht gelungen, obwohl DFT-Kalkulationen belegen, dass der Einbau möglich sein sollte. Wie mehrmals betont sind Solvothermalsynthesen komplex und es ist die große Herausforderung, die richtigen Synthesebedingungen zu finden, um Sn-POVs zu präparieren.

6. Publikationsliste und Konferenzbeiträge

Publikationen

1) M. Wendt, L. K. Mahnke, N. Heidenreich, W. Bensch, *Eur. J. Inorg. Chem.* **2016**, 5393.

„*Nucleation and Crystal Growth of a {$V_{14}Sb_8O_{42}$}-Cluster from a {$V_{15}Sb_6O_{42}$} Polyoxovanadate: In Situ X-ray Diffraction Studies"*

Eigenanteil: Maßgeblich an der Idee und Konzeption beteiligt, beteiligt an den *in situ* Messungen am DESY, maßgeblich an der Auswertung sowie an der Interpretation und Diskussion der Ergebnisse beteiligt.

2) L. K. Mahnke, A. Kondinski, U. Warzok, C. Näther, J. van Leusen, C. A. Schalley, K. Yu. Monakhov, P. Kögerler, W. Bensch, *Angew. Chem. Int. Ed.* **2018**, *7*, 2972.

„Conformational Isomerism in Polyoxovanadates"

Eigenanteil: Maßgeblich an der Konzeption beteiligt, wesentlicher Anteil an der Erstellung des Manuskripts, Durchführung der Synthesen, sowie der Charakterisierung (IR, CHN, XRD, TG, EDX, SEM, BVS) und maßgeblich an der Interpretation und Diskussion der Ergebnisse beteiligt.

3) M. Wendt, L. K. Mahnke, C. Näther, J. van Leusen, P. Kögerler, W. Bensch, *Dalton Trans.*, **2018**, *47*, 6672-6674.

„Ordnung muss sein: Heteroelement order and disorder in polyoxovanadates"

Eigenanteil: Maßgeblich an der Konzeption beteiligt, Durchführung der Synthese der Verbindung 3, sowie der Analytik (IR, CHN, XRD, TG, EDX, SEM). Durchführung der Bond-valence-sum-analysis aller drei Verbindungen. Maßgeblich an der Interpretation der Ergebnisse beteiligt.

4) L. K. Mahnke, U. Warzok, M. Lin, C. Näther, C. A. Schalley, W. Bensch, *Chem. Eur. J.* **2018**, *24*, 5522.

„The New Water-Soluble Cluster Compound $\{Zn(en)_3\}_3[V_{15}Sb_6O_{42}(H_2O)]\cdot(ethylenediamine)_3\cdot 10\ H_2O$ *as a Synthon for the Generation of two New Antimonato Polyoxovanadates"*

Eigenanteil: Maßgeblich an der Konzeption beteiligt, federführend in der Erstellung des Manuskripts, Durchführung der Synthesen, sowie der Charakterisierung (IR, CHN, XRD, TG, EDX, SEM, BVS) und federführend in der Interpretation und Diskussion der Ergebnisse.

5) L. K. Mahnke, M. Wendt, C. Näther, W. Bensch, *Cryst. Growth Des.* **2018**, *18*, 6100.

„Rational Syntheses of Three New $\{V_{14}Sb_8\}$*-Clusters Applying a Water Soluble High-Nuclearity Cluster as Synthon"*

Eigenanteil: Maßgeblich an der Konzeption beteiligt, federführend in der Erstellung des Manuskripts, Durchführung der Synthesen, sowie der Charakterisierung (IR, CHN, XRD, TG, EDX, SEM, BVS) und federführend in der Interpretation und Diskussion der Ergebnisse.

6) U. Warzok, L. K. Mahnke, W. Bensch, *Chem. Eur. J.* **2019**, *25*, 1405.

„Soluble Hetero-Polyoxovanadates and Their Solution Chemistry Analyzed by Electrospray Ionization Mass Spectrometry"

Eigenanteil: Maßgeblich an der Konzeption beteiligt, wesentlicher Anteil an der Erstellung des Manuskripts, federführend bei der Erstellung der Grafiken.

Konferenzen:

DESY Users Meeting in Hamburg, Germany (27.01.2016 - 29.01.2016)

MATsynCELL spring meeting in Kiel, Germany (27.04.2016)

RACIRI Summer School 2016 in Repino, Russland (21.08.2016 - 27.08.2016)

MATsynCELL and C2 autumn meeting in Uppsala, Schweden (06.10.2016 - 07.10.2016)

20. Norddeutsches Doktorandenkolloquium in Kiel, Germany (21.09.17-22.09.2017)

19th International Symposium on the Reactivity of Solids in Bayreuth, Germany (15.08.2018 - 18.08.2018)

54. Hemdsärmelkolloquium in Kiel, Germany (07.03.2019-09.03.2019)

Presentation:

MATsynCELL spring meeting in Kiel, Germany (27.4.2016)

"In situ XRD Studies on Hetero-Polyoxovanadates – Nucleation and Formation of a $\{V_{14}Sb_8O_{42}\}$ from a $\{V_{15}Sb_6O_{42}\}$-Cluster"

Poster:

RACIRI Summer School 2016 in Repino, Russland (21.08.2016-27.08.2016)

"Nucleation and Formation of a $\{V_{14}Sb_8O_{42}\}$-Cluster from a $\{V_{15}Sb_6O_{42}\}$ Hetero-Polyoxovanadate – In situ XRD Studies"

MATsynCELL autumn meeting in Uppsala, Schweden (06.10.2016-07.10.2016)

"Nucleation and Formation of a $\{V_{14}Sb_8O_{42}\}$-Cluster from a $\{V_{15}Sb_6O_{42}\}$ Hetero-Polyoxovanadate – In situ XRD Studies"

19th International Symposium on the Reactivity of Solids (ISRS-19) in Bayreuth, Germany (15.08.2018-18.08.2018)

"Innovations in Polyoxovanadate Chemistry – New Water Soluble Precursors"

Messzeiten:

Messzeiten am Deutschen Elektronen Synchrotron in Hamburg, Deutschland.

Oktober 2015	Beamline P07	*in situ* XRD
Juni 2016	Beamline P08	*in situ* XRD
Juli 2016	Beamline P02.1	PDF, *in situ* XRD
Juli 2016	Beamline P08	*in situ* XRD
Juli 2016	Beamline P09	*in situ* XRD
November 2016	Beamline P64	*in situ* EXAFS
Dezember 2016	Beamline P02.1	cryo-PDF und cryo-XRD
April 2017	Beamline P2.01	PDF und *in situ* XRD
September 2018	Beamline P2.01	PDF und *in situ* XRD

Messzeiten an der Diamond-Light-Source, Großbritannien.

Februar 2017	Beamline I15	*in situ* XRD, Kappilaren

7. Hintergrundinformationen zu den Veröffentlichungen

7.1. Supporting Information der Publikation „*Nucleation and Crystal Growth of a {$V_{14}Sb_8O_{42}$}-Cluster from a {$V_{15}Sb_6O_{42}$} Polyoxovanadate: In-Situ X-ray Diffraction Studies*"

Eur. J. Inorg. Chem. **2016** · ISSN 1099–0682

SUPPORTING INFORMATION

DOI: 10.1002/ejic.201601025
Title: Nucleation and Crystal Growth of a $\{V_{14}Sb_8O_{42}\}$ Cluster from a $\{V_{15}Sb_6O_{42}\}$ Polyoxovanadate: In Situ XRD Studies
Author(s): Michael Wendt, Lisa K. Mahnke, Niclas Heidenreich, Wolfgang Bensch*

Characterization of $[\{Ni(en)_2\}_2V_{14}Sb_8O_{42}] \cdot 5.5H_2O$ (II):

Figure S1 shows a) a powder pattern of the product obtained during the *in-situ* experiment compared with the calculated pattern using the data published in [1] (note: the background results from the solution) and b) an *ex-situ* X-ray powder pattern of the *in-situ* reaction product to obtain a pattern with better resolution. The comparison demonstrates phase purity of the product. The IR spectrum shows the characteristic band of the V=O vibration at about 970 cm^{-1} and the vibrations of the ethylediamine ligand (1017, 1601, 2878 and 2924 cm^{-1}). Absorptions of crystal water molecules are located between 3200 and 3500 cm^{-1} (Figure S2). The morphology of the crystals is shown in Figure S3.

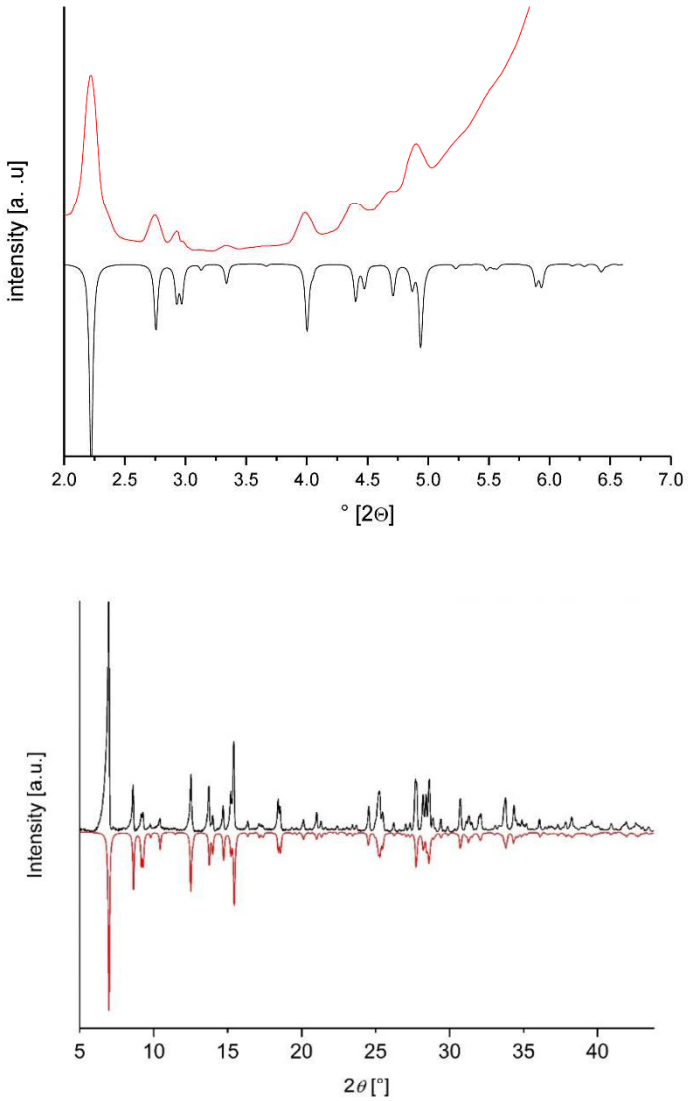

Figure S1. Single *in-situ* X-ray powder diffraction pattern of the product **II** (red) compared with the calculated pattern (black)[1] (top) and a powder diffraction of the same product measured *ex-situ* to obtain a better quality (bottom).

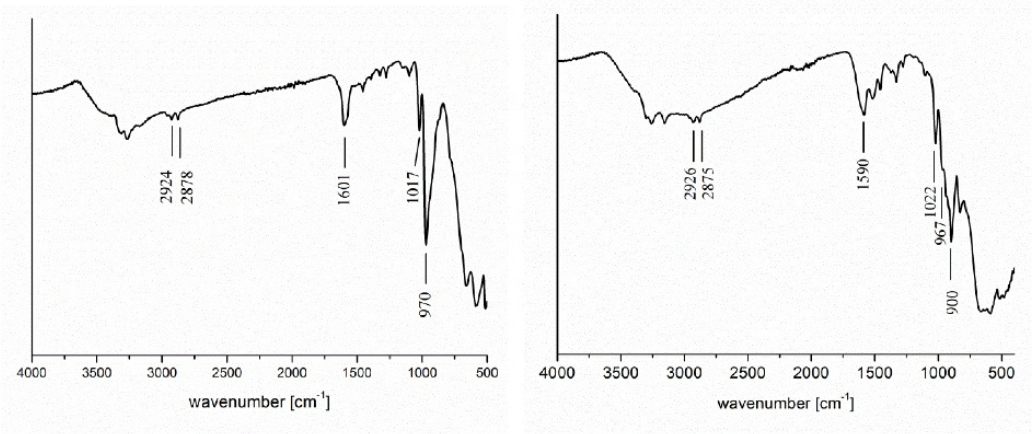

Figure S2. IR spectra of **II** after dynamic synthesis (left) and from the bulk material of the evaporated solution (right).

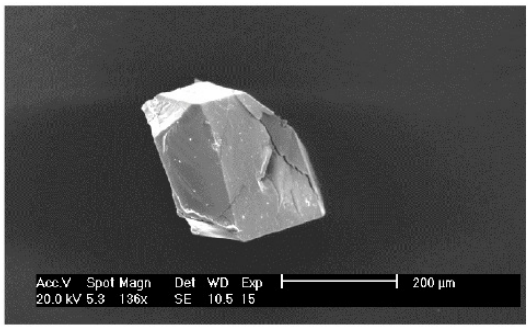

Figure S3. SEM picture of a crystal of **II**.

Evaluation of the kinetic data:

Additionally to the plots of $t/t_{0.5}$ against α for the kinetic growth models at T = 134 °C in the main text, Figure S4 shows the corresponding plots at T = 144 and 154 °C. Table S1 represents the different growth models and the corresponding formula.

Table S1. Different growth models and its corresponding equations and values for *m* reported in literature.

Growth model[2]	Rate equation $f(\alpha) = kt$	*m*
<u>Diffusion-controlled:</u> $D_1(\alpha)$	$\alpha^2 = 0.25\ (t/t_{0.5})$	0.62

$D_2(\alpha)$	$(1-\alpha)\ln(1-\alpha)+\alpha = 0.1534\ (t/t_{0.5})$	0.57
$D_3(\alpha)$ [Jander]	$[1-(1-\alpha)^{1/3}]^2 = 0.0425\ (t/t_{0.5})$	0.54
$D_4(\alpha)$[Ginstling-Brounshtein]	$1-2\,\alpha/3-(1-\alpha)^{2/3} = 0.0367\ (t/t_{0.5})$	0.57
Phase-boundary-controlled:		
$R_2(\alpha)$	$1-(1-\alpha)^{1/2} = 0.2929\ (t/t_{0.5})$	1.11
$R_3(\alpha)$	$1-(1-\alpha)^{1/3} = 0.2063\ (t/t_{0.5})$	1.07
First order		
$F_1(\alpha)$	$[-\ln(1-\alpha)] = 0.6931\ (t/t_{0.5})$	1.00
Nucleation [Avrami-Eroféev]:		
$A_3(\alpha)$	$[-\ln(1-\alpha)]^{1/3} = 0.885\ (t/t_{0.5})$	3.00

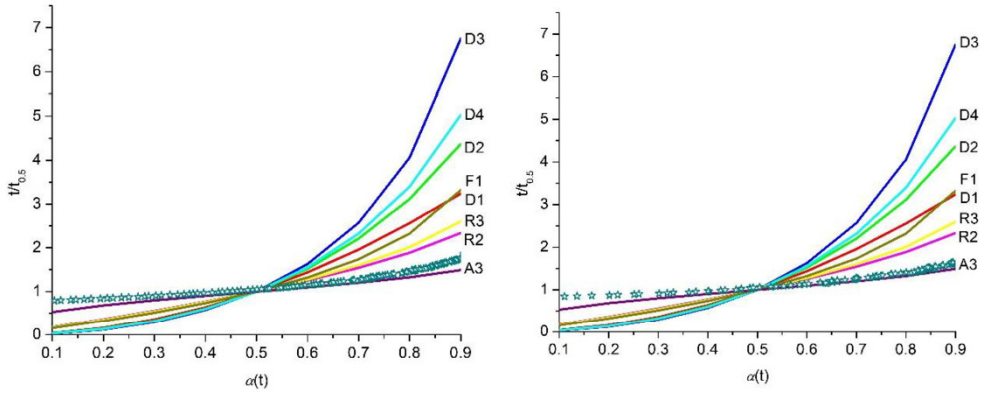

Figure S4. Kinetic growth models plotting $t/t_{0.5}$ as a function of α for T= 144 °C (left) and T = 154 °C (right); symbols represent the experimental data.

[1] L. Yu, J.-P. Liu, J.-P. Wang, J.-Y. Niu, *Chem. Res. Chinese U.* **2009**, *25*, 426.

[2] J. H. Sharp, G. W. Brindley, B. N. N. Achar, *J. Am. Ceram. Soc.* **1966**, *49*, 379.

7.2 . Supporting Information der Publikation „Conformational Isomerism in Polyoxovanadates”

Supporting Information

Configurational Isomerism in Polyoxovanadates

Lisa K. Mahnke, Aleksandar Kondinski, Ulrike Warzok, Christian Näther, Jan van Leusen, Christoph A. Schalley, Kirill Yu. Monakhov,* Paul Kögerler,* and Wolfgang Bensch**

anie_201712417_sm_miscellaneous_information.pdf

1. Computational Details

Density functional theory (DFT) calculations were carried out with the Amsterdam Density Functional program (ADF2014).[1,2] Numerical integration was performed using Becke grid integration.[3,4] Geometry optimization was conducted using GGA Becke exchange[5] plus the Perdew 86 correlation[6] (BP) functional and all-electron Slater basis sets of triple-ζ quality with one polarization function (TZP).[7] The spin-unrestricted (= U) formalism was used for all open-shell electronic systems. Scalar relativistic effects were accounted for using the zeroth-order regular approximation (ZORA).[8-10] Solvation effects were introduced using the COnductor-like Screening MOdel (COSMO) with the default parameters for water (ε = 78.39; solvent radius = 1.93 Å) where solvent-excluding surface (SES) correction was included.[11,12] Next to geometry optimizations at COSMO/ZORA-Scalar-UBP86/TZP, unrestricted single-point calculations using the hybrid UB3LYP functional[13] were performed to calculate different molecular properties (binding energies, atomic spin densities, frontier molecular orbitals and molecular electrostatic potentials) of the $[V_{14}Sb_8O_{42}]^{4-}$ isomers. The choice of the B3LYP functional for the description of the electronic structure of heteroPOVs systems was dictated by the fact that hybrid DFT functionals usually yield reliable atomic spin populations at the metal sites.[14,15]

2. Isomer Assignment and Modeling

The three rotational isomers α-/γ-/β-$[V_{14}Sb_8O_{42}]^{4-}$ exhibit four, four and three inequivalent V atomic positions, respectively.[16] These chemically inequivalent positions can be assigned as V^1, V^2, V^3, and V^4 (see Figure S1). In order to reach a systematic assignment of the positional isomers belonging to the different rotational isomer topology, we have introduced the numerals 1, 2, 3 and 4 that indicate a flip or an inversion of the vanadyl V=O vector at the specified V atom position (with respect to the basal O_4 plane). We note that these structural scenarios could not only be considered as configurational but also as conformational isomerism, according to the broader IUPAC definition that also includes polytopal rearrangements (https://goldbook.iupac.org/html/C/C01258.html). Following this, to differentiate the rotational isomers with a V=O flip from those where the V=O flip is absent, we have introduced the star notation (*i.e.* α*, β* and γ*). The combination of the two notations can provide systematic assignment to all 11 positional isomers as: α_1*, α_2*, α_3*, α_4*, β_1*, β_2*, β_3*, β_4*, γ_1*, γ_2* and γ_3* (see Figure S2).[17,18] The star notation is not unusual in polyoxometalate chemistry and has been previously used for the description of the Wells-Dawson-type cluster isomers, while the numerical index has been used to distinguish between monolacunary β-Keggin-type isomers: (*e.g.* β_1-$[XW_{11}O_{39}]^{n-}$, β_2-$[XW_{11}O_{39}]^{n-}$ and β_3-$[XW_{11}O_{39}]^{n-}$). The initial geometries for the optimization calculations of the eleven positional isomers were obtained by the modification of a single O atom position in the geometry of the pre-optimized α-/β-/γ-$[V_{14}Sb_8O_{42}]^{4-}$ POVs.

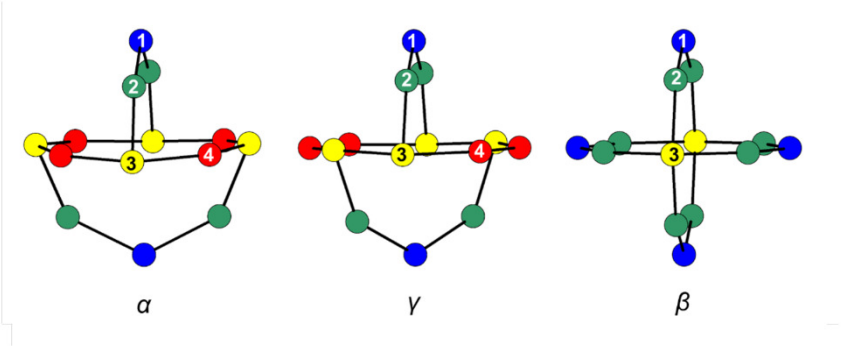

Figure S1: The assignment of the different V atom positions in the *α*-/*β*-/*γ*-$[V_{14}Sb_8O_{42}]^{4-}$ clusters. The positionally inequivalent V centers are depicted in blue, green, yellow, and red.

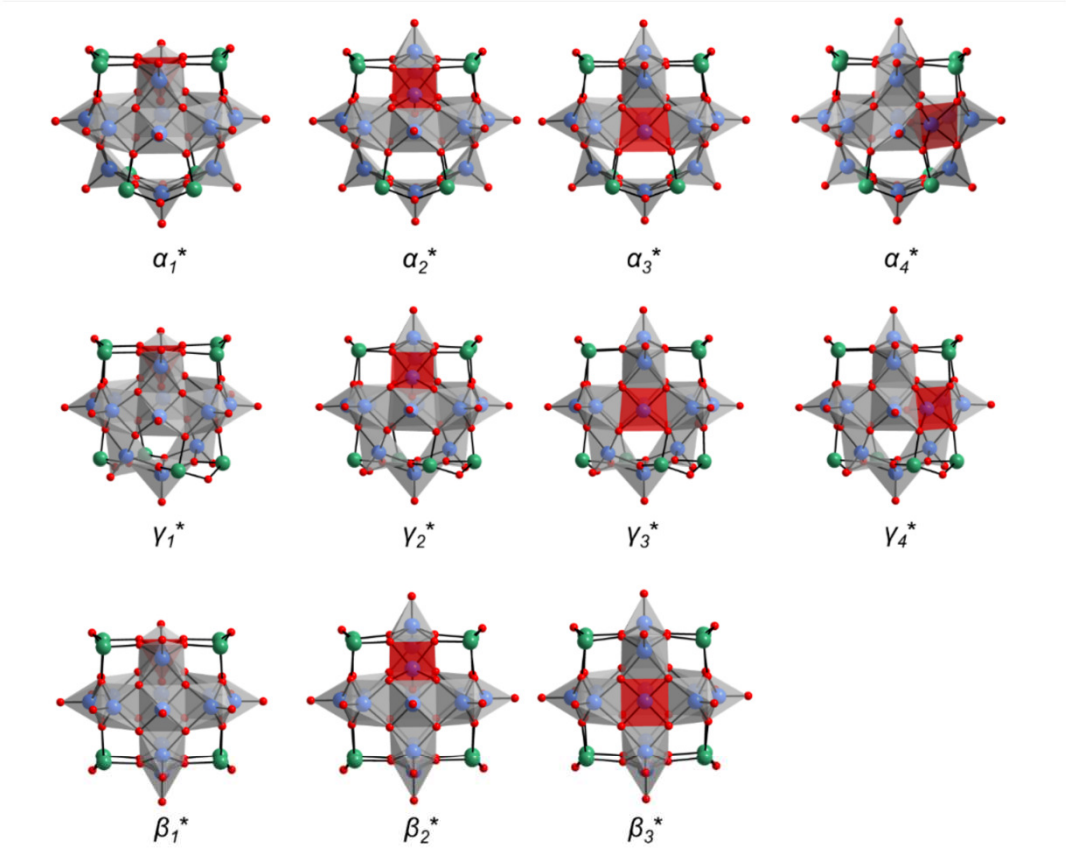

Figure S2: Combined polyhedral and ball-and-stick representation of the eleven different positional isomers belonging to *α**-/*β**-/*γ**-$[V_{14}Sb_8O_{42}]^{4-}$ cluster family (V: blue, O: red, Sb: green, {VO_5}: transparent gray square pyramids). To indicate the position of a V=O flip, a single {VO_5} unit in each isomer is highlighted as red square pyramid.

Geometric Properties

The calculated and experimentally derived bond distances for α_1*-$[V_{14}Sb_8O_{42}]^{4-}$ are compared in Table S1. The different intra-cluster V···V distances in α-/α_1*-$[V_{14}Sb_8O_{42}]^{4-}$ are presented in Figure S3 and compared to each other in Table S2.

Table S1: Comparison of the DFT-calculated and experimentally determined bond ranges for V–O_t (terminal), V–O_b (bridging) and Sb–O bonds in α_1*-$[V_{14}Sb_8O_{42}]^{4-}$ in compound **2** (all in Å). Calculations were performed at COSMO/ZORA-SCALAR-UBP86/TZP.

Bond type	Theory	Experiment (compound 2)
V–O (terminal)	1.613 – 1.642	1.591(6) – 1.629(7)
V–O (bridging)	1.957 – 2.005	1.901(7) – 2.002(6)
Sb–O	2.007 – 2.030	1.895(8) – 2.000(8)

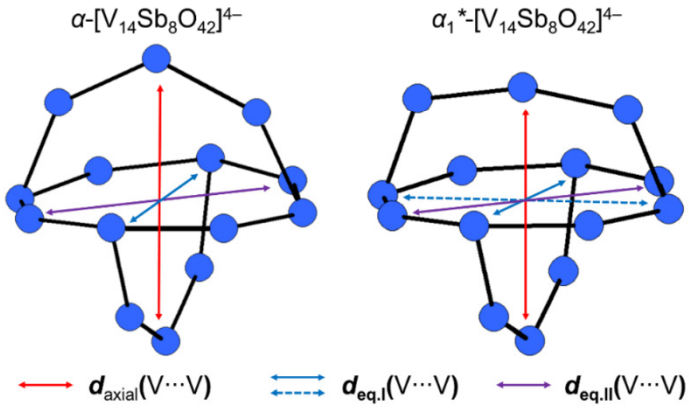

Figure S3: Definition of the different intra-cluster V···V distances in α-/α_1*-$[V_{14}Sb_8O_{42}]^{4-}$ isomers.

Table S2: Comparison of the V···V inter-cluster distances in α- and α_1*-$[V_{14}Sb_8O_{42}]^{4-}$ cluster structures derived from DFT calculations (in Å). Calculations were performed at COSMO/ZORA-SCALAR-UBP86/TZP.

Interatomic distance type	α-$[V_{14}Sb_8O_{42}]^{4-}$	α_1*-$[V_{14}Sb_8O_{42}]^{4-}$
d_{axial}(V···V)	7.858	6.695
$d_{eq.I}$(V···V)	8.091	8.048; 8.168
$d_{eq.II}$(V···V)	7.880	7.857

Electronic Properties and Relative Stability

The relative stabilities of α_1*-$[V_{14}Sb_8O_{42}]^{4-}$ with respect of the other $[V_{14}Sb_8O_{42}]^{4-}$ isomers are summarized in Tables S3-S6. The bonding energies of all possible $[V_{14}Sb_8O_{42}]^{4-}$ isomers relative to the most stable α isomer are sketched in Figure S5.

The HOMO of α_1*-$[V_{14}Sb_8O_{42}]^{4-}$ is predominantly constructed by V-centered *d* atomic-like orbitals (>70 %) and minor contributions from the O-centered 2*p*-like orbitals, whereas the LUMO has major contributions from V- and Sb-centered *d* and the *p* atomic-like orbitals (each of *ca.* 40%) and minor contributions of O-centered 2*p*-like orbitals (Figure S4). The calculated HOMO-LUMO gap of α_1*-$[V_{14}Sb_8O_{42}]^{4-}$ is *ca.* 3.9 eV and is the largest among the unconventional α*-/β*-/γ*-$[V_{14}Sb_8O_{42}]^{4-}$ isomers (see Table S3). The energetic position of the LUMO suggests that upon electrochemical reduction V^{IV} and Sb^{III} centers are possibly simultaneously reduced. Furthermore, the electropositive Sb^{III} centers (Figure S5) and the available *p* atomic-like orbitals in the LUMO indicate opportunities for further directed interactions with electron donating ligands such as primary and secondary organic amines.

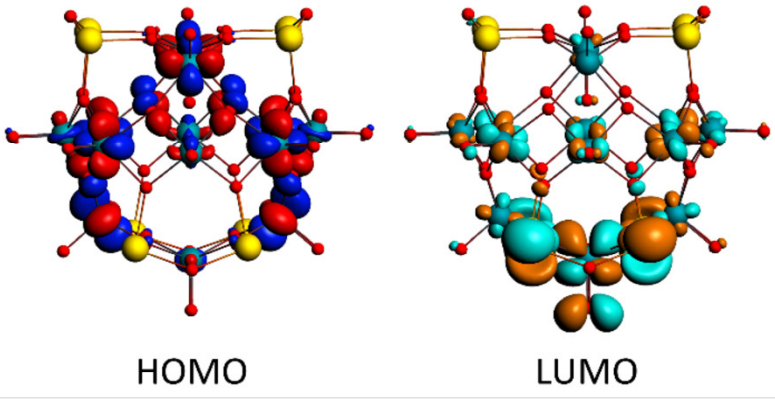

Figure S4: The α-spin HOMO (left) and LUMO (right) of α_1*-$[V_{14}Sb_8O_{42}]^{4-}$, calculated at the COSMO/ZORA-SCALAR-UB3LYP/TZP level of theory. Color code: V: turquoise, O: red, Sb: yellow.

Table S3: Selected energy values as calculated at COSMO/ZORA-SCALAR-UB3LYP/TZP for the α-/β-/γ-/α_1*-$[V_{14}Sb_8O_{42}]^{4-}$ isomers. E_b denotes the total bonding energy, ΔE_b is the bonding energy relative to α-$[V_{14}Sb_8O_{42}]^{4-}$, E_{HOMO} is the energy of the α-spin (i.e. all-parallel spin) HOMO, E_{LUMO} is the energy of the α-spin LUMO and $E_{HOMO-LUMO}$ is the HOMO-LUMO gap energy.

	α-$[V_{14}Sb_8O_{42}]^{4-}$	γ-$[V_{14}Sb_8O_{42}]^{4-}$	β-$[V_{14}Sb_8O_{42}]^{4-}$	α_1*-$[V_{14}Sb_8O_{42}]^{4-}$
E_{HOMO} / eV	–6.0	–5.9	–5.8	–6.0
E_{LUMO} / eV	–2.1	–2.3	–2.3	–2.1
$E_{HOMO-LUMO}$ / eV	3.9	3.6	3.5	3.9
E_b / kJ·mol^{-1}	–59053.9	–59036.8	–59015.2	–59003.6
ΔE_b / kJ·mol^{-1}	0.0	17.1	38.7	50.3

Table S4: The energies of and the contributions (in %) to the HOMOs and LUMOs centered on vanadium, oxygen and antimony in α_1*-$[V_{14}Sb_8O_{42}]^{4-}$.

α-spin	*E* / eV	V	O	Sb	β-spin	*E* / eV	V	O	Sb
HOMO	–6.0	71.9	15.1	0.0	HOMO	–7.5	1.2	52.1	40.6
LUMO	–2.1	38.5	10.3	42.1	LUMO	–2.0	64.3	7.6	18.8
$\Delta_{(LUMO-HOMO)}$	3.9	–33.4	–4.8	42.1	$\Delta_{(LUMO-HOMO)}$	5.5	63.1	–44.5	–21.8

Table S5: The energies of and the contributions to (in %) of the HOMOs and LUMOs centered on vanadium, oxygen and antimony in α-$[V_{14}Sb_8O_{42}]^{4-}$.

α-spin	*E* / eV	V	O	Sb	β-spin	*E* / eV	V	O	Sb
HOMO	–6.0	75.3	16.0	0.0	HOMO	–7.5	3.1	52.6	42.6
LUMO	–2.1	39.7	10.6	41.4	LUMO	–1.9	73.6	0.0	14.9
$\Delta_{(LUMO-HOMO)}$	3.9	–35.6	–6.4	41.4	$\Delta_{(LUMO-HOMO)}$	5.6	70.5	–52.6	–27.7

Table S6: Important energy values as calculated at COSMO/ZORA-SCALAR-UB3LYP/TZP for the α*-/β*-/γ* $[V_{14}Sb_8O_{42}]^{4-}$ positional isomers. E_b is the total bonding energy, ΔE_b is the bonding energy relative to α-$[V_{14}Sb_8O_{42}]^{4-}$, E_{HOMO} is the energy of the α-spin HOMO, E_{LUMO} is the energy of the α-spin LUMO and $E_{HOMO-LUMO}$ is the HOMO-LUMO gap energy. For representation of the positional isomers see Figure S2.

	α_1*-$[V_{14}Sb_8O_{42}]^{4-}$	α_2*-$[V_{14}Sb_8O_{42}]^{4-}$	α_3*-$[V_{14}Sb_8O_{42}]^{4-}$	α_4*-$[V_{14}Sb_8O_{42}]^{4-}$
E_{HOMO} / eV	–6.0	–5.9	–5.9	–5.9
E_{LUMO} / eV	–2.1	–2.1	–2.1	–2.1
$E_{HOMO-LUMO}$ / eV	3.9	3.8	3.8	3.8
E_b / kJ·mol^{-1}	–59004	–59025	–58987	–59019
ΔE_b / kJ·mol^{-1}	0	–21.0	17.1	–15.0
	γ_1*-$[V_{14}Sb_8O_{42}]^{4-}$	γ_2*-$[V_{14}Sb_8O_{42}]^{4-}$	γ_3*-$[V_{14}Sb_8O_{42}]^{4-}$	γ_4*-$[V_{14}Sb_8O_{42}]^{4-}$
E_{HOMO} / eV	–6.1	–5.8	–5.7	–5.4
E_{LUMO} / eV	–2.4	–2.2	–2.2	–2.2
$E_{HOMO-LUMO}$ / eV	3.7	3.6	3.5	3.2
E_b / kJ·mol^{-1}	–58899	–59004	–58960	–59004
ΔE_b / kJ·mol^{-1}	104.6	–0.6	43.2	–0.3
	β_1*-$[V_{14}Sb_8O_{42}]^{4-}$	β_2*-$[V_{14}Sb_8O_{42}]^{4-}$	β_3*-$[V_{14}Sb_8O_{42}]^{4-}$	
E_{HOMO} / eV	–5.7	–5.7	–5.6	
E_{LUMO} / eV	–2.2	–2.0	–5.6	
$E_{HOMO-LUMO}$ / eV	3.5	3.7	3.4	
E_b / kJ·mol^{-1}	–58978	–58993	–58899	
ΔE_b / kJ·mol^{-1}	25.5	10.2	104.8	

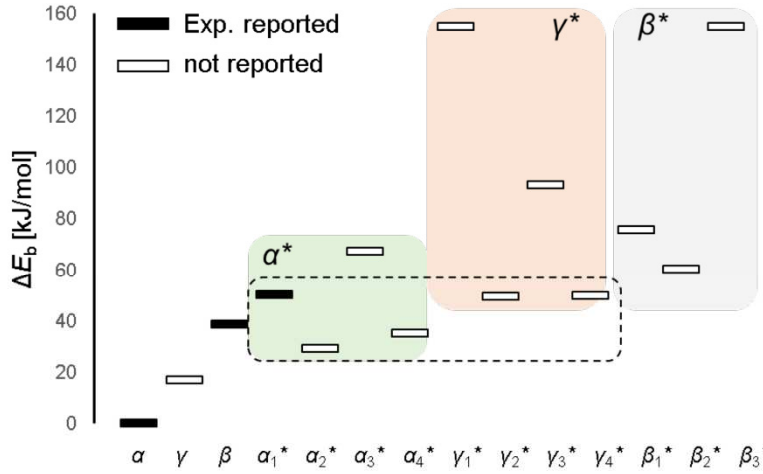

Figure S5. Diagram depicting the relative energies of the $[V_{14}Sb_8O_{42}]^{4-}$ isomers relative to α-$[V_{14}Sb_8O_{42}]^{4-}$ (based on Tables S3 and S6). Unconventional and novel isomers with a comparable stability to α_1*-$[V_{14}Sb_8O_{42}]^{4-}$ are encircled with a dashed line.

Spin Densities and Molecular Electrostatic Potential

The spin density isosurface and molecular electrostatic potential (MEP) of α_1*-$[V_{14}Sb_8O_{42}]^{4-}$ are presented in Figure S6. The spin density isosurface represents the single spin orbitals, which fit well with the model of the POV where all V centers are of formal oxidation state +IV. According to the MEP, all terminal and bridging oxo ligands show high negative potentials. All oxo ligands can be involved in ionic bonding with dissolved cations or in the crystal lattice, however protonation in such systems is mainly expected to occur at the bridging oxo ligands.

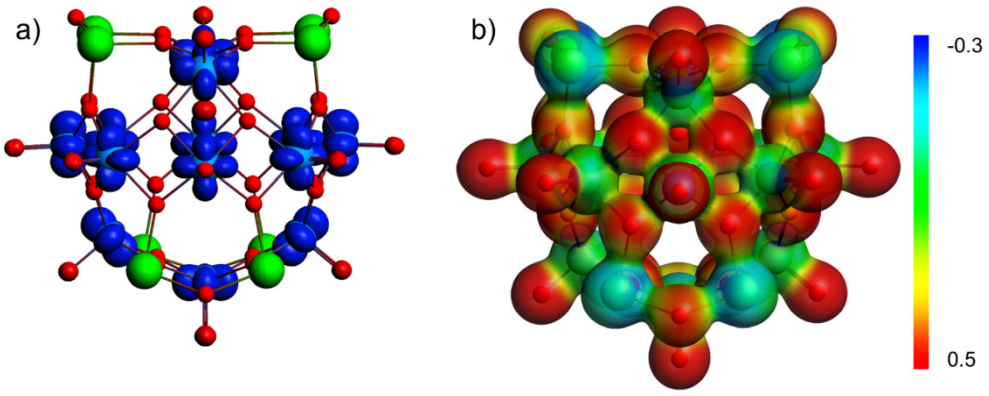

Figure S6. a) Spin density isosurface indicating accumulation of α spins for α_1*-$[V_{14}Sb_8O_{42}]^{4-}$; b) Molecular electrostatic potential (MEP) isosurface of α_1*-$[V_{14}Sb_8O_{42}]^{4-}$, with the most negative potentials in red. The α_1*-$[V_{14}Sb_8O_{42}]^{4-}$ structure is shown in a ball-and-stick representation (V: blue, O: red, Sb: green).

Simulation of the IR Spectrum of α_1*-$[V_{14}Sb_8O_{42}]^{4-}$

The fingerprint range of the calculated IR spectrum (400 – 1000 cm^{-1}) of α_1*-$[V_{14}Sb_8O_{42}]^{4-}$ (Figure S7) is in good qualitative agreement with the experimental spectrum. The largest discrepancies between the calculated and the experimentally measured IR absorption bands (*ca.* 16 cm^{-1}) are noted for the stretching modes of the terminal V–O bonds. Such discrepancies as well as a split of the $\tilde{\nu}(V–O_{term})$ absorption are expected when considering that our molecular model does not include the ion pairing effects as present in the crystal structure of α_1*-$[V_{14}Sb_8O_{42}]^{4-}$. Interpretation of the six characteristic modes is provided in Table S7.

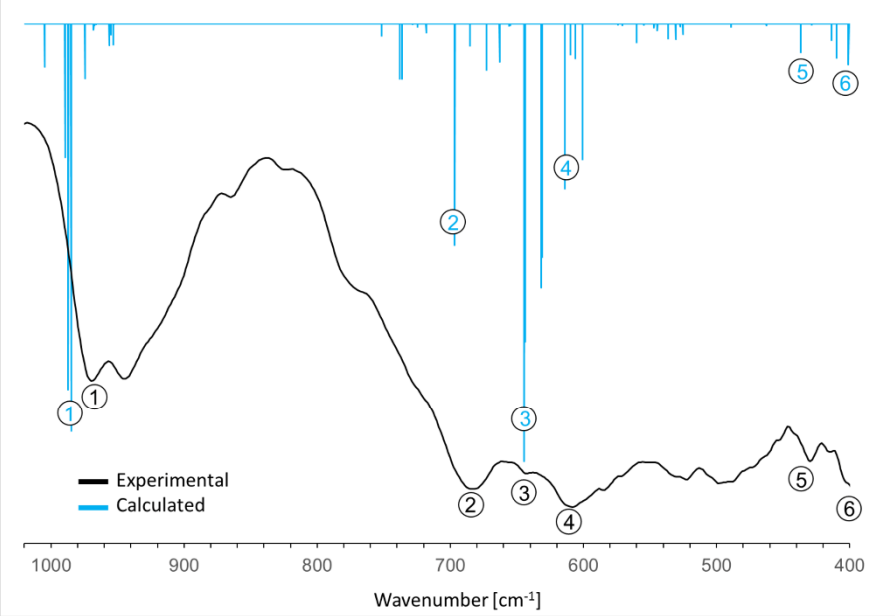

Figure S7. Comparison of the experimentally measured (black) and calculated (blue) IR spectra of α_1*-$[V_{14}Sb_8O_{42}]^{4-}$.

Table S7. Approximate assignment of the characteristic normal modes and the respective wavenumbers as calculated at LDA/ZORA-scalar/TZP/COSMO and the experimentally derived values for α_1*-$[V_{14}Sb_8O_{42}]^{4-}$ (see IR spectra in Figure S9). O_t: terminal oxygen atoms, O^{2V}: μ_3-oxygen atoms binding to two other V centers.

Region	Theory: $\tilde{\nu}$ / cm^{-1}	Experiment: $\tilde{\nu}$ /cm^{-1}	Assignment
1	985	969	$\nu(V–O_t)$
2	697	687	$\nu(Sb–O^{2V})$
3	643	642	$\nu(Sb–O)$
4	613	609	$\nu(V–O^{2V})$
5	436	431	$\delta(V–O)$
6	401	401	$\delta(Sb–O)$

3. Additional Experimental and Analytical Data for Compound 2

Determination of synthesis yield: The synthesis of **2** requires the use of an excess of precursor **1**, a portion of which is not dissolved in the reaction solution, which complicates the determination of the yield percentage as referenced to **1**. The exact synthesis procedure is as follows: the reaction mixture is heated to 150 °C and is held at this temperature for 4 h, resulting in the formation of a clear (no Tyndall effect) brown solution. Upon cooling to about 80 – 90 °C (for filtration), the solution becomes turbid (the separated solid is X-ray amorphous and contains V, Sb, and Ni). After filtration, a clear brown solution is obtained. This solution is kept at room temperature, and after 9 d crystals form that are separated by filtration. The color of the solution then appears slightly brighter. This solution is then stored for another couple of days in a vial with a perforated plastic cap, which yields some additional crystals of **2**. We thus report the yield obtained after 9 d, which corresponds to the amount of material crystallized from the supersaturated solution.

Instrumentation: IR spectra (KBr pellets) were measured from 400 to 4000 cm^{-1} using a Genesis FTIR spectrometer (ATI Mattson). C/H/N analysis was performed with an EURO EA Elemental Analyzer (EURO VECTOR Instruments). EDX analyses were performed using a Philips Environmental Scanning Electron Microscope ESEM XL30 equipped with an EDX detector. The X-ray diffraction powder pattern was recorded using a STOE STADI-P diffractometer in transmission geometry with Cu-Kα radiation (λ = 1.540598 Å) equipped with a Mythen 1 K detector and curved with a Ge(111) monochromator. Differential thermal analysis and thermogravimetry (DTA-TG) have been performed on a Netzsch STA-409CD instrument under nitrogen atmosphere (purity 5.0; heating 4 K min^{-1}, flow rate: 75 mL min^{-1}, in Al_2O_3 crucibles).

The X-ray powder diffraction pattern of **2** (Figure S8) is in full agreement with the pattern calculated from single-crystal data (red). Furthermore, Figure S9 compares the IR spectrum of **2** with that of the cyclen ligand, demonstrating the presence of cyclen in **2**, as well as the characteristic V^{IV}=O vibration at 970 cm^{-1}, the M-O-M absorption at 682 cm^{-1}, and vibrations of ethylenediamine and cyclen (3236, 2924, 2867, 1615, 1447 and 946 cm^{-1}), see Table S8.

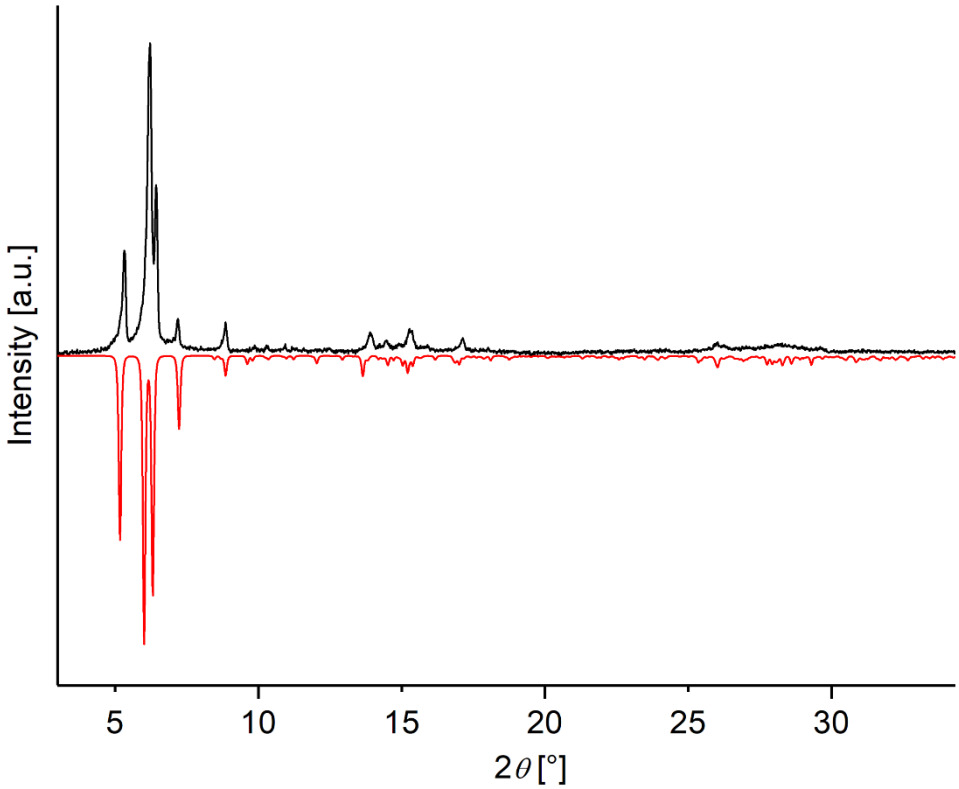

Figure S8. X-ray powder diffraction pattern of **2** (black) and the pattern calculated from single crystal structure data (red).

Table S8. Characteristic IR absorption peaks and assignments for compound **2**.

$\tilde{\nu}$ / cm^{-1}	
3236	NH stretch
2924 and 2867	CH stretch
1615	deformation of secondary amine
1447	CH_2 deformation
970	V^{IV}=O stretch
946	C-C (cyclen) skeletal vibration
682	M-O-M stretch

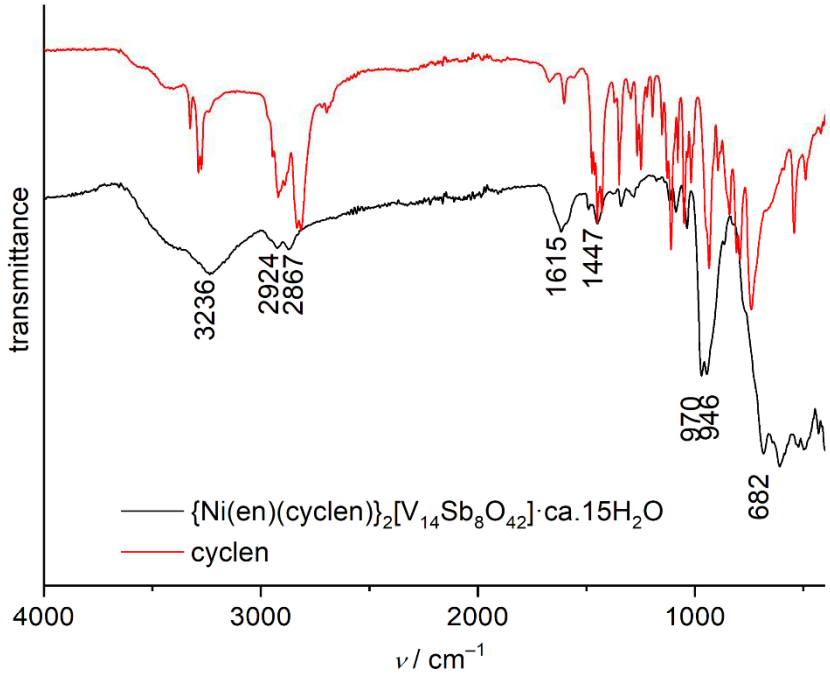

Figure S9. IR spectrum of compound **2** compared to that of cyclen.

Thermogravimetric analysis (Figure S10) revealed three broad steps up to 900 °C. A mass loss of 5.8 % up to 215 °C corresponds to the loss of ~10 crystal water molecules (calcd.: 5.77 %). The other mass loss steps cannot be unambiguously explained.

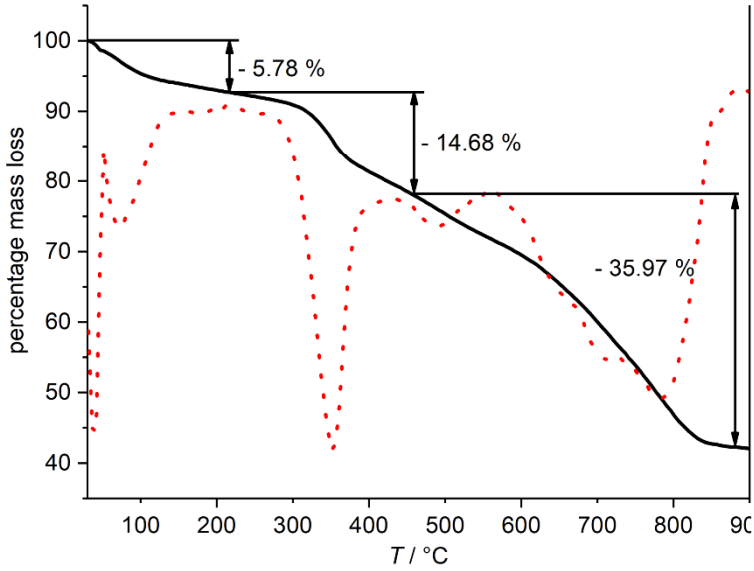

Figure S10. TG (black) and DTG (red) curves of compound **2**.

4. Crystallographic Details

Data collection has been performed with a STOE Imaging Plate Diffraction System (IPDS-1) with Mo-Kα radiation (λ = 0.71073 Å). A numerical absorption correction was performed ($T_{min/max}$: 0.3227/0.6947). The crystal structure has been solved with SHELXS-97 and refined against F^2 using SHELXL-2014.

Table S9. Selected structural data and refinement results for compound **2**.

Formula	$C_{40}H_{112}N_{24}Ni_4O_{86}Sb_{16}V_{28}$
Crystal system	monoclinic
Space group	$P2_1/n$
a	19.4201(4) Å
b	24.4157(4) Å
c	20.6579(4) Å
α	90°
β	117.1620(10)°
γ	90°
Volume	8714.8(3) Å^3
T	170(2) K
Z	2
Crystal size	0.06 × 0.10 × 0.16 mm^3
Density (calcd.)	2.254 Mg m^{-3}
Absorption coefficient μ	4.351 mm^{-1}
Θ_{max}	26.005°
Reflections collected	92336
R_{int}	0.0652
Independent reflections	17119
Reflections with $F_0 > 4\sigma(F_0)$	14585
R_1 [$F_0 > 4\sigma(F_0)$]	0.0624
R_1 for all data	0.0703
wR_2 [$F_0 > 4\sigma(F_0)$]	0.1696
wR_2 for all data	0.1752
Goodness of fit (F^2)	1.034
$\Delta\rho_{max/min}$	2.219 / –1.328 e Å^{-3}

All non-hydrogen atoms were refined anisotropically. The C-H and N-H hydrogen atoms were positioned with idealized geometry and refined isotropically with $U_{iso}(H) = 1.2\ U_{eq}(C)$ using a riding model. One of the two crystallographically independent Ni complexes is completely disordered. The Ni cation could be easily located but anisotropic refinement led to relatively high anisotropic displacement parameters. Some of the C and N atoms of the ligands could also be located but none of their positions are fully occupied, and even with e.g. half occupancy they exhibited very large isotropic displacement parameters. Several attempts were made to find a reasonable split model

using restraints but without any success. There are also several electron density peaks that are indicative for disordered water molecules (O···O distance about 2.8 A), but even here no split model could be found. Lowering the symmetry does not solve this problem and there is also no hint for superstructure reflections. Therefore, these water molecules and one of the two Ni complexes were removed using Squeeze in Platon (Fig. S17). The Ni complex was considered in the calculation of the formula and the molecular weight.

V=O_{term} bonds range from 1.591(6) to 1.629(7) Å (average: 1.610 Å), V–(μ-O) from 1.901(7) to 2.002(6) Å (avg. 1.966 Å), Sb–O from 1.895(8) to 2.000(8) Å (avg. 1.957 Å), shortest V···V separations: 2.911(3) – 3.068(2) Å (avg. 2.967 Å).

Crystals of compound **2** were obtained with a platelet-like morphology (Fig. S11).

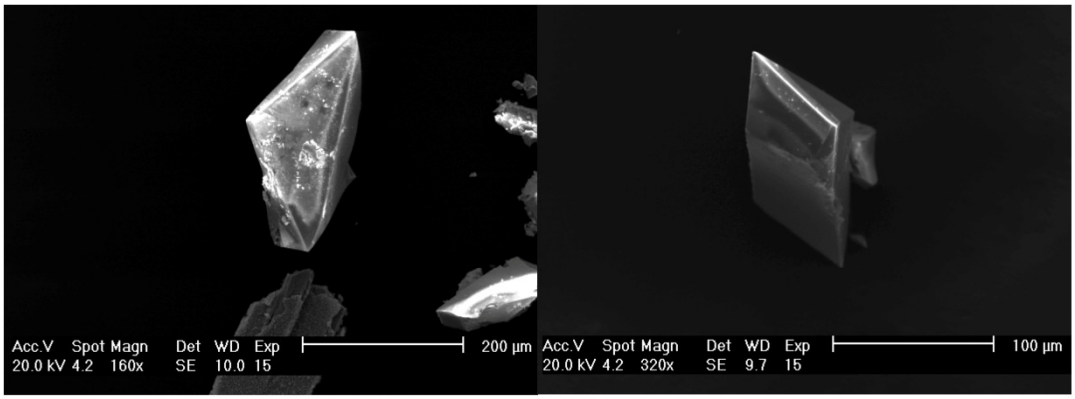

Figure S11. SEM images of two crystals of compound **2**.

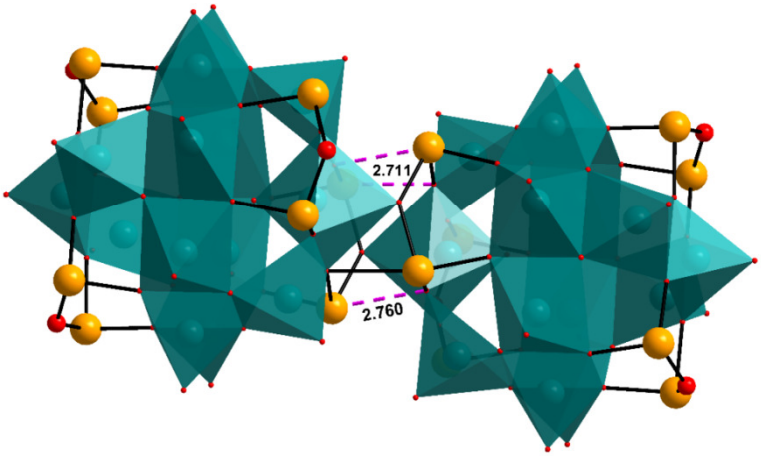

Figure S12. Shortest inter-cluster Sb–O contacts (dashed purple lines) in {$V_{14}Sb_8$} dimers in **2**.

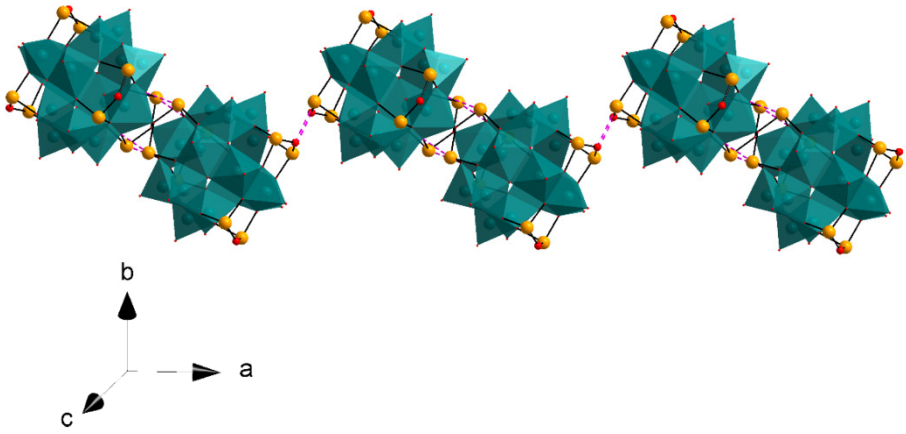

Figure S13. Arrangement of cluster dimers to form a zig-zag chain directed along [100] in the crystal structure of **2**.

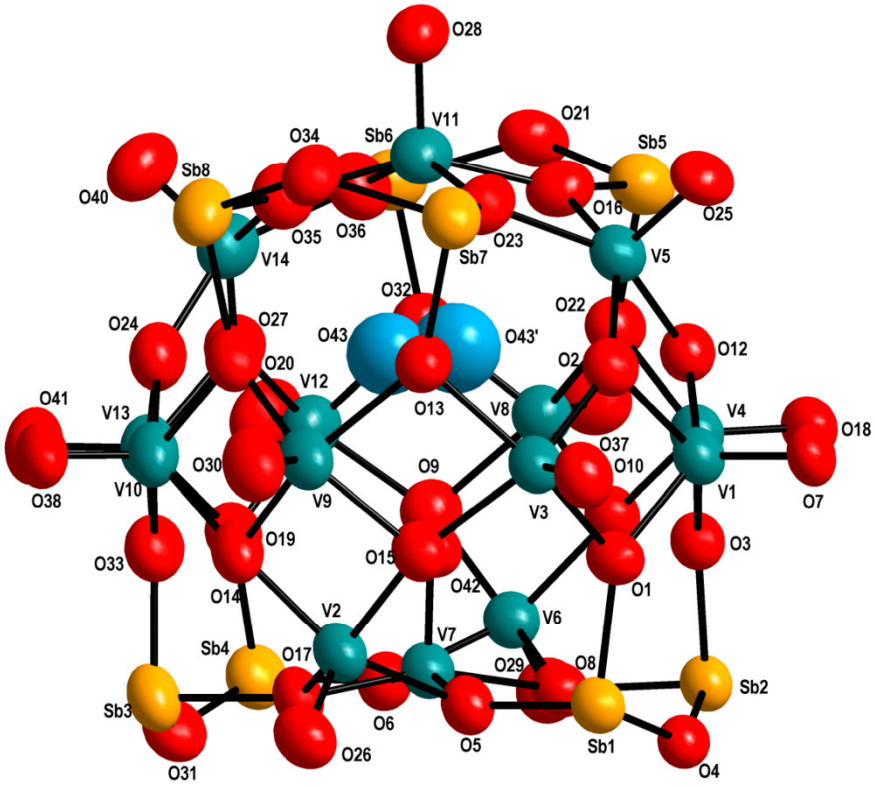

Figure S14. Drawing of the α_1*-$[V_{14}Sb_8O_{42}]^{4-}$ anion in compound **2** on the 50% probability level together with atom labeling.

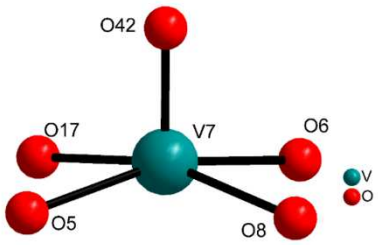

Figure S15. The $\{VO_5\}$ unit with the O42 atom pointing into the interior of the cluster.

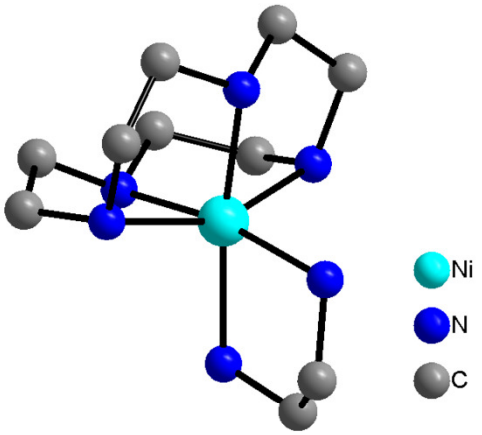

Figure S16. The distorted octahedral $[Ni(cyclen)(en)]^{2+}$ complex in the structure of **II**; H atoms have been omitted for clarity.

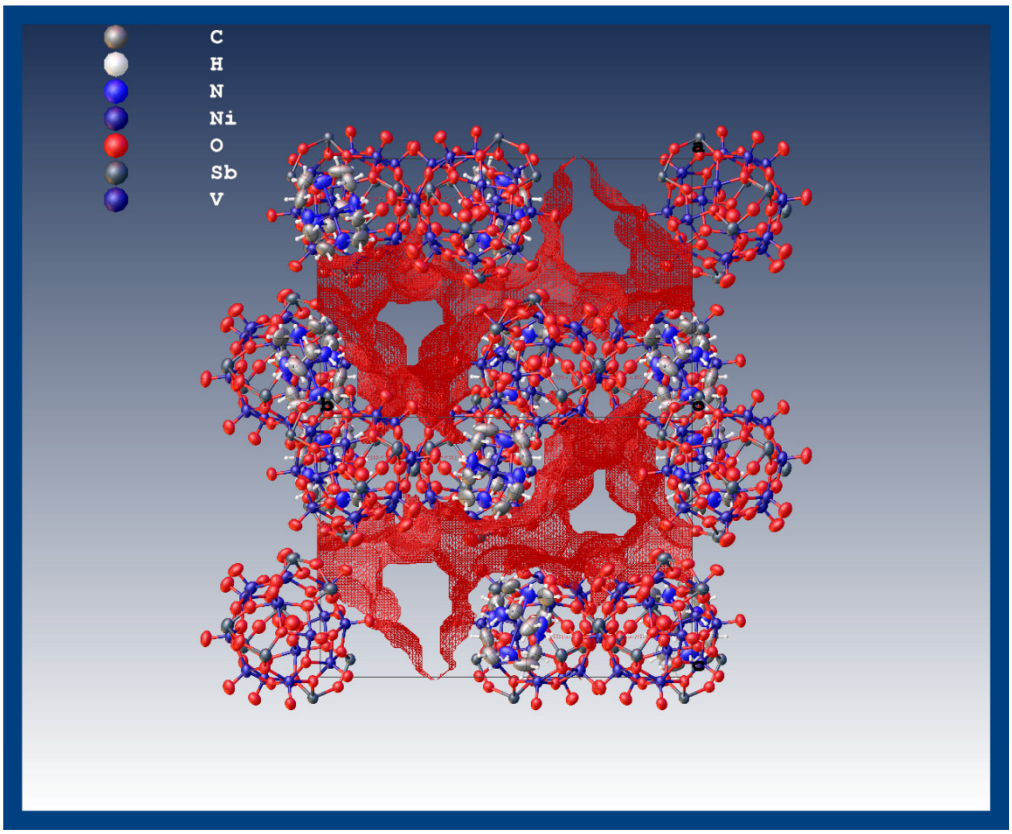

Figure S17. Void space for **2** calculated with the software package olex[2] showing large voids where the removed $[Ni(en)(cyclen)]^{2+}$ complex and the water molecules may be located (plane view [101]).

Table S10. Geometric parameters of possible hydrogen bonds (Å and °) in the structure of **2**.

D-H···A	d(D-H)	d(H···A)	d(D···A)	<(DHA)
C(3)-H(3B)···O(25)#2	0.99	2.37	3.322(16)	160.6
C(4)-H(4B)···O(10)#3	0.99	2.43	3.210(15)	135.6
N(3)-H(3)···O(7)#3	1.00	2.65	3.378(14)	129.6
N(3)-H(3)···O(10)#3	1.00	2.55	3.200(14)	122.6
C(5)-H(5B)···O(7)#3	0.99	2.65	3.370(15)	130.1
N(4)-H(4)···O(38)	1.00	1.83	2.826(12)	177.9
N(11)-H(11A)···O(10)#3	0.91	2.17	3.046(13)	160.2
N(12)-H(12D)···O(38)	0.91	2.46	2.981(12)	116.9

Symmetry transformations used to generate equivalent atoms: #1: $-x+1, -y+1, -z+1$ #2: $x-1/2, -y+1/2, z-1/2$ #3: $-x+3/2, y-1/2, -z+3/2$

5. Electrospray Ionization Mass Spectrometry

Electrospray ionization quadrupole-time-of-flight high resolution mass spectrometric (ESI-Q-TOF-HRMS) experiments were performed with a Synapt G2-S HDMS (Waters Co., Milford, MA, USA) instrument. The following settings were used: flow rate 5 mL min^{-1}, spray voltage 1.5 kV, sample cone voltage 70 V, source offset 80 V, source temperature 80 °C, desolvation temperature 150 °C, nebulizer gas 6 bar, desolvation gas flow 500 L^{-1}. Around these initial settings, the parameters were optimized for maximum abundance of the desired intact cluster ions and minimum abundance of fragments. To determine exact masses, the recorded MS spectra were recalibrated using a leucin-enkephalin lockspray (*m/z* 556.28). For collision-induced dissociation (CID), N_2 was used as the collision gas. Fragmentation experiments were conducted in the transfer cell of the Synapt G2-S HDMS instrument with collision energies of 20–50 V. For IM-MS separation of the monomeric and dimeric complexes that appear at the same *m/z*, the following settings were used: T-wave velocity 2.4 m s^{-1}, T-wave peak height 42.6 V, gas flow T-wave mobility cell: nitrogen (89.2 mL min^{-1}). Data acquisition and processing were carried out using MassLynx (version 4.1).

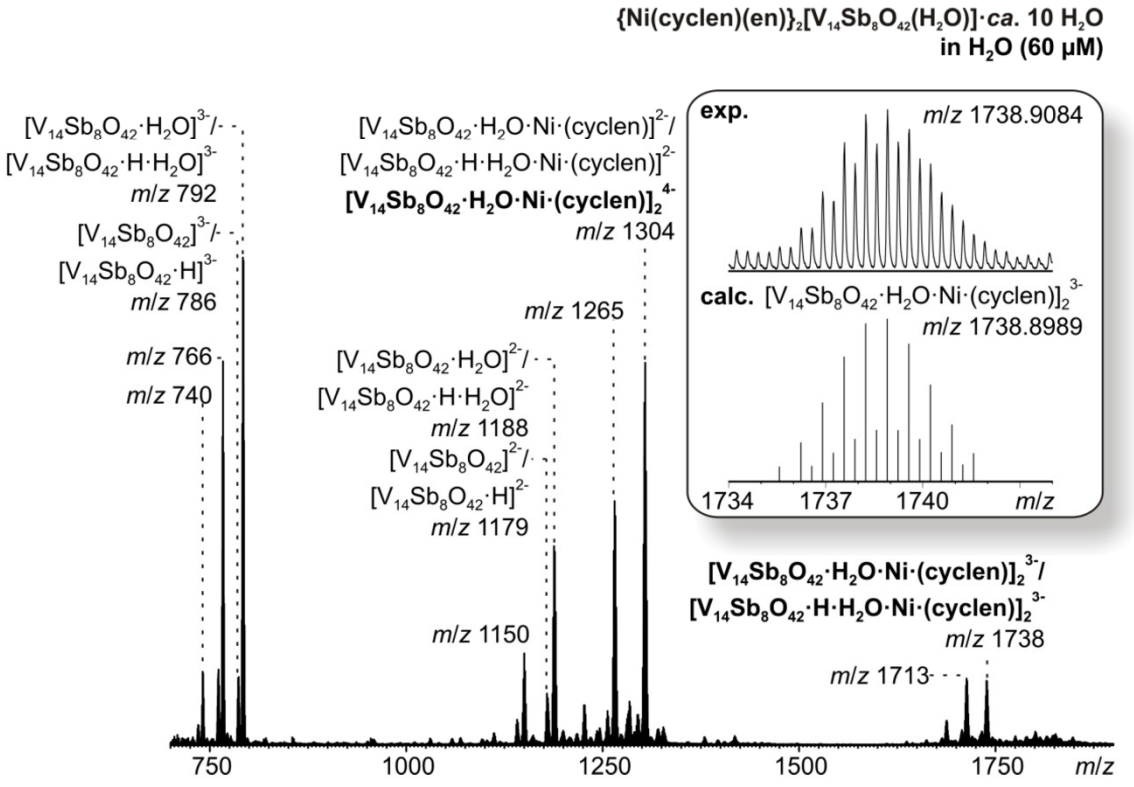

Figure S18: ESI-Q-TOF-HRMS spectrum of compound **2** (60 µM in H_2O) and experimental and calculated isotopic pattern (inset).

In agreement with our previous mass spectrometry study on compound **1**,[19] the observed isotopic pattern of all observed signals for compound **2** reveals actually two patterns which overlap and which are shifted against each other by *m/z* 0.33. For example, the signal at *m/z* 792 can be assigned to $[V_{14}Sb_8O_{42}(H_2O)]^{3-}$ and $[V_{14}Sb_8O_{42}{\cdot}H{\cdot}(H_2O)]^{3-}$, the latter of which contains a quadruply charged cluster core with one charge compensated by a proton. The same assignments can be made for signals belonging to dimeric complexes.

Besides the known signals indicated in the mass spectrum of $\{Ni(cyclen)(en)_2\}_2[V_{14}Sb_8O_{42}(H_2O)]$, a series of peaks exists for which no conclusive assignment could be made (*m/z* 740, 766, 1150, 1265, 1713). Based on previous results, it can be assumed that they belong to structurally closely related cluster species, for which we were nevertheless unable to find a fully convincing elemental composition, which is in line with the experimental data. As the powder diffraction patterns of a sample that was used for the mass spectrometric experiments clearly showed the sample not to contain significant amounts of impurities, we assume that these signals correspond to a marginal level of impurities, which are more easily ionized and thus appear with higher intensities in the mass spectra than expected from their abundance in the sample.

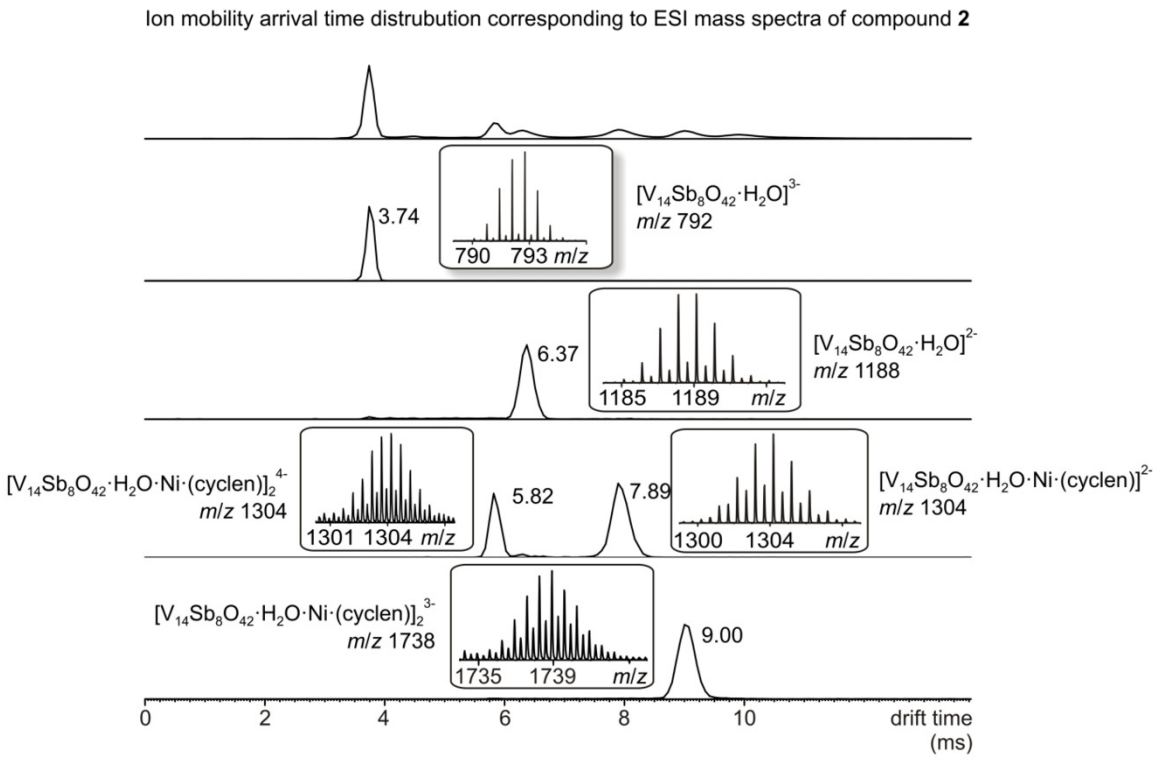

Figure S19. Separation of ions by ion mobility mass spectrometry. Arrival time distributions corresponding to all ions generated by electrospray ionization of compound **2** (top) and separated ion species (below).

The ESI-MS spectrum of a representative α-isomer analogue $\{Zn(en)\}_2[V_{14}Sb_8O_{42}(H_2O)]$, which does not form dimeric arrangements in the crystal structure, neither shows any dimer formation in solution in the same concentration range (Figure S20).

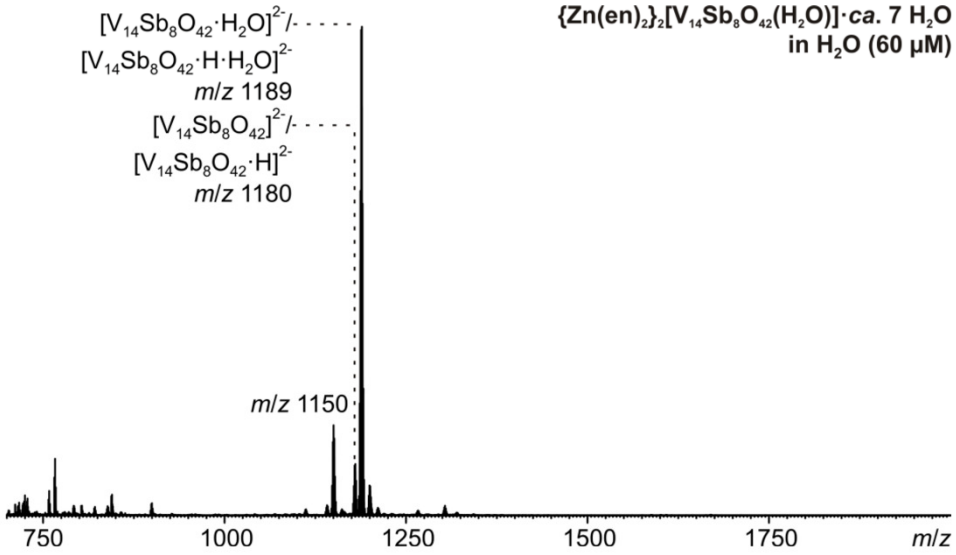

Figure S20. ESI-Q-TOF-HRMS spectrum of the representative α-$\{V_{14}Sb_8O_{42}\}$ isomer cluster in the compound $\{Zn(en)\}_2[V_{14}Sb_8O_{42}(H_2O)]$ (60 µM in H_2O).

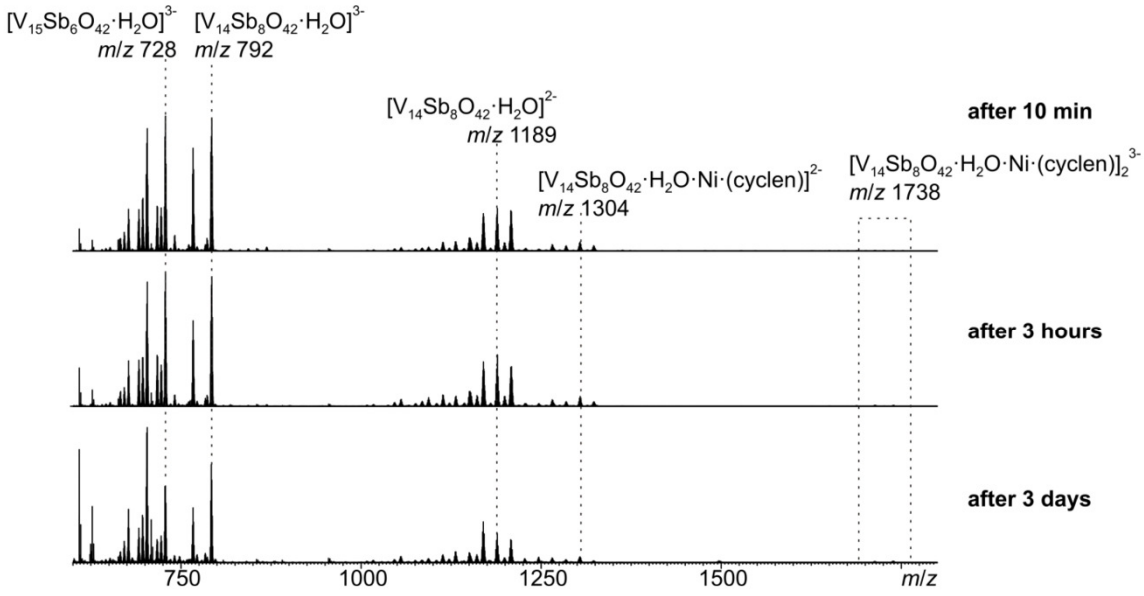

Figure S21. ESI-Q-TOF-HRMS spectrum of reaction mixture to obtain **2** at different times after filtration of the crude reaction mixture.

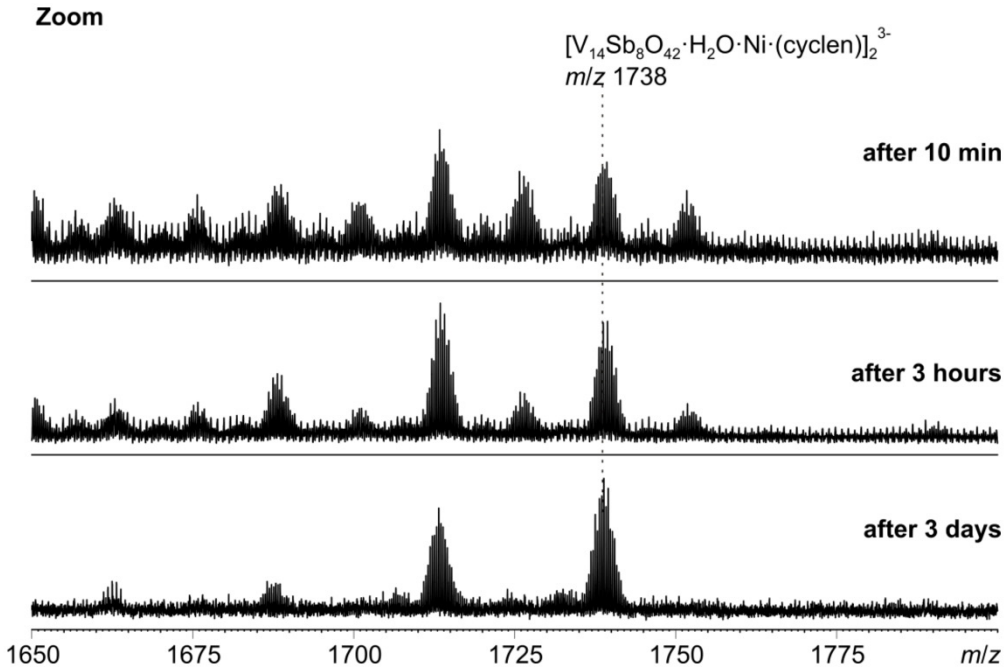

Figure S22. ESI-Q-TOF-HRMS spectrum of reaction mixture to obtain **2** at different times after filtration of the crude reaction mixture; zoom into the region around the signals for the $[V_{14}Sb_8O_{42}\cdot H_2O\cdot Ni(cyclen)]_2^{3-}$/ $[V_{14}Sb_8O_{42}\cdot H\cdot H_2O\cdot Ni(cyclen)]_2^{3-}$ ions.

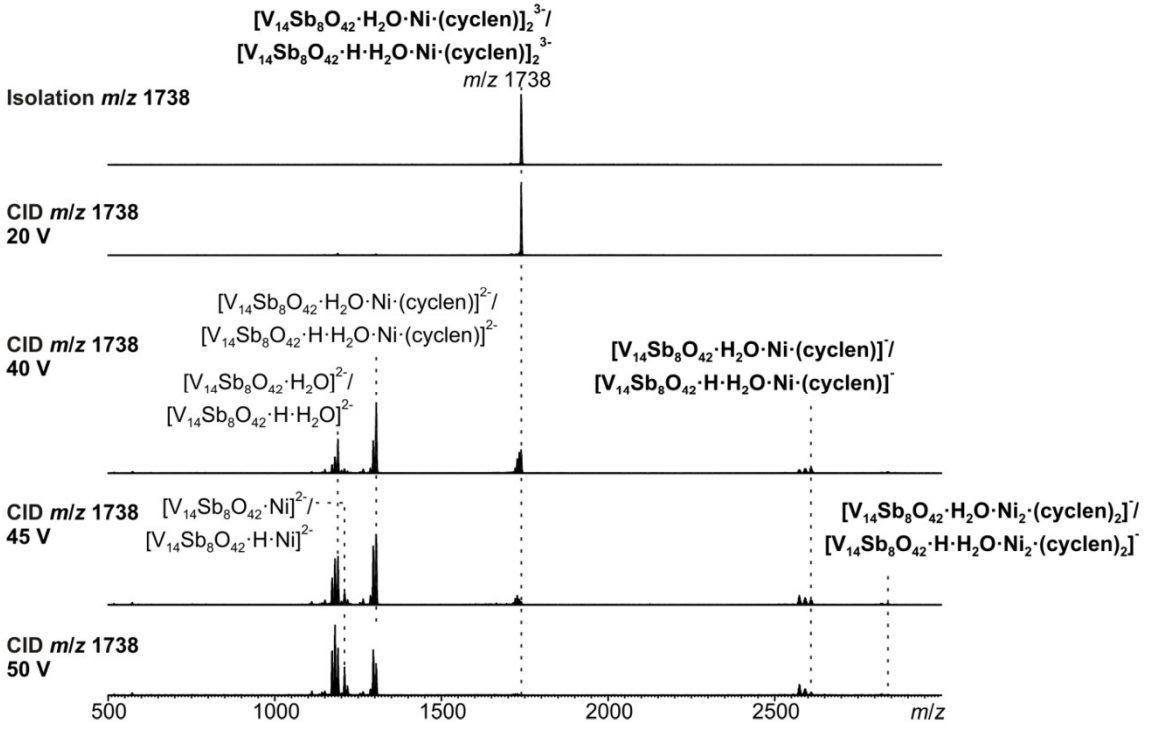

Figure S23. Collision-induced dissociation (CID) experiment of complex ions $[\mathbf{N}\cdot H_2O\cdot Ni(cyclen)]_2^{3-}$/ $[\mathbf{N}\cdot H\cdot H_2O\cdot Ni(cyclen)]_2^{3-}$, with $\mathbf{N} = \{V_{14}Sb_8O_{42}\}$ (full spectrum).

6. Magnetochemical Data and Interpretation

Temperature- (2.0 K–290 K, 1.0 T) and field-dependent (0.1 T–5.0 T, 2.0 K) magnetic susceptibility measurements were performed on a polycrystalline sample of **2** using a Quantum Design MPMS-5XL SQUID magnetometer. The data were corrected for the diamagnetic contributions of the compound ($\chi_{dia} = -1.57\times10^{-3}$ cm^3 mol^{-1}) and the sample holder.

The magnetic data of **2** are compared to those of β-$[V_{14}Sb_8O_{42}]^{4-}$. In both compounds, strong antiferromagnetic exchange interactions between the s = 1/2 vanadyl groups are present. For $T <$ 55 K, the slight distortion of the octahedral ligand field of the Ni^{2+} centers, resulting in a small zero-field splitting, contributes to the more distinct decrease of $\chi_m T$ due to the thermal depopulation of the split multiplet states. At 2.0 K, the molar magnetization M_m continuously increases with the applied field up to 5.8 $N_A\,\mu_B$ at 5.0 T. At this field, the magnetization does not indicate saturation, but is larger than the saturation value of two high-spin Ni^{2+} centers (4.0–4.9 $N_A\,\mu_B$), in line with dominant antiferromagnetic exchange interactions, but also with non-negligible contributions from α_1*-$[V_{14}Sb_8O_{42}]^{4-}$, hinting at a multiplet ground state. A qualitative estimate of the magnetic properties of the α_1*-$[V_{14}Sb_8O_{42}]^{4-}$ cluster is derived from modeling the Ni^{2+} centers as non-coupled, spin-only centers of effective spin S_{Ni} = 1 using CONDON 2.0.[20] A mean value of g_{eff} = 2.23 for the Ni^{2+} centers (Figure S24, dashed lines) then reasonably reproduces the data, as the corresponding plots of the difference data (Figure S24, full dots) reveal two physical features: Firstly, inflection points in the M_m vs. B plots vanish for $g_{eff} \leq 2.23$. Secondly, $\chi_m T$ remains positive at the lowest temperatures for $g_{eff} \approx 2.23$. A further comparison of the estimated contributions of α_1*-$[V_{14}Sb_8O_{42}]^{4-}$ and the magnetic data of β-$[V_{14}Sb_8O_{42}]^{4-}$ (Figure S24, open triangles) reveals obvious discrepancies in magnitude and, in particular, shape of the corresponding representations, which is primary due to the distinctly different exchange pathways in both polyoxoanions.

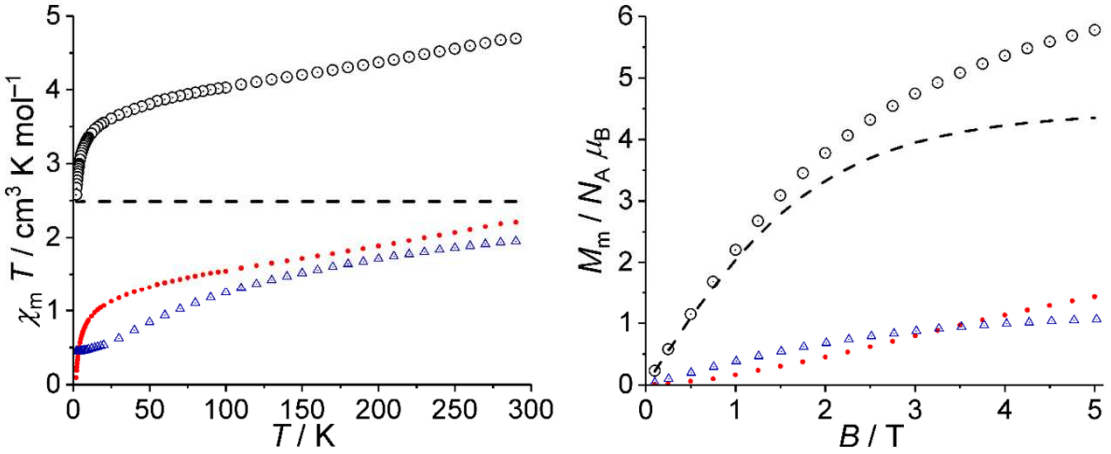

Figure S24. Temperature dependence of $\chi_m T$ (left) and field dependence of the molar magnetization M_m (right). Open circles: experimental data of **2** at 0.1 T; blue triangles: experimental data of β-$[V_{14}Sb_8O_{42}]^{4-}$ at 0.1 T; dashed lines: calculated contributions of two Ni^{2+} centers assuming an effective spin S = 1 model adopting an isotropic g factor of g_{eff} = 2.23; red full dots: difference of experimental data and calculated Ni^{2+} contributions representing the potential contributions of α_1*-$[V_{14}Sb_8O_{42}]^{4-}$.

7. Cartesian Coordinates

Table S11. Cartesian coordinates (in Å) of the α-/β-/γ-$[V_{14}Sb_8O_{42}]^{4-}$ isomers and the eleven positional isomers α_n*-/β_n*-/γ_n*-$[V_{14}Sb_8O_{42}]^{4-}$.

α_1*-$[V_{14}Sb_8O_{42}]^{4-}$			
O	3.39661382	1.45658448	-1.43078316
O	5.66392524	0.00000000	-0.18305781
O	-1.44003428	-3.41469045	1.25001113
O	0.00000000	-5.72564138	0.04866966
O	-3.93586094	-3.93099692	-0.07637552
O	0.00000000	-3.79132978	3.87677227
V	0.00000000	0.00000000	3.84553964
V	0.00000000	0.00000000	-2.84913006
O	0.00000000	0.00000000	5.47228065
V	-2.82697210	0.00000000	2.48681292
Sb	-1.80555292	3.20921326	3.22227477
Sb	1.80555292	3.20921326	3.22227477
V	-4.02394310	0.00000000	-0.25187415
V	-2.76662466	2.78875885	-0.09288855
V	0.00000000	4.08421576	0.07527830
V	2.76662466	2.78875885	-0.09288855
V	2.76662466	-2.78875885	-0.09288855
V	4.02394310	0.00000000	-0.25187415
O	-1.21158643	1.48294025	-3.38853306
O	1.21158643	-1.48294025	-3.38853306
O	-1.21158643	-1.48294025	-3.38853306
O	1.21158643	1.48294025	-3.38853306
O	0.00000000	0.00000000	-1.23592813
V	0.00000000	-4.08421576	0.07527830
V	-2.76662466	-2.78875885	-0.09288855
V	2.82697210	0.00000000	2.48681292
O	-3.77879237	0.00000000	-4.03493875
Sb	1.80555292	-3.20921326	3.22227477
Sb	-1.80555292	-3.20921326	3.22227477
O	-1.42678100	-1.21521620	3.19940843
O	-1.42678100	1.21521620	3.19940843
O	-4.07653665	0.00000000	3.53824544
O	0.00000000	3.79132978	3.87677227
O	1.42678100	1.21521620	3.19940843
Sb	-3.21087793	1.81862552	-3.40314380
V	0.00000000	2.91563279	-2.68080154
Sb	3.21087793	-1.81862552	-3.40314380
V	0.00000000	-2.91563279	-2.68080154
Sb	-3.21087793	-1.81862552	-3.40314380
Sb	3.21087793	1.81862552	-3.40314380
O	1.42678100	-1.21521620	3.19940843
O	4.07653665	0.00000000	3.53824544
O	-3.26925543	1.26265553	1.03866465
O	-5.66392524	0.00000000	-0.18305781
O	-3.26925543	-1.26265553	1.03866465
O	-3.93586094	3.93099692	-0.07637552
O	-1.44003428	3.41469045	1.25001113
O	1.44003428	3.41469045	1.25001113
O	0.00000000	5.72564138	0.04866966
O	3.26925543	1.26265553	1.03866465
O	3.93586094	3.93099692	-0.07637552
O	3.26925543	-1.26265553	1.03866465
O	1.44003428	-3.41469045	1.25001113
O	3.93586094	-3.93099692	-0.07637552
O	-3.39661382	1.45658448	-1.43078316
O	1.26435123	3.35983504	-1.23121485
O	-1.26435123	3.35983504	-1.23121485
O	0.00000000	4.14993106	-3.74978402
O	3.39661382	-1.45658448	-1.43078316
O	3.77879237	0.00000000	-4.03493875
O	1.26435123	-3.35983504	-1.23121485
O	-1.26435123	-3.35983504	-1.23121485
O	0.00000000	-4.14993106	-3.74978402
O	-3.39661382	-1.45658448	-1.43078316

α_2*-$[V_{14}Sb_8O_{42}]^{4-}$			
Sb	3.50437612	1.80574468	-2.81800971
V	0.40021094	-0.00000000	-3.83317498
V	2.49063091	0.00000000	3.02604649
V	2.65514284	2.76461579	0.42683434
V	3.95759404	0.00000000	0.41831609
O	3.05388897	1.25739712	1.61301809
O	3.47837207	1.45427686	-0.83156058
O	3.78003839	3.94089983	0.58535432
O	1.52490279	1.42037091	-3.03427372
V	-0.10835143	4.04813838	0.21535920
O	5.57791842	0.00000000	0.68341502
O	4.16854665	-0.00000000	-3.38825527
O	3.65912200	0.00000000	4.16612168
O	0.61939874	-0.00000000	-5.44577932
O	3.05388897	-1.25739712	1.61301809
V	2.65514284	-2.76461579	0.42683434
O	1.29752260	-3.26745457	-0.89807638
V	0.24060021	-2.83822610	-2.50670216
O	-1.19726653	-3.33936421	-1.25538852
V	-2.84514575	-2.81199701	-0.35911690
O	-3.37532448	-1.26693919	0.70738812
V	-2.08764879	0.00000000	1.49294814
O	-3.37532448	1.26693919	0.70738812
V	-2.84514575	2.81199701	-0.35911690
O	-1.19726653	3.33936421	-1.25538852
V	0.24060021	2.83822610	-2.50670216
O	1.29752260	3.26745457	-0.89807638
O	1.14437609	3.35518165	1.58298387
Sb	1.28918968	3.24472945	3.59197698
O	1.04500470	1.22138297	3.64723021
V	-0.47704581	0.00000000	3.99306981
O	-1.72712197	1.20832342	3.02969913
Sb	-2.28517214	3.14987561	3.09142831
O	-1.74167150	3.49101926	1.17485775
O	-3.34950832	1.47240029	-1.76923842
Sb	-2.85557271	1.81086985	-3.69420043
O	-0.88383095	1.44014833	-3.36525041
Sb	3.50437612	-1.80574468	-2.81800971
O	3.47837207	-1.45427686	-0.83156058
O	1.14437609	-3.35518165	1.58298387
Sb	1.28918968	-3.24472945	3.59197698
O	1.04500470	-1.22138297	3.64723021
O	-1.72712197	-1.20832342	3.02969913
Sb	-2.28517214	-3.14987561	3.09142831
O	-1.74167150	-3.49101926	1.17485775
O	-3.34950832	-1.47240029	-1.76923842
Sb	-2.85557271	-1.81086985	-3.69420043
O	-0.88383095	-1.44014833	-3.36525041
O	1.52490279	-1.42037091	-3.03427372
O	-4.02654519	3.93646797	-0.48601273
O	0.41006009	-4.07430845	-3.56108553
O	-0.59979935	3.79030476	3.98524801
O	-3.32584453	-0.00000000	-4.41872541
O	3.78003839	-3.94089983	0.58535432
V	-4.05554387	-0.00000000	-0.63908698
O	-5.69543249	-0.00000000	-0.68002130
O	-4.02654519	-3.93646797	-0.48601273
V	-0.10835143	-4.04813838	0.21535920
O	-0.04051346	-5.68704788	0.16133265
O	0.41006009	4.07430845	-3.56108553
O	-0.59979935	-3.79030476	3.98524801
O	-0.04051346	5.68704788	0.16133265
O	-0.78905182	0.00000000	0.52728298
O	-0.83295266	0.00000000	5.58311210

α_3*-$[V_{14}Sb_8O_{42}]^{4-}$			
Sb	3.11836615	1.80692219	-3.26122730
V	-0.07811899	-0.00000000	-3.89088340
V	2.71855605	0.00000000	2.63119990
V	2.66989346	2.77771507	0.05006017
V	3.94648094	-0.00000000	-0.10063616
O	3.16947065	1.25900267	1.18218076
O	3.34031405	1.45815038	-1.28803239
O	3.82181180	3.93876592	0.06902314
O	1.12831656	1.42051322	-3.21699211
V	-0.08855713	4.09166691	0.17482658
O	5.58470588	-0.00000000	-0.00189599
O	3.70365012	-0.00000000	-3.90871642
O	3.96284369	0.00000000	3.68979242
O	-0.00300896	-0.00000000	-5.51590203
O	3.16947065	-1.25900267	1.18218076
V	2.66989346	-2.77771507	0.05006017
O	1.16272072	-3.28496395	-1.09284523
V	-0.08406471	-2.84472282	-2.55861310
O	-1.35855986	-3.39061686	-1.14369745
V	-2.87382172	-2.85703701	-0.03707983
O	-3.18849764	-1.26267107	1.04460501
V	-2.89466233	0.00000000	2.53409290
O	-3.18849764	1.26267107	1.04460501
V	-2.87382172	2.85703701	-0.03707983
O	-1.35855986	3.39061686	-1.14369745
V	-0.08406471	2.84472282	-2.55861310
O	1.16272072	3.28496395	-1.09284523
O	1.32446445	3.40911924	1.38023777
Sb	1.68016008	3.21571957	3.35302066
O	1.31569521	1.21660861	3.33370951
V	-0.11580841	0.00000000	3.96442270
O	-1.53385832	1.22018871	3.30493288
Sb	-1.93099144	3.21652752	3.30743498
O	-1.58710265	3.53745957	1.33968242
O	-3.49178338	1.49531710	-1.41789958
Sb	-3.29176133	1.83078589	-3.39948268
O	-1.29899565	1.47543099	-3.34887996
Sb	3.11836615	-1.80692219	-3.26122730
O	3.34031405	-1.45815038	-1.28803239
O	1.32446445	-3.40911924	1.38023777
Sb	1.68016008	-3.21571957	3.35302066
O	1.31569521	-1.21660861	3.33370951
O	-1.53385832	-1.22018871	3.30493288
Sb	-1.93099144	-3.21652752	3.30743498
O	-1.58710265	-3.53745957	1.33968242
O	-3.49178338	-1.49531710	-1.41789958
Sb	-3.29176133	-1.83078589	-3.39948268
O	-1.29899565	-1.47543099	-3.34887996
O	1.12831656	-1.42051322	-3.21699211
O	-4.09797888	3.94461772	-0.02384398
O	-0.01563320	-4.08088369	-3.62269495
O	-0.13372179	3.79673686	3.98434684
O	-3.83272429	-0.00000000	-4.02687117
O	3.82181180	-3.93876592	0.06902314
V	-2.72896337	-0.00000000	-0.36248233
O	-1.11309586	-0.00000000	-0.53335231
O	-4.09797888	-3.94461772	-0.02384398
V	-0.08855713	-4.09166691	0.17482658
O	-0.02258972	-5.72988795	0.10092650
O	-0.01563320	4.08088369	-3.62269495
O	-0.13372179	-3.79673686	3.98434684
O	-0.02258972	5.72988795	0.10092650
O	-4.22282118	0.00000000	3.48685167
O	-0.13098297	0.00000000	5.59148067

α_4*-$[V_{14}Sb_8O_{42}]^{4-}$			
Sb	3.27444141	3.65645061	0.94791258
V	3.91999423	0.11278540	-0.10542697
V	-2.58707739	1.93093713	1.86449755
V	-0.06331454	3.98860299	-0.08196092
V	0.11731040	2.86527911	2.76107103
O	-1.16665859	3.18461377	1.32059915
O	1.29602181	3.50659381	1.30777063
O	-0.12273791	5.62247530	-0.02163563
O	3.29225527	1.99688110	-0.21829210
V	-0.17954244	2.91033070	-2.94220380
O	-0.00436538	4.01675389	3.92436649
O	3.91951923	2.76902437	2.62765899
O	-3.67987868	2.79326107	2.71794500
O	5.54660861	0.10079406	-0.07268372
O	-1.14517618	1.40421950	3.10152978
V	-0.00000000	0.00000000	3.83552169
O	1.14517618	-1.40421950	3.10152978
V	2.58707739	-1.93093713	1.86449755
O	1.16665859	-3.18461377	1.32059915
V	0.06331454	-3.98860299	-0.08196092
O	-1.10133362	-3.37516534	-1.53019931
V	-2.58767839	-2.16996825	-2.05906078
O	-1.16780073	-1.50996710	-3.22007978
V	-0.00000000	0.00000000	-2.68864674
O	1.16780073	1.50996710	-3.22007978
V	2.58767839	2.16996825	-2.05906078
O	1.10133362	3.37516534	-1.53019931
O	-1.39315555	3.51529056	-1.50018323
Sb	-3.38109081	3.44198286	-1.12376495
O	-3.25449944	1.75607210	0.00168970
V	-3.91999423	-0.11278540	-0.10542697
O	-3.34436689	-0.31957727	-1.98943476
Sb	-3.24803682	0.85272508	-3.64418334
O	-1.29609675	1.31762063	-3.37700964
O	1.29609675	-1.31762063	-3.37700964
Sb	3.24803682	-0.85272508	-3.64418334
O	3.34436689	0.31957727	-1.98943476
Sb	3.30348021	1.04528929	3.44890568
O	1.32449164	1.42149703	3.36582386
O	-1.32449164	-1.42149703	3.36582386
Sb	-3.30348021	-1.04528929	3.44890568
O	-3.25828984	0.06354606	1.75149633
O	-3.29225527	-1.99688110	-0.21829210
Sb	-3.27444141	-3.65645061	0.94791258
O	-1.29602181	-3.50659381	1.30777063
O	1.39315555	-3.51529056	-1.50018323
Sb	3.38109081	-3.44198286	-1.12376495
O	3.25449944	-1.75607210	0.00168970
O	3.25828984	-0.06354606	1.75149633
O	-0.00000000	0.00000000	-1.06902213
O	3.67987868	-2.79326107	2.71794500
O	-3.96840668	2.53762785	-2.81488788
O	3.96840668	-2.53762785	-2.81488788
O	-0.00000000	0.00000000	5.47176690
V	0.17954244	-2.91033070	-2.94220380
O	0.16439229	-3.99819788	-4.17160862
O	0.12273791	-5.62247530	-0.02163563
V	-0.11731040	-2.86527911	2.76107103
O	0.00436538	-4.01675389	3.92436649
O	3.61899011	3.07998524	-2.94139010
O	-3.91951923	-2.76902437	2.62765899
O	-0.16439229	3.99819788	-4.17160862
O	-3.61899011	-3.07998524	-2.94139010
O	-5.54660861	-0.10079406	-0.07268372

β_1*-$[V_{14}Sb_8O_{42}]^{4-}$				β_2*-$[V_{14}Sb_8O_{42}]^{4-}$			
Sb	3.29256222	-3.21288274	-1.81224403	Sb	3.17707521	-3.14383680	-2.05661837
O	3.38213821	1.21420157	1.46639828	O	3.29895966	1.06668774	1.41492954
Sb	-3.11117006	3.21250023	1.80194429	Sb	-3.20894419	3.02888969	1.92096813
O	-3.21990396	1.21961386	-1.43298042	O	-3.34717106	1.27490180	-1.44514521
Sb	3.29256222	-3.21288274	1.81224403	Sb	3.22853439	-3.38017329	1.53916909
O	-1.11838286	3.30317519	-1.43465742	O	-1.21953051	3.32031998	-1.30177261
Sb	-3.11117006	3.21250023	-1.80194429	Sb	-3.21085081	3.28694093	-1.67469347
O	0.07801585	-3.81266122	-4.07080468	O	-0.00000000	-0.60463670	-0.89454076
Sb	-3.11784148	-3.20469937	-1.80214341	Sb	-3.17707521	-3.14383680	-2.05661837
O	1.30991636	3.32412153	1.44568149	O	1.21790826	3.15147956	1.55765846
Sb	3.29957398	3.21195815	1.81131489	Sb	3.20894419	3.02888969	1.92096813
O	-1.11838286	3.30317519	1.43465742	O	-1.21790826	3.15147956	1.55765846
Sb	-3.11784148	-3.20469937	1.80214341	Sb	-3.22853439	-3.38017329	1.53916909
O	1.36694553	-1.27465778	3.44896383	O	1.27032486	-1.55314607	3.22444322
Sb	3.29957398	3.21195815	-1.81131489	Sb	3.21085081	3.28694093	-1.67469347
O	-1.18004003	-1.26813418	3.39429285	O	-1.27032486	-1.55314607	3.22444322
V	2.78668394	-0.00079432	-2.94763304	V	2.70371227	0.16216522	-2.95204306
O	1.36870055	1.27512767	3.44987619	O	1.27003444	0.98785742	3.37162222
V	-2.59610857	0.00355664	2.88024508	V	-2.67696569	-0.24931110	2.77064616
O	-3.73854249	-3.82948935	-0.00000000	O	-3.83746314	-3.87874005	-0.30569007
V	2.79996793	-0.00183800	-0.00000000	V	3.94093533	-0.05482132	-0.08835828
O	-3.22190508	-1.21163235	-1.43283938	O	-3.36515824	-1.16790625	-1.61832795
V	-3.86372105	0.00464181	-0.00000000	V	-3.94093533	-0.05482132	-0.08835828
O	0.07622909	-5.56959669	-0.00000000	O	-0.00000000	-5.66209471	-0.45949974
V	2.78668394	-0.00079432	2.94763304	V	2.67696569	-0.24931110	2.77064616
O	1.36870055	1.27512767	-3.44987619	O	1.27629381	1.44982197	-3.42981346
V	-2.59610857	0.00355664	-2.88024508	V	-2.70371227	0.16216522	-2.95204306
O	0.08304848	3.81625690	-4.07043430	O	-0.00000000	4.02607248	-3.87849284
V	0.09647085	2.68680578	2.89002372	V	0.00000000	2.43434084	2.95277562
O	1.30330163	-3.32154792	-1.44492962	O	1.21496449	-3.19804805	-1.56120759
V	0.09192397	-2.68401377	-2.88990349	V	-0.00000000	-1.71489666	-2.07392205
O	3.92935100	-0.00179009	4.11659850	O	3.81024028	-0.33228404	3.94556330
V	0.08310200	0.00112244	4.19008471	V	0.00000000	-0.32712425	4.06711968
O	-1.17828181	1.27344076	-3.39575951	O	-1.27629381	1.44982197	-3.42981346
V	0.08310200	0.00112244	-4.19008471	V	-0.00000000	0.18914055	-4.22440662
O	0.05212960	0.00043026	5.84314132	O	0.00000000	-0.42535232	5.71781812
V	0.09192397	-2.68401377	2.88990349	V	0.00000000	-2.96295787	2.68822187
O	0.05212960	0.00043026	-5.84314132	O	-0.00000000	0.20622100	-5.87760259
V	0.09647085	2.68680578	-2.89002372	V	-0.00000000	2.80509899	-2.79054625
O	-1.17828181	1.27344076	3.39575951	O	-1.27003444	0.98785742	3.37162222
V	0.08679928	-3.94420143	-0.00000000	V	-0.00000000	-4.04761280	-0.24067338
O	1.30330163	-3.32154792	1.44492962	O	1.22392225	-3.57116829	1.24584042
V	0.09503007	3.94661976	-0.00000000	V	0.00000000	3.86522589	0.16387224
O	-1.12519169	-3.30086575	-1.43583737	O	-1.21496449	-3.19804805	-1.56120759
O	3.90154575	-3.82314250	-0.00000000	O	3.83746314	-3.87874005	-0.30569007
O	-1.12519169	-3.30086575	1.43583737	O	-1.22392225	-3.57116829	1.24584042
O	-3.73028519	3.83838650	-0.00000000	O	-3.82468182	3.78263230	0.16884247
O	1.36694553	-1.27465778	-3.44896383	O	1.27669614	-1.09007837	-3.43468643
O	3.38170474	-1.21499822	-1.46836565	O	3.36515824	-1.16790625	-1.61832795
O	-1.18004003	-1.26813418	-3.39429285	O	-1.27669614	-1.09007837	-3.43468643
O	-3.21990396	1.21961386	1.43298042	O	-3.29895966	1.06668774	1.41492954
O	3.90858593	3.82293859	-0.00000000	O	3.82468182	3.78263230	0.16884247
O	3.92935100	-0.00179009	-4.11659850	O	3.79748293	0.21170555	-4.16619536
O	-3.71860438	0.00413658	-4.06786096	O	-3.79748293	0.21170555	-4.16619536
O	-3.71860438	0.00413658	4.06786096	O	-3.81024028	-0.33228404	3.94556330
O	0.08304848	3.81625690	4.07043430	O	0.00000000	3.47293171	4.21481645
O	3.38213821	1.21420157	-1.46639828	O	3.34717106	1.27490180	-1.44514521
O	0.07801585	-3.81266122	4.07080468	O	0.00000000	-4.10397172	3.85874385
O	-3.22190508	-1.21163235	1.43283938	O	-3.27324483	-1.37123184	1.24670589
O	0.08599335	5.57215260	-0.00000000	O	0.00000000	5.48818555	0.26252188
O	1.18673646	-0.00228263	-0.00000000	O	5.56668820	-0.06030472	-0.05501145
O	1.30991636	3.32412153	-1.44568149	O	1.21953051	3.32031998	-1.30177261
O	-5.49006222	0.00665638	-0.00000000	O	-5.56668820	-0.06030472	-0.05501145
O	3.38170474	-1.21499822	1.46836565	O	3.27324483	-1.37123184	1.24670589

β_3*-$[V_{14}Sb_8O_{42}]^{4-}$			
Sb	-3.20885741	-3.21509873	-1.92494523
O	1.21289031	-3.31358496	1.32622512
Sb	3.20301373	3.21348660	1.70649469
O	1.22969453	3.43521153	-1.53484084
Sb	-3.22228854	-3.21251315	1.67842602
O	3.44085922	1.22465761	-1.52439554
Sb	3.22140376	3.21458868	-1.89708751
O	-3.77301599	-0.00000000	-4.24246615
Sb	-3.20885741	3.21509873	-1.92494523
O	3.30477570	-1.22123352	1.33622318
Sb	3.20301373	-3.21348660	1.70649469
O	3.30477570	1.22123352	1.33622318
Sb	-3.22228854	3.21251315	1.67842602
O	-1.28926909	-1.27115911	3.26267713
Sb	3.22140376	-3.21458868	-1.89708751
O	-1.28926909	1.27115911	3.26267713
V	0.01169533	-2.76648467	-2.94908575
O	1.25290764	-1.27091738	3.27421584
V	-0.01533497	2.68469702	2.75554073
O	-3.83964841	3.83777970	-0.12357474
V	-0.00204611	-3.99497082	-0.08345471
O	-1.21982411	3.43606751	-1.54720256
V	-0.00204611	3.99497082	-0.08345471
O	-5.62210840	-0.00000000	-0.04894207
V	-0.01533497	-2.68469702	2.75554073
O	1.30537432	-1.29167841	-3.28562397
V	0.01169533	2.76648467	-2.94908575
O	3.80719126	-0.00000000	-4.20839387
V	2.66919438	0.00000000	2.76873512
O	-3.42773481	-1.22458764	-1.55606131
V	-2.75381625	-0.00000000	-2.96258779
O	-0.02177341	-3.80422214	3.94675142
V	-0.02177706	0.00000000	4.03971416
O	1.30537432	1.29167841	-3.28562397
V	0.00975285	-0.00000000	-2.65228826
O	-0.02942698	0.00000000	5.69324476
V	-2.70086501	0.00000000	2.74350087
O	-0.00290412	-0.00000000	-1.01999640
V	2.77854474	-0.00000000	-2.93598188
O	1.25290764	1.27091738	3.27421584
V	-3.99621512	-0.00000000	-0.10235513
O	-3.32230127	-1.22098371	1.30540677
V	3.99258507	-0.00000000	-0.06417935
O	-3.42773481	1.22458764	-1.55606131
O	-3.83964841	-3.83777970	-0.12357474
O	-3.32230127	1.22098371	1.30540677
O	3.83627646	3.83736449	-0.09067523
O	-1.27949915	-1.29325286	-3.30065039
O	-1.21982411	-3.43606751	-1.54720256
O	-1.27949915	1.29325286	-3.30065039
O	1.21289031	3.31358496	1.32622512
O	3.83627646	-3.83736449	-0.09067523
O	0.01800138	-3.79010785	-4.22544007
O	0.01800138	3.79010785	-4.22544007
O	-0.02177341	3.80422214	3.94675142
O	3.78265646	0.00000000	3.96562910
O	1.22969453	-3.43521153	-1.53484084
O	-3.82573192	0.00000000	3.92969548
O	-1.22912542	3.31119698	1.31375272
O	5.61793331	0.00000000	0.00740448
O	-0.00376409	-5.62022089	-0.01835796
O	3.44085922	-1.22465761	-1.52439554
O	-0.00376409	5.62022089	-0.01835796
O	-1.22912542	-3.31119698	1.31375272

γ_1*-$[V_{14}Sb_8O_{42}]^{4-}$			
Sb	-0.19446154	3.69231241	-3.28627062
V	-0.00000000	0.00000000	-2.80774146
V	2.72480235	0.89035598	2.54650992
V	1.80764021	3.46581700	-0.11110135
V	3.88496314	1.19810655	-0.20022661
O	2.75050713	2.19132250	1.05791845
O	2.86428962	2.39816112	-1.41510449
O	2.53084137	4.92303281	-0.01281548
O	-0.77522570	1.75068057	-3.36758274
O	-1.82590741	5.26708708	-0.13877553
O	5.45066475	1.69856473	-0.18178821
O	1.66823456	3.41979288	-3.97682382
O	3.85836215	1.32314066	3.64008372
O	-0.00000000	0.00000000	-1.19474748
O	3.63626493	-0.18103144	1.16701421
V	3.71174919	-1.77604888	0.01392544
O	2.48318167	-2.62348513	-1.25533353
V	2.62936649	-1.31649593	-2.74142702
O	-0.22540940	-3.58165565	-1.30735522
V	-1.80764021	-3.46581700	-0.11110135
O	-2.75050713	-2.19132250	1.05791845
V	-2.72480235	-0.89035598	2.54650992
O	-3.63626493	0.18103144	1.16701421
V	-3.71174919	1.77604888	0.01392544
O	-2.48318167	2.62348513	-1.25533353
V	-2.62936649	1.31649593	-2.74142702
O	0.22540940	3.58165565	-1.30735522
O	0.24117360	3.54676831	1.12485384
Sb	0.66389610	3.60490143	3.11011742
O	0.97712508	1.60127210	3.20282824
V	-0.00000000	0.00000000	3.84306942
O	-1.74895603	0.70902796	3.20269960
Sb	-2.75674745	2.47849385	3.21193374
O	-2.52704877	2.80542040	1.23184854
O	-3.67117108	0.38196156	-1.36017996
Sb	-3.04605062	-2.07832881	-3.39913207
O	-1.86048285	-0.42386760	-3.37973876
Sb	3.04605062	2.07832881	-3.39913207
O	3.67117108	-0.38196156	-1.36017996
O	2.52704877	-2.80542040	1.23184854
Sb	2.75674745	-2.47849385	3.21193374
O	1.74895603	-0.70902796	3.20269960
O	-0.97712508	-1.60127210	3.20282824
Sb	-0.66389610	-3.60490143	3.11011742
O	-0.24117360	-3.54676831	1.12485384
O	-2.86428962	-2.39816112	-1.41510449
Sb	0.19446154	-3.69231241	-3.28627062
O	0.77522570	-1.75068057	-3.36758274
O	1.86048285	0.42386760	-3.37973876
O	5.20582274	-2.46321445	0.03544959
O	3.67435753	-1.89283890	-3.85664994
O	-1.21231888	3.61295860	3.81459778
O	-1.66823456	-3.41979288	-3.97682382
O	-3.67435753	1.89283890	-3.85664994
V	-3.88496315	-1.19810655	-0.20022661
O	-5.45066475	-1.69856473	-0.18178821
O	-2.53084137	-4.92303281	-0.01281548
V	1.33385312	-3.71474661	-0.07256839
O	1.82590741	-5.26708708	-0.13877553
O	-5.20582274	2.46321445	0.03544959
O	1.21231887	-3.61295860	3.81459778
V	-1.33385312	3.71474661	-0.07256839
O	-3.85836215	-1.32314066	3.64008372
O	-0.00000000	0.00000000	5.46980922

γ_2*-$[V_{14}Sb_8O_{42}]^{4-}$			
Sb	0.38036773	-3.65323211	-3.25914405
V	0.02108662	-0.01661835	-4.03322549
V	-2.72286144	-1.05103811	2.58422847
V	-1.64286969	-3.54008839	-0.09302908
V	-3.86805079	-1.45379006	-0.14133530
O	-2.68459084	-2.37321392	1.10488848
O	-2.81542064	-2.59890609	-1.39018367
O	-2.22814499	-5.06008577	-0.00964668
O	0.90304282	-1.69961294	-3.47530092
O	2.08303836	-5.05918429	-0.14140159
O	-5.41947106	-2.00329693	-0.16698545
O	-1.49139684	-3.52440138	-3.95972754
O	-3.80467197	-1.57407594	3.69084635
O	-0.10176116	0.03758237	-5.65644387
O	-3.73988735	-0.05454544	1.23433242
V	-3.83926888	1.52530430	0.06526617
O	-2.56557147	2.41636157	-1.14471519
V	-1.80090127	0.71061614	-1.79668138
O	-0.10574051	3.69230219	-1.25558652
V	1.48930044	3.63404051	-0.09470529
O	2.50416139	2.41900071	1.06737420
V	2.56903100	1.12059114	2.54889568
O	3.55890048	0.12341962	1.17463006
V	3.72054508	-1.45871339	0.02710664
O	2.53567422	-2.37164664	-1.23150422
V	2.65537854	-1.09766632	-2.74511707
O	-0.06449919	-3.47264470	-1.28902292
O	-0.08490710	-3.51272876	1.15093891
Sb	-0.50313306	-3.60497103	3.13203063
O	-0.92619140	-1.62756674	3.21847444
V	-0.06876309	0.03340973	3.86197076
O	1.72181450	-0.54584454	3.21867658
Sb	2.83226974	-2.24594112	3.23804985
O	2.62594301	-2.56800611	1.25506209
O	3.57752673	-0.07323964	-1.34921721
Sb	2.84121732	2.33362446	-3.39226647
O	1.84416047	0.55699719	-3.49652020
Sb	-2.92255263	-2.23539104	-3.37804062
O	-3.59637474	0.10491189	-1.28477125
O	-2.79118428	2.65859975	1.32191695
Sb	-2.97061758	2.32115137	3.30255021
O	-1.87179278	0.61288204	3.26065520
O	0.77992502	1.69564077	3.20384811
Sb	0.37879943	3.67979089	3.17826704
O	-0.03915001	3.66859352	1.19243139
O	2.54221641	2.58055850	-1.41271280
Sb	-0.52052686	3.62552043	-3.24472432
O	-0.78333349	1.62022259	-3.23507437
O	-1.71223019	-0.61735751	-3.27625123
O	-5.37208288	2.11556097	-0.02530400
O	-0.77729606	0.22290643	-0.64142305
O	1.37104999	-3.48651572	3.83100931
O	1.35260795	3.55232981	-3.96794891
O	3.80372497	-1.63695591	-3.77422032
V	3.68572154	1.51091748	-0.20076557
O	5.20614147	2.13936077	-0.21498221
O	2.16854013	5.11562693	-0.03313074
V	-1.63723958	3.66256921	0.03714938
O	-2.30409272	5.14794565	-0.05895670
O	5.25520794	-2.05262960	0.02906772
O	-1.49351059	3.55606924	3.87579767
V	1.48958396	-3.54304142	-0.04690111
O	3.66756366	1.64024668	3.64126882
O	-0.05088625	0.03146456	5.48858476

γ_3*-$[V_{14}Sb_8O_{42}]^{4-}$			
Sb	0.32473663	-3.67614632	-3.21600979
V	-0.11934957	-0.02120055	-3.91358613
V	-2.68629311	-1.13497941	2.66327530
V	-1.59769356	-3.70737685	-0.01663950
V	-2.50296422	-0.98071030	-0.17529916
O	-2.46886335	-2.40435734	1.16456775
O	-2.61845355	-2.56797151	-1.32190019
O	-2.35368337	-5.15285737	0.05350388
O	0.68517626	-1.68296262	-3.18883355
O	2.23303501	-5.16309364	-0.02107745
O	-1.02208266	-0.30966702	-0.25136681
O	-1.55168551	-3.53677642	-3.90815311
O	-3.86445721	-1.66396885	3.66751078
O	-0.05035930	-0.05413586	-5.53878816
O	-3.53537789	-0.09458716	1.21213398
V	-3.88334886	1.48410224	0.08256008
O	-2.74445321	2.46171762	-1.18371428
V	-2.75010017	1.15295510	-2.68522221
O	-0.10975681	3.54872966	-1.23289648
V	1.46727729	3.55281918	-0.03552004
O	2.48571213	2.35451231	1.14533945
V	2.55057002	1.05784580	2.63913540
O	3.53442430	0.05570254	1.27319765
V	3.67694438	-1.52845881	0.12791173
O	2.48566787	-2.44802647	-1.12008874
V	2.50056807	-1.13148952	-2.59532232
O	-0.02461703	-3.78437307	-1.21237464
O	-0.05344130	-3.76133813	1.24134361
Sb	-0.50137322	-3.70348977	3.22805878
O	-0.92214157	-1.71963891	3.37193055
V	-0.06856921	-0.03426801	3.97107236
O	1.71860529	-0.61145569	3.32935676
Sb	2.82183298	-2.31987497	3.33613265
O	2.58568751	-2.63698576	1.35779520
O	3.51832780	-0.13959579	-1.24473075
Sb	2.80498221	2.22475844	-3.31161497
O	1.66835481	0.54512995	-3.26278651
Sb	-3.00853268	-2.29573378	-3.28861800
O	-3.66208714	0.10747791	-1.32093712
O	-2.81193638	2.61605032	1.31314712
Sb	-2.99227093	2.23374172	3.29222692
O	-1.87611852	0.53197001	3.37139331
O	0.75855154	1.62688630	3.28454909
Sb	0.33246428	3.60551563	3.19175968
O	-0.08700073	3.52409278	1.20891655
O	2.60154575	2.56549541	-1.33293591
Sb	-0.50164443	3.65395952	-3.22027751
O	-0.95705385	1.68359996	-3.33834714
O	-1.96749476	-0.54865356	-3.40750863
O	-5.45040910	1.98353762	0.12103194
O	-3.86237355	1.68043602	-3.75921811
O	1.36848160	-3.56917338	3.93524319
O	1.37349151	3.50039190	-3.90606730
O	3.56389657	-1.66172321	-3.71611798
V	3.68262607	1.44437778	-0.10304859
O	5.21715474	2.03858227	-0.09731982
O	2.09154043	5.05710089	0.05660356
V	-1.66768112	3.59020048	0.01349052
O	-2.24725640	5.11336896	-0.04209988
O	5.20968802	-2.12723043	0.12229731
O	-1.54160822	3.48610887	3.88975516
V	1.52437164	-3.69584679	0.04870056
O	3.64633894	1.59286952	3.72629935
O	-0.04494192	-0.01042315	5.59784305

γ_4*-$[V_{14}Sb_8O_{42}]^{4-}$			
Sb	0.43331570	-3.74522039	-3.23593772
V	-0.03217260	-0.09323393	-3.90231484
V	-2.72809865	-1.11228192	2.67041169
V	-1.09473448	-2.52096629	-0.10715294
V	-3.84225842	-1.55876844	-0.07738166
O	-2.58414685	-2.38758499	1.18276847
O	-2.68044119	-2.65935322	-1.29575775
O	-0.49041454	-1.02847318	-0.23632622
O	0.84405630	-1.76451389	-3.29261552
O	2.19087928	-5.23345332	-0.02669111
O	-5.34891034	-2.21889725	-0.08639921
O	-1.45485828	-3.59916169	-3.89730898
O	-3.82495097	-1.66110193	3.75205367
O	-0.03012332	-0.06779684	-5.52873540
O	-3.75215856	-0.15145182	1.29363139
V	-3.83723419	1.42115895	0.13289807
O	-2.61739270	2.30241025	-1.11727404
V	-2.68088480	0.99325971	-2.59875496
O	-0.05432308	3.50968743	-1.20867385
V	1.53319129	3.51804037	-0.02920789
O	2.54419601	2.30436352	1.14537210
V	2.59536608	0.99010421	2.62519210
O	3.59740254	0.00324154	1.25963717
V	3.79310282	-1.57500641	0.11103055
O	2.63783914	-2.52097670	-1.15617324
V	2.62931485	-1.18449355	-2.62868347
O	0.05017770	-3.70297310	-1.24942873
O	0.01189549	-3.53645426	1.17851509
Sb	-0.51411035	-3.69986813	3.13140465
O	-0.94175491	-1.72607150	3.31505371
V	-0.05095860	-0.07310583	3.93243357
O	1.72559354	-0.67624463	3.26604190
Sb	2.83203824	-2.38334039	3.32469643
O	2.73655357	-2.72691904	1.33350304
O	3.60587168	-0.18424990	-1.25624566
Sb	2.85053733	2.19859969	-3.31587095
O	1.76457348	0.48323437	-3.28480524
Sb	-2.92681106	-2.37838272	-3.28722072
O	-3.70853382	0.01668534	-1.23309177
O	-2.72054972	2.52107414	1.35812157
Sb	-2.93067476	2.26081128	3.34798120
O	-1.86052790	0.53299154	3.35452400
O	0.80497290	1.58023215	3.26664940
Sb	0.42513410	3.56997618	3.20561902
O	-0.01565547	3.51132810	1.22667939
O	2.64238875	2.51106576	-1.33247920
Sb	-0.48759820	3.55029225	-3.19040321
O	-0.88433122	1.56516009	-3.23706832
O	-1.84622886	-0.66603584	-3.31088178
O	-5.35477967	2.05694263	0.10893752
O	-3.76615251	1.53160088	-3.69391286
O	1.34657730	-3.61441928	3.87906178
O	1.38023086	3.43129110	-3.90454379
O	3.72614267	-1.67451714	-3.73475144
V	3.74105775	1.39891394	-0.10883872
O	5.27079355	2.00524142	-0.10241502
O	2.17174124	5.01656861	0.05262097
V	-1.60548363	3.51718170	0.04743681
O	-2.24181679	5.01533840	-0.04064310
O	5.34317958	-2.12778804	0.11076674
O	-1.44594360	3.48552424	3.91621142
V	1.61145288	-3.70923600	0.01594659
O	3.68505246	1.49563601	3.73255859
O	-0.01329260	-0.07290883	5.55841214

α-$[V_{14}Sb_8O_{42}]^{4-}$			
Sb	0.98821602	3.54621144	-3.33509803
V	-0.00000000	0.00000000	-3.92890497
V	2.00306181	2.00306181	2.56818900
V	-0.00000000	3.94111904	0.00000000
V	2.86045830	2.86045830	-0.18096994
O	1.42827718	3.20407435	1.11263612
O	1.38956567	3.45997163	-1.35848342
O	-0.00000000	5.57588633	0.00000000
O	-0.14987211	1.86488965	-3.27145206
V	-2.86045830	2.86045830	0.18096994
O	4.01847943	4.01847943	-0.09707146
O	2.67436455	2.67436455	-3.97967275
O	2.88399356	2.88399356	3.62236830
O	-0.00000000	0.00000000	-5.55497723
O	3.20407435	1.42827718	1.11263612
V	3.94111904	0.00000000	0.00000000
O	3.20407435	-1.42827718	-1.11263612
V	2.00306181	-2.00306181	-2.56818900
O	1.42827718	-3.20407435	-1.11263612
V	-0.00000000	-3.94111904	0.00000000
O	-1.42827718	-3.20407435	1.11263612
V	-2.00306181	-2.00306181	2.56818900
O	-3.20407435	-1.42827718	1.11263612
V	-3.94111904	0.00000000	0.00000000
O	-3.20407435	1.42827718	-1.11263612
V	-2.00306181	2.00306181	-2.56818900
O	-1.42827718	3.20407435	-1.11263612
O	-1.38956567	3.45997163	1.35848342
Sb	-0.98821602	3.54621144	3.33509803
O	0.14987211	1.86488965	3.27145206
V	-0.00000000	0.00000000	3.92890497
O	-1.86488965	-0.14987211	3.27145206
Sb	-3.54621144	0.98821602	3.33509803
O	-3.45997163	1.38956567	1.35848342
O	-3.45997163	-1.38956567	-1.35848342
Sb	-3.54621144	-0.98821602	-3.33509803
O	-1.86488965	0.14987211	-3.27145206
Sb	3.54621144	0.98821602	-3.33509803
O	3.45997163	1.38956567	-1.35848342
O	3.45997163	-1.38956567	1.35848342
Sb	3.54621144	-0.98821602	3.33509803
O	1.86488965	0.14987211	3.27145206
O	-0.14987211	-1.86488965	3.27145206
Sb	0.98821602	-3.54621144	3.33509803
O	1.38956567	-3.45997163	1.35848342
O	-1.38956567	-3.45997163	-1.35848342
Sb	-0.98821602	-3.54621144	-3.33509803
O	0.14987211	-1.86488965	-3.27145206
O	1.86488965	-0.14987211	-3.27145206
O	-5.57588633	0.00000000	0.00000000
O	2.88399356	-2.88399356	-3.62236830
O	-2.67436455	2.67436455	3.97967275
O	-2.67436455	-2.67436455	-3.97967275
O	5.57588633	0.00000000	0.00000000
V	-2.86045830	-2.86045830	-0.18096994
O	-4.01847943	-4.01847943	-0.09707146
O	-0.00000000	-5.57588633	0.00000000
V	2.86045830	-2.86045830	0.18096994
O	4.01847943	-4.01847943	0.09707146
O	-2.88399356	2.88399356	-3.62236830
O	2.67436455	-2.67436455	3.97967275
O	-4.01847943	4.01847943	0.09707146
O	-2.88399356	-2.88399356	3.62236830
O	-0.00000000	0.00000000	5.55497723

β-$[V_{14}Sb_8O_{42}]^{4-}$				*γ*-$[V_{14}Sb_8O_{42}]^{4-}$			
Sb	4.53781017	0.00000000	-1.79771358	Sb	0.43137630	-3.64595155	-3.20715804
O	1.48717542	3.20497255	1.42816433	V	-0.00000000	0.00000000	-3.93280477
Sb	-4.53781017	0.00000000	1.79771358	V	-2.64186751	-1.09688964	2.63266132
O	-3.20497255	-1.48717542	-1.42816433	V	-1.56845985	-3.60607348	-0.03669544
Sb	4.53781017	0.00000000	1.79771358	V	-3.77715146	-1.48759533	-0.11255422
O	-3.20497255	1.48717542	-1.42816433	O	-2.57293738	-2.38961264	1.13584608
Sb	-4.53781017	0.00000000	-1.79771358	O	-2.68241662	-2.59770452	-1.34004567
O	2.69907709	-2.69907709	-4.06344634	O	-2.20059314	-5.10638385	0.04496396
Sb	0.00000000	-4.53781017	-1.79771358	O	0.84308896	-1.66199445	-3.26498691
O	-1.48717542	3.20497255	1.42816433	O	2.20059314	-5.10638385	-0.04496396
Sb	0.00000000	4.53781017	1.79771358	O	-5.30823232	-2.08778978	-0.10183468
O	-3.20497255	1.48717542	1.42816433	O	-1.43792294	-3.51538030	-3.91046512
Sb	0.00000000	-4.53781017	1.79771358	O	-3.73356254	-1.62775508	3.72483470
O	1.79691742	0.00000000	3.36416363	O	-0.00000000	0.00000000	-5.55914164
Sb	0.00000000	4.53781017	-1.79771358	O	-3.62425436	-0.09435739	1.26058855
O	0.00000000	-1.79691742	3.36416363	V	-3.77715146	1.48759533	0.11255422
V	1.90850751	1.90850751	-2.87356768	O	-2.57293738	2.38961264	-1.13584608
O	0.00000000	1.79691742	3.36416363	V	-2.64186751	1.09688964	-2.63266132
V	-1.90850751	-1.90850751	2.87356768	O	-0.01666976	3.58420760	-1.21928358
O	0.00000000	-5.42681011	0.00000000	V	1.56845985	3.60607348	-0.03669544
V	2.80606170	2.80606170	0.00000000	O	2.57293738	2.38961264	1.13584608
O	-1.48717542	-3.20497255	-1.42816433	V	2.64186751	1.09688964	2.63266132
V	-2.80606170	-2.80606170	0.00000000	O	3.62425436	0.09435739	1.26058855
O	3.95461417	-3.95461417	0.00000000	V	3.77715146	-1.48759533	0.11255422
V	1.90850751	1.90850751	2.87356768	O	2.57293738	-2.38961264	-1.13584608
O	0.00000000	1.79691742	-3.36416363	V	2.64186751	-1.09688964	-2.63266132
V	-1.90850751	-1.90850751	-2.87356768	O	0.01666976	-3.58420760	-1.21928358
O	-2.69907709	2.69907709	-4.06344634	O	-0.01666976	-3.58420760	1.21928358
V	-1.90850751	1.90850751	2.87356768	Sb	-0.43137630	-3.64595155	3.20715804
O	3.20497255	-1.48717542	-1.42816433	O	-0.84308896	-1.66199445	3.26498691
V	1.90850751	-1.90850751	-2.87356768	V	-0.00000000	0.00000000	3.93280477
O	2.69907709	2.69907709	4.06344634	O	1.79742359	-0.57149724	3.30357783
V	0.00000000	0.00000000	4.13627063	Sb	2.90371169	-2.27703000	3.32164155
O	-1.79691742	0.00000000	-3.36416363	O	2.68241662	-2.59770452	1.34004567
V	0.00000000	0.00000000	-4.13627063	O	3.62425436	-0.09435739	-1.26058855
O	0.00000000	0.00000000	5.78652738	Sb	2.90371169	2.27703000	-3.32164155
V	1.90850751	-1.90850751	2.87356768	O	1.79742359	0.57149724	-3.30357783
O	0.00000000	0.00000000	-5.78652738	Sb	-2.90371169	-2.27703000	-3.32164155
V	-1.90850751	1.90850751	-2.87356768	O	-3.62425436	0.09435739	-1.26058855
O	-1.79691742	0.00000000	3.36416363	O	-2.68241662	2.59770452	1.34004567
V	2.80606170	-2.80606170	0.00000000	Sb	-2.90371169	2.27703000	3.32164155
O	3.20497255	-1.48717542	1.42816433	O	-1.79742359	0.57149724	3.30357783
V	-2.80606170	2.80606170	0.00000000	O	0.84308896	1.66199445	3.26498691
O	1.48717542	-3.20497255	-1.42816433	Sb	0.43137630	3.64595155	3.20715804
O	5.42681011	0.00000000	0.00000000	O	0.01666976	3.58420760	1.21928358
O	1.48717542	-3.20497255	1.42816433	O	2.68241662	2.59770452	-1.34004567
O	-5.42681011	0.00000000	0.00000000	Sb	-0.43137630	3.64595155	-3.20715804
O	1.79691742	0.00000000	-3.36416363	O	-0.84308896	1.66199445	-3.26498691
O	3.20497255	1.48717542	-1.42816433	O	-1.79742359	-0.57149724	-3.30357783
O	0.00000000	-1.79691742	-3.36416363	O	-5.30823232	2.08778978	0.10183468
O	-3.20497255	-1.48717542	1.42816433	O	-3.73356254	1.62775508	-3.72483470
O	0.00000000	5.42681011	0.00000000	O	1.43792294	-3.51538030	3.91046512
O	2.69907709	2.69907709	-4.06344634	O	1.43792294	3.51538030	-3.91046512
O	-2.69907709	-2.69907709	-4.06344634	O	3.73356254	-1.62775508	-3.72483470
O	-2.69907709	-2.69907709	4.06344634	V	3.77715146	1.48759533	-0.11255422
O	-2.69907709	2.69907709	4.06344634	O	5.30823232	2.08778978	-0.10183468
O	1.48717542	3.20497255	-1.42816433	O	2.20059314	5.10638385	0.04496396
O	2.69907709	-2.69907709	4.06344634	V	-1.56845985	3.60607348	0.03669544
O	-1.48717542	-3.20497255	1.42816433	O	-2.20059314	5.10638385	-0.04496396
O	-3.95461417	3.95461417	0.00000000	O	5.30823232	-2.08778978	0.10183468
O	3.95461417	3.95461417	0.00000000	O	-1.43792294	3.51538030	3.91046512
O	-1.48717542	3.20497255	-1.42816433	V	1.56845985	-3.60607348	0.03669544
O	-3.95461417	-3.95461417	0.00000000	O	3.73356254	1.62775508	3.72483470
O	3.20497255	1.48717542	1.42816433	O	-0.00000000	0.00000000	5.55914164

References

(1) te Velde, G.; Bickelhaupt, F. M.; Baerends, E. J.; Fonseca Guerra, C.; Van Gísbergen, S. J. A.; Snijders, J. G.; Ziegler, T. *J. Comput. Chem.* **2001**, *22*, 931–967.

(2) ADF **2014**, SCM, Theoretical Chemistry, Vrije Univesity, Amsterdam, The Netherlands, http://www.scm.com/

(3) Becke, A. D. *J. Chem. Phys.* **1988**, *88*, 2547–2553.

(4) Franchini, M.; Philipsen, P. H. T.; Visscher, L. *J. Comput. Chem.* **2013**, *34*, 1819–1827.

(5) Becke, A. D. *Phys. Rev. A: At., Mol., Opt. Phys.* **1988**, *38*, 3098–3100.

(6) Perdew, J. *Phys. Rev. B: Condens. Matter Mater. Phys.* **1986**, *33*, 8822–8824.

(7) van Lenthe, E.; Baerends, E. J. *J. Comput. Chem.* **2003**, *24*, 1142–1156.

(8) van Lenthe, E.; Baerends, E. J.; Snijders, J. G. *J. Chem. Phys.* **1993**, *99*, 4597–4610.

(9) van Lenthe, E.; Baerends, E. J.; Snijders, J. G. *J. Chem. Phys.* **1994**, *101*, 9783–9792.

(10) van Lenthe, E.; Ehlers, A.; Baerends, E. *J. Chem. Phys.* **1999**, *110*, 8943–8953.

(11) Klamt, A. *J. Phys. Chem.* **1995**, *99*, 2224–2235.

(12) Pye, C. C.; Ziegler, T. *Theor. Chem. Acc.* **1999**, *101*, 396–408.

(13) Stephens, P. J.; Devlin, F. J.; Chabalowski, C. F.; Frisch, M. J. *J. Phys. Chem.* **1994**, *98*, 11623–11627.

(14) Aparicio, P. A.; López, X.; Poblet, J. M. *J. Mol. Eng. Mater.* **2014**, *2*, 1440004.

(15) Rodriguez-Fortea, A.; de Graaf, C.; Poblet, J. M. *Chem. Phys. Lett.* **2006**, *428*, 88–92.

(16) Kondinski, A.; Heine, T.; Monakhov, K. Y. *Inorg. Chem.* **2016**, *55*, 3777–3788.

(17) Baker, L. C. W.; Figgis, J. S. *J. Am. Chem. Soc.* **1970**, *92*, 3794–3797.

(18) Pope, M. T. *Heteropoly and Isopoly Oxometalates*, Springer-Verlag, Berlin, **1983**.

(19) Wendt, M.; Warzok, U.; Näther, C.; van Leusen, J.; Kögerler, P.; Schalley, C. A.; Bensch, W. *Chem. Sci.* **2016**, *7*, 2684–2694.

(20) van Leusen, J.; Speldrich, M.; Schilder, H.; Kögerler, P. *Coord. Chem. Rev.* **2015**, *289-290*, 137–148.

7.3 Supporting Information der Publikation „*Ordnung muss sein: hetero-element order and disorder in polyoxovanadates*"

Electronic Supplementary Material (ESI) for Dalton Transactions.

Ordnung muss sein: heteroelement order and disorder in polyoxovanadates

M. Wendt[a], L. K. Mahnke[a], C. Näther[a], J. van Leusen[b], P. Kögerler[b] and W. Bensch[a]

Content

[a] Dr. Michael Wendt, M. Sc. L. K. Mahnke, Prof. Dr. C. Näther, Prof. Dr. W. Bensch
Institut für Anorganische Chemie
Christian-Albrechts-Universität zu Kiel, 24118 Kiel, Germany
E-mail: wbensch@ac.uni-kiel.de

[b] Dr. Jan van Leusen, Prof. Dr. P. Kögerler
Institut für Anorganische Chemie
RWTH Aachen University, 52074 Aachen, Germany
E-mail: paul.koegerler@ac.rwth-aachen.de

Syntheses

General: The purchased chemicals ($NiCl_2 \cdot 6H_2O$, NH_4VO_3, Sb_2O_3 (Merck), GeO_2 (ABCR), diethylenetriamine (Acros), ethylenediamine (Fluka) and phenanthroline (ABCR)) were used without further purifications. The solvothermal reactions of **1** and **2** were performed in DURAN® glass tubes with an inner volume of 11 mL for 7 d at 150 °C. The products consisting of brown crystals were filtered off and washed with water after cooling to room temperature.

*Synthesis of $\{Ni(en)_3\}_3[H_4V_{15}Sb_2Ge_4O_{46}]\cdot en\cdot\approx 10H_2O$ (**1**):*

Compound **1** was obtained by using a solution of 1.7 mL ethylendiamine and 2.3 mL H_2O was given to a mixture of 0.1256 g (1.07 mmol) NH_4VO_3, 0.1234 g (0.423 mmol) Sb_2O_3, 0.0442 g (0.423 mmol) GeO_2 and 0.1251 g (0.526 mmol) $NiCl_2 \cdot 6H_2O$ (pH > 13). Yield based on V was 67 %. Elemental analyses: C 8.00, H 3.25, N 9.92 %; calc. for $C_{20}H_{104}Ge_4N_{20}Ni_3O_{56}Sb_2V_{15}$: C 8.02, H 3.50, N 9.35 %.

EDX ratio: 4.0 (Ge, 16.7 at%) : 3.0 (Ni, 12.5 at%) : 2.0 (Sb, 14.8 at%) : 15.0 (V, 62.5 at%)

*Synthesis of $\{Ni(en)_3\}_3[H_3V_{15}Sb_3Ge_3O_{45}]\cdot\approx 15H_2O$ (**2**):*

A solution of 1.7 mL ethylenediamine and 2.3 mL H_2O were given to a mixture of 0.0944 g (0.800 mmol) NH_4VO_3, 0.0920 g (0.315 mmol) Sb_2O_3, 0.0330 g (0.315 mmol) GeO_2 and 0.0936 g (0.393 mmol) $NiCl_2 \cdot 6H_2O$ (pH > 13) afforded crystallization of **2**. Yield based on V was 88 %. Elemental analyses: C 7.17, H 3.29, N 8.54 %; calc. for $C_{18}H_{105}Ge_3N_{18}Ni_3O_{60}Sb_3V_{15}$: C 7.07, H 3.46, N 8.25 %.

EDX ratio: 3.0 (Ge, 12.5 at%) : 3.0 (Ni, 12.5 at%) : 3.0 (Sb, 12.5 at%) : 15.0 (V, 62.5 at%)

*Synthesis of $\{Ni(en_3)\}_3[V_{15}Ge_3Sb_3O_{45}]\cdot\approx 9H_2O$ (**3**)*

Compound **3** was obtained using the precursor compound $\{Ni(en)_3\}_3[V_{15}Sb_6O_{42}(H_2O)_x]\cdot ca.15H_2O$ (**4**). **4** was synthesized using the published protocol.[ii] 0.1461 g (0.048 mmol) of the precursor compound **4** were mixed with 0.0222 g (0.212 mmol) GeO_2 (Fluka) and a solution of 3.9 mL dist. water and 0.1 mL ethylenediamine (pH ≈ 11). The mixture was heated for 24 h at 150°C. The product was washed with dist. water and ethanol. The brown crystals have been cleaned by sonication in ethanol. Yield based on V: 46 %. Elemental analyses: C 7.00, H 3.00, N 7.92 %; calc. for $C_{18}H_{101}Ge_3N_{18}Ni_3O_{58}Sb_3V_{15}$: C 7.16, H 3.37, N 8.34 %.

EDX ratio: 3.0 (Ge, 12.3 at%) : 3.3 (Ni, 13.1 at%) : 3.6 (Sb, 14.8 at%) : 14.6 (V, 59.8 at%)

Characterization Methods

X-ray powder patterns were recorded on a STOE Stadi-P powder diffractometer with a Ge monochromator with $Cu_{K\alpha1}$ radiation and a Mythen 1k detector.

A EURO EA elemental analyzer of EURO VECTOR instruments was used for elemental analysis.

DTA-TG measurements were done in Al_2O_3 crucibles with a Netzsch STA 409 CD under a nitrogen flow of 75 mL min^{-1} at a heating rate of 4K min^{-1}.

A Philips Environmental Scanning Electron Microscope ESEM XL30 equipped with an EDX detector enabled investigations for energy dispersive X-ray analyses (EDX).

A Genesis FTIRTM spectrometer from ATI Mattson was used for collecting IR spectra in the range from 400 to 4000 cm^{-1}.

Magnetic data of **1-3** were collected using a Quantum Design MPMS-5XL SQUID magnetometer. Samples were compacted and immobilized into cylindrical PTFE capsules. Temperature-dependent data were recorded in the range 2.0 – 290 K at 0.1 T, and field dependent data in the range 0 – 5.0 T at 2.0 K. The data were corrected for the diamagnetic contributions of both the sample holders and the compounds ($\chi_{m,dia}$ / 10^{-3} cm^3 mol^{-1} = –1.50 (**I**), –1.53 (**II**), –1.88 (**III**)).

Tab. S 1: EDX Data of compounds **1-3**.

	V [at%]	**Sb [at%]**	**Ge [at%]**	**Ni [at%]**
$[V_{15}Sb_2Ge_4Ni_3]$ (1)	62.51	8.33	16.66	12.50
$[V_{15}Sb_3Ge_3Ni_3]$ (2)	62.51	12.50	12.50	12.50
$[V_{15}Sb_3Ge_3Ni_2]$ (3)	59.80	14.80	12.30	13.10

Tab. S 2: BVS calculations for determination of the oxidations state of V for compounds **1-3** With b = 0.37 and R0 for V-O = 1.773.[1]

$\{Ni(en)_3\}_3[H_4V_{15}Sb_2Ge_4O_{46}] \cdot en$ (I)

	distances	exp[(R0-R)/b]
V(1)-O	1.613	1.54
	1.916	0.68
	1.934	0.65
	1.968	0.59
	2.008	0.53
		3.99
V(2)-O	1.621	1.51
	1.914	0.68
	1.916	0.68
	1.973	0.58
	1.982	0.57
		4.02
V(3)-O	1.607	1.57
	1.923	0.67
	1.941	0.64
	1.959	0.60
	2.019	0.51
		3.99
V(4)-O	1.612	1.55
	1.913	0.68
	1.944	0.63
	1.959	0.60
	2.003	0.54
		4.00
V(5)-O	1.607	1.57
	1.929	0.66
	1.943	0.63
	1.966	0.59
	1.997	0.55
		3.99
V(6)-O	1.607	1.57
	1.91	0.69
	1.941	0.64
	1.992	0.55
	2.005	0.53
		3.98

$\{Ni(en)_3\}_3[H_3V_{15}Sb_3Ge_3O_{46}]$ (II)

	distances	exp[(R0-R)/b]
V(1)-O	1.62	1.53
	1.94	0.64
	1.94	0.64
	1.95	0.61
	2.00	0.54
		3.97
V(2)-O	1.61	1.55
	1.93	0.66
	1.94	0.64
	2.01	0.52
	1.98	0.57
		3.93
V(3)-O	1.61	1.54
	1.92	0.67
	1.94	0.63
	1.94	0.63
	1.98	0.57
		4.04
V(4)-O	1.63	1.48
	1.91	0.69
	1.94	0.64
	1.97	0.58
	1.99	0.55
		3.95
V(5)-O	1.61	1.56
	1.92	0.68
	1.94	0.64
	1.98	0.57
	1.99	0.56
		4.02
V(6)-O	1.62	1.53
	1.92	0.67
	1.92	0.66
	1.99	0.56
	1.99	0.56
		3.98

$\{Ni(en)_3\}_3[H_3V_{15}Sb_3Ge_3O_{46}]$ (III)

	distances	exp[(R0-R)/b]
V(1)-O	1.615	1.53
	1.948	0.62
	1.954	0.61
	1.958	0.61
	2.001	0.54
		3.92
V(2)-O	1.603	1.58
	1.925	0.66
	1.932	0.65
	1.955	0.61
	2.011	0.53
		4.03
V(3)-O	1.606	1.57
	1.927	0.66
	1.932	0.65
	1.965	0.60
	2.002	0.54
		4.01
V(4)-O	1.596	1.61
	1.91	0.69
	1.947	0.62
	1.974	0.58
	2.016	0.52
		4.03
V(5)-O	1.603	1.58
	1.911	0.69
	1.954	0.61
	1.954	0.61
	2.015	0.52
		4.02
V(6)-O	1.608	1.56
	1.922	0.67
	1.95	0.62
	1.976	0.58
	2.006	0.53
		3.96

V(7)-O	1.609	1.56
	1.936	0.64
	1.936	0.64
	1.943	0.63
	2.025	0.51
		3.98

V(7)-O	1.62	1.51
	1.92	0.67
	1.93	0.65
	1.95	0.61
	2.01	0.53
		3.97

V(7)-O	1.597	1.61
	1.925	0.66
	1.934	0.65
	1.978	0.57
	1.979	0.57
		4.07

V(8)-O	1.609	1.56
	1.909	0.69
	1.941	0.64
	1.98	0.57
	2.007	0.53
		3.99

V(8)-O	1.61	1.56
	1.93	0.66
	1.93	0.66
	2.00	0.55
	2.00	0.55
		3.98

V(8)-O	1.607	1.57
	1.922	0.67
	1.937	0.64
	1.948	0.62
	2.006	0.53
		4.03

V(9)-O	1.611	1.55
	1.935	0.65
	1.944	0.63
	1.952	0.62
	2.021	0.51
		3.95

V(9)-O	1.607	1.57
	1.939	0.64
	1.943	0.63
	1.943	0.63
	1.998	0.54
		4.01

V(10)-O	1.621	1.51
	1.91	0.69
	1.932	0.65
	1.953	0.61
	1.988	0.56
		4.02

V(10)-O	1.616	1.53
	1.896	0.72
	1.921	0.67
	1.966	0.59
	1.998	0.54
		4.05

V(11)-O	1.597	1.61
	1.936	0.64
	1.936	0.64
	1.986	0.56
	1.997	0.55
		4.00

V(11)-O	1.605	1.57
	1.927	0.66
	1.945	0.63
	1.973	0.58
	1.999	0.54
		3.99

V(12)-O	1.608	1.56
	1.936	0.64
	1.936	0.64
	1.964	0.60
	2.022	0.51
		3.96

V(12)-O	1.625	1.49
	1.909	0.69
	1.953	0.61
	1.954	0.61
	2.024	0.51
		3.92

V(13)-O	1.62	1.51
	1.916	0.68
	1.936	0.64
	1.972	0.58
	1.997	0.55
		3.97

V(13)-O	1.608	1.56
	1.912	0.69
	1.917	0.68
	1.989	0.56
	2.012	0.52
		4.01

5

V(14)-O	1.624	1.50
	1.929	0.66
	1.935	0.65
	1.957	0.61
	1.994	0.55
		3.96

V(14)-O	1.606	1.57
	1.93	0.65
	1.949	0.62
	1.95	0.62
	2.028	0.50
		3.97

V(15)-O	1.611	1.55
	1.909	0.69
	1.952	0.62
	1.978	0.57
	2	0.54
		3.97

V(15)-O	1.61	1.55
	1.924	0.66
	1.934	0.65
	1.958	0.61
	1.962	0.60
		4.07

Tab. S 3: BVS calculations for determination of the oxidations state of the O-H groups for compounds **1-3** with b = 0.94 and R0 for O-H = 0.569. [i]

$\{Ni(en)_3\}_3[H_4V_{15}Sb_2Ge_4O_{46}] \cdot en$ (I)

	distances	*exp[(R0-R)/b]*
O(4)-X	1.701	1.22
	0.7	0.87
		2.09
O(11)-X	1.733	1.12
	0.7	0.87
		1.99
O(18)-X	1.65	1.40
	0.7	0.87
		2.27
O(14)-X	1.546	1.86
	0.7	0.87
		2.73

$\{Ni(en)_3\}_3[H_3V_{15}Sb_3Ge_3O_{45}]$ (II)

	distances	*exp[(R0-R)/b]*
O(1)-X	1.712	1.19
	0.7	0.87
		2.06
O(2)-X	1.731	1.13
	0.7	0.87
		2.00
O(3)-X	1.692	1.25
	0.7	0.87
		2.12

$\{Ni(en)_3\}_3[H_3V_{15}Sb_3Ge_3O_{45}]$ (III)

	distances	*exp[(R0-R)/b]*
O(6)-X	1.657	1.38
	0.7	0.87
		2.25
O(12)-X	1.637	1.45
	0.7	0.87
		2.32
O(18)-X	1.672	1.32
	0.7	0.87
		2.19

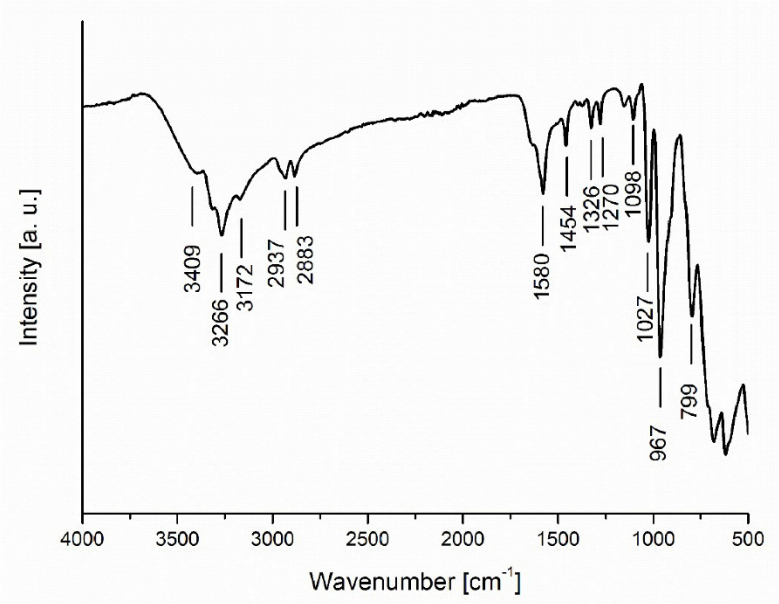

Fig. S 1: IR spectrum of compound **1**.

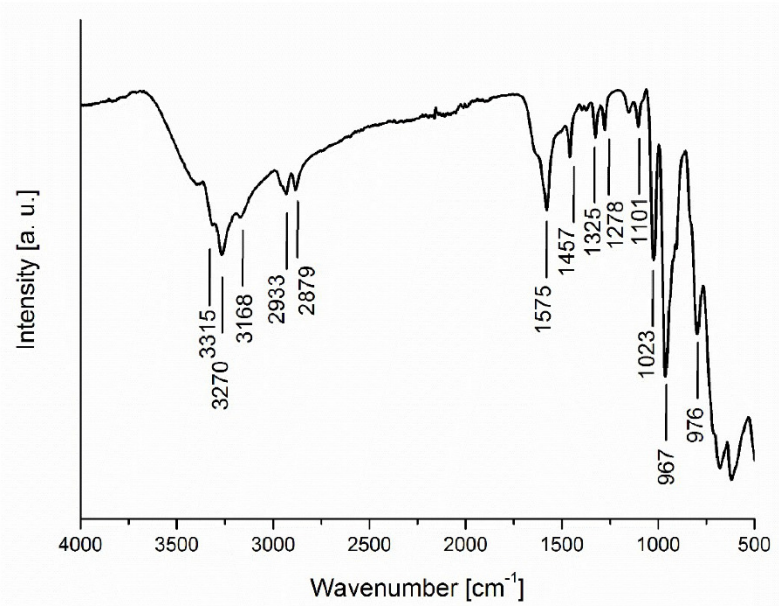

Fig. S 2: IR spectrum of compound **2**.

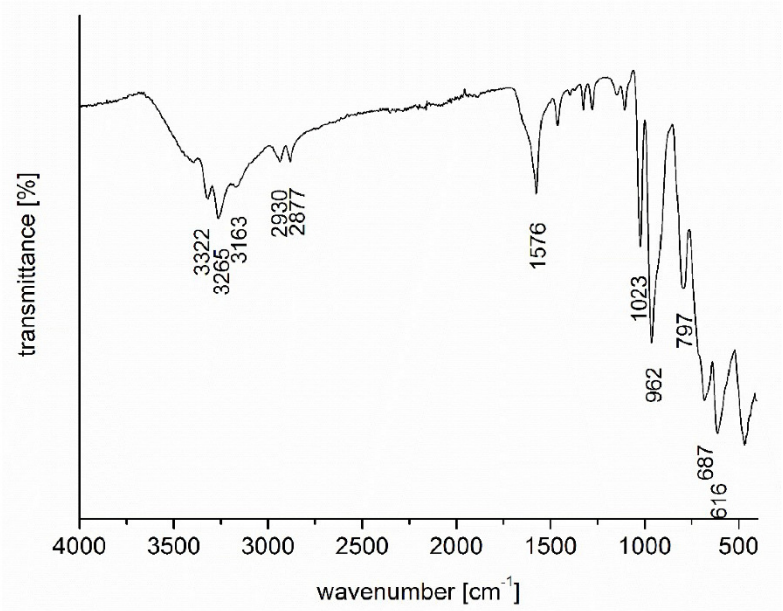

Fig. S 3: IR spectrum of compound **3**.

Tab. S 4: Selected data of data acquisition and crystal structure refinement results for **1-3**.

	1	**2**	**3**
Formula	$C_{20}H_{84}Ge_4N_{20}Ni_3O_{46}Sb_2V_{15}$	$C_{18}H_{75}Ge_3N_{18}Ni_3O_{45}Sb_3V_{15}$	$C_{18}H_{93}Ge_3N_{18}Ni_3O_{54}Sb_3V_{15}$
MW / g·mol^{-1}	2815.16	2787.21	2949.35
crystal system	monoclinic	monoclinic	monoclinic
space group	$P2_1$	$C2$	$P2_1$
***a* /Å**	12.6027(7)	18.1983(12)	14.9473(3)
***b* / Å**	26.4698(17)	22.7116(15)	18.8080(3)
***c* / Å**	15.1116(9)	14.4488(10)	16.1556(3)
***α* / °**	90	90	90
***β* / °**	114.801(6)	126.600(6)	112.6160(10)
***γ* / °**	90	90	90
***V* / Å^3**	4576.2(5)	4794.3(6)	4192.55(14)
***T* / K**	200	200	170
Z	2	2	2
***Density* / Mg/m^3**	2.043	1.931	2.336
***μ* / mm^{-1}**	4.005	3.787	4.343
θ_{max} / °	26.98	27.996	28.003
measured refl.	32887	29983	51412
unique refl.	19699	11322	17911
R_{int}	0.0292	0.0563	0.0568
refl. with $F_0>4\sigma(F_0)$	18236	10041	16811
Parameters	1003	512	1104
$R_1[F_0>4\sigma(F_0)]$	0.0344	0.0314	0.0469
wR_2 **(all refl.)**	0.0873	0.0775	0.1181
GOF	1.037	0.996	1.025
$\Delta\rho_{max/min}$ /e·Å^{-3}	1.830, -1.833	0.721, -0.690	2.251/-1.978
Flack x parameter	-	0.017(8)	-
BASF parameter	0.038(11)	-	0.12(2)

Single crystal X-ray analysis

The data were measured using an Imaging Plate Diffraction System (IPDS-2) from STOE, Germany with MoKα-radiation. For all compounds a numerical absorption correction was performed. The structure were solved with SHELXT and refined using SHELXL-2014. All non-hydrogen atoms, except the O atoms of lower occupancy connected to the Ge atoms in **1** and **2** were refined anisotropic. The C-H and N-H H atoms were positioned with idealized geometry and refined isotropic with $U_{iso}(H) = 1.2U_{eq}(C)$ using a riding model. In all compounds the O-H H atoms were not located but considered in the calculation of the formula and the molecular mass. In compound **3**, some of the ethylenediamine molecules are disordered and were refined using a split model. For this compound the Flack-x parameter is close to 0, but not within the estimated standard deviation. Therefore, a twin-refinement was performed, which was also performed for compound **1**. In compound **1** and **2**, some of the Ge and Sb atoms occupy the same crystallographic positions. In the

beginning the site occupation factor was refined but finally it was fixed to the refined values. In both of these compounds there are also additional water molecules that are disordered and for which no reasonable structure model was found. Therefore, the data were corrected for disordered solvent using the Squeeze option in Platon. For compound **1** a void volume of 824.5 Å^3 is calculated which can host ≈ 10 H_2O molecules per formula unit. For **2**, the calculated void space is 1202 Å^3 which is large enough for 15 water molecules per formula unit.

CCDC 1503959 (Compound **1**), CCDC 1503958 (Compound **2**) and CCDC 1820425 (Compound **3**) contain the supplementary crystallographic data for this paper. These data can be obtained free charge from the Cambridge Crystallographic Data Centre via http://www.ccdc.cam.ac.uk/data_request/cif.

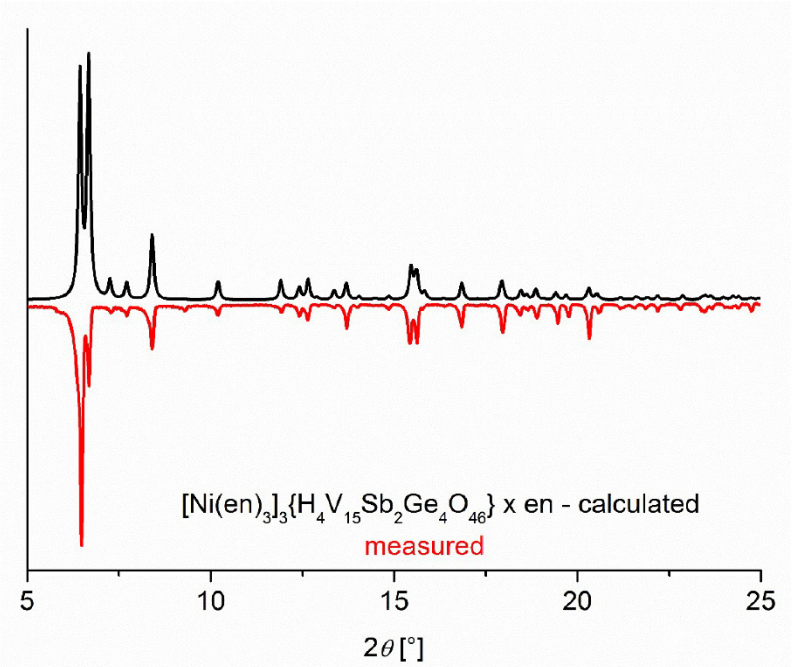

Fig. S 4: Powder pattern of compound **1** compared with calculated Data.

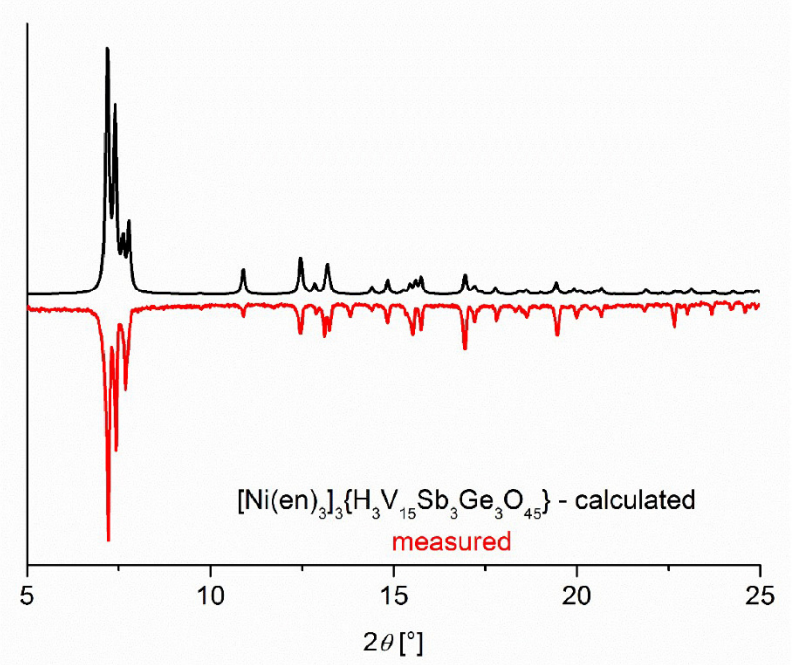

Fig. S 5: Powder pattern of compound **2** compared with calculated Data.

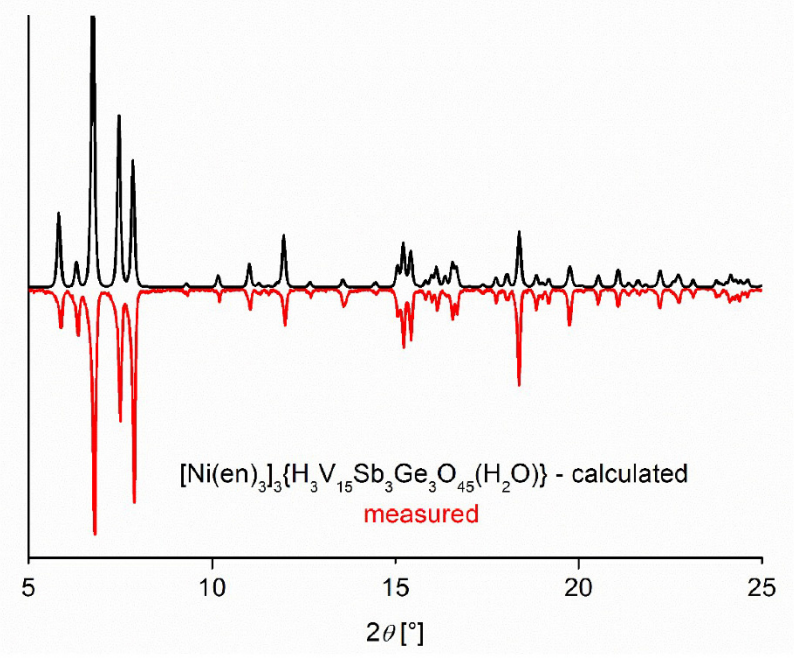

Fig. S 6: Powder pattern of compound **3** compared with calculated Data.

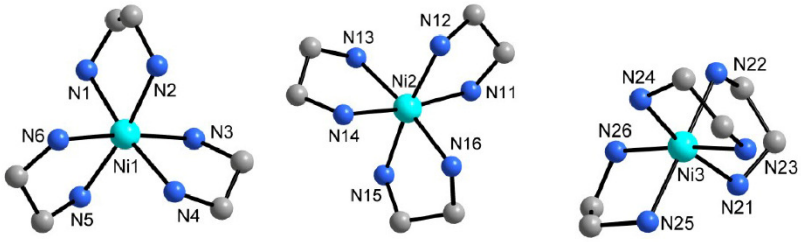

Fig. S 7: View of the three different $[Ni(en)_3]^{2+}$ complexes in compound **1**; all of the complexes are Λ-isomers. Grey spheres represent C atoms; H atoms are omitted for clarity.

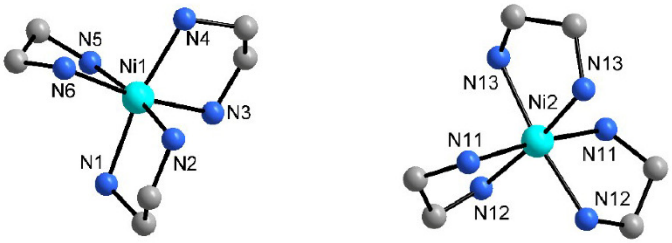

Fig. S 8: The two isomeric structures of $[Ni(en)_3]^{2+}$ of compound **2**: left: Δ-isomer, right: Λ- isomer. Grey: C atoms; H atoms are omitted for clarity. Only selected atoms are labeled.

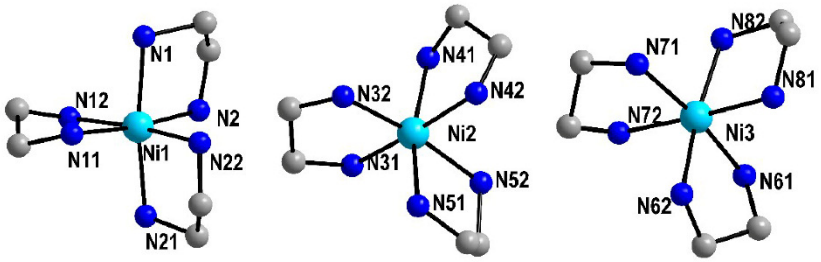

Fig. S 9: View of the three different $[Ni(en)_3]^{2+}$ complexes in compound **3**; Ni(1) is a Δ-isomer and Ni(2) and Ni(3) are Λ-isomers. Grey: C atoms; H atoms are omitted for clarity. Only selected atoms are labeled.

Tab. S 5: Selected bond lengths [Å] for the anion in compound **1**.

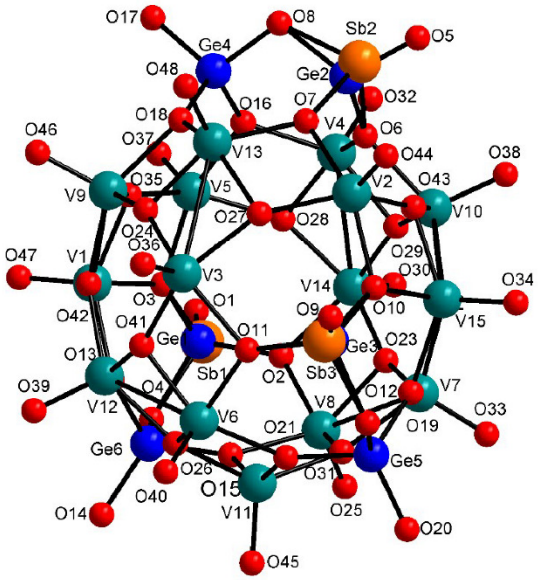

Sb(1)-O(2)	1.966(5)	V(5)-O(37)	1.613(6)
Sb(1)-O(4)	1.970(6)	V(5)-O(35)	1.927(5)
Sb(1)-O(3)	2.044(5)	V(5)-O(28)	1.942(5)
Sb(1)-N(31)	2.507(11)	V(5)-O(3)	1.963(6)
Sb(2)-O(8)	1.957(6)	V(5)-O(16)	1.995(5)
Sb(2)-O(7)	1.985(5)	V(6)-O(40)	1.610(5)
Sb(2)-O(6)	1.993(5)	V(6)-O(41)	1.909(5)
Sb(3)-O(11)	1.863(13)	V(6)-O(26)	1.937(5)
Sb(3)-O(12)	1.930(13)	V(6)-O(11)	1.993(6)
Sb(3)-O(10)	2.033(10)	V(6)-O(21)	2.005(5)
Ge(1)-O(1)	1.66(2)	V(7)-O(33)	1.609(5)
Ge(1)-O(3)	1.676(7)	V(7)-O(23)	1.937(5)
Ge(1)-O(2)	1.801(8)	V(7)-O(22)	1.939(5)
Ge(1)-O(4)	1.823(8)	V(7)-O(31)	1.940(5)
Ge(2)-O(5)	1.66(2)	V(7)-O(19)	2.027(5)
Ge(2)-O(6)	1.727(14)	V(8)-O(25)	1.611(5)
Ge(2)-O(7)	1.795(15)	V(8)-O(23)	1.910(5)
Ge(2)-O(8)	1.850(16)	V(8)-O(31)	1.940(5)
Ge(3)-O(9)	1.614(10)	V(8)-O(2)	1.985(5)
Ge(3)-O(10)	1.766(8)	V(8)-O(15)	2.005(6)
Ge(3)-O(12)	1.810(9)	V(9)-O(46)	1.611(5)
Ge(3)-O(11)	1.837(9)	V(9)-O(42)	1.933(5)
Ge(4)-O(17)	1.729(6)	V(9)-O(24)	1.945(5)
Ge(4)-O(16)	1.740(5)	V(9)-O(35)	1.949(5)
Ge(4)-O(18)	1.743(5)	V(9)-O(18)	2.024(5)
Ge(4)-O(8)	1.745(6)	V(10)-O(38)	1.617(5)
Ge(5)-O(20)	1.653(6)	V(10)-O(22)	1.930(5)
Ge(5)-O(19)	1.767(5)	V(10)-O(29)	1.936(5)
Ge(5)-O(21)	1.780(5)	V(10)-O(43)	1.955(5)
Ge(5)-O(12)	1.789(6)	V(10)-O(6)	1.984(6)
Ge(6)-O(14)	1.703(6)	V(11)-O(45)	1.598(5)

Ge(6)-O(15)	1.747(5)	V(11)-O(31)	1.938(5)
Ge(6)-O(13)	1.748(5)	V(11)-O(26)	1.943(5)
Ge(6)-O(4)	1.751(6)	V(11)-O(15)	1.989(5)
Ge(6)-Ge(1)	2.938(5)	V(11)-O(21)	1.995(5)
V(1)-O(47)	1.615(5)	V(12)-O(39)	1.609(5)
V(1)-O(42)	1.916(5)	V(12)-O(41)	1.934(5)
V(1)-O(35)	1.935(5)	V(12)-O(42)	1.938(5)
V(1)-O(3)	1.967(5)	V(12)-O(26)	1.960(5)
V(1)-O(13)	2.005(5)	V(12)-O(13)	2.026(5)
V(2)-O(44)	1.621(5)	V(13)-O(48)	1.621(5)
V(2)-O(27)	1.914(5)	V(13)-O(24)	1.915(6)
V(2)-O(43)	1.915(5)	V(13)-O(27)	1.938(5)
V(2)-O(10)	1.977(5)	V(13)-O(7)	1.968(5)
V(2)-O(7)	1.985(6)	V(13)-O(18)	1.998(5)
V(3)-O(36)	1.606(5)	V(14)-O(30)	1.622(5)
V(3)-O(24)	1.924(5)	V(14)-O(29)	1.924(5)
V(3)-O(41)	1.942(5)	V(14)-O(23)	1.939(5)
V(3)-O(27)	1.959(5)	V(14)-O(28)	1.956(5)
V(3)-O(11)	2.020(5)	V(14)-O(2)	1.989(6)
V(4)-O(32)	1.610(5)	V(15)-O(34)	1.610(5)
V(4)-O(29)	1.910(5)	V(15)-O(22)	1.905(5)
V(4)-O(28)	1.945(5)	V(15)-O(43)	1.953(5)
V(4)-O(6)	1.961(5)	V(15)-O(10)	1.978(5)
V(4)-O(16)	2.005(5)	V(15)-O(19)	1.999(6)

Tab. S 6: Bond lengths [Å] and angles [°] for the Ni complexes in compound **1**.

Ni(1)-N(6)	2.111(7)	Ni(1)-N(2)	2.138(7)
Ni(1)-N(5)	2.124(8)	Ni(1)-N(4)	2.141(7)
Ni(1)-N(1)	2.126(8)	Ni(1)-N(3)	2.156(8)
N(6)-Ni(1)-N(1)	92.6(3)	N(1)-Ni(1)-N(4)	171.3(3)
N(5)-Ni(1)-N(1)	93.7(3)	N(2)-Ni(1)-N(4)	93.2(3)
N(6)-Ni(1)-N(2)	90.4(3)	N(6)-Ni(1)-N(3)	173.1(3)
N(5)-Ni(1)-N(2)	170.4(3)	N(5)-Ni(1)-N(3)	94.5(4)
N(1)-Ni(1)-N(2)	81.1(3)	N(1)-Ni(1)-N(3)	93.4(3)
N(6)-Ni(1)-N(4)	93.9(3)	N(2)-Ni(1)-N(3)	93.9(3)
N(5)-Ni(1)-N(4)	92.9(3)	N(4)-Ni(1)-N(3)	80.4(3)
Ni(2)-N(12)	2.117(7)	Ni(2)-N(15)	2.127(7)
Ni(2)-N(14)	2.117(7)	Ni(2)-N(16)	2.139(8)
Ni(2)-N(13)	2.119(7)	Ni(2)-N(11)	2.146(7)
N(12)-Ni(2)-N(14)	93.2(3)	N(13)-Ni(2)-N(16)	172.8(3)
N(12)-Ni(2)-N(13)	91.6(3)	N(15)-Ni(2)-N(16)	81.0(3)
N(14)-Ni(2)-N(13)	82.2(3)	N(12)-Ni(2)-N(11)	81.4(3)
N(12)-Ni(2)-N(15)	172.7(3)	N(14)-Ni(2)-N(11)	172.3(3)
N(14)-Ni(2)-N(15)	92.4(3)	N(13)-Ni(2)-N(11)	92.5(3)
N(13)-Ni(2)-N(15)	93.7(3)	N(15)-Ni(2)-N(11)	93.4(3)
N(12)-Ni(2)-N(16)	94.2(3)	N(16)-Ni(2)-N(11)	92.7(3)
N(14)-Ni(2)-N(16)	93.1(3)		
Ni(3)-N(25)	2.109(7)	Ni(3)-N(22)	2.126(7)
Ni(3)-N(24)	2.110(7)	Ni(3)-N(26)	2.127(7)
Ni(3)-N(23)	2.120(7)	Ni(3)-N(21)	2.139(8)
N(25)-Ni(3)-N(24)	92.5(3)	N(23)-Ni(3)-N(26)	173.5(3)
N(25)-Ni(3)-N(23)	91.6(3)	N(22)-Ni(3)-N(26)	93.7(3)
N(24)-Ni(3)-N(23)	82.7(3)	N(25)-Ni(3)-N(21)	95.8(3)
N(25)-Ni(3)-N(22)	175.0(3)	N(24)-Ni(3)-N(21)	169.9(3)
N(24)-Ni(3)-N(22)	90.5(3)	N(23)-Ni(3)-N(21)	91.3(3)
N(23)-Ni(3)-N(22)	92.7(3)	N(22)-Ni(3)-N(21)	81.6(3)
N(25)-Ni(3)-N(26)	82.0(3)	N(26)-Ni(3)-N(21)	90.8(3)
N(24)-Ni(3)-N(26)	96.1(3)		

Tab. S 7: Geometric parameters for the proposed hydrogen bonds for compound **1** [Å and °].

D-H...A	d(D-H)	d(H...A)	d(D...A)	<(DHA)
N(1)-H(1A)...O(20)#1	0.91	2.62	3.318(10)	134.0
C(2)-H(2D)...O(36)#2	0.99	2.64	3.432(15)	136.7
N(2)-H(2A)...O(24)#2	0.91	2.37	3.247(10)	161.5
N(2)-H(2B)...O(46)#2	0.91	2.60	3.126(9)	117.9
N(3)-H(3A)...O(5)#3	0.91	2.28	3.19(3)	175.5
N(3)-H(3B)...O(33)#1	0.91	2.20	3.013(10)	148.0
C(3)-H(3C)...O(25)#1	0.99	2.50	3.418(13)	154.0
N(4)-H(4A)...O(42)#2	0.91	2.32	3.100(9)	143.8
N(4)-H(4A)...O(46)#2	0.91	2.52	3.296(9)	143.2
N(4)-H(4B)...O(39)#2	0.91	2.38	3.109(8)	137.1
N(5)-H(5B)...O(38)#3	0.91	2.22	3.030(10)	147.5
C(5)-H(5C)...O(39)#2	0.99	2.60	3.410(12)	139.1
C(5)-H(5D)...O(34)#3	0.99	2.52	3.477(12)	162.5
N(6)-H(6A)...O(39)#2	0.91	2.63	3.330(9)	134.8
N(6)-H(6A)...O(41)#2	0.91	2.31	3.148(9)	152.9
N(6)-H(6B)...O(36)#2	0.91	2.52	3.188(10)	130.1
N(11)-H(11A)...O(30)	0.91	2.44	3.110(8)	130.9
N(11)-H(11B)...O(29)	0.91	2.29	3.125(8)	151.5
N(11)-H(11B)...O(38)	0.91	2.63	3.362(9)	137.8
C(12)-H(12D)...O(47)#4	0.99	2.41	3.392(13)	170.6
N(12)-H(12A)...O(39)#4	0.91	2.41	3.176(10)	141.5
N(13)-H(13A)...O(38)	0.91	2.29	3.019(9)	136.4
N(13)-H(13B)...O(22)	0.91	2.26	3.071(8)	147.6
N(13)-H(13B)...O(33)	0.91	2.64	3.385(9)	139.8
C(14)-H(14D)...O(48)#5	0.99	2.49	3.444(11)	161.4
N(14)-H(14A)...O(46)#5	0.91	2.31	3.115(9)	147.0
N(15)-H(15A)...O(33)	0.91	2.32	3.079(9)	141.1
N(15)-H(15B)...O(23)	0.91	2.37	3.129(9)	140.7
N(15)-H(15B)...O(30)	0.91	2.60	3.401(9)	147.9
N(21)-H(21A)...O(48)#6	0.91	2.37	3.186(9)	148.8
N(22)-H(22A)...O(30)	0.91	2.22	3.122(8)	169.7
N(22)-H(22B)...O(40)#2	0.91	2.28	3.137(9)	157.5
N(23)-H(23A)...O(48)#6	0.91	2.22	3.047(8)	150.7
N(23)-H(23B)...O(40)#2	0.91	2.18	3.036(9)	155.5
C(23)-H(23C)...O(21)#2	0.99	2.65	3.567(12)	154.1
C(23)-H(23D)...O(44)#6	0.99	2.39	3.371(13)	169.5
C(24)-H(24C)...O(37)	0.99	2.64	3.383(12)	132.0
N(24)-H(24A)...O(28)	0.91	2.38	3.140(8)	141.6
N(25)-H(25A)...O(27)#6	0.91	2.65	3.144(8)	114.7
N(25)-H(25A)...O(48)#6	0.91	2.58	3.224(9)	128.4
N(25)-H(25B)...O(44)#6	0.91	2.55	3.446(10)	167.2
C(25)-H(25C)...O(9)#6	0.99	2.62	3.257(14)	122.3
C(25)-H(25D)...O(32)	0.99	2.66	3.374(11)	129.3
N(26)-H(26A)...O(32)	0.91	2.21	2.995(9)	144.2
N(31)-H(31A)...O(25)	0.91	2.28	3.127(12)	155.5
C(31)-H(31C)...O(30)	0.99	2.51	3.489(17)	171.5

Symmetry transformations used to generate equivalent atoms: #1 -x+1,y-1/2,-z+1 #2 -x+1,y-1/2,-z #3 -x+2,y-1/2,-z+1 #4 x+1,y,z+1 #5 x,y,z+1 #6 -x+2,y-1/2,-z

Tab. S 8: Bond lengths [Å] for the anion in compound **2**.

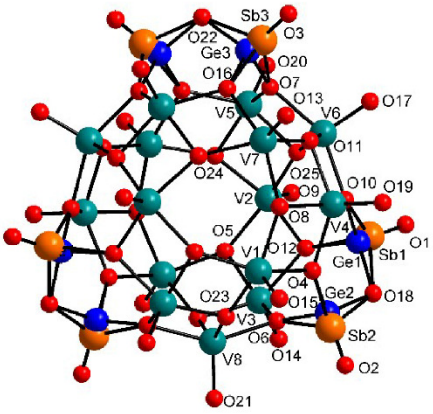

Sb(1)-O(12)	1.946(4)	V(3)-O(23)	1.947(4)
Sb(1)-O(18)	1.976(4)	V(3)-O(12)	1.977(4)
Sb(1)-O(10)	1.990(5)	V(3)-O(6)	1.979(4)
Sb(2)-O(4)	1.948(5)	V(4)-O(19)	1.629(4)
Sb(2)-O(18)	1.977(5)	V(4)-O(8)	1.910(4)
Sb(2)-O(6)	1.979(4)	V(4)-O(11)	1.937(4)
Sb(3)-O(7)	1.920(5)	V(4)-O(10)	1.974(4)
Sb(3)-O(22)	1.970(3)	V(4)-O(4)	1.991(4)
Sb(3)-O(16)	2.053(5)	V(5)-O(20)	1.611(5)
Ge(1)-O(1)	1.721(16)	V(5)-O(24)	1.919(4)
Ge(1)-O(18)	1.737(6)	V(5)-O(25)	1.939(4)
Ge(1)-O(10)	1.769(7)	V(5)-O(7)	1.982(5)
Ge(1)-O(12)	1.770(6)	V(5)-O(16)#1	1.982(5)
Ge(1)-Ge(2)	2.848(4)	V(6)-O(17)	1.614(4)
Ge(2)-O(2)	1.716(7)	V(6)-O(25)	1.919(4)
Ge(2)-O(18)	1.721(5)	V(6)-O(11)	1.920(5)
Ge(2)-O(4)	1.759(5)	V(6)-O(10)	1.989(4)
Ge(2)-O(6)	1.769(4)	V(6)-O(7)	1.989(4)
Ge(3)-O(3)	1.686(8)	V(7)-O(13)	1.616(4)
Ge(3)-O(16)	1.702(5)	V(7)-O(24)#1	1.920(4)
Ge(3)-O(22)	1.758(4)	V(7)-O(8)	1.934(4)
Ge(3)-O(7)	1.820(5)	V(7)-O(11)	1.956(4)
Ge(3)-Ge(3)#1	2.924(4)	V(7)-O(16)	2.011(4)
V(1)-O(15)	1.620(4)	V(8)-O(21)	1.609(6)
V(1)-O(8)#1	1.935(4)	V(8)-O(23)#1	1.921(4)
V(1)-O(5)	1.944(4)	V(8)-O(23)	1.921(4)
V(1)-O(23)	1.960(4)	V(8)-O(6)#1	1.991(4)
V(1)-O(4)#1	1.997(4)	V(8)-O(6)	1.991(4)
V(2)-O(9)	1.612(5)	O(4)-V(1)#1	1.997(4)
V(2)-O(24)	1.930(4)	O(8)-V(1)#1	1.935(4)
V(2)-O(5)	1.936(4)	O(16)-V(5)#1	1.982(4)
V(2)-O(25)	1.945(4)	O(22)-Ge(3)#1	1.758(4)
V(2)-O(12)	2.009(4)	O(22)-Sb(3)#1	1.970(3)
V(3)-O(14)	1.619(4)	O(24)-V(7)#1	1.920(4)
V(3)-O(5)	1.916(4)		

Symmetry transformations used to generate equivalent atoms: #1 -x+2,y,-z+2 #2 -x+1,y,-z+1

Tab. S 9: Bond lengths [Å] and angles [°] for the Ni complexes in compound **2**.

Ni(1)-N(5)	2.110(6)	Ni(2)-N(11)#2	2.129(6)
Ni(1)-N(2)	2.116(6)	Ni(2)-N(11)	2.129(6)
Ni(1)-N(6)	2.134(6)	Ni(2)-N(13)	2.133(6)
Ni(1)-N(4)	2.135(5)	Ni(2)-N(13)#2	2.133(6)
Ni(1)-N(3)	2.142(6)	Ni(2)-N(12)#2	2.134(6)
Ni(1)-N(1)	2.147(5)	Ni(2)-N(12)	2.134(6)
N(5)-Ni(1)-N(2)	170.8(2)	N(11)#2-Ni(2)-N(11)	173.7(3)
N(5)-Ni(1)-N(6)	82.7(3)	N(11)#2-Ni(2)-N(13)	91.5(2)
N(2)-Ni(1)-N(6)	91.2(3)	N(11)-Ni(2)-N(13)	93.2(3)
N(5)-Ni(1)-N(4)	95.0(2)	N(11)#2-Ni(2)-N(13)#2	93.2(2)
N(2)-Ni(1)-N(4)	92.0(2)	N(11)-Ni(2)-N(13)#2	91.5(2)
N(6)-Ni(1)-N(4)	91.5(2)	N(13)-Ni(2)-N(13)#2	81.0(3)
N(5)-Ni(1)-N(3)	92.3(3)	N(11)#2-Ni(2)-N(12)#2	81.3(3)
N(2)-Ni(1)-N(3)	94.6(2)	N(11)-Ni(2)-N(12)#2	94.2(2)
N(6)-Ni(1)-N(3)	170.9(2)	N(13)-Ni(2)-N(12)#2	94.6(2)
N(4)-Ni(1)-N(3)	81.3(2)	N(13)#2-Ni(2)-N(12)#2	173.0(2)
N(5)-Ni(1)-N(1)	92.2(2)	N(11)#2-Ni(2)-N(12)	94.2(2)
N(2)-Ni(1)-N(1)	81.7(2)	N(11)-Ni(2)-N(12)	81.3(3)
N(6)-Ni(1)-N(1)	97.2(2)	N(13)-Ni(2)-N(12)	173.0(2)
N(4)-Ni(1)-N(1)	169.3(2)	N(13)#2-Ni(2)-N(12)	94.6(2)
N(3)-Ni(1)-N(1)	90.6(2)	N(12)#2-Ni(2)-N(12)	

Symmetry transformations used to generate equivalent atoms: #1 -x+2,y,-z+2 #2 -x+1,y,-z+1

Tab. S 10: Geometric parameters of the proposed hydrogen bonds for compound **2** [Å and °].

D-H...A	d(D-H)	d(H...A)	d(D...A)	<(DHA)
N(1)-H(1C)...O(9)#3	0.91	2.40	3.125(7)	136.9
C(1)-H(1B)...O(1)#3	0.99	2.64	3.218(18)	117.2
C(2)-H(2A)...O(25)#3	0.99	2.57	3.442(9)	146.5
C(2)-H(2B)...O(1)#3	0.99	2.53	3.149(17)	120.5
N(2)-H(2C)...O(17)#4	0.91	2.07	2.958(7)	166.0
N(3)-H(3C)...O(17)#4	0.91	2.45	3.217(7)	142.6
C(4)-H(4A)...O(17)#4	0.99	2.62	3.449(8)	141.1
C(4)-H(4B)...O(2)#1	0.99	2.48	3.242(10)	133.5
N(4)-H(4C)...O(23)	0.91	2.44	3.222(6)	144.0
N(5)-H(5C)...O(21)	0.91	2.10	2.947(7)	153.5
N(6)-H(6C)...O(20)#3	0.91	2.22	3.062(9)	152.9
N(6)-H(6D)...O(14)	0.91	2.27	3.101(7)	151.1
N(11)-H(11C)...O(15)	0.91	2.22	3.092(7)	160.4
C(11)-H(11B)...O(9)#2	0.99	2.56	3.435(9)	146.8
N(12)-H(12C)...O(5)#2	0.91	2.24	3.109(7)	159.3
N(12)-H(12D)...O(15)#2	0.91	2.55	3.101(8)	119.7
N(13)-H(13C)...O(13)#1	0.91	2.52	3.323(8)	148.0
N(13)-H(13C)...O(24)	0.91	2.41	3.096(7)	132.5
N(13)-H(13D)...O(9)	0.91	2.20	3.017(7)	149.6

Symmetry transformations used to generate equivalent atoms:
#1 -x+2,y,-z+2 #2 -x+1,y,-z+1 #3 -x+3/2,y-1/2,-z+1; #4 x-1/2,y-1/2,z.

Tab. S 11: Selected bond lengths [Å] for the anion in compound **3**.

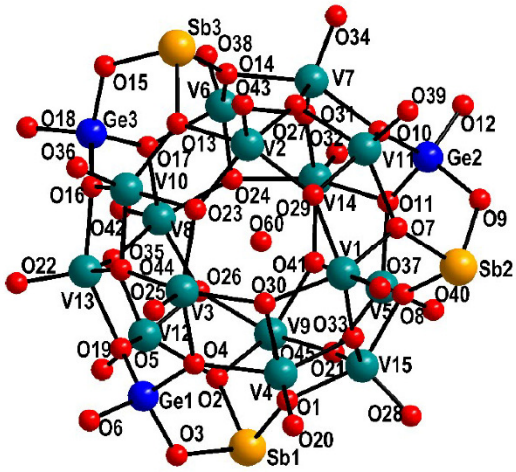

Sb(1)-O(1)	1.966(8)	Sb(2)-O(8)	1.984(8)
Sb(1)-O(3)	1.986(8)	Sb(3)-O(14)	1.935(7)
Sb(1)-O(2)	1.990(7)	Sb(3)-O(13)	1.955(8)
Sb(2)-O(7)	1.963(7)	Sb(3)-O(15)	1.971(9)
Sb(2)-O(9)	1.978(8)		
Ge(1)-O(6)	1.657(9)	Ge(2)-O(10)	1.770(8)
Ge(1)-O(5)	1.747(8)	Ge(2)-O(9)	1.771(8)
Ge(1)-O(4)	1.748(8)	Ge(3)-O(18)	1.671(10)
Ge(1)-O(3)	1.753(8)	Ge(3)-O(16)	1.731(8)
Ge(2)-O(12)	1.635(9)	Ge(3)-O(17)	1.732(8)
Ge(2)-O(11)	1.755(9)	Ge(3)-O(15)	1.750(9)
V(1)-O(37)	1.615(8)	V(8)-O(35)	1.949(8)
V(1)-O(30)	1.948(8)	V(8)-O(17)	2.006(9)
V(1)-O(33)	1.955(8)	V(8)-V(12)	2.853(3)
V(1)-O(29)	1.958(8)	V(9)-O(45)	1.607(9)
V(1)-O(7)	2.004(7)	V(9)-O(26)	1.938(8)
V(2)-O(43)	1.604(8)	V(9)-O(41)	1.942(8)
V(2)-O(29)	1.927(8)	V(9)-O(21)	1.942(8)
V(2)-O(23)	1.933(8)	V(9)-O(2)	1.997(7)
V(2)-O(27)	1.956(7)	V(10)-O(36)	1.619(8)
V(2)-O(13)	2.009(8)	V(10)-O(23)	1.898(8)
V(3)-O(25)	1.606(8)	V(10)-O(44)	1.922(8)
V(3)-O(30)	1.926(8)	V(10)-O(13)	1.969(8)
V(3)-O(23)	1.930(8)	V(10)-O(16)	1.998(8)
V(3)-O(44)	1.967(8)	V(11)-O(39)	1.606(9)
V(3)-O(4)	2.005(8)	V(11)-O(29)	1.923(7)
V(4)-O(20)	1.596(8)	V(11)-O(27)	1.943(8)
V(4)-O(30)	1.913(8)	V(11)-O(7)	1.971(8)
V(4)-O(33)	1.947(7)	V(11)-O(10)	2.000(7)
V(4)-O(1)	1.975(8)	V(12)-O(19)	1.621(9)
V(4)-O(4)	2.016(8)	V(12)-O(26)	1.912(8)
V(5)-O(40)	1.605(8)	V(12)-O(35)	1.952(8)
V(5)-O(41)	1.910(7)	V(12)-O(2)	1.956(7)
V(5)-O(21)	1.952(8)	V(12)-O(5)	2.024(7)
V(5)-O(8)	1.954(8)	V(13)-O(22)	1.605(9)

V(5)-O(11)	2.015(8)	V(13)-O(44)	1.912(8)
V(6)-O(38)	1.609(8)	V(13)-O(35)	1.916(8)
V(6)-O(24)	1.920(8)	V(13)-O(5)	1.988(8)
V(6)-O(31)	1.952(8)	V(13)-O(16)	2.015(8)
V(6)-O(14)	1.977(8)	V(14)-O(32)	1.607(7)
V(6)-O(17)	2.005(8)	V(14)-O(24)	1.932(8)
V(7)-O(34)	1.597(9)	V(14)-O(41)	1.950(8)
V(7)-O(31)	1.924(8)	V(14)-O(31)	1.951(8)
V(7)-O(27)	1.934(8)	V(14)-O(11)	2.027(8)
V(7)-O(14)	1.980(8)	V(15)-O(28)	1.609(7)
V(7)-O(10)	1.982(8)	V(15)-O(21)	1.926(8)
V(7)-V(11)	3.038(2)	V(15)-O(33)	1.933(7)
V(8)-O(42)	1.606(8)	V(15)-O(1)	1.960(8)
V(8)-O(24)	1.922(8)	V(15)-O(8)	1.960(8)
V(8)-O(26)	1.937(8)		

Tab. S 12: Bond lengths [Å] and angles of the Ni complexes [°] for compound **3**.

Ni(1)-N(22)	2.104(12)	Ni(1)-N(21)	2.129(12)
Ni(1)-N(11)	2.111(10)	Ni(1)-N(12)	2.130(10)
Ni(1)-N(2)	2.120(10)	Ni(1)-N(1)	2.138(13)
N(22)-Ni(1)-N(11)	172.4(5)	N(21)-Ni(1)-N(12)	94.2(4)
N(22)-Ni(1)-N(2)	93.7(5)	N(22)-Ni(1)-N(1)	92.3(6)
N(11)-Ni(1)-N(2)	92.8(5)	N(11)-Ni(1)-N(1)	92.5(6)
N(22)-Ni(1)-N(21)	81.9(5)	N(2)-Ni(1)-N(1)	81.7(5)
N(11)-Ni(1)-N(21)	94.0(5)	N(21)-Ni(1)-N(1)	170.8(5)
N(2)-Ni(1)-N(21)	91.6(5)	N(12)-Ni(1)-N(1)	93.0(5)
N(22)-Ni(1)-N(12)	91.5(4)	C(1')-N(1)-Ni(1)	109.3(16)
N(11)-Ni(1)-N(12)	82.4(4)	C(1)-N(1)-Ni(1)	103.7(12)
N(2)-Ni(1)-N(12)	172.7(5)		
Ni(2)-N(31)	2.01(2)	Ni(2)-N(32)	2.130(12)
Ni(2)-N(52')	2.07(4)	Ni(2)-N(51')	2.14(3)
Ni(2)-N(42)	2.120(16)	Ni(2)-N(52)	2.164(16)
Ni(2)-N(41)	2.123(11)	Ni(2)-N(51)	2.167(18)
N(31)-Ni(2)-N(52')	64.8(12)	N(42)-Ni(2)-N(51')	113.2(15)
N(31)-Ni(2)-N(42)	175.3(7)	N(41)-Ni(2)-N(51')	164.6(14)
N(52')-Ni(2)-N(42)	116.3(11)	N(32)-Ni(2)-N(51')	91.3(12)
N(31)-Ni(2)-N(41)	94.9(7)	N(31)-Ni(2)-N(52)	92.8(8)
N(52')-Ni(2)-N(41)	86.0(11)	N(42)-Ni(2)-N(52)	89.3(6)
N(42)-Ni(2)-N(41)	80.7(5)	N(41)-Ni(2)-N(52)	95.0(6)
N(31)-Ni(2)-N(32)	85.1(7)	N(32)-Ni(2)-N(52)	170.4(5)
N(52')-Ni(2)-N(32)	149.8(11)	N(31)-Ni(2)-N(51)	98.4(8)
N(42)-Ni(2)-N(32)	93.5(5)	N(42)-Ni(2)-N(51)	86.2(6)
N(41)-Ni(2)-N(32)	94.5(5)	N(41)-Ni(2)-N(51)	165.9(6)
N(31)-Ni(2)-N(51')	71.4(15)	N(32)-Ni(2)-N(51)	91.4(6)
N(52')-Ni(2)-N(51')	81.9(15)	N(52)-Ni(2)-N(51)	79.7(6)
Ni(3)-N(61)	2.101(12)	Ni(3)-N(71)	2.136(13)
Ni(3)-N(72)	2.109(13)	Ni(3)-N(62)	2.136(10)
Ni(3)-N(81)	2.123(10)	Ni(3)-N(82)	2.150(10)
N(61)-Ni(3)-N(72)	92.0(6)	N(81)-Ni(3)-N(62)	90.9(4)
N(61)-Ni(3)-N(81)	90.5(4)	N(71)-Ni(3)-N(62)	93.4(5)
N(72)-Ni(3)-N(81)	176.8(6)	N(61)-Ni(3)-N(82)	95.7(4)
N(61)-Ni(3)-N(71)	171.9(6)	N(72)-Ni(3)-N(82)	96.1(5)
N(72)-Ni(3)-N(71)	81.2(7)	N(81)-Ni(3)-N(82)	81.6(4)
N(81)-Ni(3)-N(71)	96.5(5)	N(71)-Ni(3)-N(82)	89.4(5)
N(61)-Ni(3)-N(62)	82.4(4)	N(62)-Ni(3)-N(82)	172.2(4)
N(72)-Ni(3)-N(62)	91.4(5)		

Tab. S 13: Geometric parameters of the proposed hydrogen bonds for compound **3** [Å and °].

D-H...A	d(D-H)	d(H...A)	d(D...A)	<(DHA)
N(1)-H(1F)...O(56)#1	0.91	2.63	3.44(2)	148.7
N(1)-H(1H)...O(51)	0.91	2.41	3.28(3)	162.4
C(2)-H(2A)...O(28)	0.99	2.61	3.465(17)	144.1
N(2)-H(2F)...O(29)#2	0.91	2.30	3.181(13)	161.8
N(11)-H(11C)...O(43)#2	0.91	2.35	3.085(13)	138.0
N(11)-H(11D)...O(23)#2	0.91	2.34	3.140(12)	145.9
N(11)-H(11D)...O(25)#2	0.91	2.64	3.427(15)	144.6
C(12)-H(12B)...O(38)#1	0.99	2.38	3.247(15)	145.4
N(12)-H(12C)...O(32)#1	0.91	2.27	3.118(14)	155.1
N(12)-H(12D)...O(54)#3	0.91	2.41	3.290(18)	162.1
N(21)-H(21D)...O(30)#2	0.91	2.28	3.167(14)	165.0
C(21)-H(21A)...O(37)#2	0.99	2.58	3.374(16)	137.7
C(22)-H(22A)...O(32)#1	0.99	2.49	3.407(16)	154.8
N(22)-H(22C)...O(45)	0.91	2.16	3.022(14)	158.1
N(22)-H(22D)...O(12)#1	0.91	2.47	3.147(14)	131.3
N(22)-H(22D)...O(56)#1	0.91	2.28	3.16(2)	161.6
N(31)-H(31E)...O(6)#4	0.91	2.38	3.23(2)	155.6
N(31)-H(31E)...O(6)#4	0.91	2.38	3.23(2)	155.6
N(31)-H(31G)...O(58)#4	0.91	2.58	3.40(3)	149.8
C(31')-H(31D)...O(6)#4	0.99	2.40	3.14(4)	130.9
N(32)-H(32E)...O(24)	0.91	2.34	3.139(13)	146.9
N(32)-H(32F)...O(32)	0.91	2.26	2.990(14)	136.6
N(41)-H(41D)...O(25)#4	0.91	2.29	3.162(16)	159.5
C(41)-H(41A)...O(20)#4	0.99	2.41	3.34(2)	156.2
C(42)-H(42A)...O(12)#1	0.99	2.61	3.57(3)	163.9
N(42)-H(42C)...O(41)	0.91	2.25	3.079(15)	151.2
N(42)-H(42D)...O(45)	0.91	2.30	3.013(13)	135.3
N(51)-H(51E)...O(26)	0.91	2.24	3.127(18)	166.1
N(52)-H(52F)...O(12)#1	0.91	2.44	3.28(2)	154.2
N(52')-H(52G)...O(58)#4	0.91	2.66	3.54(4)	164.4
N(52')-H(52H)...O(9)#1	0.91	2.12	2.99(4)	158.4
N(61)-H(61C)...O(39)#2	0.91	2.21	3.095(14)	164.7
C(61)-H(61B)...O(43)#2	0.99	2.39	3.358(17)	167.2
C(62)-H(62B)...O(34)#2	0.99	2.53	3.321(18)	136.5
N(62)-H(62C)...O(38)#6	0.91	2.59	3.418(15)	151.6
N(62)-H(62D)...O(18)#6	0.91	2.32	3.186(14)	159.0
N(71)-H(71E)...O(15)#6	0.91	2.39	3.226(14)	153.1
N(71)-H(71H)...O(19)#7	0.91	2.50	3.393(18)	166.6
N(71)-H(71E)...O(15)#6	0.91	2.39	3.226(14)	153.1
N(71)-H(71H)...O(19)#7	0.91	2.50	3.393(18)	166.6
C(72)-H(72A)...O(18)#6	0.99	2.66	3.57(3)	153.1
C(71')-H(71D)...O(18)#6	0.99	2.48	3.44(5)	164.9
N(72)-H(72E)...O(20)	0.91	2.02	2.897(14)	161.9
N(81)-H(81C)...O(38)#6	0.91	2.06	2.958(12)	168.9
N(81)-H(81D)...O(59)#3	0.91	2.56	3.44(3)	162.1
C(81)-H(81B)...O(19)#7	0.99	2.42	3.197(17)	134.4
N(82)-H(82C)...O(28)	0.91	2.56	3.234(14)	131.0
N(82)-H(82C)...O(33)	0.91	2.55	3.389(12)	153.6
N(82)-H(82D)...O(19)#7	0.91	2.50	3.188(15)	132.4

Symmetry transformations used to generate equivalent atoms: #1 -x+2,y+1/2,-z+1; #2-x+1,y+1/2,-z+1; #3 x,y,z-1; #4 x+1,y,z; #5 -x+2,y+1/2,-z+2; #6 x-1,y,z-1; #7 -x+1,y-1/2,-z+1.

Tab. S 14: Mixed occupancies of the heteroatom positions in **1** and **2**.

Compound		**Ge[%]**	**Sb [%]**
1	Ge(1):Sb(1)	20	80
1	Ge(2):Sb(2)	10	90
1	Ge(3):Sb(3)	70	30
2	Ge(1):Sb(1)	30	70
2	Ge(2):Sb(2)	65	35
2	Ge(3):Sb(3)	55	45

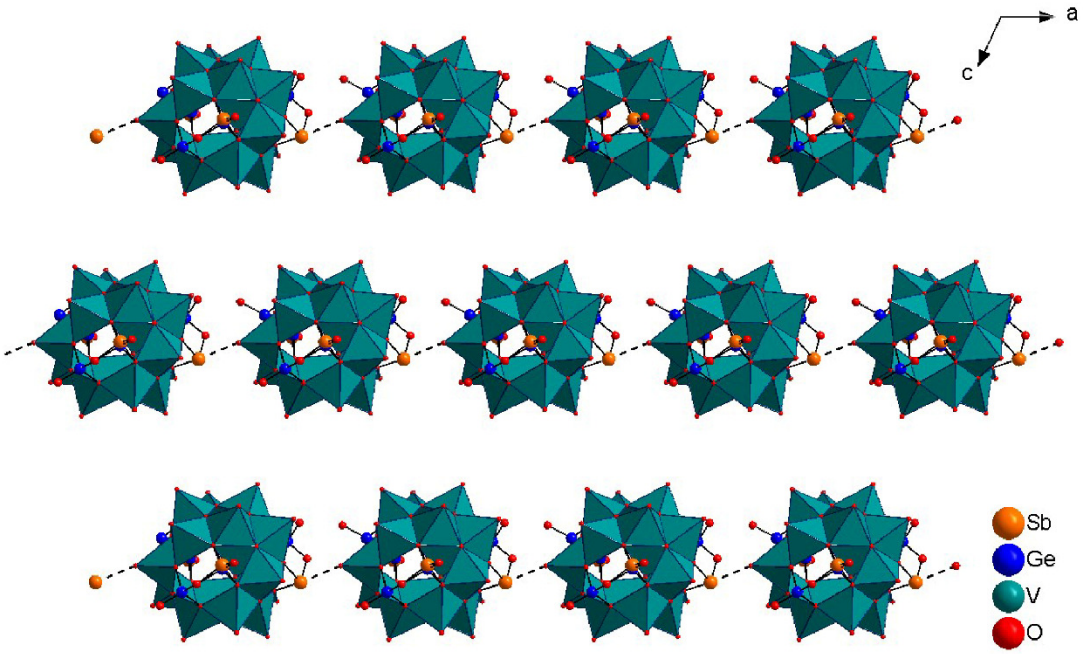

Fig. S 10: Chains of cluster anions generated by short Sb···O intercluster interactions (dashed lines) along [100].

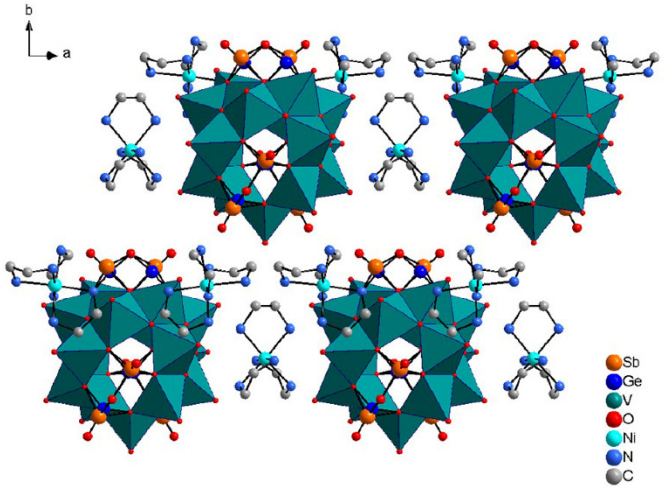

Fig. S 11: Alternating cations and the cluster anions in **2**. H-atoms have been omitted for clarity.

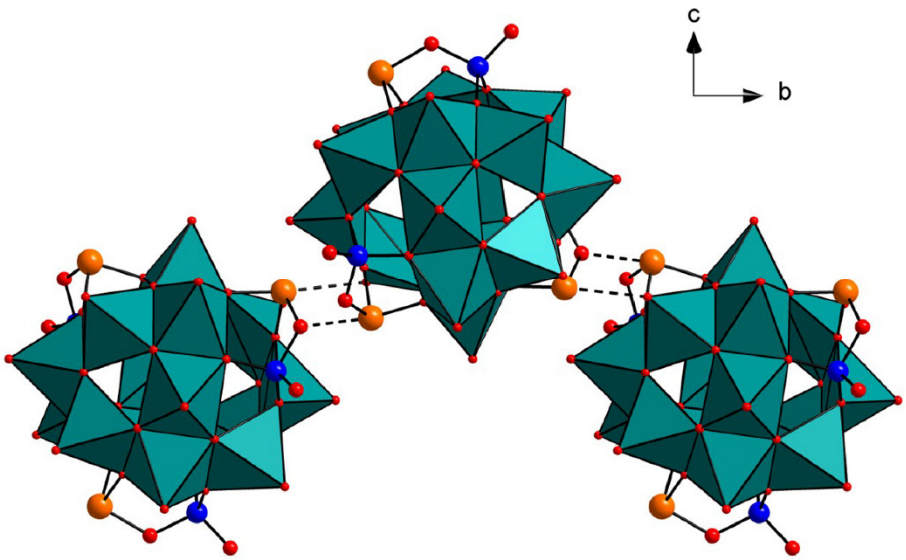

Fig. S 12: Intermolecular Sb···O contacts (dashed lines) between the anions in the structure of **3** generating a wavy chain along [010].

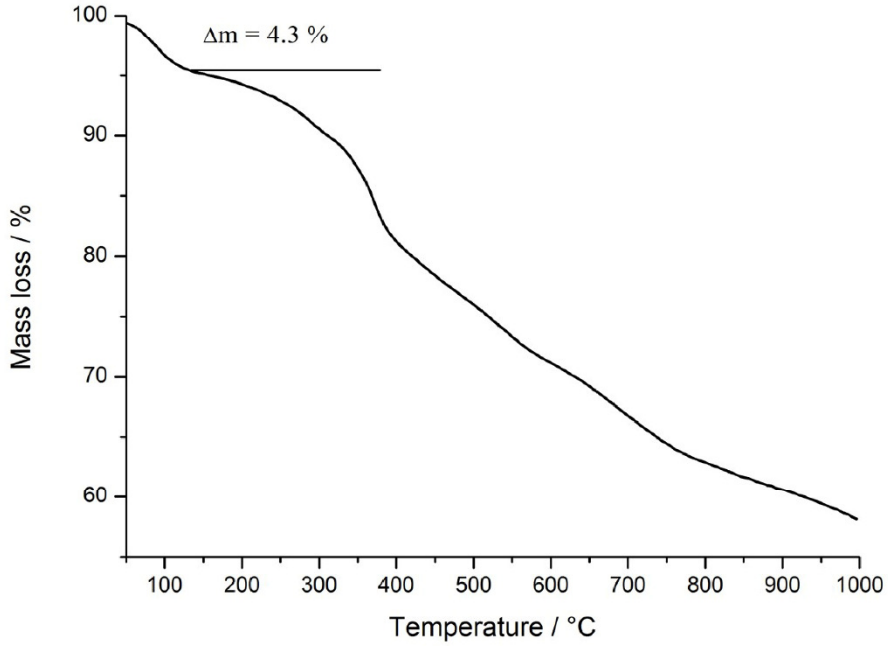

Fig. S 13: TG curve of compound **1**.

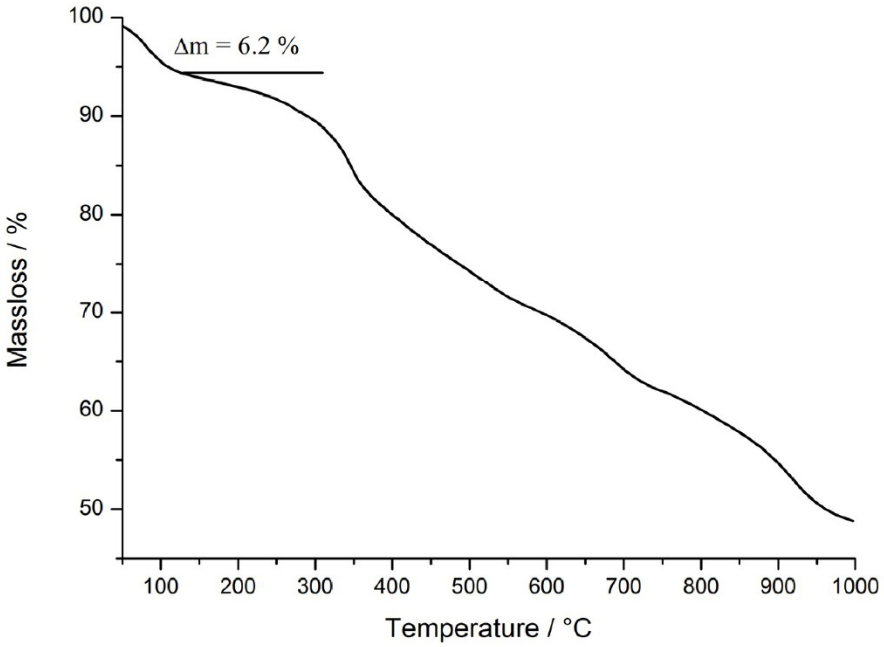

Fig. S14: TG curve of compound **2**.

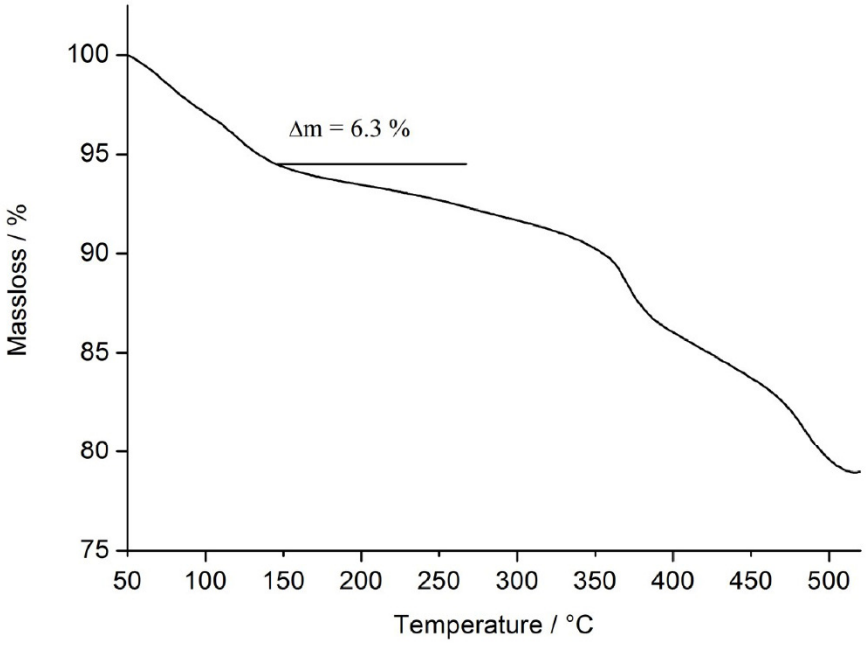

Fig. S15: TG curve of compound **3**.

7.4 Supporting Information der Publikation *„The New Water-Soluble Cluster Compound {Zn(en)$_3$}$_3$[V$_{15}$Sb$_6$O$_{42}$(H$_2$O)]·(ethylenediamine)$_3$·10H$_2$O as a Synthon for the Generation of two New Antimonato Polyoxovanadates"*

CHEMISTRY
A European Journal

Supporting Information

New Water-Soluble Cluster Compound {Zn(en)$_3$}$_3$[V$_{15}$Sb$_6$O$_{42}$(H$_2$O)]·(Ethylenediamine)$_3$·10 H$_2$O as a Synthon for the Generation of Two New Antimonato Polyoxovanadates

Lisa K. Mahnke,[a] Ulrike Warzok,[b] Mengxi Lin,[a] Christian Näther,[a] Christoph A. Schalley,[b] and Wolfgang Bensch*[a]

chem_201705732_sm_miscellaneous_information.pdf

Content

1. Solubility Test

The absorbance of differently concentrated aqueous solutions of **II** ($\{Zn(en)_3\}_3[V_{15}Sb_6O_{42}(H_2O)]\cdot 3en\cdot 10H_2O$ (en = ethylenediamine)) was measured with UV-Vis spectroscopy (Fig. S1, left) and the saturated solution was diluted by a factor of 25 to determine maximal solubility.

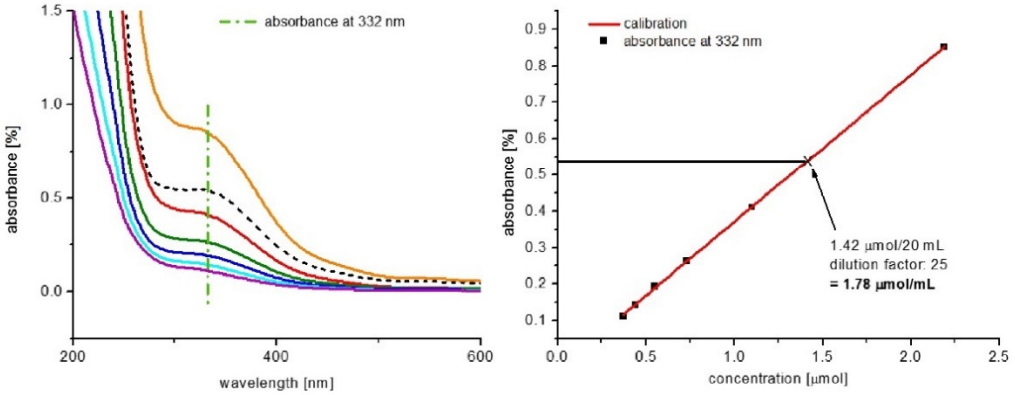

Fig. S 1: Left: UV-Vis absorbance curves with 7.2 (orange), 3.6 (red), 2.4 (green), 1.8 (blue), 1.44 (light blue) and 1.2 (magenta) mg of compound **II** in 20 mL dist. Water; dotted line: max. solubility product (compound **II**) diluted by a factor of 25. Right: calibration line (red) of different absorbance data (black points) and the max. solubility diluted by a factor of 25 (cross).

2. Mass spectrometry

For time-dependent measurements of the $\{V_{15}Sb_6\} \rightarrow \{V_{14}Sb_8\}$ transformation of compounds ($\{Ni(en)_3\}_3[V_{15}Sb_8O_{42}(H_2O)]\cdot\sim15H_2O$[2]) (**I**) and **II** in different aqueous solutions, 60 µM solutions from crystalline samples **I** and **II** were prepared in H_2O, aqueous 1% NH_4OAc solution and aqueous 1% NH_3 solution, respectively. Solutions were kept at 4 °C, aliquots were taken after the indicated time and directly subjected to the mass spectrometric analysis.

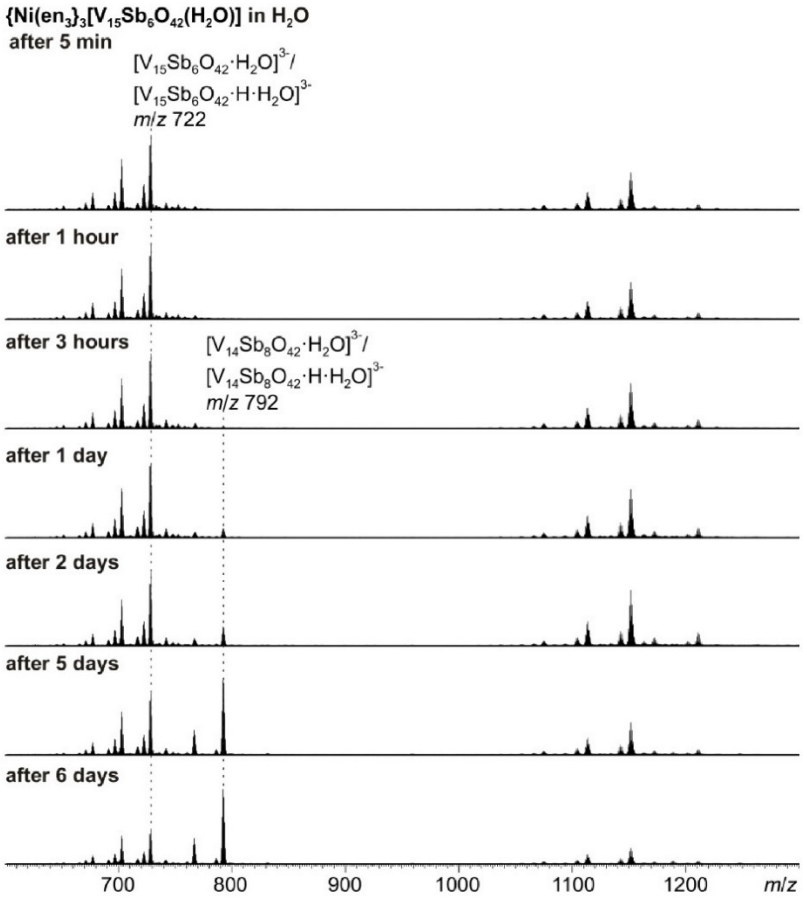

Fig. S 2: ESI-Q-TOF-HRMS spectra of compound **I** (60 µM in H_2O) after different reaction times. Labeled peaks were used for graphical analysis.

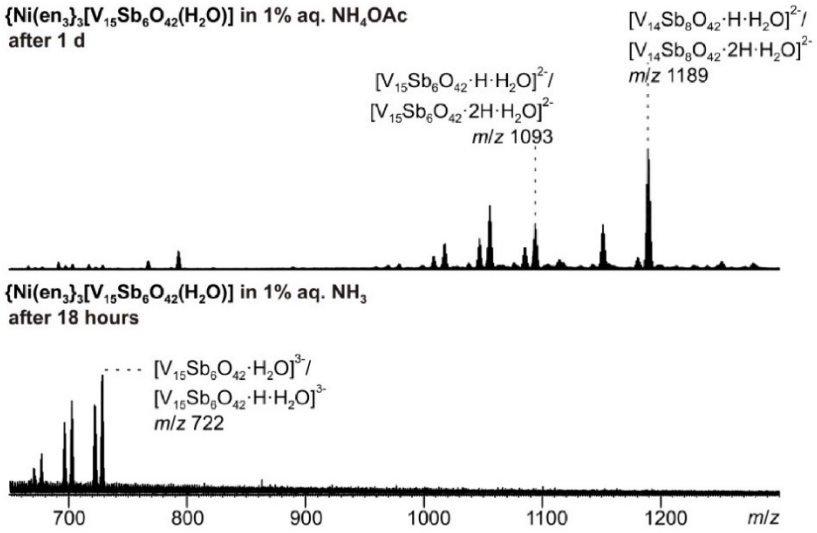

Fig. S 3: ESI-Q-TOF-HRMS spectra of compound **I.** Top: 60 µM in aqueous 1% NH_4OAc solution after 1 day; Bottom: 60 µM in aqueous 1% NH_3 solution after 18 hours, longer reaction times led to decomposition.

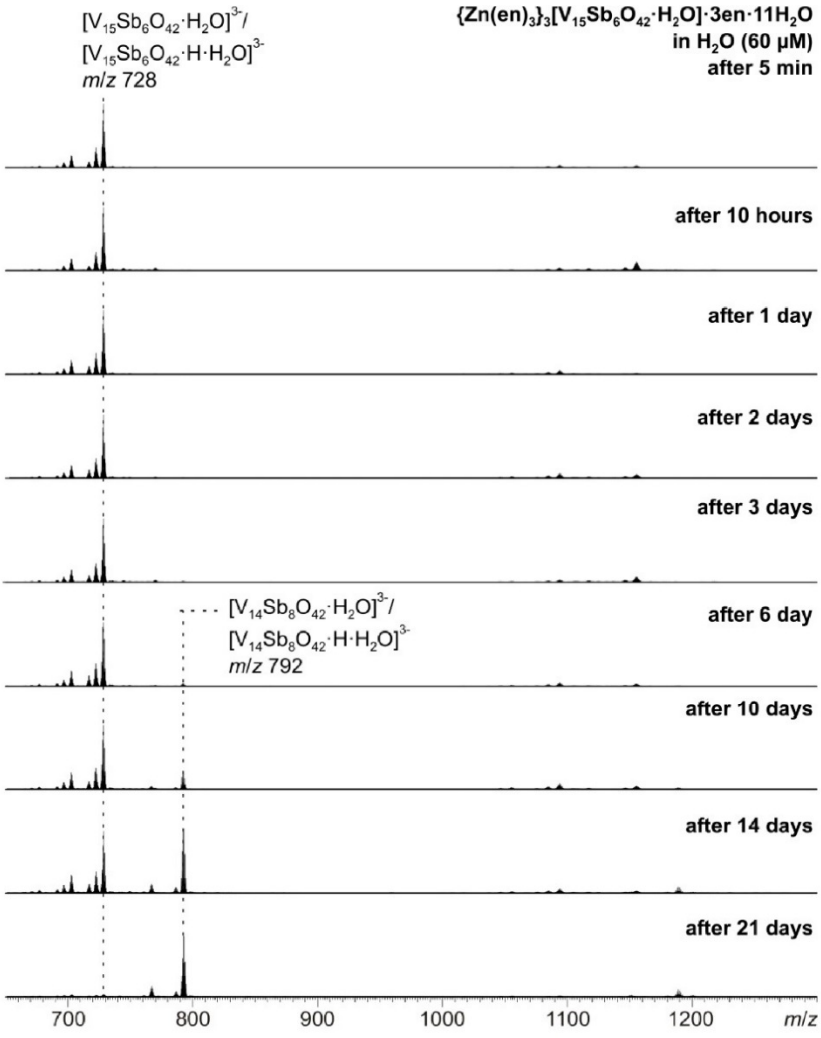

Fig. S 4: ESI-Q-TOF-HRMS spectra of compound **II** (60 µM in H_2O) after different reaction times. Labeled peaks were used for graphical analysis.

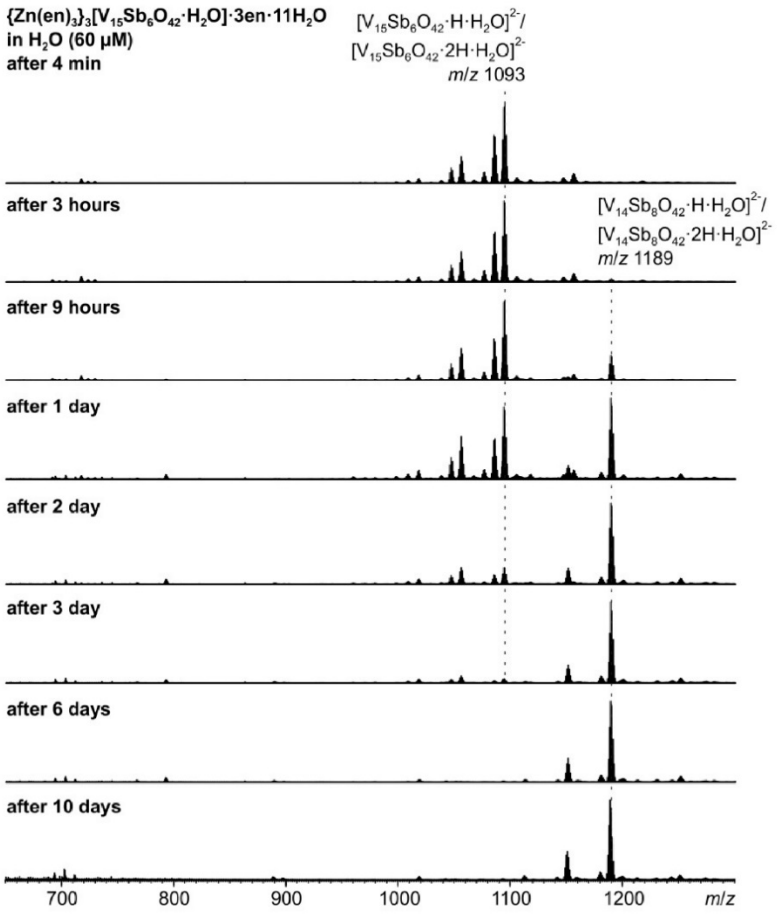

Fig. S 5: ESI-Q-TOF-HRMS spectra of compound **II** (60 µM in aqueous 1% NH_4OAc solution) after different reaction times. Labeled peaks were used for graphical analysis.

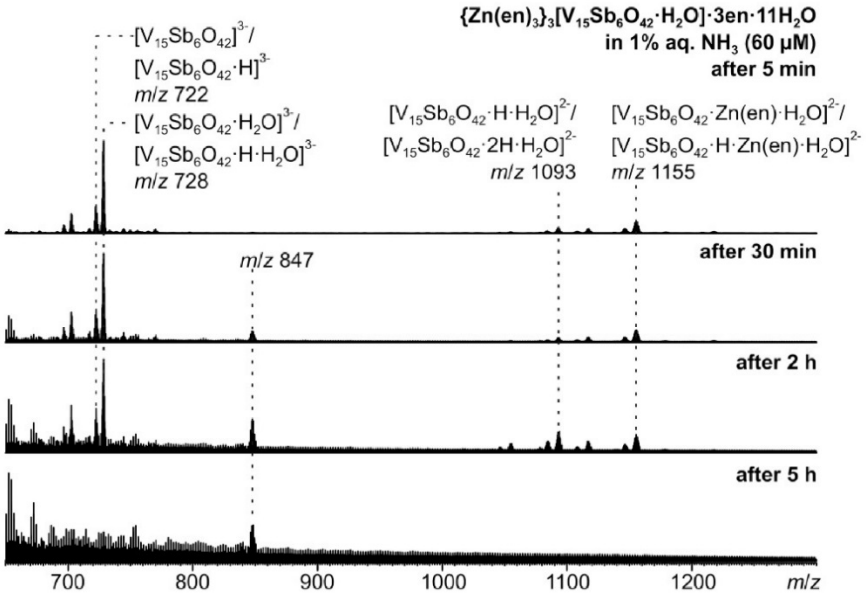

Fig. S 6: ESI-Q-TOF-HRMS spectra of compound **II** (60 µM in aqueous 1% NH_3 solution) after different reaction times.

3. Single crystal data

Table S 1: Selected crystal data and refinement results for compounds **II**-**IV**.

Compound	**II**	**III**	**IV**
Formula	$C_{24}H_{106}N_{24}O_{53}Sb_6V_{15}Zn_3$	$C_{76}H_{112}N_{16}O_{66}Sb_6V_{15}Zn_3$	$C_{12}H_{71}N_{12}O_{53.5}Sb_6V_{15}Zn_3$
Weight [g.mol^{-1}]	3270.03	3996.56	2930.51
Crystal system	monoclinic	monoclinic	monoclinic
Space group	$P2_1$	$C2/c$	$P2_1/c$
***a* [Å]**	14.2860(2)	21.2237(5)	15.1955(3)
***b* [Å]**	22.7600(2)	31.1346(6)	18.1415(3)
***c* [Å]**	15.0139(2)	18.7156(4)	27.6042(6)
***α* [°]**	90	90	90
***β* [°]**	103.0330(10)	91.983(2)	105.726(2)
***γ* [°]**	90	90	90
***V* [Å^3]**	4756.01(10)	12359.7(5)	7324.8(3)
Z	2	4	4
***D*$_{calc}$ [mg·m^3]**	2.28390	2.122	2.657
***μ* [mm^{-1}]**	3.904	3.029	5.049
Min/max trans.	0.4911/0.6428	0.5539/0.6729	4152/0.5790
***Θ*$_{max}$ [°]**	27.003	26.004	25.141
Measured refl.	75994	41666	50802
Independent refl.	20786	12153	13000
***R*$_{int}$**	0.0313	0.0524	0.0437
Refl.[$F_0>4\sigma(F_0)$]	19916	12153	11467
Parameters	1144	822	932
***R*$_1$ [$F_0>4\sigma(F_0)$]**	0.0388	0.0473	0.0525
***wR*$_2$**	0.1036	0.1292	0.1344
GOF	1.053	1.041	1.114
***Δρ*$_{max/min}$ [e·Å^{-3}]**	1.89/-1.209	0.97/-0.85	1.64/-1.39
Flack X-parameter	0.012(5)	-	-

4. Bond lengths and angles

4.1. Compound **II** $\{Zn(en)_3\}_3[V_{15}Sb_6O_{42}(H_2O)]\cdot 3en\cdot 10H_2O$ bond lengths and angles

Table S 2: Selected bond lengths [Å] and angles [°] (compound **II**).

Sb(1)-O(1)	1.920(8)	Sb(4)-O(2)	1.926(7)
Sb(1)-O(9)	1.945(6)	Sb(4)-O(40)	1.944(7)
Sb(1)-O(36)	1.948(7)	Sb(4)-O(31)	2.015(6)
Sb(2)-O(16)	1.950(7)	Sb(5)-O(3)	1.917(7)
Sb(2)-O(12)	1.950(7)	Sb(5)-O(42)	1.939(6)
Sb(2)-O(1)	1.963(8)	Sb(5)-O(37)	1.972(6)
Sb(3)-O(2)	1.950(7)	Sb(6)-O(21)	1.946(6)
Sb(3)-O(22)	1.953(6)	Sb(6)-O(3)	1.954(7)
Sb(3)-O(8)	2.024(6)	Sb(6)-O(6)	2.026(7)
V(1)-O(11)	1.634(7)	V(7)-V(12)	3.026(2)
V(1)-O(13)	1.918(7)	V(7)-V(8)	3.045(2)
V(1)-O(23)	1.952(7)	V(8)-O(38)	1.628(7)
V(1)-O(8)	1.964(6)	V(8)-O(19)	1.922(6)
V(1)-O(40)	1.969(7)	V(8)-O(10)	1.928(7)
V(1)-V(10)	2.902(2)	V(8)-O(15)	1.949(6)
V(1)-V(12)	2.961(2)	V(8)-O(9)	2.005(7)
V(1)-V(3)	3.051(2)	V(8)-V(9)	2.895(2)
V(2)-O(29)	1.625(7)	V(9)-O(4)	1.632(7)
V(2)-O(41)	1.920(6)	V(9)-O(10)	1.919(7)
V(2)-O(17)	1.944(6)	V(9)-O(15)	1.960(6)
V(2)-O(31)	1.961(6)	V(9)-O(6)	1.965(7)
V(2)-O(22)	1.968(7)	V(9)-O(42)	1.970(7)
V(2)-V(4)	2.871(2)	V(9)-V(14)	2.984(2)
V(2)-V(15)	2.994(2)	V(10)-O(27)	1.615(7)
V(2)-V(11)	3.037(2)	V(10)-O(13)	1.930(7)
V(3)-O(35)	1.605(6)	V(10)-O(20)	1.937(7)
V(3)-O(13)	1.933(7)	V(10)-O(23)	1.965(6)
V(3)-O(7)	1.942(6)	V(10)-O(12)	2.020(7)
V(3)-O(18)	1.962(7)	V(10)-V(13)	3.055(2)
V(3)-O(40)	1.983(6)	V(11)-O(26)	1.608(7)
V(3)-V(6)	2.863(2)	V(11)-O(41)	1.918(6)
V(4)-O(30)	1.622(7)	V(11)-O(34)	1.929(7)
V(4)-O(10)	1.923(7)	V(11)-O(19)	1.943(6)
V(4)-O(41)	1.932(6)	V(11)-O(22)	2.011(6)
V(4)-O(17)	1.950(6)	V(12)-O(39)	1.622(7)
V(4)-O(42)	2.003(6)	V(12)-O(34)	1.926(7)
V(4)-V(9)	3.054(2)	V(12)-O(23)	1.928(6)
V(5)-O(32)	1.612(7)	V(12)-O(8)	1.956(7)
V(5)-O(7)	1.927(6)	V(12)-O(16)	1.976(7)
V(5)-O(20)	1.938(7)	V(13)-O(5)	1.615(7)
V(5)-O(28)	1.946(7)	V(13)-O(20)	1.899(7)
V(5)-O(21)	2.011(7)	V(13)-O(28)	1.930(7)
V(5)-V(13)	2.845(2)	V(13)-O(12)	1.976(7)
V(5)-V(6)	3.042(2)	V(13)-O(36)	1.988(7)
V(6)-O(24)	1.615(7)	V(13)-V(14)	3.021(2)
V(6)-O(7)	1.916(7)	V(14)-O(33)	1.626(7)
V(6)-O(18)	1.944(6)	V(14)-O(28)	1.920(7)
V(6)-O(21)	1.972(6)	V(14)-O(15)	1.932(6)
V(6)-O(37)	1.974(6)	V(14)-O(6)	1.951(7)
V(6)-V(15)	3.018(2)	V(14)-O(36)	1.975(7)
V(7)-O(14)	1.623(7)	V(15)-O(25)	1.616(7)
V(7)-O(19)	1.904(7)	V(15)-O(18)	1.933(7)
V(7)-O(34)	1.935(6)	V(15)-O(17)	1.937(7)
V(7)-O(16)	1.979(7)	V(15)-O(31)	1.959(6)
V(7)-O(9)	1.986(7)	V(15)-O(37)	1.981(6)
V(7)-V(11)	2.819(2)		
Zn(1)-N(22)	2.163(8)	Zn(2)-N(51)	2.197(8)
Zn(1)-N(11)	2.180(9)	Zn(2)-N(52)	2.200(8)
Zn(1)-N(2)	2.184(9)	Zn(2)-N(41)	2.206(8)
Zn(1)-N(12)	2.185(8)	Zn(3)-N(71)	2.174(9)
Zn(1)-N(1)	2.205(8)	Zn(3)-N(62)	2.175(10)
Zn(1)-N(21)	2.263(8)	Zn(3)-N(82)	2.179(9)
Zn(2)-N(31)	2.175(9)	Zn(3)-N(81)	2.186(9)
Zn(2)-N(42)	2.183(9)	Zn(3)-N(72)	2.193(9)
Zn(2)-N(32)	2.184(8)	Zn(3)-N(61)	2.209(9)
N(1)-C(1)	1.474(14)	N(61)-C(61)	1.445(17)
C(1)-C(2)	1.482(16)	C(61)-C(62)	1.48(2)
C(2)-N(2)	1.492(13)	C(62)-N(62)	1.495(16)
N(11)-C(11)	1.490(15)	N(71)-C(71)	1.461(13)
C(11)-C(12)	1.489(16)	C(71)-C(72)	1.521(17)

C(12)-N(12)	1.454(14)	C(72)-N(72)	1.463(16)
N(21)-C(21)	1.480(15)	N(81)-C(81)	1.463(15)
C(21)-C(22)	1.519(17)	C(81)-C(82)	1.478(17)
C(22)-N(22)	1.486(13)	C(82)-N(82)	1.495(15)
N(31)-C(31)	1.467(12)	N(91)-C(91)	1.42(2)
C(31)-C(32)	1.516(17)	C(91)-C(92)	1.50(2)
C(32)-N(32)	1.480(14)	C(92)-N(92)	1.49(2)
N(41)-C(41)	1.527(16)	N(93)-C(93)	1.463(19)
C(41)-C(42)	1.479(19)	C(93)-C(94)	1.49(2)
C(42)-N(42)	1.473(14)	C(94)-N(94)	1.51(3)
N(51)-C(51)	1.488(12)	N(95)-C(95)	1.64(3)
C(51)-C(52)	1.494(15)	C(95)-C(96)	1.75(3)
C(52)-N(52)	1.469(13)	C(96)-N(96)	1.55(3)
N(22)-Zn(1)-N(11)	165.1(3)	N(32)-Zn(2)-N(52)	92.3(3)
N(22)-Zn(1)-N(2)	92.6(3)	N(51)-Zn(2)-N(52)	79.3(3)
N(11)-Zn(1)-N(2)	100.5(3)	N(31)-Zn(2)-N(41)	93.4(3)
N(22)-Zn(1)-N(12)	93.1(3)	N(42)-Zn(2)-N(41)	79.8(4)
N(11)-Zn(1)-N(12)	79.6(3)	N(32)-Zn(2)-N(41)	99.5(3)
N(2)-Zn(1)-N(12)	91.7(3)	N(51)-Zn(2)-N(41)	90.9(3)
N(22)-Zn(1)-N(1)	96.6(3)	N(52)-Zn(2)-N(41)	165.7(3)
N(11)-Zn(1)-N(1)	92.7(3)	N(71)-Zn(3)-N(62)	92.9(4)
N(2)-Zn(1)-N(1)	79.7(3)	N(71)-Zn(3)-N(82)	171.5(4)
N(12)-Zn(1)-N(1)	167.3(3)	N(62)-Zn(3)-N(82)	92.8(4)
N(22)-Zn(1)-N(21)	79.5(3)	N(71)-Zn(3)-N(81)	95.6(4)
N(11)-Zn(1)-N(21)	88.9(3)	N(62)-Zn(3)-N(81)	169.1(4)
N(2)-Zn(1)-N(21)	166.5(3)	N(82)-Zn(3)-N(81)	79.5(4)
N(12)-Zn(1)-N(21)	99.7(3)	N(71)-Zn(3)-N(72)	79.8(3)
N(1)-Zn(1)-N(21)	90.2(3)	N(62)-Zn(3)-N(72)	96.3(4)
N(31)-Zn(2)-N(42)	168.7(3)	N(82)-Zn(3)-N(72)	93.3(4)
N(31)-Zn(2)-N(32)	79.7(3)	N(81)-Zn(3)-N(72)	92.0(3)
N(42)-Zn(2)-N(32)	92.4(4)	N(71)-Zn(3)-N(61)	97.2(3)
N(31)-Zn(2)-N(51)	88.5(3)	N(62)-Zn(3)-N(61)	80.2(4)
N(42)-Zn(2)-N(51)	100.5(4)	N(82)-Zn(3)-N(61)	90.0(4)
N(32)-Zn(2)-N(51)	164.6(3)	N(81)-Zn(3)-N(61)	91.9(4)
N(31)-Zn(2)-N(52)	96.7(3)	N(72)-Zn(3)-N(61)	175.3(4)
N(42)-Zn(2)-N(52)	91.7(3)		

4.2. Compound **III** ($\{Zn(phen)_3\}_2[Zn(en)_2V_{15}Sb_6O_{42}(H_2O)]\cdot 23H_2O$) bond lengths and angles

Table S 3: Selected bond lengths [Å] and angles [°] for compound **III**.

Sb(1)-O(3)	1.937(4)	O(2)-Sb(3)#1	1.940(3)
Sb(1)-O(5)	1.961(4)	O(7)-Sb(2)#1	1.938(4)
Sb(1)-O(18)	1.971(4)	O(8)-V(5)#1	1.940(4)
Sb(2)-O(3)	1.925(4)	O(10)-Zn(1)	2.241(4)
Sb(2)-O(7)#1	1.938(4)	O(11)-V(4)#1	1.912(4)
Sb(2)-O(15)	1.947(4)	O(18)-V(5)#1	1.991(4)
Sb(3)-O(21)	1.930(4)	O(18)-V(2)#1	2.000(4)
Sb(3)-O(20)	1.933(4)	O(21)-V(4)#1	2.006(4)
Sb(3)-O(2)	1.940(3)	Zn(1)-N(2)	2.120(5)
		Zn(1)-N(2)#2	2.120(5)
V(1)-O(17)	1.613(4)	Zn(1)-N(1)	2.127(5)
V(1)-O(4)	1.914(4)	Zn(1)-N(1)#2	2.127(5)
V(1)-O(11)	1.924(4)	Zn(2)-N(51)	2.156(6)
V(1)-O(6)	1.949(4)	Zn(2)-N(32)	2.182(5)
V(1)-O(21)	2.020(4)	Zn(2)-N(52)	2.201(6)
V(1)-V(7)	2.8449(13)	Zn(2)-N(31)	2.205(6)
V(1)-V(4)#1	3.0612(14)	N(2)-Zn(1)-N(2)#2	180.0
V(2)-O(13)	1.604(4)	N(2)-Zn(1)-N(1)	82.4(2)
V(2)-O(14)	1.926(4)	N(2)#2-Zn(1)-N(1)	97.6(2)
V(2)-O(19)	1.954(4)	N(2)-Zn(1)-N(1)#2	97.6(2)
V(2)-O(7)	1.977(4)	N(2)#2-Zn(1)-N(1)#2	82.4(2)
V(2)-O(18)#1	2.000(4)	N(1)-Zn(1)-N(1)#2	180.0
V(2)-V(3)	2.8639(14)	N(2)-Zn(1)-O(10)	85.40(18)
V(2)-V(8)	3.0261(11)	N(2)#2-Zn(1)-O(10)	94.60(18)
V(2)-V(5)	3.0371(14)	N(1)-Zn(1)-O(10)	88.98(18)
V(3)-O(9)	1.616(4)	N(1)#2-Zn(1)-O(10)	91.02(18)
V(3)-O(14)	1.931(4)	N(2)-Zn(1)-O(10)#2	94.60(18)
V(3)-O(4)	1.933(4)	N(2)#2-Zn(1)-O(10)#2	85.40(18)
V(3)-O(19)	1.955(4)	N(1)-Zn(1)-O(10)#2	91.02(18)
V(3)-O(15)	2.008(4)	N(1)#2-Zn(1)-O(10)#2	88.98(18)
V(3)-V(7)	3.0541(14)	O(10)-Zn(1)-O(10)#2	180.00(19)
V(4)-O(12)	1.607(4)	N(12)-Zn(2)-N(11)	78.3(2)
V(4)-O(11)#1	1.911(4)	N(12)-Zn(2)-N(51)	163.3(2)
V(4)-O(8)	1.934(4)	N(11)-Zn(2)-N(51)	90.8(2)
V(4)-O(20)	1.977(4)	N(12)-Zn(2)-N(32)	101.5(2)
V(4)-O(21)#1	2.006(4)	N(11)-Zn(2)-N(32)	164.9(2)
V(4)-V(5)#1	2.8214(14)	N(51)-Zn(2)-N(32)	92.4(2)
V(4)-V(6)	3.0140(14)	N(12)-Zn(2)-N(52)	91.9(2)
V(4)-V(1)#1	3.0612(14)	N(11)-Zn(2)-N(52)	94.9(2)
V(5)-O(10)	1.632(4)V(5)-O(14)	N(51)-Zn(2)-N(52)	76.4(2)
V(5)-O(11)	1.917(4)	N(32)-Zn(2)-N(52)	100.2(2)
V(5)-O(8)#1	1.939(4)	N(12)-Zn(2)-N(31)	95.1(2)
V(5)-O(18)#1	1.991(4)	N(11)-Zn(2)-N(31)	89.1(2)
V(5)-V(4)#1	2.8214(14)	N(51)-Zn(2)-N(31)	97.2(2)
V(6)-O(22)	1.612(4)	N(32)-Zn(2)-N(31)	75.9(2)
V(6)-O(6)	1.920(4)	N(52)-Zn(2)-N(31)	172.5(2)
V(6)-O(8)	1.926(4)		
V(6)-O(5)	1.989(4)		
V(6)-O(20)	2.002(4)		
V(6)-V(7)	2.9991(14)		
V(7)-O(16)	1.624(4)	π- π –interactions	3.918
V(7)-O(4)	1.899(4)	π- π –interactions	3.918
V(7)-O(6)	1.945(4)	π- π –interactions	3.918
V(7)-O(5)	1.970(4)	π- π –interactions	3.918
V(7)-O(15)	1.990(4)	π- π -interactions	3.888
V(8)-O(1)	1.600(6)	π- π –interactions	3.888
V(8)-O(19)	1.955(4)	π- π –interactions	3.888
V(8)-O(19)#1	1.955(4)	π- π –interactions	3.888
V(8)-O(7)	1.975(4)	π- π –interactions	3.885
V(8)-O(7)#1	1.975(4)	π- π –interactions	3.885
V(8)-V(2)#1	3.0261(11)	π- π –interactions	3.715
		π- π –interactions	3.715
Zn(1)-O(10)#2	2.241(4)	π- π –interactions	3.702
N(1)-C(1)	1.486(9)	π- π –interactions	3.702
C(1)-C(2)	1.512(10)	π- π -interactions	3.588
C(2)-N(2)	1.482(9)	π- π –interactions	3.588
Zn(2)-N(12)	2.142(6)		
Zn(2)-N(11)	2.153(5)		

4.3. Compound **IV** ($\{\{Zn(en)_2(H_2O)_2\}(Zn(en)_2)\}[Zn(en)_2V_{15}Sb_6O_{42}(H_2O)]\cdot 8.5H_2O$) bond lengths and angles

Table S 4: Selected bond lengths [Å] and angles [°] for compound **IV**.

Sb(1)-O(5)	1.941(6)	V(9)-V(15)	2.895(2)
Sb(1)-O(13)	1.950(6)	V(10)-O(33)	1.606(6)
Sb(1)-O(18)	1.951(6)	V(10)-O(36)	1.933(6)
Sb(2)-O(20)	1.951(6)	V(10)-O(41)	1.939(6)
Sb(2)-O(13)	1.962(7)	V(10)-O(1)	1.958(6)
Sb(2)-O(14)	1.981(6)	V(10)-O(25)	1.994(6)
Sb(3)-O(2)	1.924(6)	V(11)-O(42)	1.623(6)
Sb(3)-O(26)	1.950(6)	V(11)-O(22)	1.907(6)
Sb(3)-O(16)	1.975(6)	V(11)-O(12)	1.947(6)
Sb(4)-O(3)	1.932(6)	V(11)-O(4)	1.955(6)
Sb(4)-O(26)	1.964(6)	V(11)-O(2)	2.011(6)
Sb(4)-O(25)	1.971(6)	V(12)-O(31)	1.603(6)
Sb(5)-O(27)	1.944(7)	V(12)-O(28)	1.934(6)
Sb(5)-O(8)	1.962(6)	V(12)-O(22)	1.935(6)
Sb(5)-O(6)	1.975(6)	V(12)-O(19)	1.960(6)
Sb(6)-O(27)	1.936(6)	V(12)-O(18)	1.990(6)
Sb(6)-O(7)	1.953(6)	V(12)-V(15)	3.052(2)
Sb(6)-O(34)	1.965(6)	V(13)-O(23)	1.625(6)
		V(13)-O(29)	1.896(6)
V(1)-O(40)	1.626(6)	V(13)-O(8)	1.951(6)
V(1)-O(15)	1.932(6)	V(13)-O(9)	1.965(6)
V(1)-O(9)	1.938(6)	V(13)-O(34)	1.966(6)
V(1)-O(14)	1.946(6)	V(14)-O(38)	1.608(6)
V(1)-O(8)	1.960(6)	V(14)-O(24)	1.937(6)
V(1)-V(15)	2.968(2)	V(14)-O(4)	1.952(6)
V(1)-V(13)	3.018(2)	V(14)-O(7)	1.966(6)
V(2)-O(30)	1.616(6)	V(14)-O(16)	1.966(6)
V(2)-O(41)	1.930(6)	V(15)-O(37)	1.603(6)
V(2)-O(24)	1.944(6)	V(15)-O(28)	1.919(6)
V(2)-O(16)	1.954(6)	V(15)-O(15)	1.939(6)
V(2)-O(25)	1.966(6)	V(15)-O(18)	1.968(7)
V(2)-V(8)	2.907(2)	V(15)-O(14)	1.981(6)
V(2)-V(14)	2.973(2)		
V(2)-V(10)	3.045(2)	O(23)-Zn(1)	2.344(6)
V(3)-O(35)	1.614(6)	Zn(1)-N(1)	2.021(8)
V(3)-O(1)	1.909(6)	Zn(1)-N(11)	2.042(8)
V(3)-O(19)	1.937(6)	Zn(1)-N(12)	2.043(8)
V(3)-O(5)	1.977(6)	Zn(1)-N(2)	2.118(9)
V(3)-O(3)	1.979(6)	Zn(2)-N(31)	2.113(10)
V(3)-V(4)	3.027(2)	Zn(2)-N(32)	2.135(9)
V(3)-V(6)	3.029(2)	Zn(2)-N(21)	2.137(10)
V(4)-O(17)	1.606(6)	Zn(2)-N(22)	2.167(11)
V(4)-O(36)	1.907(6)	Zn(2)-O(48)	2.249(9)
V(4)-O(1)	1.945(6)	Zn(2)-O(49)	2.279(9)
V(4)-O(20)	1.974(6)	Zn(3)-N(41)	1.973(10)
V(4)-O(5)	1.996(7)	Zn(3)-N(51)	2.005(10)
V(4)-V(10)	2.858(2)	Zn(3)-N(52)	2.013(10)
V(4)-V(5)	3.037(2)	Zn(3)-N(42)	2.018(9)
V(5)-O(10)	1.620(6)		
V(5)-O(36)	1.916(6)	N(1)-Zn(1)-N(11)	131.0(3)
V(5)-O(29)	1.949(6)	N(1)-Zn(1)-N(12)	138.7(3)
V(5)-O(9)	1.961(6)	N(11)-Zn(1)-N(12)	87.5(3)
V(5)-O(20)	2.027(6)	N(1)-Zn(1)-N(2)	84.2(3)
V(5)-V(13)	2.864(2)	N(11)-Zn(1)-N(2)	104.8(4)
V(6)-O(21)	1.614(6)	N(12)-Zn(1)-N(2)	101.7(3)
V(6)-O(22)	1.914(6)	N(1)-Zn(1)-O(23)	84.6(3)
V(6)-O(19)	1.939(6)	N(11)-Zn(1)-O(23)	85.5(3)
V(6)-O(3)	1.970(6)	N(12)-Zn(1)-O(23)	84.3(3)
V(6)-O(2)	2.000(6)	N(2)-Zn(1)-O(23)	168.2(3)
V(6)-V(12)	2.820(2)	C(1)-N(1)-Zn(1)	109.6(6)
V(6)-V(11)	3.053(2)	N(31)-Zn(2)-N(32)	84.2(4)
V(7)-O(11)	1.623(6)	N(31)-Zn(2)-N(21)	94.3(4)
V(7)-O(12)	1.903(6)	N(32)-Zn(2)-N(21)	108.7(4)
V(7)-O(4)	1.943(6)	N(31)-Zn(2)-N(22)	173.0(4)
V(7)-O(7)	1.962(6)	N(32)-Zn(2)-N(22)	91.7(4)
V(7)-O(6)	1.991(6)	N(21)-Zn(2)-N(22)	81.6(4)

V(7)-V(11)	2.866(2)	N(31)-Zn(2)-O(48)	92.3(4)
V(7)-V(14)	3.013(2)	N(32)-Zn(2)-O(48)	86.0(4)
V(7)-V(9)	3.053(2)	N(21)-Zn(2)-O(48)	164.4(4)
V(8)-O(32)	1.615(6)	N(22)-Zn(2)-O(48)	93.0(4)
V(8)-O(41)	1.922(6)	N(31)-Zn(2)-O(49)	93.9(4)
V(8)-O(29)	1.934(6)	N(32)-Zn(2)-O(49)	164.6(3)
V(8)-O(24)	1.960(6)	N(21)-Zn(2)-O(49)	86.7(4)
V(8)-O(34)	2.019(6)	N(22)-Zn(2)-O(49)	91.5(4)
V(8)-V(13)	3.030(2)	O(48)-Zn(2)-O(49)	78.7(4)
V(9)-O(39)	1.600(6)	N(41)-Zn(3)-N(51)	128.0(4)
V(9)-O(12)	1.940(6)	N(41)-Zn(3)-N(52)	125.2(4)
V(9)-O(28)	1.951(6)	N(51)-Zn(3)-N(52)	85.9(4)
V(9)-O(15)	1.966(6)	N(41)-Zn(3)-N(42)	87.9(4)
V(9)-O(6)	2.038(6)	N(51)-Zn(3)-N(42)	119.7(4)
		N(52)-Zn(3)-N(42)	113.0(4)

Table S 5: Selected bond lengths [Å] for compounds **II**-**IV**.

Comp.	Type	min. bond length [Å]	max. bond length [Å]	average [Å]
	Sb-O	1.917(7)	2.026(7)	1.958
	V-μ_2/μ_3-O	1.904(7)	2.020(7)	1.918
II	**terminal V=O**	1.605(6)	1.634(7)	1.620
	Zn-N	2.163(8)	2.263(8)	2.191
	V-V	2.819(2)	3.055(2)	2.971
	Sb-N	2.613(10)	2.656(13)	-
	Sb-O	1.925(4)	1.971(4)	1.942
	V-μ_2/μ_3-O	1.899(4)	2.020(4)	1.956
III	**terminal V=O**	1.600(6)	1.632(4)	1.614
	V-V	2.821(14)	3.061(14)	2.969
	Zn(1)-N	2.120(5)	2.127(5)	-
	Zn(1)-O	2.241(4)	2.241(4)	-
	Zn(2)-N	2.142(6)	2.205(6)	2.153
	Sb-O	1.924(6)	1.981(6)	1.955
	V-μ_2/μ_3-O	1.896(6)	2.038(6)	1.955
	terminal V=O	1.600(6)	1.626(6)	1.614
IV	**V-V**	2.820(2)	3.053(2)	2.973
	Zn(1)-N	2.021(8)	2.118(9)	2.056 Å
	Zn(2)-N	2.113(10)	2.167(11)	2.138
	Zn(3)	1.973(10)	2.018(9)	2.003
	Zn(1)-O	2.344(6)	2.344(6)	-
	Zn(2)-O	2.249(9)	2.279(9)	-

Table S 6: Selected angles [°] for compound **II**-**IV**.

Comp.	angle	min. angle [°]	max. angle [°]
II	**N-Zn-N**	79.3(3)	99.7(3)
	trans N-Zn-N	164.6(3)	175.3(4)
III	**N-Zn-N**	78.3(2)	172.5(2)
	trans N-Zn-N	163.3(2)	180.0(19)
	bite N-Zn(1)-N	82.4(2)	-
	corr. N-Zn(1)-N	97.6(2)	-
IV	**N-Zn(1)-N**	87.5(3)	137.7(3)
	basal O-Zn(1)-N	84.5(3)	85.5(3)
	trans O-Zn(1)-N	168.2(3)	-
IV	**N-Zn(3)-N**	85.9(4)	128.0(4)

5. BVS

Table S 7: Results of bond valence sum calculations of compounds **II**-**IV**.[1]

Compound II		**Compound III**		**Compound IV**	
V(1)	3.94	V(1)	4.02	V(1)	4.01
V(2)	3.99	V(2)	3.97	V(2)	4.02
V(3)	4.02	V(3)	3.97	V(3)	4.02
V(4)	3.99	V(4)	4.01	V(4)	4.02
V(5)	4.02	V(5)	4.02	V(5)	3.92
V(6)	4.02	V(6)	3.97	V(6)	3.99
V(7)	3.98	V(7)	3.98	V(7)	3.99
V(8)	3.97	V(8)	3.98	V(8)	3.97
V(9)	3.94			V(9)	3.94
V(10)	3.95			V(10)	4.01
V(11)	4.05			V(11)	3.96
V(12)	4.01			V(12)	4.04
V(13)	4.02			V(13)	4.02
V(14)	4.03			V(14)	4.01
V(15)	3.99			V(15)	4.06
average	**3.99**	**average**	**3.99**	**average**	**4.00**
Sb(1)	3.15	Sb(1)	3.35	Sb(1)	3.43
Sb(2)	3.00	Sb(2)	3.53	Sb(2)	3.28
Sb(3)	2.85	Sb(3)	3.55	Sb(3)	3.42
Sb(4)	2.95			Sb(4)	3.36
Sb(5)	3.10			Sb(5)	3.31
Sb(6)	2.85			Sb(6)	3.40
average	**2.98**	**average**	**3.48**	**average**	**3.37**

General characterization methods

IR spectra were measured from 400 to 4000 cm^{-1} using a Genesis FTIRTM spectrometer (ATI Mattson) at room temperature. UV/VIS spectra were recorded on an Agilent 8453 spectrometer (Agilent Technologies) in a range of 190 nm to 1100 nm (deviation: ± 0.5 nm; wavelength reproducibility: ± 0.02 nm). CHN analyses were performed with a EA Elemental Analyzer (EURO VECTOR Instruments).

EDX analyses were performed with a Environmental Scanning Electron Microscope ESEM XL30 (Philips) equipped with an EDX detector.

The powder patterns were recorded using a STADI-P diffractometer in transmission geometry with Cu-Kα_1 radiation (STOE, λ = 1.540598 Å, Ge(111) monochromator) with a Mythen 1 K detector. The powder patterns of the compounds are compared with calculated patterns demonstrating phase purity of the materials (Fig. S 7 – S 9).

Electrospray ionisation quadrupole-time-of-flight high resolution mass spectrometric (ESI-Q-TOF-HRMS) experiments were performed with a Synapt G2-S HDMS (Waters Co., Milford, MA, USA) instrument. The flow rate was set to 3-5 µL min^{-1}, the spray voltage to 1.6 kV, the sample cone voltage to 10 V, the source offset to 80 V, the nebuliser gas to 6 bar and the desolvation gas flow to 500 L h^{-1}. 60 µM solutions from crystalline samples **I** and **II** were prepared in H_2O, aqueous 1% NH_4OAc solution and aqueous 1% NH_3 solution, respectively. Time-dependent measurements were conducted on samples kept at 4 °C from which aliquots were taken and directly subjected to the mass spectrometric experiments. All reaction times given therefore refer to the reaction at 4 °C.

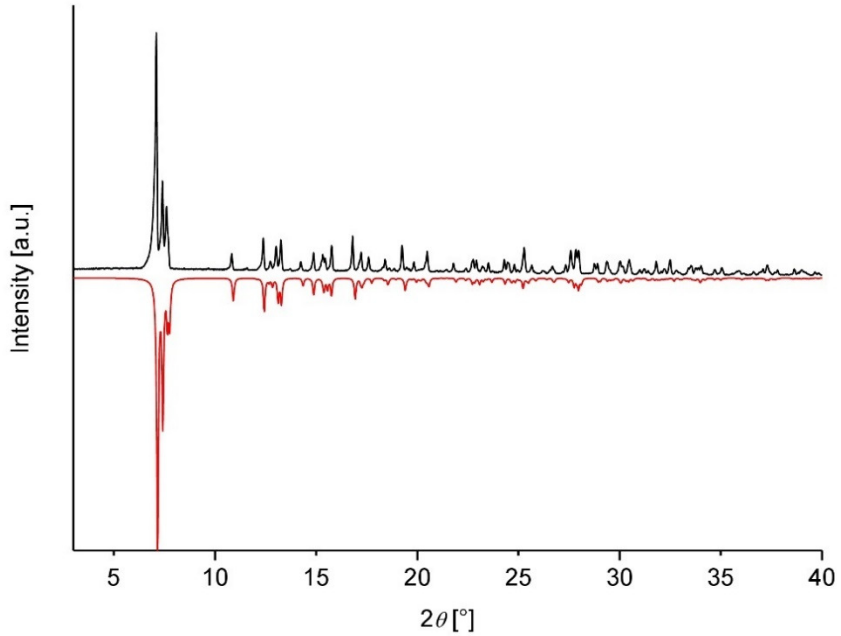

Fig. S 7: The X-ray powder pattern of the new water soluble hetero-POV $\{Zn(en)_3\}_3[V_{15}Sb_6O_{42}(H_2O)]\cdot 3en\cdot 10.5H_2O$ (**II**) (black) and the calculated pattern using single crystal data (red).

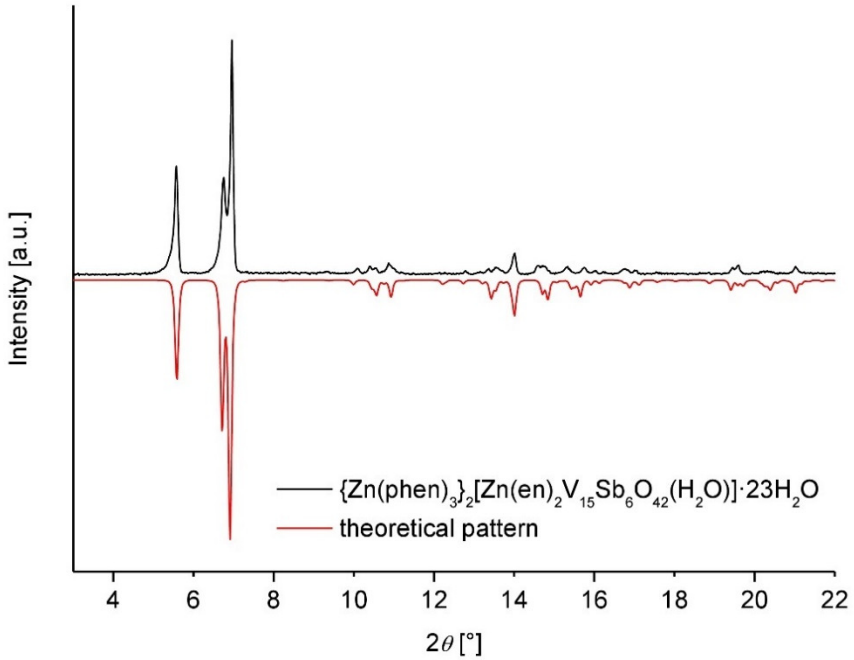

Fig. S 8: The X-ray powder pattern of $\{Zn(phen)_3\}_2[Zn(en)_2V_{15}Sb_6O_{42}(H_2O)]\cdot 23H_2O$ (**III**) (black) the calculated pattern using single crystal data (red).

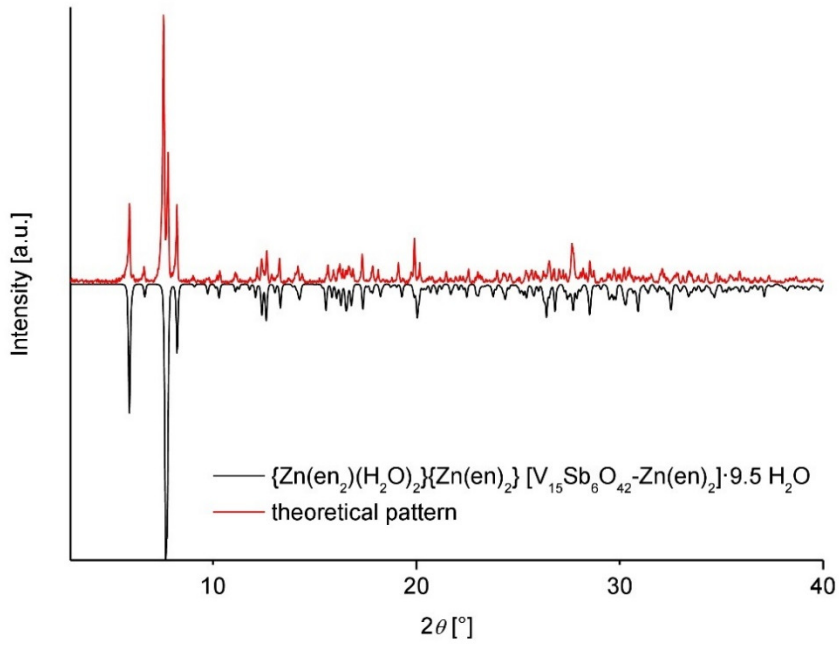

Fig. S 9: The X-ray powder pattern of $\{Zn(en_2)(H_2O)_2\}\{Zn(en)_2\}$ $[V_{15}Sb_6O_{42}\text{-}Zn(en)_2]\cdot 9.5\ H_2O$ (**IV**) (black) and the calculated pattern using single crystal data (red).

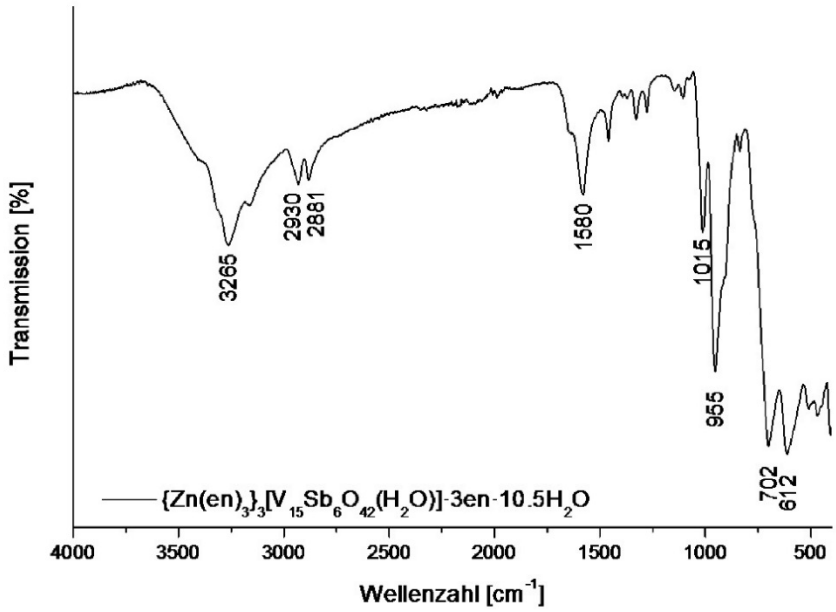

Fig. S 10: IR spectrum of $\{Zn(en)_3\}_3[V_{15}Sb_6O_{42}(H_2O)]\cdot 3en\cdot 10.5H_2O$ (**II**).

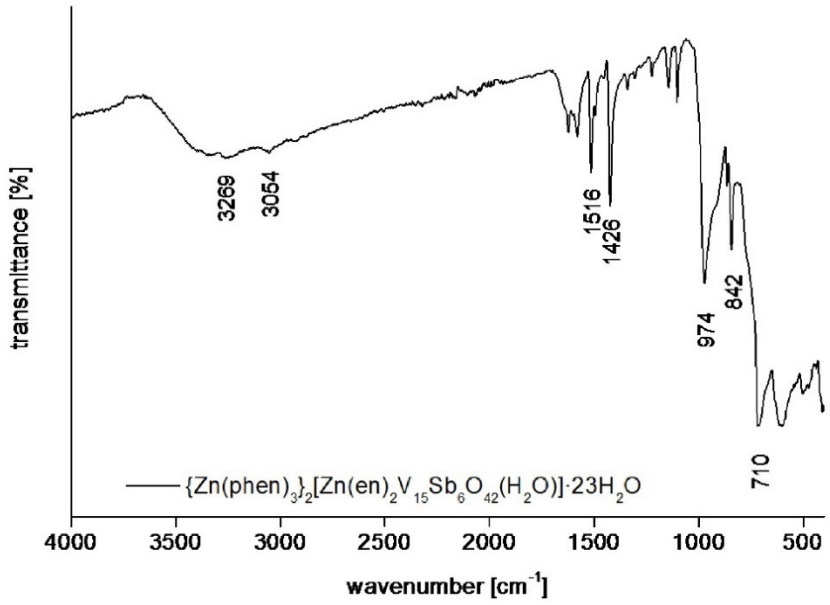

Fig. S 11: IR spectrum of $\{Zn(phen)_3\}_2[Zn(en)_2V_{15}Sb_6O_{42}(H_2O)]\cdot 23H_2O$ (**III**).

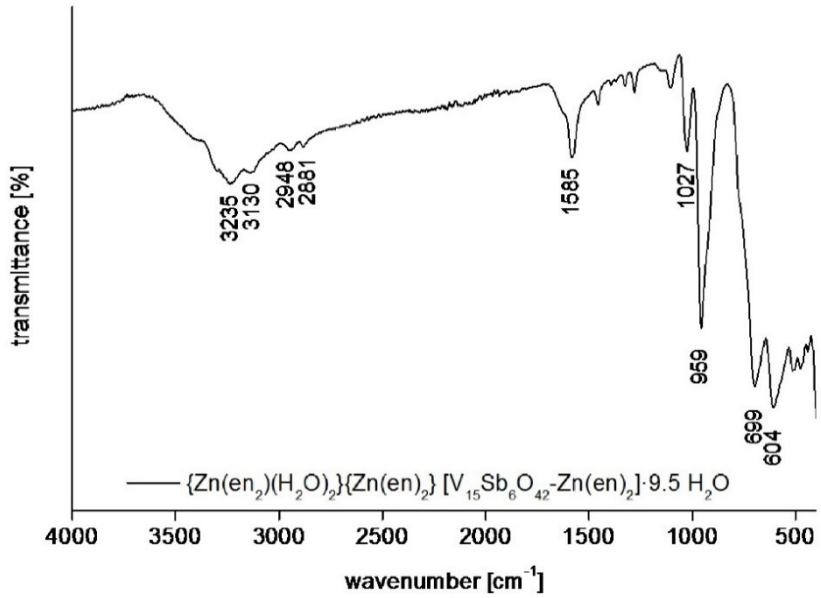

Fig. S 12: IR spectrum of $\{Zn(en_2)(H_2O)_2\}\{Zn(en)_2\}$ $[V_{15}Sb_6O_{42}\text{-}Zn(en)_2]\cdot 9.5\ H_2O$ (**IV**).

6. Compound **II**

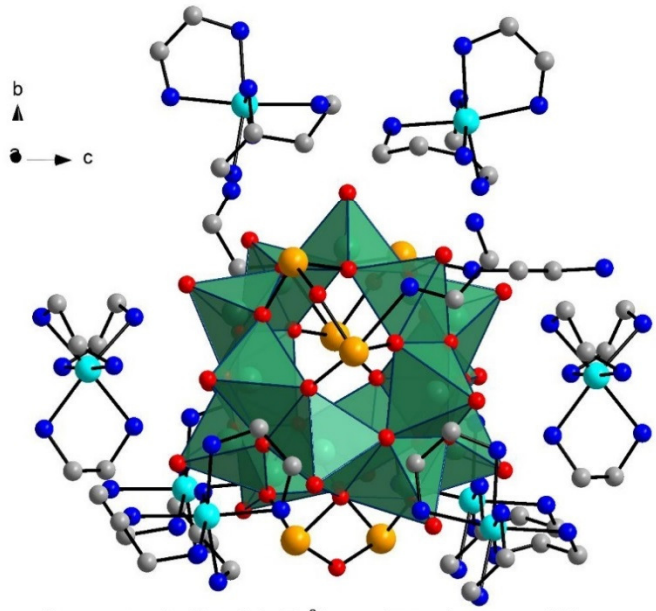

Fig. S 13: One cluster anion surrounded by eight Zn^{2+} complexes (compound **II**)

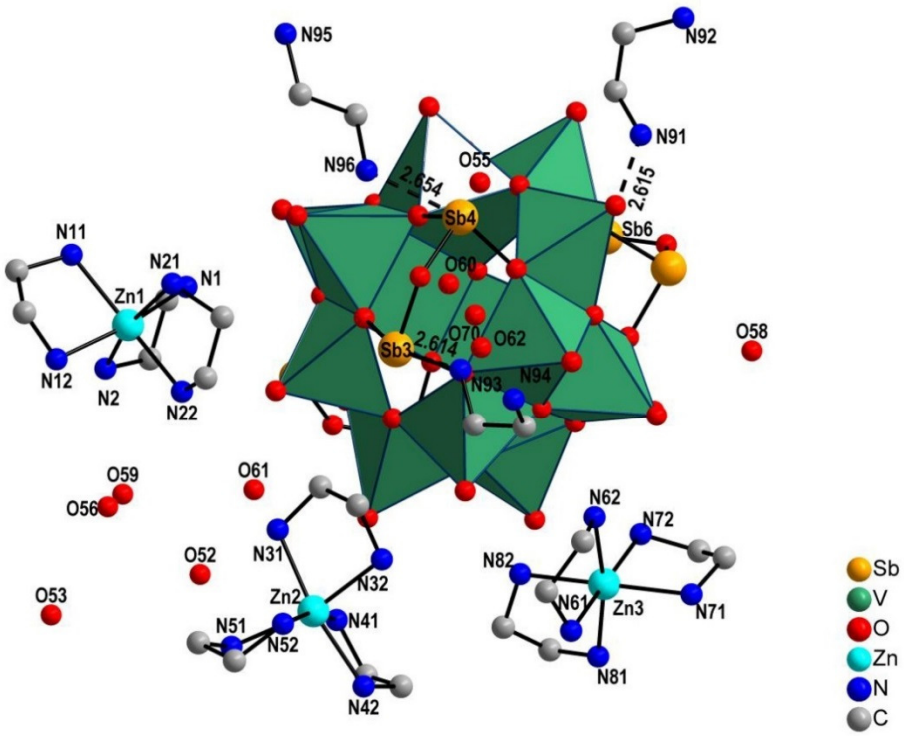

Fig. S 14: View of the constituents in the structure of compound **II** with water-molecules and selected atom labels.

Table S 8: Geometric parameters of hydrogen bonds [Å and °] (compound **II**).

D-H...A	d(D-H)	d(H...A)	d(D...A)	<(DHA)
Complexes (H) – Cluster (O)				
N(1)-H(1B)...O(39)	0.91	2.55	3.320(11)	143.1
N(2)-H(2D)...O(18)#1	0.91	2.43	3.274(10)	155.2
N(2)-H(2D)...O(24)#1	0.91	2.61	3.184(10)	121.6
N(11)-H(11B)...O(25)#1	0.91	2.10	2.959(11)	158.0
N(12)-H(12C)...O(24)#1	0.91	2.18	3.021(11)	152.6
N(12)-H(12D)...O(5)#3	0.91	2.22	3.083(10)	157.1
N(21)-H(21B)...O(32)#3	0.91	2.48	3.230(11)	140.5
C(22)-H(22B)...O(28)#3	0.99	2.57	3.418(12)	143.1
N(22)-H(22D)...O(39)	0.91	2.01	2.903(11)	168.0
N(31)-H(31B)...O(33)#3	0.91	2.08	2.952(10)	159.0
C(31)-H(31B)...O(34)	0.99	2.48	3.355(12)	147.2
N(32)-H(32D)...O(26)	0.91	2.30	3.068(10)	142.3
N(41)-H(41A)...O(29)#5	0.91	2.34	3.079(11)	138.1
N(41)-H(41B)...O(14)	0.91	2.39	3.160(11)	142.3
N(42)-H(42D)...O(25)#5	0.91	2.07	2.975(11)	170.4
N(51)-H(51B)...O(17)#5	0.91	2.37	3.128(10)	140.6
N(51)-H(51B)...O(25)#5	0.91	2.60	3.385(11)	144.6
C(51)-H(51B)...O(33)#3	0.99	2.60	3.453(11)	144.7
N(52)-H(52D)...O(33)#3	0.91	2.49	3.263(11)	142.5
N(61)-H(61A)...O(27)	0.91	2.63	3.400(14)	142.9
N(61)-H(61B)...O(13)	0.91	2.50	3.180(11)	132.2
N(61)-H(61B)...O(35)	0.91	2.24	3.069(12)	151.9
N(62)-H(62D)...O(26)#7	0.91	2.44	3.206(12)	141.7
N(62)-H(62D)...O(41)#7	0.91	2.44	3.229(11)	145.4
N(71)-H(71A)...O(35)	0.91	2.47	3.066(11)	123.5
N(71)-H(71B)...O(7)	0.91	2.21	3.051(10)	153.9
C(71)-H(71B)...O(59)#8	0.99	2.65	3.306(17)	123.9
N(72)-H(72C)...O(38)#7	0.91	2.56	3.363(12)	147.6
N(72)-H(72D)...O(10)#7	0.91	2.63	3.266(10)	127.2
N(72)-H(72D)...O(30)#7	0.91	2.27	3.147(11)	161.2
N(81)-H(81B)...O(20)	0.91	2.39	3.102(11)	135.1
N(81)-H(81B)...O(27)	0.91	2.47	3.287(11)	149.5
N(82)-H(82C)...O(26)#7	0.91	2.28	3.044(11)	140.9
N(82)-H(82D)...O(19)#7	0.91	2.30	3.042(11)	138.1
N(82)-H(82D)...O(38)#7	0.91	2.49	3.283(11)	146.1
Ethylenediamine (H) – Crystal water (O)				
N(1)-H(1A)...O(54)	0.91	2.27	3.120(14)	155.6
N(2)-H(2C)...O(59)	0.91	2.31	3.188(15)	161.2
N(11)-H(11A)...O(51)#2	0.91	2.30	3.126(13)	150.9
N(21)-H(21A)...O(54)	0.91	2.48	3.314(15)	152.9
N(22)-H(22C)...O(56)#3	0.91	2.64	3.509(14)	159.5
N(22)-H(22C)...O(59)	0.91	2.61	3.319(14)	135.8
N(31)-H(31A)...O(52)#3	0.91	2.61	3.397(14)	144.7
N(32)-H(32C)...O(57)#4	0.91	2.21	3.113(13)	172.1
N(42)-H(42C)...O(54)#4	0.91	2.39	3.273(15)	162.6
N(51)-H(51A)...O(52)#3	0.91	2.27	3.144(14)	162.1
N(52)-H(52C)...O(51)#3	0.91	2.46	3.244(12)	144.0
N(62)-H(62C)...O(52)#6	0.91	2.51	3.191(16)	131.4
N(71)-H(71A)...O(59)#8	0.91	2.62	3.328(15)	135.0
N(72)-H(72C)...O(51)#7	0.91	2.60	3.345(12)	139.6
N(81)-H(81A)...O(32)	0.91	2.29	3.083(11)	145.7

Ethylenediamine (N) – Crystalwater (O)

N1	O54	3.123
N2	O59	3.192
N51	O52	3.146
N62	O52	3.180
N91	O60	2.924
N92	O55	2.772
N95	O57	2.792
O51	N11	3.123
O52	N51	3.146
O52	N62	3.180
O52	N62	3.180
O52	N62	3.180
O52	N51	3.146
O52	N51	3.146
O55	N92	2.772
O57	N32	3.116
O59	N2	3.192
O59	N2	3.192
O59	N2	3.192
O60	N93	3.125

O60	N93	3.125
O60	N91	2.924

Table S 9: O-O-distances compound **II**

Atom 1	Atom 2	distance [Å]
O52	O61	2.645
O52	O61	2.645
O52	O59	2.807
O52	O61	2.645
O52	O61	2.645
O53	O58	2.853
O53	O56	2.948
O53	O58	2.853
O53	O56	2.948
O53	O58	2.853
O54	O57	2.768
O55	O60	2.872
O55	O60	2.872
O56	O53	2.948
O56	O59	2.802
O56	O59	2.802
O56	O59	2.802
O56	O53	2.948
O58	O53	2.853
O59	O52	2.807
O59	O52	2.807
O59	O52	2.807
O59	O56	2.802

7. Compound **III**

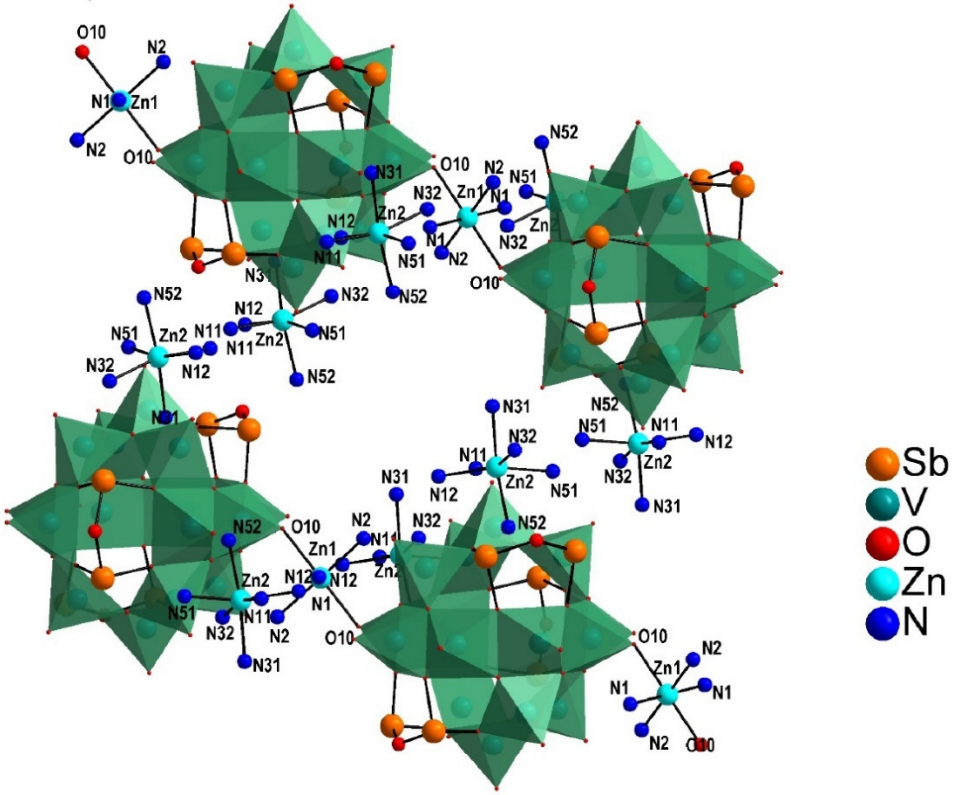

Fig. S 15: View of the constituents in the structure of compound **III** with selected atom labels.

Table S 10: O-O distances between crystal water O atoms and O atoms of the cluster anion (compound **III**).

Atom 1	Atom 2	distance [Å]
O(10)	O(36)	2.779
O(16)	O(31)	2.695
O(16)	O(34)	2.820
O(17)	O(32)	2.745
O(22)	O(39)	2.874
O(3)	O(34)	3.127
O(33)	O(9)	2.767

Table S 11: O-H-distances between crystal water and cationic-complexes (compound **III**).

Atom 1	Atom 2	distance [Å]
O(33)	H(13)	2.588
O(36)	H(2N2)	2.666
O(37)	H(55)	2.552
O(38)	H(59)	2.640
O(39)	H(31)	2.558
O(40)	H(36)	2.538

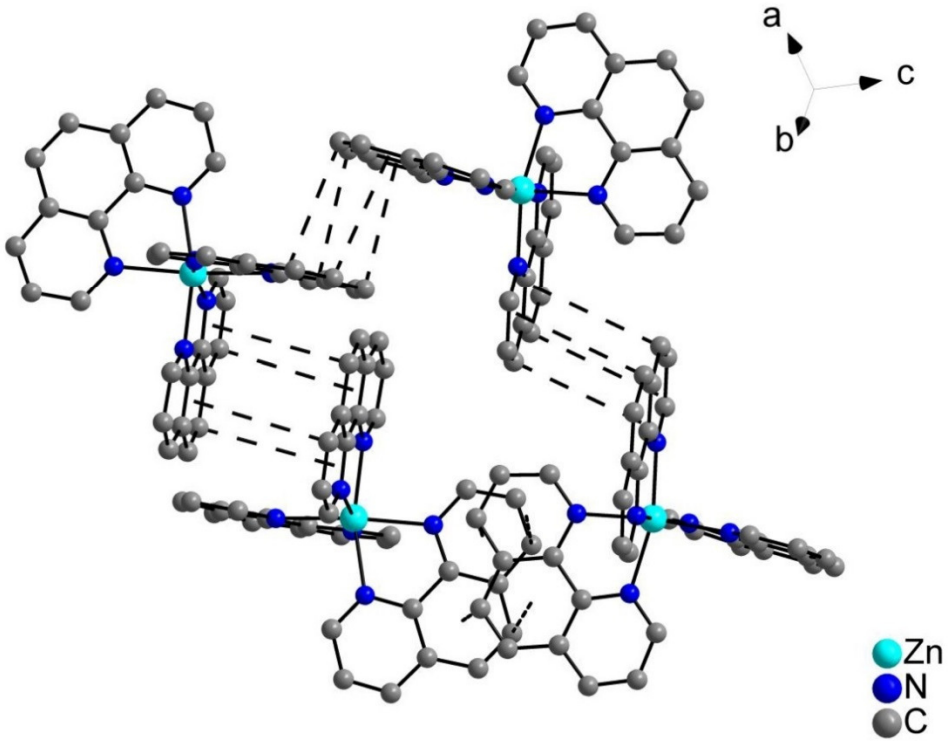

Fig. S 16: Proposed π-π-stacking interactions between phen ligands of the $[Zn(phen)_3]^{2+}$-complexes in compound **III** (H-atoms have been omitted for clarity).

Table S 12: Geometric parameters of hydrogen bonds in compound **III** [Å and °].

D-H...A	d(D-H)	d(H...A)	d(D...A)	<(DHA)
Complexes (H) – Cluster (O)				
N(1)-H(1N1)...O(14)	0.91	2.27	3.122(6)	154.8
C(1)-H(1A)...O(12)#3	0.99	2.58	3.562(8)	169.7
N(2)-H(1N2)...O(11)#2	0.91	2.30	3.166(7)	159.7
N(2)-H(1N2)...O(17)#2	0.91	2.62	3.242(7)	126.0
C(11)-H(11)...N(51)	0.95	2.69	3.233(9)	116.9
C(12)-H(12)...O(16)#5	0.95	2.47	3.222(8)	136.5
C(19)-H(19)...O(9)#6	0.95	2.51	3.385(10)	153.7
C(31)-H(31)...N(11)	0.95	2.62	3.182(9)	118.3
C(32)-H(32)...O(12)#7	0.95	2.39	3.042(8)	125.9
C(39)-H(39)...O(12)	0.95	2.42	3.093(10)	127.9
C(39)-H(39)...O(21)#1	0.95	2.64	3.555(9)	160.9
C(52)-H(52)...O(6)#7	0.95	2.65	3.447(9)	141.9
C(52)-H(52)...O(17)#7	0.95	2.58	3.443(9)	150.9
Complexes (H) – Crystal water (O)				
N(1)-H(2N1)...O(41)#3	0.91	2.52	3.214(10)	133.1
N(2)-H(2N2)...O(33A)#4	0.91	2.12	3.00(4)	163.1
C(31)-H(31)...O(39)	0.95	2.56	3.219(12)	126.9
C(59)-H(59)...O(38)	0.95	2.64	3.340(12)	130.8

8. Compound **IV**

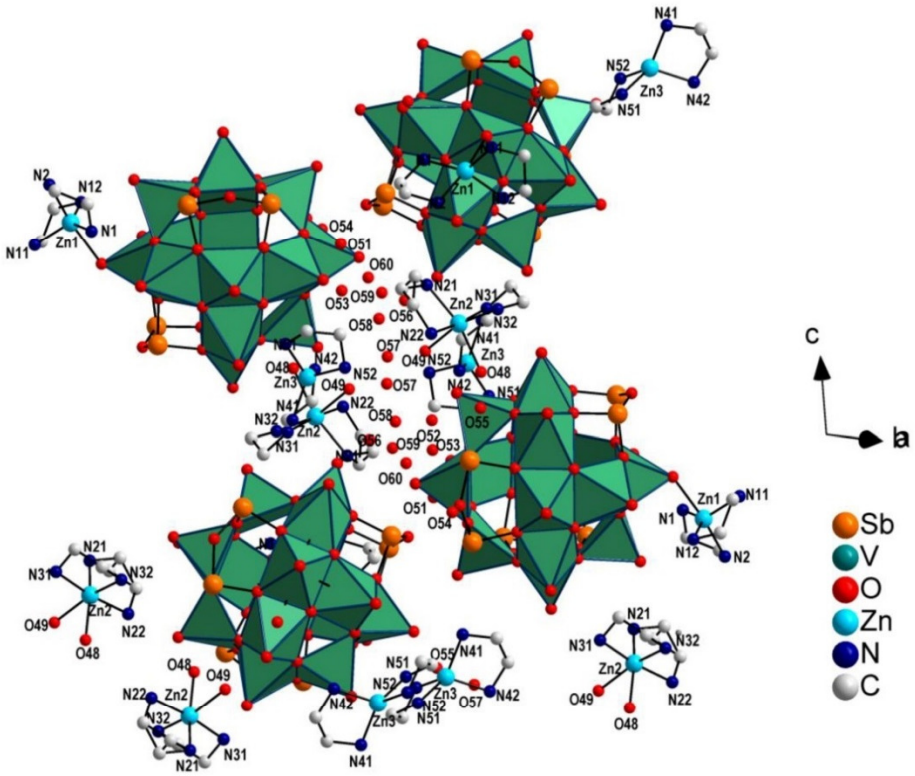

Fig. S 17: Constituents in the structure of compound **IV** with selected atom labels.

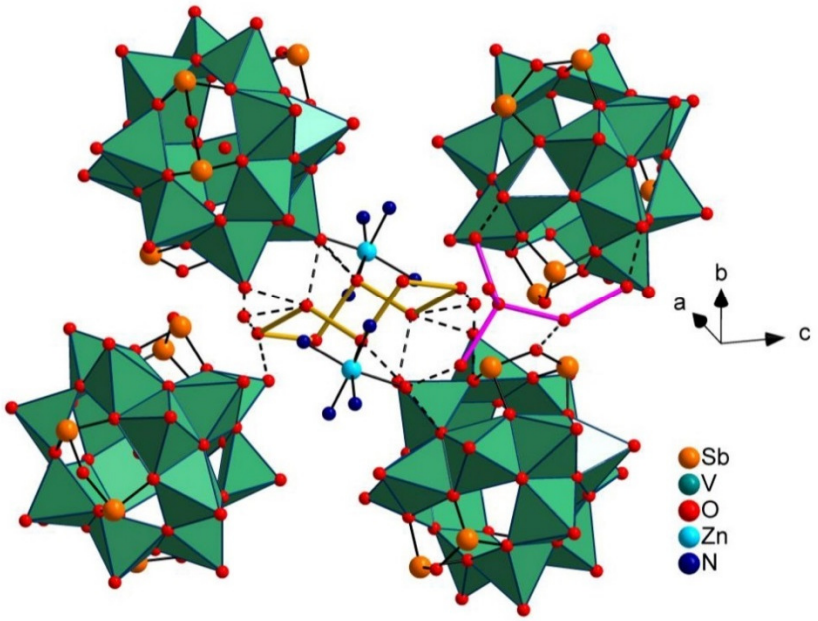

Fig. S 18: Water cluster in the structure of compound **IV**; yellow: R8 ring formed with one water-molecule of the Zn^{2+} complexes, pink: D4 chain.

Table S 13: Geometric parameters of hydrogen bonds in compound **IV** [Å and °].

D-H...A	d(D-H)	d(H...A)	d(D...A)	<(DHA)
Complexes (H) – Cluster (O)				
N(1)-H(1C)...O(9)	0.91	2.08	2.960(10)	162.4
N(2)-H(2C)...O(33)#3	0.91	2.47	3.289(12)	149.8
N(2)-H(2C)...O(41)#3	0.91	2.45	3.104(11)	128.9
N(11)-H(11C)...O(33)#3	0.91	2.01	2.885(10)	162.0
N(11)-H(11D)...O(6)#4	0.91	2.45	3.313(10)	159.6
N(11)-H(11D)...O(11)#4	0.91	2.55	3.116(10)	121.2
C(12)-H(12A)...O(25)#3	0.99	2.63	3.614(12)	175.4
N(12)-H(12C)...O(29)	0.91	2.55	3.354(10)	148.0
N(21)-H(21C)...O(10)#2	0.91	2.14	3.010(11)	159.9
C(22)-H(22F)...O(32)#6	0.99	2.48	3.312(17)	141.0
N(22)-H(22D)...O(38)#6	0.91	2.29	3.181(13)	166.9
N(31)-H(31C)...O(11)#1	0.91	2.33	3.141(11)	148.9
N(31)-H(31D)...O(17)#2	0.91	2.41	3.311(11)	169.3
C(31)-H(31A)...O(33)#2	0.99	2.49	3.223(14)	130.4
N(32)-H(32C)...O(30)#6	0.91	2.18	3.072(11)	167.1
N(41)-H(41C)...O(37)#9	0.91	2.13	2.891(12)	140.7
N(41)-H(41D)...O(35)#2	0.91	2.28	3.142(12)	158.1
C(41)-H(41B)...O(1)#2	0.99	2.52	3.471(13)	161.9
C(41)-H(41A)...O(39)#1	0.99	2.52	3.241(14)	129.4
C(42)-H(42A)...O(42)#1	0.99	2.65	3.334(13)	126.1
N(42)-H(42D)...O(12)#1	0.91	2.29	3.150(11)	157.5
N(51)-H(51C)...O(37)#9	0.91	2.59	3.276(11)	132.3
N(51)-H(51D)...O(28)#1	0.91	2.23	3.102(11)	159.8
N(51)-H(51D)...O(37)#1	0.91	2.56	3.132(12)	121.2
C(52)-H(52B)...O(31)#1	0.99	2.40	3.282(13)	148.6
N(52)-H(52D)...O(40)#9	0.91	2.08	2.981(12)	171.1
Complexes (H) – Crystal water (O)				
N(1)-H(1D)...O(52)#1	0.91	2.06	2.944(11)	163.4
C(2)-H(2A)...O(51)#2	0.99	2.60	3.555(13)	161.7
N(2)-H(2D)...O(30)#3	0.91	2.29	2.997(11)	133.8
C(12)-H(12B)...O(51)#5	0.99	2.46	3.414(14)	161.6
N(12)-H(12D)...O(30)#3	0.91	2.29	3.048(10)	140.1
N(22)-H(22C)...O(57)	0.91	2.14	3.028(17)	163.5
C(32)-H(32B)...O(54)#7	0.99	2.42	3.399(14)	172.6
N(32)-H(32D)...O(55)#8	0.91	2.54	3.325(13)	144.7
N(42)-H(42C)...O(57)#2	0.91	2.55	3.196(16)	128.8
N(52)-H(52C)...O(57)#2	0.91	2.36	3.170(17)	147.9

10. SEM pictures

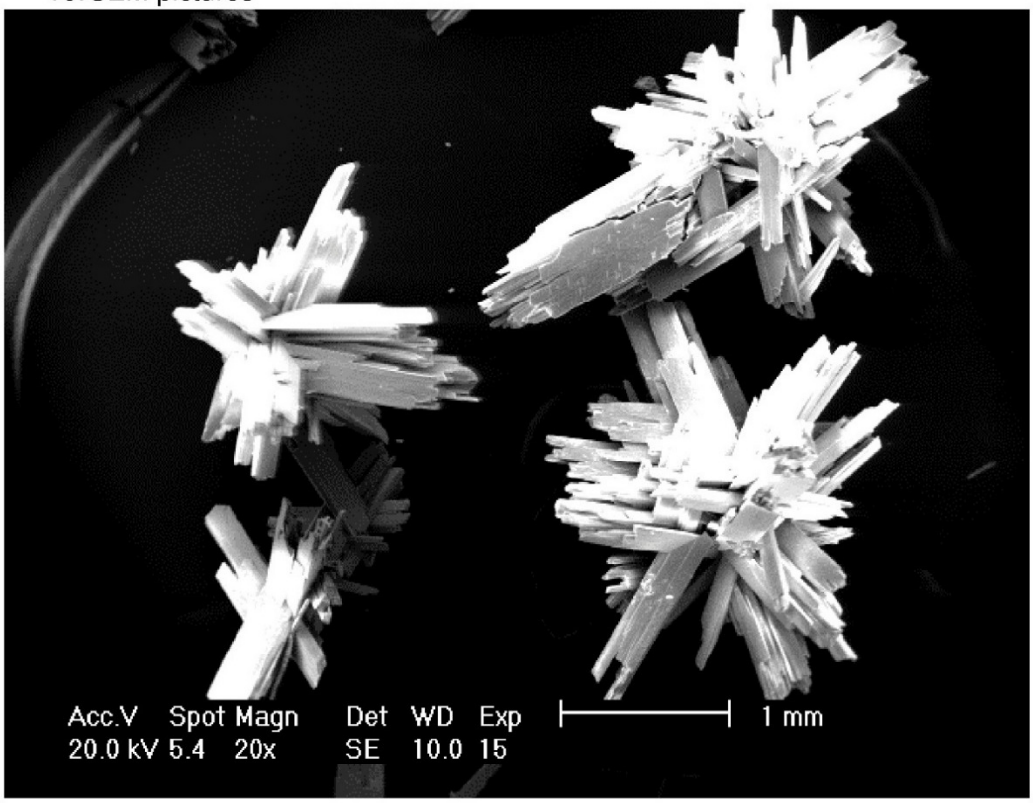

Fig. S 19: SEM picture of compound **II**.

Fig. S 20: Photograph of the crystals through a microscope.

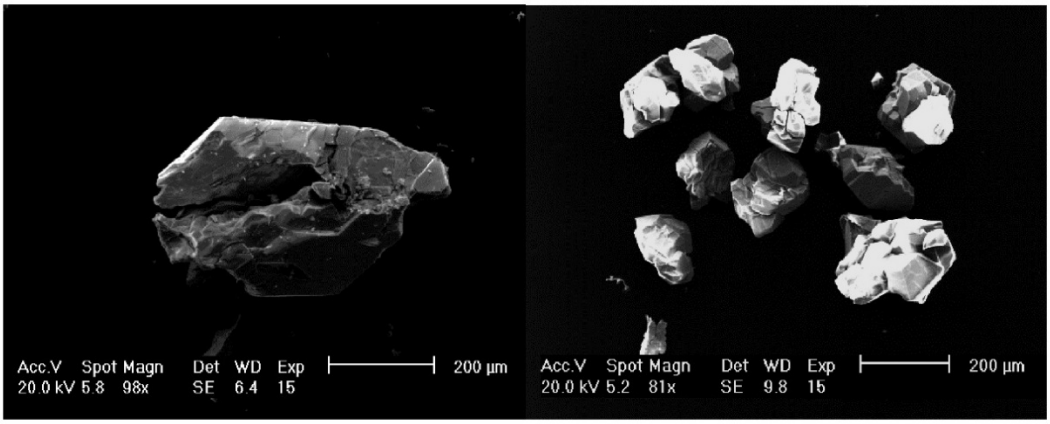

Fig. S 21: SEM picture of compound **III**.

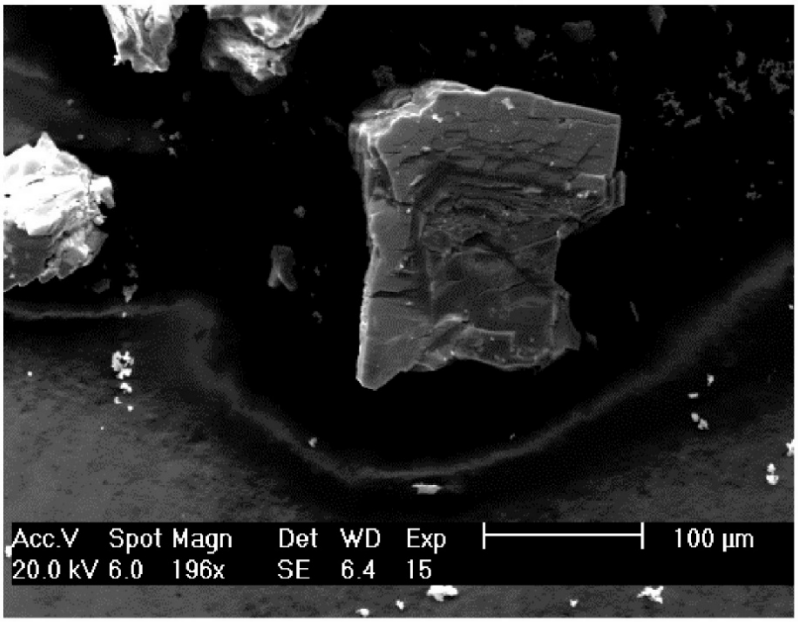

Fig. S 22: SEM picture of compound **IV**.

11. Literature

[1] a) I. D. Brown, D. Altermatt, *Acta Crystallogr B* **1985**, *41*, 244–247. b) M. O'Keefe, N. E. Brese, *J. Am. Chem. Soc.* **1991**, *113*, 3226–3229.

[2] M. Wendt, U. Warzok, C. Näther, J. van Leusen, P. Kögerler, C. A. Schalley, W. Bensch, *Chem. Sci.* **2016**, *7*, 2684–2694.

7.5 Supporting Information der Publikation *„Rational Syntheses of Three New {$V_{14}Sb_8$}-Clusters Applying a Water Soluble High-Nuclearity Cluster as Synthon"*

Rational Syntheses of Three New {$V_{14}Sb_8$}-Clusters Applying a Water Soluble High-Nuclearity Cluster as Synthon

*Lisa K. Mahnke, Michael Wendt, Christian Näther, Wolfgang Bensch**

Institut für Anorganische Chemie, Christian-Albrechts-Universität zu Kiel, Max-Eyth-Straße 2,

24118 Kiel, Germany, wbensch@ac.uni-kiel.de

Content

Further synthetic information

Synthesis of $\{Zn(phen)_3\}_2[V_{14}Sb_8O_{42}]\cdot 0.5phen\cdot 18H_2O$ (**1**) without compound Zn-$\{V_{15}Sb_8\}$: 0.1567 g NH_4VO_3, 0.0773 g Sb_2O_3, 0.1961 g $Zn(NO_3)_2\cdot 6H_2O$, 0.3565 g phenanthroline and a mixture of 3.7 mL dist. H_2O and 0.3 mL methylamine (40%) were heated at 150°C for 7d. Yield: ca. 79 %.

Synthesis of $\{Fe(phen)_3\}_2[V_{14}Sb_8O_{42}(H_2O)]\cdot phen\cdot 11\ H_2O$ (**3**) without Zn-$\{V_{15}Sb_8\}$: 0.0640 g NH_4VO_3, 0.1225 g Sb_2O_3, 0.0621 g $FeCl_2\cdot 4H_2O$, 0.4005 g phenanthroline and a mixture of 2.3 mL dist. H_2O and 0.067 mL diethylenetriamine were heated at 150°C for 7d. Yield: ca. 51 %.

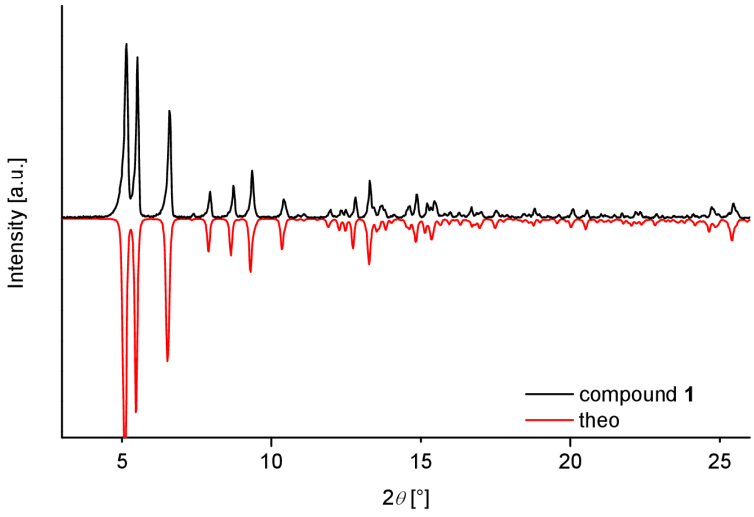

Figure S 1. X-ray powder diffraction pattern of compound **1**.

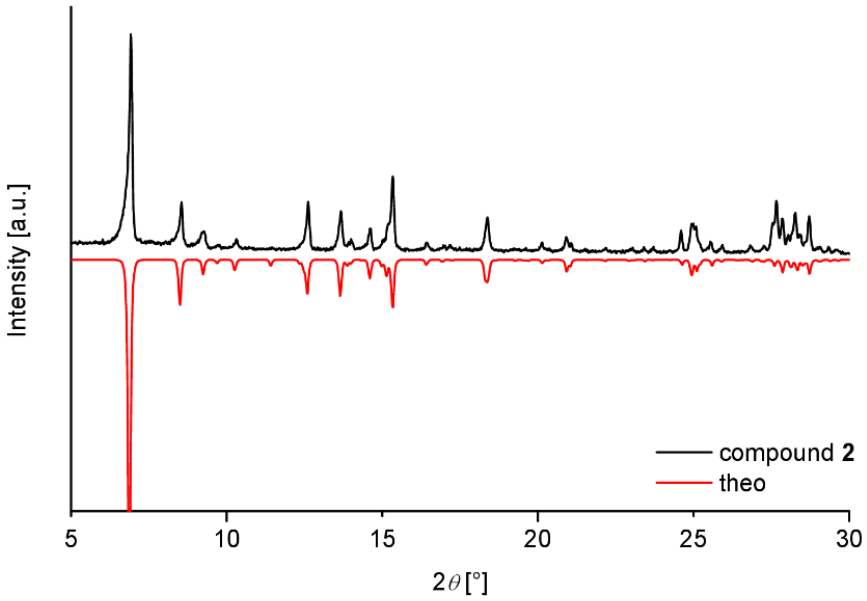

Figure S 2. X-ray powder diffraction pattern of compound **2**.

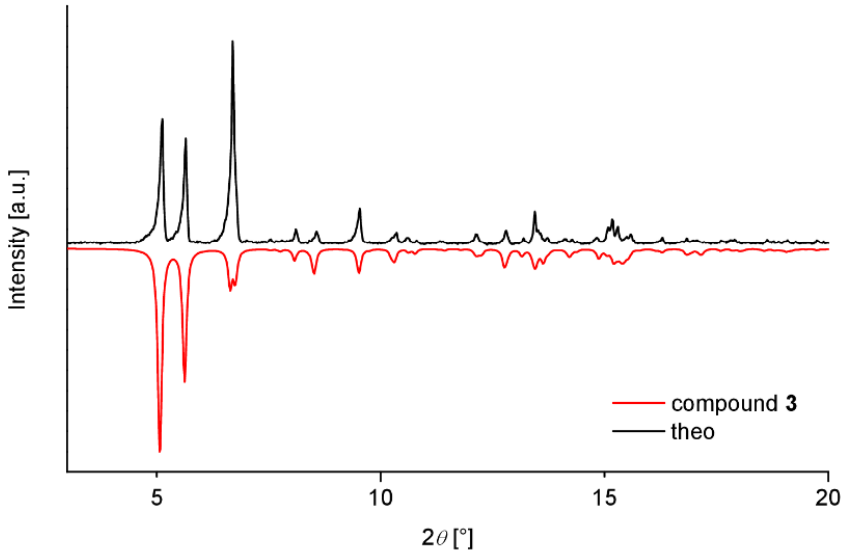

Figure S 3. X-ray powder diffraction pattern of compound **3**.

Table S 1. Selected bond lengths [Å] and angles [°] compound **1**. Symmetry transformations used to generate equivalent atoms: #1 -x+2,-y+1,-z+1

Sb(1)-O(12)	1.956(5)	V(5)-O(19)	1.996(5)	**Complexes**	
Sb(1)-O(3)	1.964(5)	V(6)-O(10)	1.603(5)	Zn(1)-N(41)	2.137(7)
Sb(1)-O(16)	1.969(6)	V(6)-O(8)	1.927(5)	Zn(1)-N(1)	2.142(7)
Sb(2)-O(17)	1.938(5)	V(6)-O(18)	1.946(5)	Zn(1)-N(22)	2.146(6)
Sb(2)-O(16)	1.958(6)	V(6)-O(23)	1.970(5)	Zn(1)-N(42)	2.179(7)
Sb(2)-O(2)	1.988(5)	V(6)-O(38)	1.972(6)	Zn(1)-N(2)	2.187(7)
Sb(3)-O(4)	1.932(6)	V(7)-O(35)	1.621(5)	Zn(1)-N(21)	2.201(7)
Sb(3)-O(6)	1.935(5)	V(7)-O(36)	1.931(5)	Zn(2)-N(61)	2.132(7)
Sb(3)-O(38)	1.956(5)	V(7)-O(15)	1.932(5)	Zn(2)-N(81)	2.137(7)
Sb(4)-O(4)	1.929(5)	V(7)-O(3)	1.961(5)	Zn(2)-N(62)	2.146(7)
Sb(4)-O(41)	1.946(5)	V(7)-O(7)	1.990(5)	Zn(2)-N(101)	2.148(7)
Sb(4)-O(28)	1.994(6)	V(8)-O(27)	1.594(5)	Zn(2)-N(82)	2.168(7)
Sb(5)-O(34)	1.941(5)	V(8)-O(5)	1.953(5)	Zn(2)-N(102)	2.195(6)
Sb(5)-O(25)	1.950(5)	V(8)-O(28)	1.963(5)		
Sb(5)-O(7)	1.957(5)	V(8)-O(23)	1.971(5)	N(41)-Zn(1)-N(1)	163.7(3)
Sb(6)-O(1)	1.934(5)	V(8)-O(38)	1.978(5)	N(41)-Zn(1)-N(22)	93.6(3)
Sb(6)-O(30)	1.934(5)	V(9)-O(40)	1.597(5)	N(1)-Zn(1)-N(22)	99.6(3)
Sb(6)-O(25)	1.959(5)	V(9)-O(8)	1.951(5)	N(41)-Zn(1)-N(42)	77.5(3)
Sb(7)-O(9)	1.931(5)	V(9)-O(15)	1.964(5)	N(1)-Zn(1)-N(42)	92.1(3)
Sb(7)-O(19)	1.941(5)	V(9)-O(12)	1.976(5)	N(22)-Zn(1)-N(42)	162.7(3)
Sb(7)-O(23)	1.963(6)	V(9)-O(6)	1.976(5)	N(41)-Zn(1)-N(2)	91.3(3)
Sb(8)-O(9)	1.941(5)	V(10)-O(13)	1.599(5)	N(1)-Zn(1)-N(2)	76.9(3)
Sb(8)-O(33)	1.952(5)	V(10)-O(11)	1.934(5)	N(22)-Zn(1)-N(2)	100.3(2)
Sb(8)-O(5)	1.997(6)	V(10)-O(36)	1.947(5)	N(42)-Zn(1)-N(2)	94.7(3)
V(1)-O(20)	1.604(5)	V(10)-O(41)	1.992(5)	N(41)-Zn(1)-N(21)	97.0(3)
V(1)-O(2)	1.954(5)	V(10)-O(34)	1.997(5)	N(1)-Zn(1)-N(21)	95.3(3)
V(1)-O(3)	1.955(5)	V(11)-O(29)	1.596(5)	N(22)-Zn(1)-N(21)	77.4(3)
V(1)-O(1)	1.964(5)	V(11)-O(18)	1.925(5)	N(42)-Zn(1)-N(21)	89.0(3)
V(1)-O(7)	1.979(5)	V(11)-O(8)	1.929(5)	N(2)-Zn(1)-N(21)	171.4(3)
V(1)-V(7)	3.0961(18)	V(11)-O(12)	1.955(5)	N(61)-Zn(2)-N(81)	99.0(2)
V(1)-V(4)	3.1064(17)	V(11)-O(17)	1.991(5)	N(61)-Zn(2)-N(62)	78.3(3)
V(2)-O(42)	1.608(5)	V(12)-O(21)	1.608(5)	N(81)-Zn(2)-N(62)	96.8(3)
V(2)-O(11)	1.936(5)	V(12)-O(36)	1.921(5)	N(61)-Zn(2)-N(101)	96.2(2)
V(2)-O(22)	1.942(5)	V(12)-O(15)	1.928(6)	N(81)-Zn(2)-N(101)	162.4(3)
V(2)-O(5)	1.965(5)	V(12)-O(41)	1.987(5)	N(62)-Zn(2)-N(101)	95.0(3)
V(2)-O(28)	1.979(5)	V(12)-O(6)	1.995(5)	N(61)-Zn(2)-N(82)	95.9(2)
V(3)-O(31)	1.603(5)	V(13)-O(14)	1.609(5)	N(81)-Zn(2)-N(82)	77.8(3)
V(3)-O(22)	1.932(5)	V(13)-O(39)	1.916(5)	N(62)-Zn(2)-N(82)	171.4(3)
V(3)-O(37)	1.948(5)	V(13)-O(18)	1.953(5)	N(101)-Zn(2)-N(82)	91.9(2)
V(3)-O(30)	1.983(5)	V(13)-O(17)	1.974(5)	N(61)-Zn(2)-N(102)	168.9(2)
V(3)-O(33)	1.987(5)	V(5)-O(37)	1.930(5)	N(81)-Zn(2)-N(102)	88.4(2)
V(4)-O(26)	1.599(5)	V(5)-O(39)	1.936(5)	N(62)-Zn(2)-N(102)	92.8(2)
V(4)-O(39)	1.934(5)	V(13)-O(19)	1.980(5)	N(101)-Zn(2)-N(102)	78.0(2)
V(4)-O(37)	1.947(5)	V(14)-O(22)	1.935(5)	N(82)-Zn(2)-N(102)	93.7(2)
V(4)-O(2)	1.986(5)	V(14)-O(32)	1.597(5)		
V(4)-O(1)	2.010(5)	V(14)-O(11)	1.945(5)		
V(5)-O(24)	1.598(5)	V(14)-O(34)	1.979(5)		
V(5)-O(33)	1.981(5)	V(14)-O(30)	1.987(5)		

Table S 2. Selected bond lengths [Å] and angles [°] compound **2**.

Sb(1)-O(15)	1.963(4)	O(14)-V(4)#1	1.951(4)	**Complexes**	
Sb(1)-O(13)	1.978(3)	Sb(3)-O(16)	1.962(3)		
Sb(1)-O(20)	1.981(4)	Sb(3)-O(11)	1.965(4)	Zn(1)-N(4)	2.120(5)
Sb(2)-O(15)	1.940(4)	Sb(3)-O(17)#1	1.969(4)	Zn(1)-N(2)	2.122(5)
Sb(2)-O(9)	1.953(3)	Sb(4)-O(11)	1.938(4)	Zn(1)-N(1)	2.123(5)
Sb(2)-O(10)	1.957(4)	Sb(4)-O(19)	1.939(3)	O(3)-Zn(1)	2.202(4)
O(17)-Sb(3)#1	1.969(4)	Sb(4)-O(18)#1	1.969(4)	N(4)-Zn(1)-N(2)	170.1(2)
V(1)-O(1)	1.599(4)	O(18)-Sb(4)#1	1.969(4)	N(4)-Zn(1)-N(1)	96.3(2)
V(1)-O(14)	1.945(4)	V(4)-O(14)#1	1.951(4)	N(2)-Zn(1)-N(1)	83.3(2)
V(1)-O(12)#1	1.949(4)	V(4)-O(12)	1.958(4)	N(4)-Zn(1)-N(3)	82.3(2)
V(1)-O(16)	1.977(4)	V(5)-O(5)	1.600(4)	N(2)-Zn(1)-N(3)	99.1(2)
V(1)-O(9)	1.991(4)	V(5)-O(21)#1	1.950(4)	N(1)-Zn(1)-N(3)	174.0(2)
V(2)-O(2)	1.604(4)	V(5)-O(14)	1.959(4)	N(4)-Zn(1)-O(3)	98.30(18)
V(2)-O(13)	1.938(4)	V(5)-O(10)	1.973(4)	N(2)-Zn(1)-O(3)	91.57(17)
V(2)-O(16)	1.957(4)	V(5)-O(18)	1.989(4)	Zn(1)-N(3)	2.139(5)
V(2)-O(19)	1.962(4)	V(6)-O(6)	1.608(4)	Zn(1)-O(4)#3	2.204(4)
V(2)-O(9)	1.974(4)	V(6)-O(20)	1.941(4)	O(4)-Zn(1)#2	2.204(4)
V(3)-O(3)	1.611(4)	V(6)-O(18)	1.960(4)		
V(3)-O(7)	1.922(4)	V(6)-O(17)	1.968(4)	N(1)-Zn(1)-O(3)	87.54(19)
V(3)-O(21)	1.944(4)	V(6)-O(10)	1.978(4)	N(3)-Zn(1)-O(3)	86.9(2)
V(3)-O(13)	1.967(4)	V(7)-O(8)	1.606(4)	N(4)-Zn(1)-O(4)#3	82.42(18)
V(3)-O(19)	1.969(4)	V(7)-O(7)	1.939(4)	N(2)-Zn(1)-O(4)#3	87.69(17)
V(4)-O(4)	1.628(4)	V(7)-O(12)	1.959(4)	N(1)-Zn(1)-O(4)#3	90.71(19)
V(4)-O(7)	1.930(4)	V(7)-O(17)	1.964(4)	N(3)-Zn(1)-O(4)#3	94.9(2)
V(4)-O(21)	1.950(4)	V(7)-O(20)	1.969(4)	O(3)-Zn(1)-O(4)#3	178.17(16)
O(12)-V(1)#1	1.949(4)	O(21)-V(5)#1	1.950(4)		

Table S 3. Selected bond lengths [Å] and angles [°] compound **3**.

Sb(1)-O(3)	1.960(3)	V(5)-O(9)	1.982(3)		
Sb(1)-O(1)	1.961(3)	V(5)-O(5)	1.982(3)	**Complexes**	
Sb(1)-O(2)	1.963(3)	V(6)-O(33)	1.622(3)		
Sb(2)-O(6)	1.939(4)	V(6)-O(32)	1.914(3)	Fe1-N(42)	1.965(4)
Sb(2)-O(4)	1.946(3)	V(6)-O(31)	1.928(3)	Fe1-N(21)	1.965(4)
Sb(2)-O(5)	1.975(3)	V(6)-O(1)	1.963(3)	Fe1-N(41)	1.967(4)
Sb(3)-O(8)	1.942(3)	V(6)-O(19)	1.999(3)	Fe1-N(1)	1.974(4)
Sb(3)-O(7)	1.951(3)	V(7)-O(34)	1.598(3)	Fe1-N(22)	1.974(4)
Sb(3)-O(9)	1.993(3)	V(7)-O(23)	1.927(3)	Fe1-N(2)	1.977(4)
Sb(4)-O(8)	1.936(3)	V(7)-O(25)	1.946(3)	Fe2-N(82)	1.958(4)
Sb(4)-O(10)	1.946(3)	V(7)-O(17)	1.991(3)	Fe2-N(81)	1.962(4)
Sb(4)-O(11)	1.951(3)	V(7)-O(12)	2.002(3)	Fe2-N(62)	1.964(5)
Sb(5)-O(13)	1.929(3)	V(8)-O(36)	1.609(3)	Fe2-N(61)	1.972(5)
Sb(5)-O(14)	1.934(3)	V(8)-O(22)	1.935(3)	Fe2-N(101)	1.973(5)
Sb(5)-O(12)	1.947(3)	V(8)-O(35)	1.941(3)	Fe2-N(102)	1.975(5)
Sb(6)-O(6)	1.931(4)	V(8)-O(3)	1.961(3)	N(101)-Fe2-N(102)	82.85(19)
Sb(6)-O(15)	1.944(3)	V(8)-O(18)	2.000(3)	N(42)-Fe1-N(21)	93.30(17)
Sb(6)-O(16)	1.951(3)	V(9)-O(37)	1.602(3)	N(42)-Fe1-N(41)	82.82(17)
Sb(7)-O(18)	1.937(3)	V(9)-O(35)	1.934(3)	N(21)-Fe1-N(41)	92.81(16)
Sb(7)-O(2)	1.966(3)	V(9)-O(22)	1.951(3)	N(42)-Fe1-N(1)	92.99(16)
Sb(7)-O(17)	1.987(3)	V(9)-O(16)	1.988(3)	N(21)-Fe1-N(1)	93.53(16)
Sb(8)-O(14)	1.944(3)	V(9)-O(11)	2.000(3)	N(41)-Fe1-N(1)	172.59(17)
Sb(8)-O(20)	1.950(3)	V(10)-O(38)	1.604(3)	N(42)-Fe1-N(22)	173.78(17)
Sb(8)-O(19)	1.957(3)	V(10)-O(17)	1.954(3)	N(21)-Fe1-N(22)	82.53(17)
V(1)-O(21)	1.604(3)	V(10)-O(1)	1.959(3)	N(41)-Fe1-N(22)	92.75(17)
V(1)-O(5)	1.951(3)	V(10)-O(12)	1.961(3)	N(1)-Fe1-N(22)	91.87(16)
V(1)-O(9)	1.955(3)	V(10)-O(19)	1.974(3)	N(42)-Fe1-N(2)	90.93(16)
V(1)-O(11)	1.963(3)	V(11)-O(39)	1.605(3)	N(21)-Fe1-N(2)	174.43(16)
V(1)-O(16)	1.968(3)	V(11)-O(29)	1.930(3)	N(41)-Fe1-N(2)	91.31(16)
V(2)-O(24)	1.608(3)	V(11)-O(32)	1.943(3)	N(1)-Fe1-N(2)	82.63(16)
V(2)-O(23)	1.918(3)	V(11)-O(20)	1.986(3)	N(22)-Fe1-N(2)	93.54(16)
V(2)-O(22)	1.950(3)	V(11)-O(7)	1.997(3)	N(82)-Fe2-N(81)	83.09(18)
V(2)-O(15)	1.984(3)	V(12)-O(40)	1.620(3)	N(82)-Fe2-N(62)	93.16(18)
V(2)-O(18)	1.985(3)	V(12)-O(31)	1.923(3)	N(81)-Fe2-N(62)	173.8(2)
V(3)-O(27)	1.604(3)	V(12)-O(32)	1.924(3)	N(82)-Fe2-N(61)	91.91(18)
V(3)-O(26)	1.937(3)	V(12)-O(7)	1.988(3)	N(81)-Fe2-N(61)	92.23(18)
V(3)-O(25)	1.943(3)	V(12)-O(10)	1.992(3)	N(62)-Fe2-N(61)	83.0(2)
V(3)-O(4)	1.989(3)	V(13)-O(41)	1.605(3)	N(82)-Fe2-N(101)	93.22(17)
V(3)-O(13)	1.995(3)	V(13)-O(29)	1.941(3)	N(81)-Fe2-N(101)	90.91(18)
V(4)-O(28)	1.608(3)	V(13)-O(26)	1.942(3)	N(62)-Fe2-N(101)	94.21(19)
V(4)-O(25)	1.934(3)	V(13)-O(20)	1.976(3)	N(61)-Fe2-N(101)	174.27(18)
V(4)-O(23)	1.943(3)	V(13)-O(13)	1.988(3)	N(82)-Fe2-N(102)	175.19(19)
V(4)-O(4)	1.989(3)	V(14)-O(42)	1.599(3)	N(81)-Fe2-N(102)	94.2(2)
V(4)-O(15)	1.989(3)	V(14)-O(35)	1.952(3)	N(62)-Fe2-N(102)	89.9(2)
V(5)-O(30)	1.610(3)	V(14)-O(3)	1.967(3)	N(61)-Fe2-N(102)	92.14(19)
V(5)-O(26)	1.927(3)	V(14)-O(31)	1.969(3)		
V(5)-O(29)	1.941(3)	V(14)-O(10)	1.972(3)		

Table S 4. Selected crystal data and results of the structure refinements for compounds **1-3**.

Compound	**1**	**2**	**3**
Formula	$C_{78}H_{88}N_{13}O_{60}Sb_8V_{14}Zn_2$	$C_8H_{46}N_8O_{49}Sb_8V_{14}Zn_2$	$C_{84}H_{76}Fe_2N_{14}O_{52}Sb_8V_{14}$
Weight [g·mol^{-1}]	3985.51	2856.43	3912.44
Crystal system	monoclinic	monoclinic	monoclinic
Space group	$P2_1/n$	$P2_1/n$	$P2_1/n$
***a* [Å]**	20.2184(3)	14.5165(4)	19.8981(2)
***b* [Å]**	26.6676(4)	12.8716(2)	26.2309(3)
***c* [Å]**	22.9869(4)	17.7732(4)	23.4372(2)
***α* [°]**	90	90	90
***β* [°]**	104.0630(10)	106.222(2)	106.2120(10)
***γ* [°]**	90	90	90
***V* [Å^3]**	12022.5(3)	3188.71(13)	11746.5(2)
Z	4	2	4
D_{calc} [mg·m^3]	2.202	2.975	2.212
μ [mm^{-1}]	3.282	6.106	3.191
Min/max trans.		0.3471/0.4731	0.5744/0.7055
Θ_{max} [°]	25.182	28.005	25.004
Measured refl.	36897	37489	137829
Independent refl.	21064	7658	20670
R_{int}	0.0383	0.0349	0.0620
Refl. [$F_0>4\sigma(F_0)$]	16629	6918	19281
Parameters	1493	407	1586
R_1 [$F_0>4\sigma(F_0)$]	0.0438	0.0405	0.0352
wR_2 **for all refl.**	0.1244	0.1047	0.0923
GOF	1.005	1.083	1.099
$\Delta\rho_{max/min}$ [e·Å^{-3}]	1.075/-1.018	1.230/-1.274	1.395/-1.538
BASF parameter	0.1080(8)	-	-

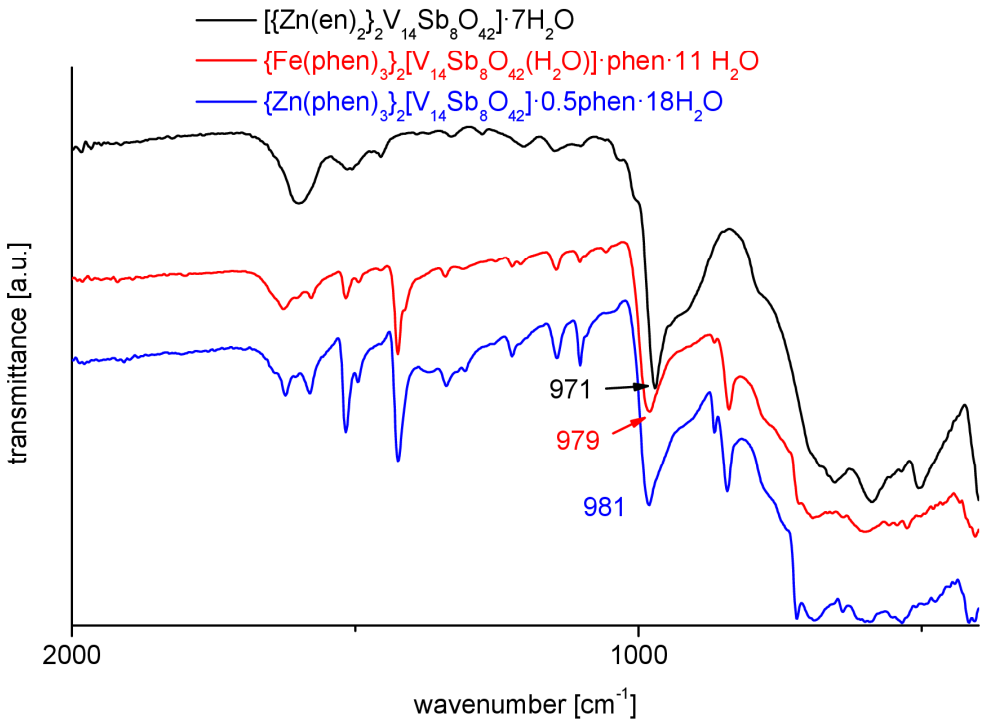

Figure S 4. IR spectra of compounds **1**-**3** and wave number of the characteristic V=O absorption.

Table S 5. Results of bond valence sum calculations for compounds **1-3**.[1–3]

compound 1		**compound 2**		**compound 3**	
V(1)	3.97	**V(1)**	3.98	**V(1)**	4.00
V(2)	4.01	**V(2)**	4.01	**V(2)**	3.99
V(3)	3.98	**V(3)**	4.03	**V(3)**	3.96
V(4)	3.96	**V(4)**	3.99	**V(4)**	3.97
V(5)	4.02	**V(5)**	3.96	**V(5)**	3.99
V(6)	4.04	**V(6)**	3.97	**V(6)**	3.99
V(7)	3.97	**V(7)**	4.00	**V(7)**	3.98
V(8)	4.00			**V(8)**	3.98
V(9)	3.98			**V(9)**	3.95
V(10)	3.97			**V(10)**	3.98
V(11)	4.10			**V(11)**	3.97
V(12)	4.00			**V(12)**	3.96
V(13)	4.00			**V(13)**	3.98
V(14)	4.17			**V(14)**	3.98
average	**4.00**	**average**	**3.99**	**average**	**3.98**
Sb(1)	2.94	**Sb(1)**	2.85	**Sb(1)**	2.95
Sb(2)	2.95	**Sb(2)**	3.04	**Sb(2)**	3.02
Sb(3)	3.11	**Sb(3)**	2.92	**Sb(3)**	2.95
Sb(4)	3.00	**Sb(4)**	3.05	**Sb(4)**	3.09
Sb(5)	3.05			**Sb(5)**	3.15
Sb(6)	3.11			**Sb(6)**	3.11
Sb(7)	3.08			**Sb(7)**	2.94
Sb(8)	2.94			**Sb(8)**	3.04
average	**3.02**	**average**	**2.97**	**average**	**3.03**

Table S 6. Distances between fully occupied water molecules in the structure of **1** forming a C8-chain[4–7] and the short N···O distance.

Atom 1	Atom 2	Distance [Å]
O(64)	N(122)	2.761(19)
O(58)	O(53)	2.797(13)
O(63)	O(54)	2.826(15)
O(59)	O(56)	2.832(14)
O(64)	O(57)	2.924(17)
O(64)	O(58)	2.767(15)
O(53)	O(59)	2.828(12)
O(56)	O(62)	2.717(12)
O(64)	O(63)	2.838(15)

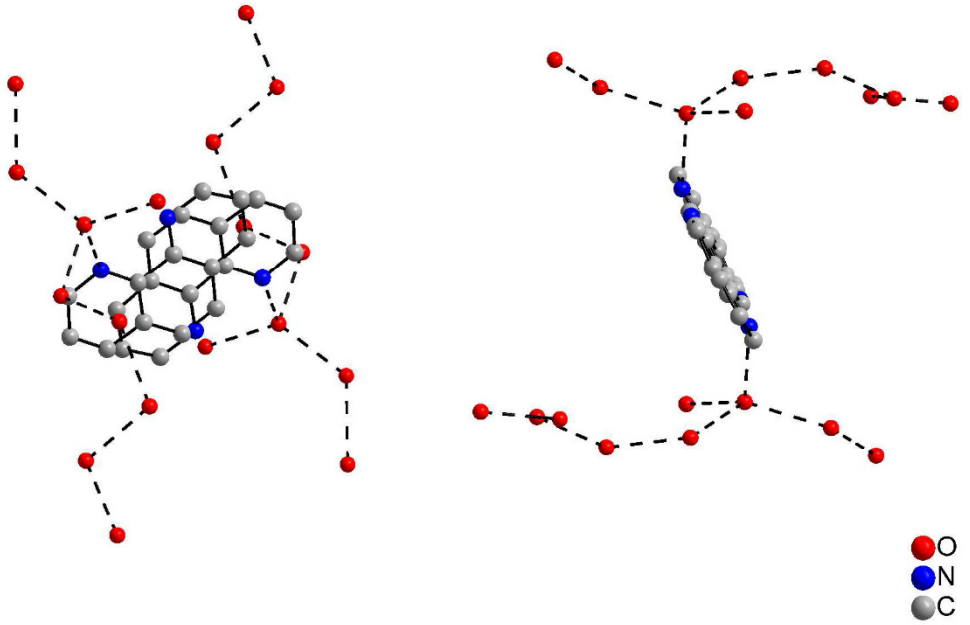

Figure S 5. The fully occupied water molecules in the structure of **1** form a C8-chain$^{4-7}$ connected via a short N-O distance to the disordered phen molecule (N(122)) with a distance of 2.761(19) Å.

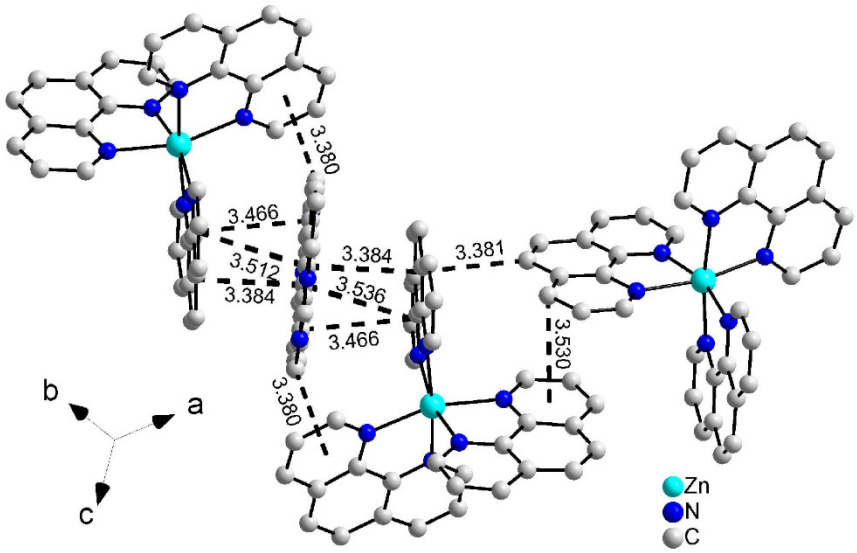

Figure S 6. Proposed π-π-interactions between the $[Zn(phen)_3]^{2+}$ complexes and the co-crystallized phen molecule in compound **1** (H atoms have been omitted for clarity).[8–17]

Table S 7. N-O-distances and angles indicating hydrogen bonding interactions in compound **2**.

Atom 1	Atom 2	Distance [Å]	Angle N-H···O
N(2)	O(33)	2.963(8)	160.07
N(3)	O(1)	2.998(8)	128.47
N(4)	O(31)	2.989(8)	163.99

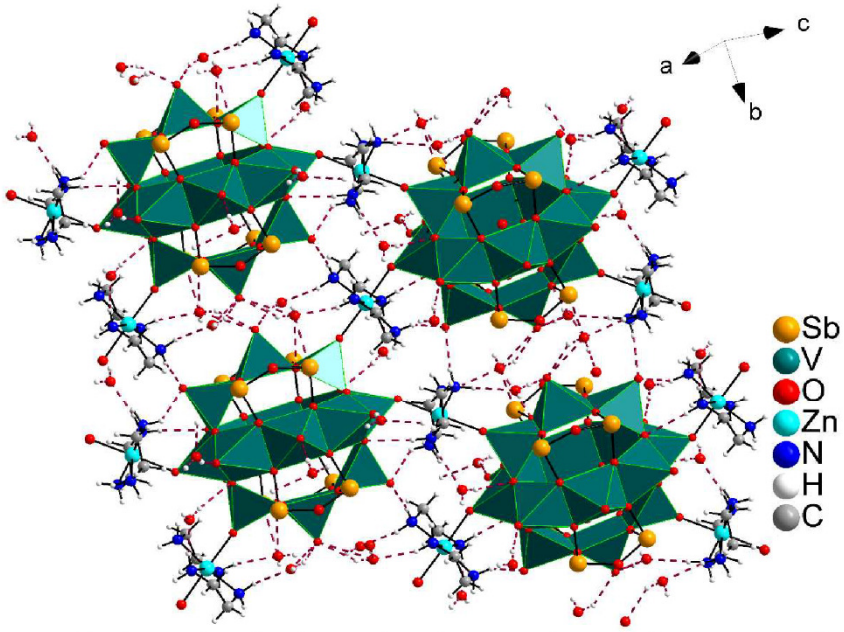

Figure S 7. Proposed hydrogen bonding interactions between the crystal water molecules and the cations/anions in the structure of compound **2**.

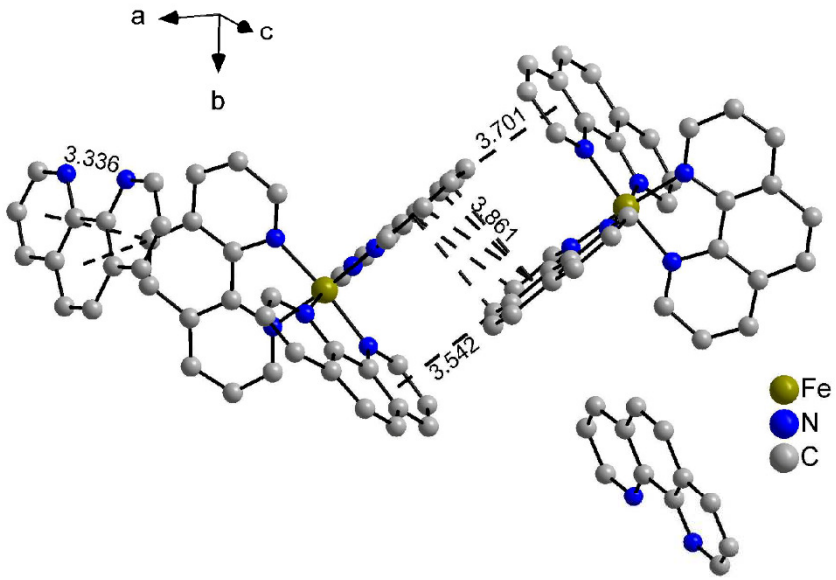

Figure S 8. Possible π-π-stacking in between the $[Fe(phen)_3]^{2+}$ complexes and the co-crystallized phen molecule in the structure of **3** (H-atoms have been omitted for clarity).[8–17]

Table S 8. Intermolecular distances indicating π-π-stacking in the structure of **3.**

Outgoing atom	**Type**	**Distance [Å]**
C(8)	sandwich	3.530(6)
C(9)	sandwich	3.706(6)
C(7)	sandwich	3.861(5)
C(82)	sandwich	3.544(8)
C(83)	sandwich	3.519(9)
C(26)	sandwich	3.336(6)
C(26)	sandwich	3.777(5)
	average	**3.610**
C(83)	T-shape	3.542(9)
C(8)	T-shape	3.701(6)
	average	**3.622**

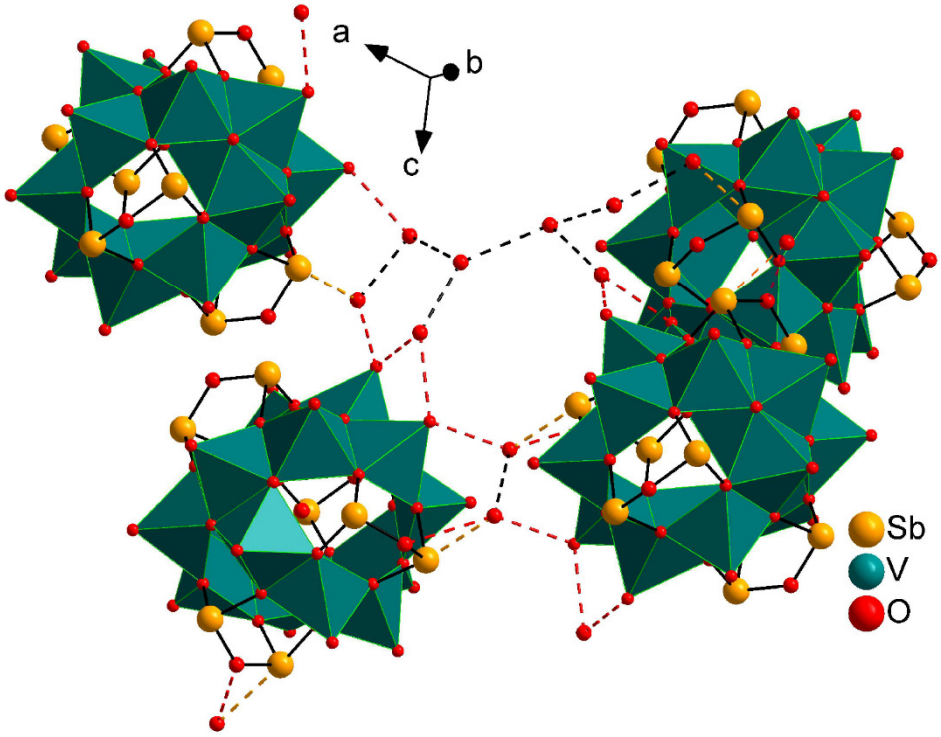

Figure S 9. Possible H-bonds between the water cluster and the anion in the structure of **3**.

References

(1) Brown, I. D.; Altermatt, D. Bond-valence parameters obtained from a systematic analysis of the Inorganic Crystal Structure Database. *Acta Crystallogr B* **1985**, *41*, 244–247.

(2) O'Keefe, M.; Brese, N. E. Atom sizes and bond lengths in molecules and crystals. *J. Am. Chem. Soc.* **1991**, *113*, 3226–3229.

(3) Palenik, R. C.; Abboud, K. A.; Palenik, G. J. Bond valence sums and structural studies of antimony complexes containing Sb bonded only to O ligands. *Inorganica Chimica Acta* **2005**, *358*, 1034–1040.

(4) Mizuse, K.; Kuo, J.-L.; Fujii, A. Structural trends of ionized water networks: Infrared spectroscopy of watercluster radical cations $(H_2O)^{n+}$ (n = 3–11). *Chem. Sci.* **2011**, *2*, 868–876.

(5) Infantes, L.; Motherwell, S. Water clusters in organic molecular crystals. *CrystEngComm* **2002**, *4*, 454.

(6) Infantes, L.; Fábián, L.; Motherwell, W. D. S. Organic crystal hydrates: What are the important factors for formation. *CrystEngComm* **2007**, *9*, 65–71.

(7) Infantes, L.; Chisholm, J.; Motherwell, S. Extended motifs from water and chemical functional groups in organic molecular crystals. *CrystEngComm* **2003**, *5*, 480.

(8) Ringer, A. L.; Sinnokrot, M. O.; Lively, R. P.; Sherrill, C. D. The effect of multiple substituents on sandwich and T-shaped pi-pi interactions. *Chem. Eur. J.* **2006**, *12*, 3821–3828.

(9) Martinez, C. R.; Iverson, B. L. Rethinking the term "pi-stacking". *Chem. Sci.* **2012**, *3*, 2191.

(10) Janiak, C. A critical account on π–π stacking in metal complexes with aromatic nitrogen-containing ligands †. *J. Chem. Soc., Dalton Trans.* **2000**, 3885–3896.

(11) Hilbert, J.; Näther, C.; Bensch, W. Utilization of mixtures of aromatic N-donor ligands of different coordination ability for the solvothermal synthesis of thiostannate containing molecules. *Dalton Trans.* **2015**, *44*, 11542–11550.

(12) Grimme, S.; Antony, J.; Ehrlich, S.; Krieg, H. A consistent and accurate ab initio parametrization of density functional dispersion correction (DFT-D) for the 94 elements H-Pu. *J. Chem. Phys.* **2010**, *132*, 154104.

(13) Grimme, S. Density functional theory with London dispersion corrections. *WIREs Comput. Mol. Sci.* **2011**, *1*, 211–228.

(14) Grimme, S. Do Special Noncovalent π–π Stacking Interactions Really Exist? *Angew. Chem. Int. Ed.* **2008**, *47*, 3430–3434.

(15) Goerigk, L.; Kruse, H.; Grimme, S. Benchmarking density functional methods against the S66 and S66x8 datasets for non-covalent interactions. *ChemPhysChem* **2011**, *12*, 3421–3433.

(16) Chi, Y.-H.; Shi, J.-M.; Li, H.-N.; Wei, W.; Cottrill, E.; Pan, N.; Chen, H.; Liang, Y.; Yu, L.; Zhang, Y.-Q. *et al.* pi-pi stacking, spin density and magnetic coupling strength. *Dalton Trans.* **2013**, *42*, 15559–15569.

(17) Bloom, J. W. G.; Wheeler, S. E. Taking the Aromaticity out of Aromatic Interactions. *Angew. Chem. Int. Ed.* **2011**, *50*, 7847.

8. Lebenslauf

9. Literaturverzeichnis

[1] S. Li, X. Yu, G. Zhang, Y. Ma, J. Yao, B. Keita, N. Louis, H. Zhao, *J. Mater. Chem.* **2011**, *21*, 2282.

[2] M. L. Campbell, D. Sulejmanovic, J. B. Schiller, E. M. Turner, S.-J. Hwu, D. C. Whitehead, *Catal. Sci. Technol.* **2016**, *6*, 3208.

[3] J.-J. Chen, M. D. Symes, S.-C. Fan, M.-S. Zheng, H. N. Miras, Q.-F. Dong, L. Cronin, *Adv. Mater.* **2015**, *27*, 4649.

[4] K. K. Kasem, F. A. Schultz, *Can. J. Chem.* **1995**, *73*, 858.

[5] J.-J. Chen, J.-C. Ye, X.-G. Zhang, M. D. Symes, S.-C. Fan, D.-L. Long, M.-S. Zheng, D.-Y. Wu, L. Cronin, Q.-F. Dong, *Adv. Energy Mater.* **2018**, *8*, 1701021.

[6] S. Herrmann, M. Kostrzewa, A. Wierschem, C. Streb, *Angew. Chem. Int. Ed.* **2014**, *53*, 13596.

[7] S. Herrmann, L. de Matteis, J. M. de La Fuente, S. G. Mitchell, C. Streb, *Angew. Chem. Int. Ed.* **2017**, *56*, 1667.

[8] J. J. Berzelius, *Ann. Phys.* **1826**, *82*, 369.

[9] J. F. Keggin, *Nature* **1933**, *131*, 908.

[10] N. V. Izarova, M. T. Pope, U. Kortz, *Angew. Chem. Int. Ed.* **2012**, *51*, 9492.

[11] Z. Lang, P. Yang, Z. Lin, L. Yan, M.-X. Li, J. J. Carbó, U. Kortz, J. M. Poblet, *Chem. Sci.* **2017**, *8*, 7862.

[12] P. Yang, H. Li, T. Ma, F. Haso, T. Liu, L. Fan, Z. Lin, C. Hu, U. Kortz, *Chem. Eur. J.* **2018**, *24*, 2466.

[13] P. Yang, Y. Xiang, Z. Lin, Z. Lang, P. Jiménez-Lozano, J. J. Carbó, J. M. Poblet, L. Fan, C. Hu, U. Kortz, *Angew. Chem. Int. Ed.* **2016**, *55*, 15766.

[14] J. E. Huheey, E. A. Keiter, R. L. Keiter, R. Steudel (Eds.) *Anorganische Chemie - Prinzipien von Struktur und Reaktivität*, de Gruyter, Berlin, **2014**.

[15] E. Riedel, C. Janiak, *Anorganische Chemie*, de Gruyter, Berlin, **2007**.

[16] M. Henry, J. P. Jolivet, J. Livage, *Aqueous chemistry of metal cations: Hydrolysis, condensation and complexation*. *In: Reisfeld R., JJørgensen C.K. (eds) Chemistry, Spectroscopy and Applications of Sol-Gel Glasses. Structure and Bonding*, Springer, Berlin, Heidelberg, **1992**.

[17] J. Livage, *Coordin. Chem. Rev.* **1998**, *178-180*, 999.

[18] F. J. C. Rossotti, H. Rossotti, J. G. Ormerod, E. Stenhagen, B. Thorell, *Acta Chem. Scand.* **1956**, *10*, 957.

[19] C. Streb, *Structure and Bonding in Molecular Vanadium Oxides: From Templates via Host-Guest Chemistry to Applications*. *In: Song YF. (eds) Polyoxometalate-Based Assemblies and Functional Materials. Structure and Bonding*, Springer, Berlin, Heidelberg, **2017**.

[20] J. J. Borrás-Almenar, E. Coronado, A. Müller, M. Pope (Eds.) *NATO Science Series, Series II*, *Vol. 98*, Springer, Dordrecht, **2003**.

[21] A. Müller, E. Krickemeyer, H. Bögge, M. Schmidtmann, F. Peters, *Angew. Chem. Int. Ed.* **1998**, *110*, 3567.

[22] A. Müller, C. Serain, *Acc. Chem. Res.* **2000**, *33*, 2.

[23] A. Müller, J. Meyer, E. Krickemeyer, E. Diemann, *Angew. Chem. Int. Ed.* **1996**, *108*, 1296.

[24] a) N. Pienack, W. Bensch, *Angew. Chem.* **2011**, *123*, 2062; b) N. Pienack, W. Bensch, *Angew. Chem. Int. Ed.* **2011**, *50*, 2014.

[25] K. Y. Monakhov, W. Bensch, P. Kögerler, *Chem. Soc. Rev.* **2015**, *44*, 8443.

[26] G. K. Johnson, E. O. Schlemper, *J. Am. Chem. Soc.* **1978**, *100*, 3645.
[27] X.-X. Hu, J.-Q. Xu, X.-B. Cui, J.-F. Song, T.-G. Wang, *Inorg. Chem. Commun.* **2004**, *7*, 264.
[28] M. Wendt, C. Näther, W. Bensch, *Chem. Eur. J.* **2016**, *22*, 7747.
[29] H.-Y. Guo, X. Zhang, X.-B. Cui, Q.-S. Huo, J.-Q. Xu, *CrystEngComm* **2016**, *18*, 5130.
[30] L. K. Mahnke, M. Wendt, C. Näther, W. Bensch, *Cryst. Groth Des.* **2018**, *18*, 6100.
[31] R. Kiebach, C. Näther, W. Bensch, *Solid State Sci.* **2006**, *8*, 964.
[32] E. Antonova, A. Wutkowski, C. Näther, W. Bensch, *Solid State Sci.* **2011**, *13*, 2154.
[33] Y. Gao, Z. Han, Y. Xu, C. Hu, *J. Clust. Sci.* **2010**, *21*, 163.
[34] E. Antonova, C. Näther, P. Kögerler, W. Bensch, *Angew. Chem. Int. Ed.* **2011**, *50*, 764.
[35] L. Yu, J.-p. Liu, J.-p. Wang, J.-y. Niu, *Chem. Res. Chinese U.* **2009**, *25 (4)*, 426.
[36] L. Zhang, X. Zhao, J. Xu, T. Wang, *Dalton Trans.* **2002**, 3275.
[37] L. K. Mahnke, A. Kondinski, U. Warzok, C. Näther, J. van Leusen, C. Schalley, K. Y. Monakhov, P. Kögerler, W. Bensch, *Angew. Chem. Int. Ed.* **2018**, *57*, 2972.
[38] L. K. Mahnke, A. Kondinski, U. Warzok, C. Näther, J. van Leusen, C. A. Schalley, K. Y. Monakhov, P. Kögerler, W. Bensch, *Angew. Chem.* **2018**, *130*, 3024.
[39] H.-Y. Guo, X. Zhang, L.-N. Xiao, X.-B. Cui, *Dalton Trans.* **2017**, *46*, 8022.
[40] M. Wendt, C. Näther, J. van Leusen, P. Kögerler, W. Bensch, *Z. Naturforsch. B* **2018**, 764.
[41] R. Kiebach, C. Näther, P. Kögerler, W. Bensch, *Dalton Trans.* **2007**, 3221.
[42] E. Antonova, C. Näther, W. Bensch, *Dalton Trans.* **2012**, *41*, 1338.
[43] E. Antonova, C. Näther, W. Bensch, *CrystEngComm* **2012**, *14*, 6853.
[44] A. Wutkowski, C. Näther, P. Kögerler, W. Bensch, *Inorg. Chem.* **2013**, *52*, 3280.
[45] E. Antonova, C. Näther, P. Kögerler, W. Bensch, *Inorg. Chem.* **2012**, *51*, 2311.
[46] M. Wendt, U. Warzok, C. Näther, J. van Leusen, P. Kögerler, C. A. Schalley, W. Bensch, *Chem. Sci.* **2016**, *7*, 2684.
[47] H. Lühmann, C. Näther, P. Kögerler, W. Bensch, *Inorg. Chim. Acta* **2014**, *421*, 549.
[48] M. Wendt, P. Polzin, J. van Leusen, C. Nather, P. Kogerler, W. Bensch, *Dalton Trans.* **2017**, *46*, 1618.
[49] M. Rasmussen, C. Näther, J. van Leusen, P. Kögerler, L. Zhechkov, T. Heine, W. Bensch, *Inorg. Chem.* **2017**, *56*, 7120.
[50] L. K. Mahnke, U. Warzok, M. Lin, C. Näther, C. A. Schalley, W. Bensch, *Chem. Eur. J.* **2018**, *24*, 5522.
[51] M. Wendt, C. Näther, J. van Leusen, P. Kögerler, W. Bensch, *Z. anorg. allg. Chem.* **2018**, *55*, 6329.
[52] M. Wendt, L. K. Mahnke, C. Näther, J. van Leusen, P. Kögerler, W. Bensch, *Dalton Trans.* **2018**, *47*, 6672.
[53] A. Wutkowski, C. Näther, P. Kögerler, W. Bensch, *Inorg. Chem.* **2008**, *47*, 1916.
[54] E. Antonova, C. Näther, P. Kögerler, W. Bensch, *Dalton Trans.* **2012**, *41*, 6957.

[55] M. Rasmussen, C. Näther, J. van Leusen, P. Kögerler, W. Bensch, *Z. anorg. allg. Chem.* **2017**, *643*, 1519.
[56] A. Kondinski, T. Heine, K. Y. Monakhov, *Inorg. Chem.* **2016**, *55*, 3777.
[57] C. Wang, G. Zhou, Z. Zhang, D. Zhu, Y. Xu, *J. Coord. Chem.* **2011**, *64*, 1198.
[58] B. Hasenknopf, *Front. Biosci.* **2005**, *10*, 275.
[59] J. T. Rhule, C. L. Hill, D. A. Judd, R. F. Schinazi, *Chem. Rev.* **1998**, *98*, 327.
[60] J.-Q. Shen, Q. Wu, Y. Zhang, Z.-M. Zhang, Y.-G. Li, Y. Lu, E.-B. Wang, *Chem. Eur. J.* **2014**, *20*, 2840.
[61] X. Li, L. Yang, C. Qin, F.-H. Liu, L. Zhao, K.-Z. Shao, Z.-M. Su, *RSC Adv.* **2015**, *5*, 59093.
[62] S. Uchida, R. Eguchi, S. Nakamura, Y. Ogasawara, N. Kurosawa, N. Mizuno, *Chem. Mater.* **2012**, *24*, 325.
[63] S. Jiang, Y. Guo, C. Wang, X. Qu, L. Li, *J. Colloid Interf. Sci.* **2007**, *308*, 208.
[64] C. Wang, X. Bu, J. Ma, C. Liu, K. Chou, X. Wang, Q. Li, *Catal. Today* **2016**, *274*, 82.
[65] S. Hayashi, S. Yamazoe, K. Koyasu, T. Tsukuda, *RSC Adv* **2016**, *6*, 16239.
[66] J. Dong, J. Hu, Y. Chi, Z. Lin, B. Zou, S. Yang, C. L. Hill, C. Hu, *Angew. Chem. Int. Ed.* **2017**, *56*, 4473.
[67] M. Lechner, K. Kastner, C. J. Chan, R. Güttel, C. Streb, *Chem. Eur. J.* **2018**, *24*, 4952.
[68] E. Ni, S. Uematsu, N. Sonoyama, *Solid State Ionics* **2014**, *268*, 222.
[69] S. Cardona-Serra, J. M. Clemente-Juan, E. Coronado, A. Gaita-Ariño, N. Suaud, O. Svoboda, R. Bastardis, N. Guihéry, J. J. Palacios, *Chem. Eur. J.* **2015**, *21*, 763.
[70] C. J. Calzado, J. M. Clemente-Juan, E. Coronado, A. Gaita-Arino, N. Suaud, *Inorg. Chem.* **2008**, *47*, 5889.
[71] S. Bertaina, S. Gambarelli, T. Mitra, B. Tsukerblat, A. Müller, B. Barbara, *Nature* **2008**, *453*, 203.
[72] M. Avrami, *J. Chem. Phys.* **1939**, *7*, 1103.
[73] M. Avrami, *J. Chem. Phys.* **1940**, *8*, 212.
[74] M. Avrami, *J. Chem. Phys.* **1941**, *9*, 177.
[75] J. D. Hancock, J. H. Sharp, *J. Am. Ceram. Soc.* **2001**, 74.
[76] H. Reinsch, N. Stock, *CrystEngComm* **2013**, *15*, 544.
[77] C. Schmidt, N. Stock, *Cryst. Groth Des.* **2011**, *11*, 5682.
[78] F. Niekiel, M. Ackermann, P. Guerrier, A. Rothkirch, N. Stock, *Inorg. Chem.* **2013**, *52*, 8699.
[79] A. F. Gualtieri, *Phys. Chem. Miner.* **2001**, *28*, 719.
[80] F. Millange, R. El Osta, M. E. Medina, R. I. Walton, *CrystEngComm* **2011**, *13*, 103.
[81] N. Heidenreich, U. Rütt, M. Köppen, A. K. Inge, S. Beier, A.-C. Dippel, R. Suren, N. Stock, *Rev. Sci. Instrum.* **2017**, *88*, 104102.
[82] N. Heidenreich, *In-situ investigation into crystallization kinetics of Zr /Hf-UiO-66*. MATsynCELL Spring Meeting, Kiel, **2016**.
[83] A. Rabenau, *Angew. Chem.* **1985**, *97*, 1017.
[84] A. Rabenau, *Angew. Chem. Int. Ed.* **1985**, *24*, 1026.
[85] W. S. Sheldrick, M. Wachhold, *Angew. Chem. Int. Ed.* **1997**, *36*, 206.
[86] Stoe & Cie, *WinXPow*, Stoe & Cie GmbH, Darmstadt, **2001**.
[87] G. M. Sheldrick, *SHELXS 97. Program for the solution of crystal structures*, Universität Göttingen, **1997**.

[88] G. M. Sheldrick, *SHELXS 97. Program for the refinement of crystal structures*, Universität Göttingen, **1997**.
[89] Stoe & Cie, *X-Red*, Stoe & Cie GmbH, Darmstadt, **1998**.
[90] Stoe & Cie, *X-Shape*, Stoe & Cie GmbH, Darmstadt, **1998**.
[91] Stoe & Cie, Stoe & Cie GmbH, Darmstadt, **2007**.
[92] K. Brandenburg, *DIAMOND*, Crystal Impact GbR, Bonn, **2014**.
[93] NETZSCH, *Netzsch TA Window Software*, Selb, **2001**.
[94] F. Porsch, *EDXPowd*, RTI GmbH, Paderborn, **2002**.
[95] A. Rothkirch, *f3tool*, DESY, Hamburg, **2010**.
[96] *olex*^{2}, OlexSys Ltd., **2004**.
[97] O. V. Dolomanov, L. J. Bourhis, R. J. Gildea, J. A. K. Howard, H. Puschmann, *J Appl Crystallogr* **2009**, *42*, 339.
[98] A. Hammersley, *Fit2D*, ESRF, Grenoble, **1987**.
[99] S. Kimball, P. Mattis, & Entwicklerteam, *Gimp*, GNU Image Manipulation Program, **1995**.

Danksagung

Ich möchte mich zuallererst bei Prof. Dr. WOLFGANG BENSCH bedanken. Danke für die Möglichkeit auf diesem spannenden Thema weiter arbeiten zu dürfen, Danke für das entgegengebrachte Vertrauen, für die Unterstützung, für den Rat, für die offene Tür und für immer neuen Input. Sie haben mich sehr voran gebracht und dafür bin ich Ihnen sehr dankbar.

Ich möchte mich ebenfalls bei Prof. Dr. CHRISTIAN NÄTHER bedanken, für die Berechnung und Verfeinerung zahlreicher Einkristallstrukturen sowie die gute Zusammenarbeit.

Bei Frau INKE JEß möchte ich mich dafür bedanken, dass Sie auch in der schlimmsten „Suppe“ noch immer den „einen“ Kristall gefunden hat.

Bei der spektroskopischen Abteilung bedanke ich mich für die zahlreichen durchgeführten Messungen.

Ich möchte mich bei allen Kooperationspartnern für die gute Zusammenarbeit bedanken, bei Dr. WARZOK, Prof. Dr. SCHALLEY, Prof. Dr. KÖGERLER, Dr. KONDINSKI, Dr. VAN LEUSEN und Prof. Dr. MONAKHOV. Besonderer Dank gilt hier ULRIKE WARZOK und ALEKSANDAR KONDINSKI für die zahlreichen Gespräche interessanten Ideen und gute Arbeit zusammen an tollen Projekten.

Meinen Bachelorstudenten, NIELS MICHAELIS und MENGXI LIN, danke ich für die tolle Arbeit, ebenso wie meinen Praktikaten, JANNIK BENECKE, JELENA PETROVIĆ und GABRIELLA STEHLÍKOVÁ - ich wünsche euch allen alles erdenklich Gute auf eurem weiteren Weg.

MAREN RASMUSSEN, ich danke dir besonders für die tolle Zusammenarbeit der letzten Monate. Du bist eine große Unterstützung und ich hoffe, dass wir tolle Ergebnisse zusammen produziert haben.

Danke auch an die „Solvos“, „neuen“ (FELIX, DANA, PHILIPP und ASSMA) wie „alten“ (CAROLIN, JESSICA, MICHAEL und JOANNA), für den Spaß und die gute Zeit, die wir gemeinsam hatten. Besonders danke ich MICHAEL WENDT, der mir so viel beigebracht hat und mir oft mehr zugetraut hat als ich mir selbst, der die besten Sprüche und lustigsten Aufmunterungen immer parat und keine Bedenken hatte seine Meinung kund zu tun. Du wirst ein großartiger Papa sein! Sowie JOANNA DOPTA, die mehr zu einer Freundin wurde als zu einer Kollegin – Ich wünsche dir alles erdenklich Gute für deinen weiteren Weg und hoffe, dass wir uns auf diesem auch weiterhin mit Rat und Tat zur Seite stehen.

NICOLE PIENACK UND ANNA-LENA HANSEN alias ÄNNA: Danke für euer offenes Ohr, eure Tipps und Tricks, für neuen Input und lustige Momente.

Ich danke dem gesamten AK BENSCH für die gute Atmosphäre, guten Gespräche, lustigen Praktikumsdienste, hin und wieder verschrobenen Kuchenessen, die Klausurkorrekturen, die man manchmal nur mit Humor ertragen konnte und für den Rückhalt. Ich hoffe man begegnet sich im weiteren Leben wieder.

Außerdem danke ich dem ganzen Institut. Allen Professoren, allen Sekretärinnen, der Werkstatt sowie jedem, der die ganze Maschinerie am Laufen hält, auch wenn es oft nicht ganz einfach ist.

Während eines Studiums, das so anstrengend sein kann wie das der Chemie braucht man Verbündete, die die guten Zeiten mit dir feiern und dich in schlechten wieder aus dem

Loch ziehen. Ich bin dankbar für jeden Tag, den wir zusammen „gekämpft“ haben. Besonders bei PIA RÖNFELDT, KIM FISCHER, SEBASTIAN LEUBNER, MELANIE KRAMME (geb. NECK), FRANZISKA BARS, ANNA REESE und JOANNA DOPTA möchte ich mich dafür bedanken. Ihr seid der Hammer!

Last but not least möchte ich mich bei meiner Familie bedanken. Besonders danken möchte ich dem innersten Kern: meiner Mama ASTRID MAHNKE, meinem Papa RALF MAHNKE und meinem Bruder JOHANNES MAHNKE. Ihr seid großartig, genauso wie ihr seid. Danke für den immensen Rückhalt, den ich durch euch immer hatte, für die zahlreichen Gespräche und dafür, dass ihr immer wieder meinen Kampfgeist geweckt habt, auch wenn ich selbst kurz vorm Aufgeben war. Danke, dass Heimat für so viel mehr stehen kann als bloß einen Ort.

„Jeder Mensch hat seine Stärken und Schwächen. Jeder stößt an Grenzen. In der Familie hat er die Chance, so angenommen zu werden, wie er ist - mit allem: Licht und Schatten.“

(Richard von Weizsäcker Weihnachtsansprache 1986, Bonn, 24. Dezember 1986.)

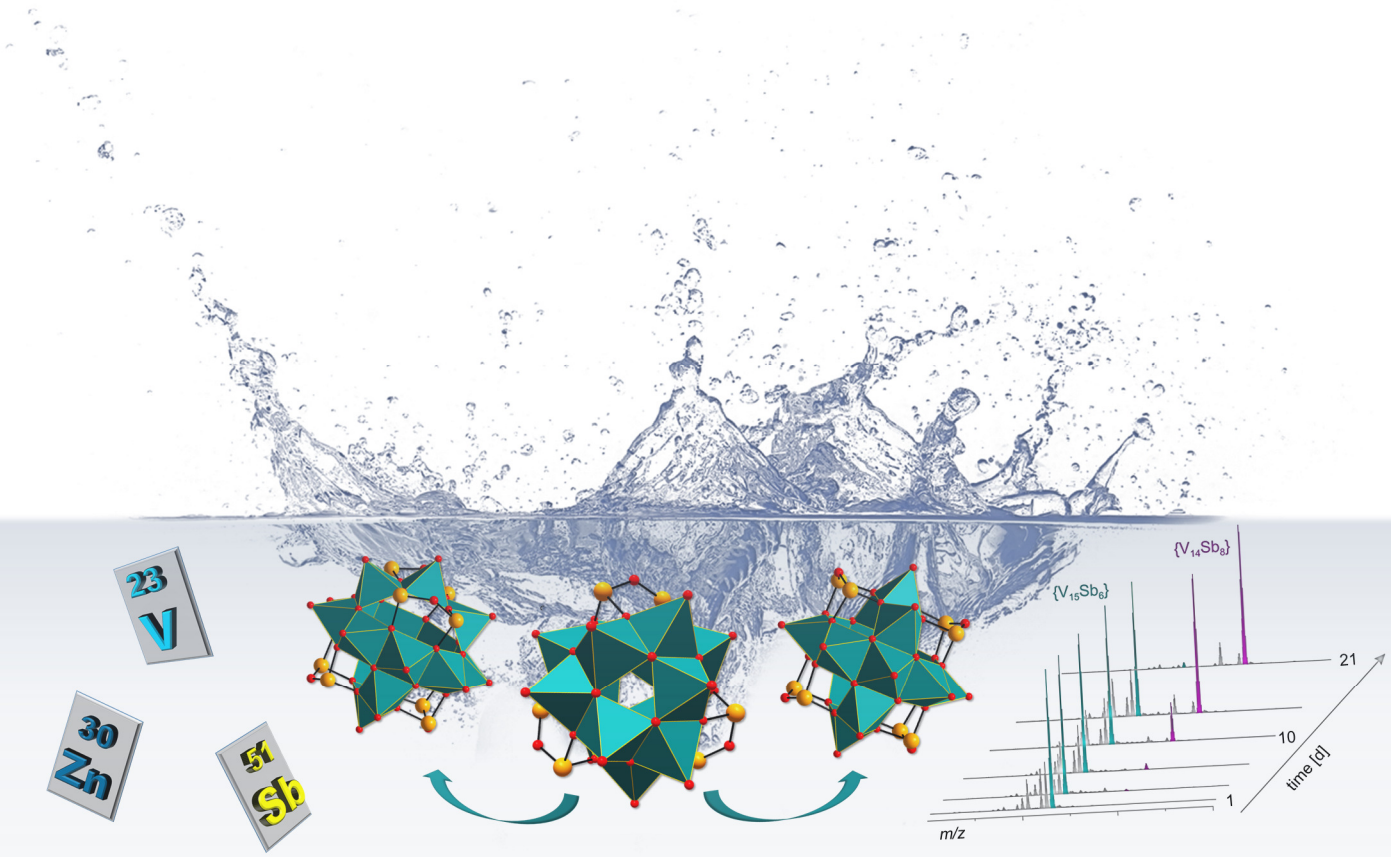
23
V
30
Zn
51
Sb
{V14Sb8}
{V15Sb6}
21
10
1
time [d]
m/z